Investigating the Molecular Composition of Rainwater and Secondary Organic Aerosol using Ultra-High Resolution Mass Spectrometry

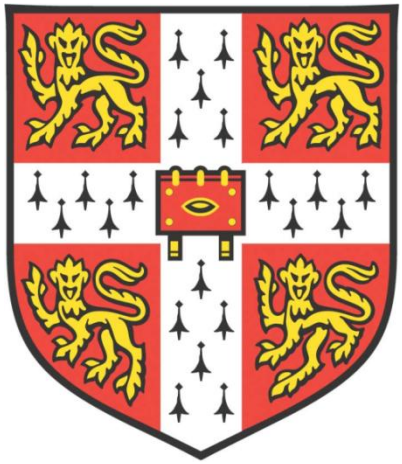

Anna Victoria Fee

Robinson College

Centre for Atmospheric Science

Department of Chemistry

University of Cambridge

This thesis is submitted for the degree of Doctor of Philosophy

December 2018

DECLARATION

This thesis is the result of my own work and includes nothing which is the outcome of work done in collaboration except where specifically indicated in the text. It is not substantially the same as any that I have submitted, or, is being concurrently submitted for a degree or diploma or other qualification at the University of Cambridge or any other University or similar institution.

In accordance with the School of Physics and Chemistry guidelines, this thesis does not exceed 60,000 words.

Signed:_____

Date:_____

Anna Victoria Fee

December 2018

ABSTRACT

Candidate Name: Anna Victoria Fee

Title of Thesis: Investigating the Molecular Composition of Rainwater and Secondary Organic Aerosol using Ultra-High Resolution Mass Spectrometry.

UHRMS has enormous potential to provide complete molecular characterisation of organic aerosol. However atmospheric aerosol often has complex, mixed organic and inorganic composition and soft ionisation techniques that have been developed to ionise organic aerosol specifically, are susceptible to salt suppression effects and competitive ionisation when applied to complex ambient aerosol.

In this thesis, characterisation experiments were conducted on a novel soft ionisation technique called Extractive Electrospray Ionisation (EESI) using mixtures of water-soluble organic compounds (WSOCs) with increasing ammonium sulphate solute concentrations. The WSOCs MS signals in the mixtures were not significantly affected by salt suppression over an atmospherically relevant range of 0-70% inorganic molar percentage relative to organic, recommending EESI-MS as a suitable technique for analysing ambient aerosol from a range of environments. EESI-MS was also used for the first time to detect Secondary Organic Aerosol (SOA) generated in the Cambridge Atmospheric Simulation Chamber (CASC) from the OH radical-initiated oxidation and ozonolysis of Anthropogenic Volatile Organic Compounds (AVOCs) and Biogenic Volatile Organic Compounds (BVOCs). Several oligomer products from complex BVOC and AVOC oxidation, previously observed in chamber studies using similar soft ionisation techniques, were detected using EESI-MS.

This thesis also includes the first study, to our knowledge, characterising the detailed molecular composition of organic compounds present in rainwater and aerosol collected during the same rain event, using chip-based direct infusion Nano-ESI and LC-ESI-MS. A Solid Phase Extraction (SPE) method was developed to extract the organic compounds from the rainwater and aerosol samples collected during the AERORAIN field campaign conducted in León, Spain, prior to MS analysis. More mono-aromatic compounds were observed in the aerosol samples whereas more poly-aromatic compounds were observed in the rainwater. HYSPLIT air mass backward trajectories revealed that both air mass origin and seasonality had strong influences on the sample composition. Samples collected during the summer and samples influenced by the Sahara desert contained the most compounds due to increased photochemical activity and extra industrial emissions from North Africa respectively. All samples contained semi-volatile oxygenated organic aerosol and multiple organosulphates were tentatively identified. Continental samples contained low-volatility oxidised organic aerosol and exhibited the most efficient aerosol scavenging and CHO and CHON compounds were preferentially scavenged over CHOS and CHONS compounds.

The combination of EESI-MS, Nano-ESI-MS and LC-ESI-MS analysis in this thesis, along with optimised analytical and data processing methods, has provided an in depth characterisation of the composition of complex aerosol, and highlights the importance of seasonality, long range transport and below-cloud scavenging on the compound distribution in ambient samples.

'Sometimes you have to make the hardest climb to see the most beautiful sunrise. I read that once on an old lady's decorative pillow. But it really is the way I feel today. I've climbed a very weird and rocky mountain…and my legs are tired, and I'm starving, but the sun is rising over a sea of love and waffles and possibility. So I'm just gonna relax and take a deep breath and enjoy this view for as long as I possibly can.'

— *Leslie Knope, Parks and Recreation*

ACKNOWLEDGEMENTS

Firstly I would like to thank my supervisor Professor Markus Kalberer for giving me the opportunity to complete my PhD and for all of his teaching, patience and support throughout my time in Cambridge. I would also like to thank the members of the Kalberer group as well as all of the members of the Centre for Atmospheric Science, past and present, for being so welcoming and providing such an enjoyable environment to work in.

Special mentions go to Dr Arthur Zielinski for all of his help and endless patience regarding the data processing codes I have used for parts of this thesis. Thanks also go to Dr Cameron Rae for providing the air mass backwards trajectory plots for the AERORAIN Campaign sample analysis. I would also like to thank Dr Chiara Giorio, Dr Peter Gallimore and Dr Ivan Kourtchev for their help and advice in the laboratory over the years and also members of the Jones group for their advice on statistical analysis.

Special thanks also go to Dr Ana Isabel Calvo Gordaliza, Professor Roberto Fraile and their colleagues at the Department of Applied Chemistry and Physics in León, Spain, who were principle investigators of the AERORAIN campaign and provided me with the rainwater and aerosol samples which were studied in this work.

Many thanks go to the staff in the Chemistry Department in Cambridge for their assistance in using the Transmission and Scanning Electron Microscopes, the images from which feature in my thesis.

I would also like to thank my Graduate Tutor Dr Paul Griffiths for his advice over the years and all of the members of Robinson College for their support and providing such a friendly community where I have made life-long friends.

Finally, for all of their support during my PhD and throughout my life, I thank my parents, family and friends, without whom I never would have made it to Cambridge.

CONTENTS

LIST OF TABLES

LIST OF FIGURES

LIST OF ABBREVIATIONS AND ACRONYMS

AI	Aromaticity Index
AMS	Aerosol Mass Spectrometer
APCI	Atmospheric Pressure Chemical Ionisation
API	Atmospheric Pressure Ionisation
APPI	Atmospheric Pressure Photoionisation
ARL	Air Resources Laboratory
AS	ammonium sulphate
ATOFMS	Aerosol Time-of-Flight Mass Spectrometer
AVOC	Anthropogenic Volatile Organic Compound
BBOA	Biomass Burning Organic Aerosol
BVOC	Biogenic Volatile Organic Compound
CASC	Cambridge Atmospheric Simulation Chamber
CCN	Cloud Condensation Nuclei
CE-ESI	Capillary Electrophoresis Electrospray Ionisation
CFT	Cloud Flow Tube
CHO	Formulae containing carbon, hydrogen and oxygen atoms
CHON	Formulae containing carbon, hydrogen, oxygen and nitrogen atoms
CHOS	Formulae containing carbon, hydrogen, oxygen and sulphur atoms
CHONS	Formulae containing carbon, hydrogen, oxygen, nitrogen and sulphur atoms
CI	Chemical Ionisation
CI	Criegee Intermediate
CPA	*cis*-pinonic acid
CPC	Condensation Particle Counter
DBE	Double Bond Equivalence
DCCA	3,3-dimethyl-2-(3-oxobutyl)cyclobutanecarboxylic acid
DESI	Desorption Electrospray Ionisation
DHHMDMCP OS	2,3-dihydroxy-2-(hydroxymethyl)-7,7-dimethylbicycloheptan-6-one organosulphate
DMA	Differential Mobility Analyser
DOC	Dissolved Organic Carbon

DOM	Dissolved Organic Matter
EC	Elemental Carbon
EDX	Energy Dispersive X-ray
EESI-MS	Extractive Electrospray Ionisation Mass Spectrometry
EI	Electron Ionisation
EIC	Extracted Ion Chromatogram
ELVOC	Extremely Low-Volatility Organic Compound
ESI-MS	Electrospray Ionisation Mass Spectrometry
FTICR	Fourier Transform Ion Cyclotron
GC	Gas Chromatography
GC-MS	Gas Chromatography Mass Spectrometry
GDAS	Global Data Assimilation System
HESI	Heated Electrospray Ionisation
HHDCA	1-hydroxy-3-(hydroxymethyl)-2,2-diemthylcyclobutane-carboxylic acid
HOA	Hydrocarbon-like Organic Aerosol
HODSA OS	3-(2-hydroxy-3-oxobutyl)-2,2-dimethylsuccinaldehyde organosulphate
HOM	Highly Oxygenated Molecule
HPLC	High Performance Liquid Chromatography
HR-Q-TOF	High-Resolution Quadrupole Time-of-Flight
(HR-)TOF-AMS	High-Resolution Time-of-Flight Aerosol Mass Spectrometer
HYSPLIT	Hybrid Single-Particle Lagrangian Integrated Trajectory
IPCC	Intergovernmental Panel on Climate Change
ITMS	Ion Trap Mass Spectrometer
IVOC	Intermediate-Volatile Organic Compound
LACIS	Liepzig Aerosol Interaction Simulator
LC	Liquid Chromatography
LC-ESI-MS	Liquid Chromatography Electrospray Ionisation Mass Spectrometry
LC-MS	Liquid Chromatography Mass Spectrometry
LDI	Laser Desorption Ionisation
LESA	Liquid Extraction Surface Analysis
LTQ	Linear Trap Quadrupole

LV-OOA	Low-Volatility Oxidised Organic Aerosol
MEMS	Microelectrical Mechanical Systems
MIS	Microelectrical Mechanical Systems Impactor Stage
MS	Mass Spectrometer or Mass Spectrometry
MS/MS or MS^n	Tandem Mass Spectrometry
MW	Molecular Weight
m/*z*	Mass-to-Charge Ratio
Nano-ESI-MS	Nanoelectrospray Ionisation Mass Spectrometer
NMR	Nuclear Magnetic Resonance
NOAA	National Oceanographic and Atmospheric Administration
NCL	National Centre for Atmospheric Research (NCAR) Command Language
OA	Organic Aerosol
OC	Organic Carbon
OOA	Oxygenated Organic Aerosol
OS	Organosulphate
PAH	Polycyclic Aromatic Hydrocarbon
POA	Primary Organic Aerosol
POM	Primary Organic Matter
PTFE	Polytetrafluoroethylene
PTR-MS	Proton Transfer Reaction Mass Spectrometry
RA	Relative Abundance
RF	Radiative Forcing
RH	Relative Humidity
RP	Reversed Phase
RT	Retention Time
SCI	Stabilised Criegee Intermediate
SEM	Scanning Electron Microscope
SFU	Stacked Filter Unit
SMPS	Scanning Mobility Particle Sizer (Spectrometer)
SOA	Secondary Organic Aerosol
SPE	Solid Phase Extraction
SVOC	Semi-Volatile Organic Compound

SV-OOA	Semi-Volatile Oxidised Organic Aerosol
TC	Total Carbon
TEM	Transmission Electron Microscope
TIC	Total Ion Current
UHPLC-MS	Ultra High Polarity Liquid Chromatography Mass Spectrometry
UHRMS	Ultra High Resolution Mass Spectrometry
UV	Ultraviolet
VOC	Volatile Organic Compound
WSOC	Water-Soluble Organic Carbon or Water Soluble Organic Compound

LIST OF APPENDICES

1 INTRODUCTION

1.1 Aerosol in the troposphere

An *aerosol* is defined as the suspension of fine solid or liquid droplets in a gas but the term is commonly used in reference to particulate matter that contains a large proportion of condensed matter other than water (Pöschl 2005). Aerosols can either be emitted directly into the atmosphere from natural and anthropogenic sources (primary aerosol) or formed via gas-to-particle conversion of Volatile Organic Compounds (VOCs) in the atmosphere (secondary aerosol). Once emitted into the atmosphere, aerosol size and chemical composition can change when a particle is "aged" through atmospheric processes including oxidation, condensation, evaporation and chemical reaction with other species. The aerosols are then removed from the atmosphere via deposition at the Earth's surface (dry deposition) or by being incorporated into cloud droplets or precipitation (wet deposition) (Seinfeld and Pandis 2006, Pöschl 2005).

1.1.1 Aerosol Size Distribution and Sources

Atmospheric aerosol have numerous significant natural sources including sea spray, biomass burning, volcanic eruptions, terrestrial dust from soil and rock debris. Anthropogenic sources include fuel combustion, meat cooking, industrial processes, vehicles and road dust and tyre debris (Mohr et al. 2009, Seinfeld and Pandis 2006).

Particles can be categorised as being 'fine' (< 2.5 μm in diameter) or 'coarse' (> 2.5 μm in diameter). Coarse particles consist mostly of sea salt, plant debris and natural and anthropogenic dust which have short atmospheric lifetimes (Seinfeld and Pandis 2006, Ziemann and Atkinson 2012). Fine particles include those in the 'Accumulation' mode (0.1 to 2.5 μm in diameter), produced from primary emissions, such as black carbon and metals from combustion. These are the main contributor to aerosol surface area and mass. Particles formed via condensation of nitrates, sulphates and organics in the gas-phase, and particles formed via the coagulation of particles in the Nuclei mode, are also classified as being 'fine'. 'Ultrafine' particles comprise 'Nucleation' or 'Nuclei' particles which are 1-10 nm in diameter and are produced from the condensation of hot combustion vapours or from the nucleation of other atmospheric species, and the 'Aitken' mode which are 10-100 nm in diameter.

1.1.2 Effects on Climate

Aerosols have important effects on climate because they can absorb and scatter shortwave and longwave radiation due to their various radiative and microphysical properties. In doing so, they exert radiative forcing effects (changes in the rate of absorption of solar radiation) which alter the radiative balance of the Earth-atmosphere system (Ramanathan et al. 2001). They also act as Cloud Condensation Nuclei (CCN) and Ice Nuclei (IN) and alter the microphysical properties of clouds, affecting their cloud optical thickness and cloud albedo which in turn, increases reflection of solar radiation by clouds. This results in a negative radiative forcing. The image in Figure 1.1, reproduced from the IPCC 2013 Climate Change Fifth Assessment Report (Myhre et al. 2013), shows the global mean radiative forcing values for different aerosol species and other atmospheric species from pre-industrial times (1750) to the year 2011.

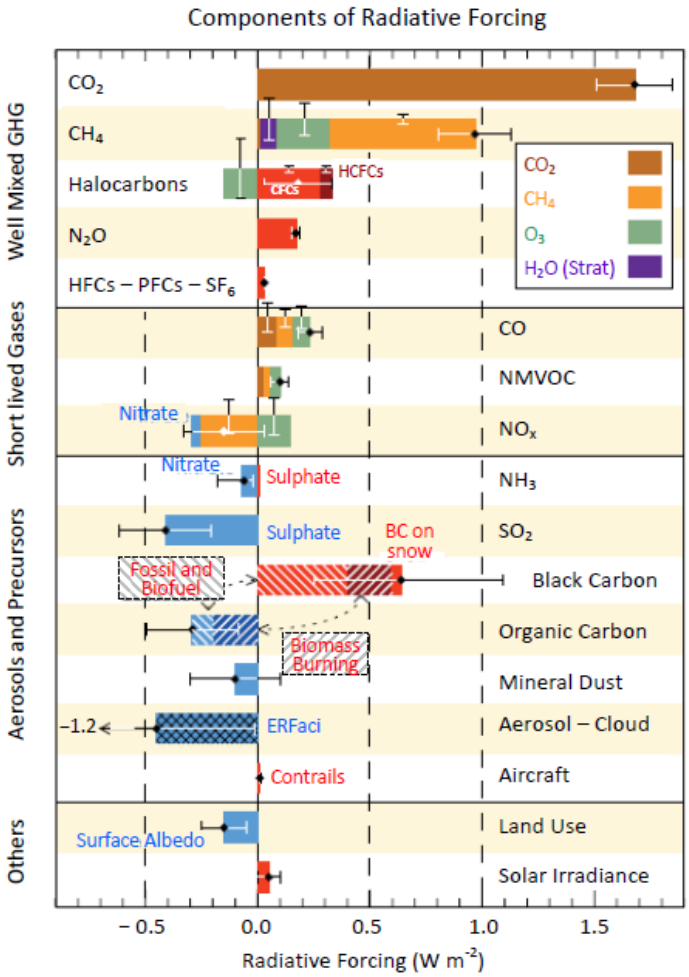

Figure 1.1. Radiative Forcings (RF) based on gaseous, aerosol and aerosol precursor compounds over the 1750–2011 year period. Red and blue bars indicate positive RF and negative RF respectively for emitted components which affect few forcing agents. Emitted components which affect many compounds are represented using several colours (figure inset). Diamond symbols represent the net impact of the individual contributions. Horizontal error bars denote uncertainty of the net impact of each individual component and vertical error bars denote relative uncertainty of the RF of that component. *ERFaci* is the Effective Radiative Forcing due to aerosol-cloud interactions, caused by BC, OC and dust emissions, and secondary aerosol from anthropogenic emissions of SO_2, NH_3 and NO_x. Image reproduced from the IPCC 2013 Climate Change Fifth Assessment Report (Myhre et al. 2013).

1.2 Organic Aerosol

Atmospheric organic aerosol (OA) is a complex mixture of different compounds with different functional groups. Some of these compounds, including Polycyclic Aromatic Hydrocarbons (PAHs) and heterocyclic amines, have high carcinogenic and mutagenic

potential (Seinfeld and Pandis 2006, Samy and Hays 2013). Approximately 300 Tg/yr of OA is emitted and OA contributes ~20–50% of the aerosol mass burden in continental mid-latitudes and as much as 90% in tropical forested areas (Kanakidou et al. 2005, Noziere et al. 2015), making it one of the two largest constituents of the global submicron aerosol burden, along with sulphate. OA is composed of both primary organic aerosol (POA) which is directly emitted into the atmosphere and secondary organic aerosol (SOA) which is photochemically produced via the oxidation of organic gas-phase precursor compounds (Hodzic et al. 2010).

1.2.1 Primary Organic Aerosol (POA) Formation

Primary Organic Aerosol (POA) is emitted directly into the atmosphere from sources including biomass burning, rubbish burning, meat cooking and fossil fuel combustion; mostly in the form of hydrocarbon-like organic aerosol (HOA) which makes a significant contribution to aerosol mass in urban areas (Zhang et al. 2007). Other types of POA include pollen, spores, bacteria and plant debris, and organic compounds which are emitted into the atmosphere in vapour form and subsequently condense into the aerosol phase without undergoing any gas-phase chemistry (Kanakidou et al. 2005).

POA comprises both intermediate-volatile organic compounds (IVOC) which preferentially remain in the gas-phase, and semi-volatile compounds (SVOC) which are characterised by relatively low volatility and partition into the aerosol phase (Hodzic et al. 2010, Robinson et al. 2007). POA produced by meat cooking tend to be characterised by long alkyl chains, including compounds like saturated alkanes and alkenes, cycloalkanes and organic acids. Vehicular emissions are largely influenced by re-condensed engine exhaust and include saturated hydrocarbons (*n*-alkanes, cycloalkanes, branched alkanes) and aromatics (Mohr et al. 2009). POA from wood burning contains a lot of biomass burning OA (BBOA) including carboxylic acids, sugars and heterocyclic amines (Samy and Hays 2013). POA is often present in high abundance in tropical air masses due to the high biomass burning activity (Pöschl 2005).

1.2.2 Secondary Organic Aerosol

Many gas-phase organic compounds undergo oxidation in the atmosphere to yield products with sufficiently low vapour pressures to partition into the aerosol phase. Those that partition into the aerosol phase are known as Secondary Organic Aerosol (SOA) and are semi-volatile or non-volatile. The concept of gas-particle-partitioning was introduced by (Pankow 1994)) and extended to include SOA formation by (Odum et al. 1996). Partitioning of a compound is described using an equilibrium partitioning coefficient, K_p (m^3 μg^{-1}):

$$K_p = \frac{C_p}{C_g C_{OA}}, \quad (1.1)$$

where C_p is the concentration of the compound in the particle phase (ng m^{-3}), C_g is the concentration of the compound in the gas phase (ng m^{-3}) and C_{OA} is the mass concentration of the total organic aerosol particle phase (µg m^{-3}), into which semi-volatile organics or highly water-soluble organics can partition. As the amount of absorbing material increases, more volatile compounds (smaller K_p) will partition into the particle phase (Hallquist et al. 2009).

Some of the organic products which do not partition into the particle phase and remain in the gas phase, can undergo further oxidation to generate additional SOA. This process is referred to as ‘oxidative ageing’ or ‘aerosol ageing’ (Kanakidou et al. 2005, Ziemann and Atkinson 2012). SOA is believed to contribute 50-85% of total OA (Glasius and Goldstein 2016) and it has been recently suggested that low-volatility SOA may account for > 50% of the CCN in continental environments (D'Andrea et al. 2013). Reaction products with higher carbon numbers and more functional groups are more likely to form SOA because these factors are associated with lower vapour pressures which are required for gas-particle partitioning.

1.3 Secondary Organic Aerosol Formation Pathways

1.3.1 Gas phase reactions of Volatile Organic Compounds (VOCs)

Arguably the most atmospherically-important mechanism for SOA formation is the oxidation of Volatile Organic Compounds (VOCs) by the hydroxyl radical (OH•), ozone (O_3) nitrate radical (NO_3•), and photolysis, which forms oxidised products of sufficiently low volatility that can partition from the gas phase into the particle phase (Kroll and Seinfeld 2008). The production of new particles via this process is known as homogeneous nucleation. Reactions with OH• and O_3 are estimated to be of significant importance during the daytime whereas VOC reactions with NO_3 are important at night (Seinfeld and Pandis 2006). Cl atoms have also been shown to react with VOCs, particularly in the Arctic and marine environments (Atkinson and Arey 2003a).

When VOCs react with a radical or ozone, a range of 'first generation products' are produced that contain at least one polar oxygenated functional group including aldehyde (-C(=O)H), ketone (-C(=O)-), alcohol (-OH), carboxylic acid (-C(=O)OH), nitrate (-ONO_2), peroxyacetylnitrate (-C(=O)OONO_2), hydroperoxide (-OOH) and percarboxylic acid (-C(=O)OOH) groups. These products tend to be less volatile and more water soluble than their parent VOCs. Further oxidation produces 'second generation products' which are even less volatile. However, gas-phase oxidation leads to a reduction in the carbon chain length and lower molecular weight compounds which are more volatile. Ultimately, repeated gas-phase oxidation of VOCs results in CO_2 (Hallquist et al. 2009).

Biogenic VOCs (BVOCs) are mostly alkenes (~50% isoprene, ~10% monoterpenes and other alkenes including sesquiterpenes) and oxygenated VOCs. BVOCs have mainly terrestrial sources including vegetative emissions but dicarboxylic acids, dimethylsulphide, ammonium salts and isoprene emissions are also produced by marine sources (Hallquist et al. 2009). BVOCs contribute ~90% of non-methane VOC global emissions but anthropogenic VOCs (AVOCs) often dominate in urban areas. AVOCs comprise ~40% alkanes, ~10% alkenes and 20% aromatics, ~10% oxygenated compounds and other unidentified VOCs (Atkinson and Arey 2003a).

The mechanisms for VOC oxidation are described here briefly. BVOCs are photolysed in the troposphere when they absorb radiation of wavelengths ≥ 290 nm. This process is

potentially very important for the formation of carbonyl compounds e.g. for methyl hydroperoxide which photolyses to produce OH• and hydroperoxide:

$$CH_3OOH + h\nu \rightarrow CH_3O\bullet + OH\bullet , \quad (1.2)$$

$$OH\bullet + CH_3OOH \rightarrow H_2O + CH_3O_2\bullet , \quad (1.3)$$

$$OH\bullet + CH_3OOH \rightarrow H_2O + CH_2OOH\bullet \rightarrow HCHO + OH\bullet \quad (1.4)$$

and alkyl nitrates including peroxy nitrates ($ROONO_2$) and peroxyacetyl nitrates (PAN; $R(O)OONO_2$) which photolyse to produce an alkoxy radical (RO•), as shown in Equation 1.5 for methyl peroxynitrate (CH_3OONO_2) (Atkinson and Arey 2003b, Atkinson 2000):

$$CH_3OONO_2 + h\nu \rightarrow CH_3OO\bullet + NO_2 . \quad (1.5)$$

Photolytic reactions generally involve bond cleavage which results in an increase in volatility but sometimes result in a reduction of SOA (Kroll and Seinfeld 2008).

An alkyl (R•) or substituted alkyl radical is also produced when a VOC reacts with an OH/NO_3 radical, a Cl atom, or O_3. Oxidation of a VOC by OH•, NO_3• or Cl atoms occurs by one of three pathways. The first is H-atom abstraction by the radical or Cl atom, from O-H, C-H or N-H bonds in the VOC, as shown in the example in Equation 1.6:

$$X + RCH_2R' \rightarrow HX + RC\bullet HR' , \quad (1.6)$$

where *X* can be OH•, NO_3• or Cl atom.

The second pathway is via radical addition across a C=C bond as shown in the example in Equation 1.7:

$$X + RCH = CHR' \rightarrow RC\bullet H - CH(X)R' , \quad (1.7)$$

where *X* can be an OH•, NO_3•, Cl atom or O_3.

The third pathway is radical addition to ring carbons of aromatic compounds as shown in the example of toluene in Figure 1.2 (Ziemann and Atkinson 2012).

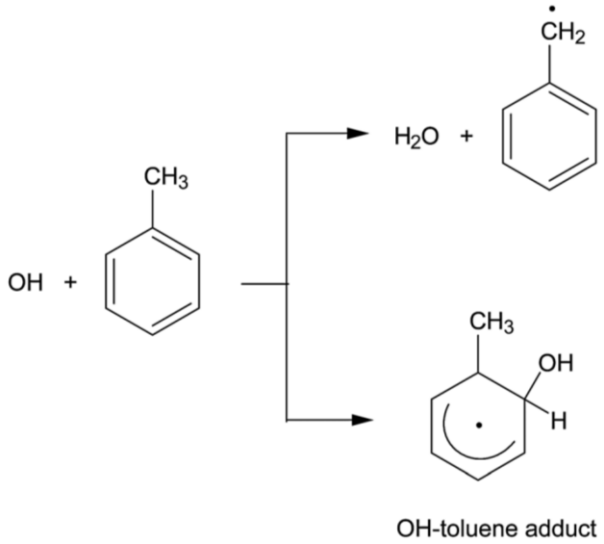

Figure 1.2. VOC oxidation via OH radical addition to the ring carbons of aromatic compounds. A substituted alkyl radical and an OH aromatic adduct are produced. Schematic from Ziemann and Atkinson (2012).

Addition reactions produce organic products with lower volatilities and although the identity of the radical makes little difference to the volatility of the product, NO_3•-initiated reactions produce higher SOA yields than OH•-initiated reactions (Kroll and Seinfeld 2008).

Reactions of VOCs with O_3 is a more complex mechanism. Addition of O_3 across a VOC C=C bond produces a primary ozonide which rapidly decomposes to produce a carbonyl and an excited carbonyl oxide called a 'Criegee intermediate' (CI). The excited CI can decompose to produce OH• and an alkyl radical (R•), or it can form a stabilised version which then reacts with water or with stabilised organics, as shown in Figure 1.3.

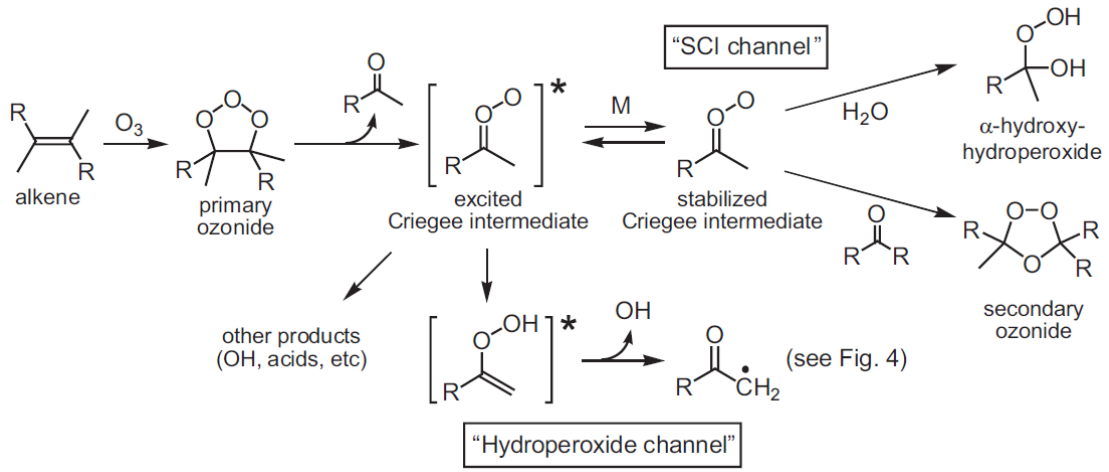

Figure 1.3. Simplified mechanism of alkene ozonolysis. Ozone (O_3) is added across the alkene C=C, producing a carbonyl and Criegee intermediate which either decomposes to produce OH and an alkyl radical ('Hydroperoxide channel') or forms a Stabilised Criegee Intermediate (SCI channel) which can react with water or organics. Schematic from Kroll and Seinfeld (2008).

The alkyl and substituted alkyl radicals produced by reactions of VOCs with radicals and ozone, go on to react with oxygen to produce peroxy radicals (RO_2•). Under low NO_x or NO_x-free conditions, RO_2• can react with HO_2 radicals to produce hydroperoxides, carboxylic acids and peroxyacids which are major contributors to SOA yields. RO_2• can also undergo 'self-reactions' (RO_2• + RO_2•) to produce alcohols and carbonyls or 'cross-reactions' to produce alkoxy (RO•) radicals. In the presence of NO_x, RO_2• reacts with NO_2 to produce peroxynitrates, or reacts with NO to produce RO• and nitrates as shown in the schematic in Figure 1.4 (Ziemann and Atkinson 2012). PANs are of sufficiently low volatility to partition into the aerosol phase, meaning they contribute to the SOA yield (Kroll and Seinfeld 2008). RO• radicals can either decompose via C-C bond scission to produce a carbonyl and alkyl radical; isomerise, or react with O_2 to produce a carbonyl and HO_2 radical (Atkinson and Arey 2003b).

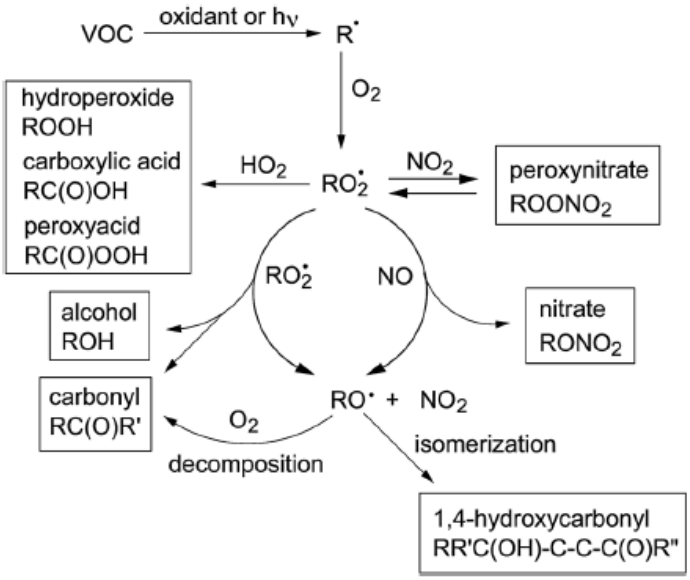

Figure 1.4. VOC oxidation mechanisms involving the formation of an alkyl (R•) or substituted alkyl radical. (e.g. hydroxyalkyl or nitrooxyalkyl radical). RO_2• and RO• denote organic peroxy and alkoxy radicals respectively. The product groups are shown in boxes. The carboxylic acid, RC(O)OH and peroxyacid RC(O)OOH, are produced via reaction of acyl peroxy radicals ($RC(O)O_2$•) with HO_2 radicals. Schematic from Ziemann and Atkinson (2012).

1.3.2 Particle phase reactions

Organic compounds can undergo particle phase reactions (including heterogeneous and multiphase reactions), while they are in the condensed phase, which influence their volatility. Oxidative reactions can occur including photolysis and oxidation via heterogeneous uptake of OH•, NO_3•, Cl and O_3 oxidants, resulting in 'aerosol ageing'. Some of the organic monomers produced by heterogeneous chemistry can then undergo condensed-phase chemistry to form oligomeric compounds (Rudich, Donahue and Mentel 2007). Semi-volatile organic compounds (SVOCs) partition between the gas and particle phases and can undergo reactions in either phase. At low total aerosol loadings, the irreversible condensation of extremely low volatile compounds (ELVOCs) have been suggested to be a primary source of SOA formation (Ehn et al. 2014).

Organic compounds can be photolysed in the particle phase. For example, irradiation of SOA and other oxidised condensed phase organics efficiently produces formaldehyde and formic acid; likely due to photolysis of peroxides in the particle phase. Ozonolysis

of oleic acid produces both volatile products from C-C bond cleavage and also high molecular weight species with low volatilities after further reactions of SCIs. In the particle phase, SCI reactions tend to proceed via the 'SCI channel' (Figure 1.3) rather than the 'hydroperoxide channel' due to increased thermalisation of the CI and higher concentrations of condensed-phase organics. Alkoxy radicals also behave differently in the particle phase from the gas phase. Oxidation and dissociation of RO• is important in both the gas and particle phase but there is no evidence to suggest that isomerisation of RO• occurs in the particle phase (Kroll and Seinfeld 2008).

Non-oxidative reactions known as "accretion reactions" also occur, producing high molecular weight species with low volatilities which have been observed in laboratory-generated SOA (Kalberer et al. 2004). Examples of accretion reactions in the troposphere include peroxyhemiacetal formations from hydroperoxides and aldehydes, aldol condensation reactions, ester, acid anhydride and organosulphate formation. Dimeric hemiacetals and esters formed from isoprene oxidation (Surratt et al. 2006) and organosulphates from isoprene and monoterpene oxidation (Gao et al. 2006) and reaction of BVOCs and sulphate (Shrivastava et al. 2017), have all been observed in ambient SOA. Other particle phase reactions which produce products with higher volatilities have been studied including carbocation rearrangements and retroaldol reactions (Kroll and Seinfeld 2008).

1.3.3 Aqueous phase reactions

Low volatility organic compounds and SOA can also be produced through aqueous reactions in clouds, fog and wet aerosol (Blando and Turpin 2000). Water soluble gases can undergo photolysis and the presence of OH• in the interstitial spaces of cloud and fog droplets allows radical-initiated oxidation of water soluble gases (Kroll and Seinfeld 2008). These photochemical reactions produce organic acids, aromatic compounds, fatty acids and aldehydes, as well has high molecular weight oligomers including organosulphates, organonitrates and nitroxy-organosulphates which have all been detected in cloud water and rainwater (Altieri, Turpin and Seitzinger 2009, Lim et al. 2010).

Unlike gas phase SOA formation which requires VOC precursors with large carbon chains (> C_7) to produce semi-volatile products with high yields, aqueous SOA precursors are water soluble and thus, smaller (C_2, C_3) (Lim et al. 2010). Glyoxal, methylglyoxal, pyruvic acid and glycoaldehyde, for example, are too volatile to act as precursors for gas phase SOA formation in significant yields but have been shown to produce low volatility products in the aqueous phase. Cloud processing of glyoxal and methylglyoxal is believed to contribute a significant amount of SOA, comparable to that produced by gas phase oxidation of monoterpene and sesquiterpenes (Volkamer, Ziemann and Molina 2009) and the total SOA burden produced by aqueous chemistry is estimated to be of the same magnitude as SOA produced by gas-particle partitioning. The shorter carbon chains in aqueous phase reactions also result in more highly oxygenated organic aerosol (OOA) being produced than would occur in gas-particle partitioning SOA formation and these OOA can act as CCN (Lim et al. 2010).

Studies of ambient SOA have observed linear correlations between SOA yield and aerosol water concentrations and high RH conditions (> 70%) which suggests that aqueous phase SOA formation dominates over partitioning of semi-volatile gas phase products, in some locations (Hennigan et al. 2009, Hennigan et al. 2008). Efficient SOA formation via aqueous chemistry pathways requires hygroscopic particles or CCN, high RH (> 70%) which enables the water soluble organic gases to partition into cloud or aerosol water, and chemistry that allows the lower volatility products to remain in the particle phase following water evaporation. This means that aqueous SOA formation is most likely to occur in conditions of high humidity and where gas phase photochemistry is favoured to produce the Water Soluble Organic Carbon (WSOC) compounds and oxidants.

1.4 Mass Spectrometry as a tool for analysing aerosol composition

One of the difficulties in characterising ambient organic aerosol is the large number of individual species present with many different functional groups, in the same sample (Hallquist et al. 2009). In the past, many different ‘offline’ techniques have been used to determine the chemical composition of ambient and laboratory-generated aerosol. These include using denuders and filters to collect aerosol, extracting target compounds using

solvent extraction and then employing a separation technique like Gas Chromatography (GC) or Liquid Chromatography (LC). These techniques offer significant identification and quantification possibilities which is why many are still used for aerosol composition analysis.

However, offline techniques have many disadvantages including being time-consuming due to the multiple sample preparation steps required before analysis. They often require transport of samples from the field to laboratory, risking sample damage or degradation. Incomplete analyte extraction and subsequent analyte loss as well as using large amounts of solvents are also issues. Ambient aerosol constantly undergoes chemical and physical changes so ideally, organic compounds need to be identified on timescales of seconds to minutes. The potential problems with offline procedures mean that the subsequent analysis of ambient aerosol may not be able to produce the exact molecular composition detail which was present in the samples when they were collected. To overcome these issues, a range of 'online' techniques have been developed to obtain information on gaseous and particulate organic compounds in real time (Noziere et al. 2015, Dalton et al. 2005).

1.4.1 High resolution mass spectrometry

Mass spectrometry (MS) allows the measurement of a wide range of organic and inorganic compounds in ambient and laboratory-generated aerosol with a fast time resolution and high sensitivity (Sullivan and Prather 2005). The principle of MS is to analyse the compounds based on the mass-to-charge ratio (m/z) of the ions they produce.

Mass spectrometers have three main components:

- An ionisation unit to produce the gas-phase ions from the aerosol sample.
- A mass analyser to separate the ions according to their m/z ratio using an electric or magnetic field.
- A detector to convert the measured current from each ion, into the relative abundance of that ion in the sample.

The main differences between mass spectrometers used for characterising organic aerosol composition are due to the type of mass analyser and ionisation techniques used to produce the ions from the sample.

1.4.2 Ionisation techniques

1.4.2.1 Hard ionisation techniques

'Hard' ionisation techniques are so-called because they use a large amount of energy to ionise samples which often fragments the sample. Electron Ionisation (EI) is a widely used technique which produces ions by colliding target analytes with 70 eV electrons. This technique produces a lot of fragmentation which enables it to provide structural information on single analytes once they have been separated from the rest of the sample using a chromatographic separation technique. The spectra produced using EI are generally specific, reproducible and comparable with database spectra. However, it is difficult to interpret fragmentation patterns of complex mixtures on EI mass spectra that have not been separated prior to MS analysis (Noziere et al. 2015).

An advantage of using thermal desorption followed by EI is that more quantitative data can be produced for organic compounds and most inorganic compounds because the ionisation occurs after the chemicals have been desorbed from the aerosol. However, it is unsuitable for less volatile compounds including sea salt and mineral dust which cannot be vapourised at 600°C. In addition, thermal desorption is not able to produce quantitative chemical information on individual particles.

Laser Desorption/Ionisation (LDI) is another hard ionisation technique which uses the light from a laser to detect the presence of a particle. It has the advantage of being able to desorb, ionise and detect all aerosol components from a single particle, in real time. This includes both the non-refractory components (e.g. ammonium nitrate, organics) and refractory components (e.g. soot, mineral dust). However, the MS signals produced using LDI are highly variable and can be affected by matrix effects. (Noziere et al. 2015, Sullivan and Prather 2005).

1.4.2.2 Soft ionisation techniques

The limitations of hard ionisation techniques has promoted the development of softer ionisation techniques which result in much less fragmentation of the organic compounds. Soft ionisation techniques can have high ionisation efficiencies but they are often susceptible to signal loss arising from the transfer of ions from the ambient pressure into the MS vacuum system which results in poor sensitivity. The lack of fragmentation of compounds when using soft ionisation techniques, although highly favourable for organic compounds, means that it is more difficult to identify specific compounds without the use of additional techniques to provide structural information. However, these softer techniques allow the user to see a much broader range of compounds and functional groups in ambient samples which is very important for characterising complex organic aerosol influenced by different seasons and environments.

Chemical Ionisation (CI) ionises the analytes by reacting them with reagent ions to produce diagnostic ions which are then detected by the MS. CI provides molecular weight information of VOCs that undergo extensive fragmentation when EI is applied (Pramanik, Ganguly and Gross 2002). Direct CI-MS techniques have short time resolutions of 0.1-1.0 seconds which allows fast measurements, making it a useful tool for analysing transport processes or detecting highly reactive species and identifying them if coupled with high resolution MS. Techniques using thermal desorption followed by CI have been developed, utilising the improved selectivity and softer ionisation of CI compared with EI which is more useful for studying organic compounds (Sullivan and Prather 2005).

Proton-Transfer-Reaction MS (PTR-MS) is the most widely used CI-MS technique in atmospheric chemistry. Organic compounds in the gas phase become ionised following protonation by hydronium ions (H_3O^+). The technique is highly sensitive, has low detection limits and causes very little fragmentation of organic compounds. It has been successfully used to study processing of SOA (Holzinger et al. 2010) and to quantify Criegee Intermediates from the ozonolysis of α-pinene (Giorio et al. 2017a).

Atmospheric Pressure Chemical Ionisation (APCI); another soft ionisation technique, uses an Atmospheric Pressure Ionisation (API) interface through which the ions enter the high vacuum part of the MS. It has an advantage over traditional CI in that the ions are formed at atmospheric pressure so large amounts of solvent do not need to be introduced directly into the vacuum system (Pramanik et al. 2002). APCI mass spectra

can provide unambiguous information on the molecular mass of compounds by producing intact molecular ions. Online APCI has successfully been used to analyse biogenic SOA from ozonolysis of monoterpenes (Warscheid and Hoffmann 2002). APCI does however produce some fragmentation which is not always ideal for analysing organic compounds.

Another more recently developed atmospheric pressure ionisation technique is Atmospheric Pressure Photoionisation (APPI) which produces photo-ions by colliding a photon emitted by a UV source with the vapourised sample (Raffaelli and Saba 2003). The UV wavelength can be optimised to improve detection limits of specific compounds.

1.4.2.3 Electrospray Ionisation (ESI)

Electrospray Ionisation MS (ESI-MS) has become the most widespread soft ionisation technique for analysing biological compounds because it allows direct analysis of non-volatile molecules from the liquid phase and can be coupled to selective separation techniques including High Performance Liquid Chromatography (HPLC) (Cech and Enke 2001). It also produces minimal fragmentation of analytes; making it very effective for detecting organic compounds. (Mazzoleni et al. 2010b, Cech and Enke 2001). ESI has been successfully applied to composition analysis for laboratory-generated (Bateman et al. 2009, Surratt et al. 2006) and ambient (Cook et al. 2017, Kourtchev et al. 2013, Wozniak et al. 2008, Mazzoleni et al. 2012b) aerosol.

ESI sources are similar in design to APCI in that they use an API interface through which the ions enter the MS (Pramanik et al. 2002). ESI-MS can be conducted in positive ionisation mode or negative ionisation mode. Compounds which readily form positively charged ions, such as proteins, due to their multiple basic amino acid residues, are ionised in positive mode to produce protonated ions ($[M+H]^+$). Compounds which can be negatively charged via deprotonation of acidic groups, such as organic acids, are ionised in negative ionisation mode to produce deprotonated ions ($[M-H]^-$).

The mechanism for ionisation in positive mode is shown in Figure 1.5 and is described here. A solution containing the analyte and polar solvent enters the ESI source through an electrospray needle with a high (2–3 kV) voltage (positive or negative depending on the target analytes) applied across it. This strong electric field causes the sample

solution to disperse and the electrospray needle has a high positive potential relative to the vacuum orifice. The negatively charged anions migrate towards the needle tip while the positively charged cations congregate around the liquid meniscus, resulting in charge separation at the surface of the liquid. The cations repel each other at the meniscus, producing a 'Taylor cone' as shown in Figure 1.5, aided by a coaxial sheath gas (dry N_2). The electrostatic repulsion increases until it overcomes the surface tension of the liquid and a charged parent droplet is dispatched from the tip of the Taylor cone. The solvent evaporates from the droplet causing the droplet to decrease in size.

Different mechanisms have been proposed for the production of analytes from charged droplets. The 'Coulomb Fission' mechanism assumes that the increased charge density from the decreasing droplet size causes the large droplet to divide into smaller and smaller droplets until only single ions remain. Alternatively, the 'Ion Evaporation' mechanism proposes that the increased charge density from the decreasing droplet size eventually results in the surface charge to surface area ratio of the droplet increasing until the Coulombic repulsion of the surface charge equals the droplet surface tension. This is termed the 'Rayleigh Stability Limit' (Rayleigh 1882), and is defined by Equation 1.8 (Cech and Enke 2001, Banerjee and Mazumdar 2012):

$$q_{Ry} = 8\pi(\varepsilon_0 \gamma R^3)^{1/2}\,, \tag{1.8}$$

where q is the charge on the droplet, ε_0 is the permittivity of the vacuum, γ is the surface tension and R is the droplet radius.

When the repulsive electrostatic forces overcome the surface tension, Coulomb fission (or 'Coulomb explosion') occurs and the parent droplet breaks up into smaller daughter droplets which have approximately 2% of the mass and 15% of the charge of the parent droplet (Taflin, Ward and Davis 1989). The solvent evaporates from the charged daughter droplets, eventually producing charged ions which pass through a heated capillary, into the analyser of a MS, under high vacuum.

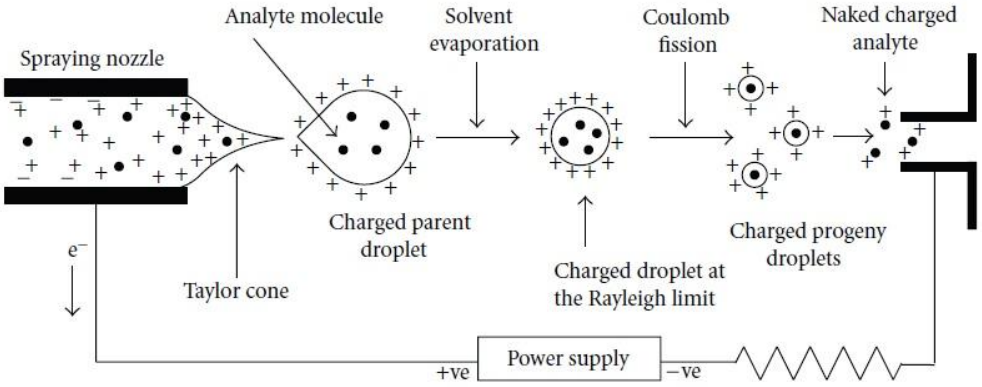

Figure 1.5. The production of charged analytes using ESI in positive ionisation mode. Anions and cations in a sample solution disperse in an electrospray needle after a high voltage is applied. Cations congregate at the liquid meniscus and repel each other to produce a Taylor Cone which releases a charged parent droplet. Solvent evaporation reduces the size of the droplet until the surface charge repulsion in the droplet equals the droplet surface tension (the 'Rayleigh Limit'). Coulomb fission occurs, producing smaller droplets which evaporate, leaving charged ions which enter the MS. Schematic from Banerjee and Mazumdar (2012).

Nanoelectrospray ionisation (Nano-ESI) (Wilm and Mann 1994) is a modified ESI technique which uses a much smaller orifice and lower flow rates than traditional ESI, and thus produces much smaller droplets of < 200 nm in diameter as opposed to 1–2 µm diameter droplets produced with traditional ESI. This means that in a given sample, a larger portion of the analyte molecules is made available for analysis. Nano-ESI also offers other advantages including higher sensitivity, low sample consumption, no cross contamination, higher tolerance towards salt contamination and virtually unlimited time for MS analysis (Schmidt, Karas and Dülcks 2003, Banerjee and Mazumdar 2012, Hop, Chen and Yu 2005).

The Advion NanoMate™ is a robotic system that uses chip-based nanoelectrospray where each chip contains 100 nozzles. This device has previously been used for UHRMS analysis to analyse forest aerosol (Kourtchev et al. 2013) and urban aerosol (Kourtchev et al. 2014b, Tong et al. 2016) and is used for part of the work described in this thesis in Chapters 1.1–8.

Other ESI techniques have been developed that allow organic aerosol samples to be extracted and analysed without the need for sample extraction. One of these is Desorption Electrospray Ionisation (DESI) which impacts charged micro-droplets onto

a fixed analyte. This process desorbs ions from the surface which are then carried into the MS (Takats et al. 2004). The lack of sample preparation allows high sample throughput analysis with a total analysis speed of < 5 seconds and DESI has been demonstrated to be less sensitive to salt effects than ESI (Ifa et al. 2010, Jackson et al. 2007).

Liquid Extraction Surface Analysis (LESA) (Eikel et al. 2011) combines micro-liquid extraction from a surface, with Nano-ESI-MS. Compared with DESI, LESA offers greater control over the extraction and improved extraction efficiency by allowing the user to optimise the contact time between the solvent droplet and sample surface. LESA has been used in conjunction with UHRMS, to analyse organic aerosol (Fuller et al. 2012).

1.4.2.4 Extractive Electrospray Ionisation (EESI).

EESI is a new soft ambient ionisation technique, first described in Chen et al., 2006. The technique uses two separate sprays; one to produce a plume of charged solvent droplets and the other to nebulise the sample solution. The solvent droplets then collide with the neutral sample and extract the compounds of interest via liquid-liquid extraction. The solvent then evaporates as with traditional ESI and the analyte ions pass through the heated capillary into the MS, as shown in Figure 1.6 (Law et al. 2010, Chen, Venter and Cooks 2006).

The mechanism of the liquid-liquid extraction from the sample analyte by the charged solvent is not completely understood. Several processes such as total coalescence, bounce, disruption and fragmentation may occur. If total coalescence is the dominant process, theoretically no extraction takes place since the two droplets just coalesce to form a larger droplet. Solvent miscibility between the two solvents and surface tension of the droplets may be an important factor for the resulting ion production if total coalescence occurs. A fluorescence study by Law et al., 2010 and a theoretical study by Wang et al., 2012 both observed a strong dependence of ion signals on the analyte solubility in both the ESI and sample spray solvents. This suggests that total coalescence is not the dominant droplet-droplet interaction and instead, a selective extraction occurs between the charged droplets and neutral analyte droplets.

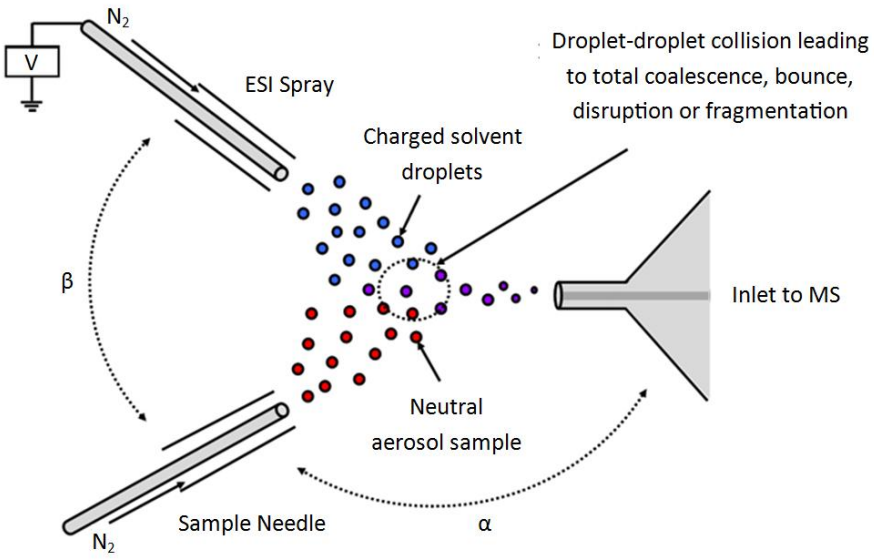

Figure 1.6. Extractive Electrospray Ionisation (EESI) mechanism. The sample solution is nebulised and collides with charged solvent droplets. The compounds of interests are extracted via liquid-liquid extraction occurs and the solvent evaporates, leaving charged ions which pass through the heated capillary into the MS. Schematic adapted from Law et al., 2010.

EESI has an advantage over traditional ESI in that the analytes are nebulised first in EESI before they are ionised and collide with the solvent droplets, meaning that they have a higher tolerance to sample matrix effects and ion suppression effects. Chen et al., 2006 also reported greater signal stability compared with ESI/APCI methods when analysing salt-rich biological samples. Additional advantages of EESI include no need for sample pre-treatment since the aerosol can be injected into the EESI source in real time, the solvents in the ESI spray can be user-specified to selectively extract analytes and EESI can tolerate high levels of moisture. These advantages make EESI, coupled with MS, an ideal method for analysing complex compound mixtures comprising volatile and non-volatile substances (Wang et al. 2012, Chen et al. 2007b).

To date, most previous studies using EESI have applied it to the analysis of biological compounds including urine, skin tissue and breath (Chen et al. 2007b, Chen et al. 2006, Chen et al. 2007c, Chen and Zenobi 2008); milk (Zhu et al. 2009); proteins (Chen et al. 2010) and also to monitor food quality (Chen et al. 2007c, Chen, Wortmann and Zenobi 2007a); and in the identification of counterfeit perfumes (Chingin et al. 2008). EESI has also been applied to the analysis of polluted water (Chen et al. 2006). These studies have demonstrated that EESI is capable of producing stable MS signals in real time, for

several hours. EESI-MS is one of the main focuses of Chapter 0 of this thesis. Further details of the technique and its application to organic aerosol analysis are described in section 3.1.

1.4.3 Mass Analysers

1.4.3.1 (Ultra-)High-Resolution MS (UHRMS)

Once ions have been generated from a sample, they must be separated according to their mass-to-charge ratio (*m*/*z*) which is determined using a mass analyser. The ability of an MS to analyse highly complex mixtures is characterised by three parameters; mass resolution, mass accuracy and dynamic range. The resolving power of an instrument is the ability to produce distinct signals for two ions with a small mass difference and is calculated using Equation 1.9:

$$\mathrm{R} = (m/z)/\text{peak width at half maximum}\,. \tag{1.9}$$

Two peaks are considered to be resolved if the valley between the peaks is 10–50% of the weaker peak intensity, depending on the type of mass analyser used. Conventional MS, such as time-of-flight (TOF) instruments have resolution powers of 10,000-20,000 which is insufficient to differentiate all of the compounds in complex organic aerosol mixtures. UHR mass analysers have resolution powers of several 100,000 which removes the need for chromatographic separation prior to MS analysis as it allows thousands of organic species to be characterised in a single mass spectrum. This makes them particularly suitable for analysing atmospheric organic aerosol which often has several thousand mass spectral peaks measured over a small mass range of a few 100 *m*/*z* (de Hoffmann and Stroobant 2002, Noziere et al. 2015, Kourtchev et al. 2013).

Mass accuracy is defined as the difference between the measured and theoretical *m*/*z* value for an ion, relative to the theoretical *m*/*z* value for that ion, and is expressed in parts per million (ppm) as shown in Equation 1.10:

$$\Delta\frac{m}{z} = \left(\frac{m/z_{\text{experimental}} - m/z_{\text{theoretical}}}{m/z_{\text{theoretical}}}\right) \times 10^6\,. \tag{1.10}$$

Using a MS capable of high resolution and high accuracy allows the complete characterisation of complex atmospheric samples and also the assignment of the elemental composition of all of the peaks observed in the mass spectrum.

The dynamic range of the MS is defined as the range of analyte concentration over which the signal from the detector is directly proportional to this concentration. This is important when trying to detect compounds of low concentrations in an aerosol mixture which also contains compounds with much higher concentrations.

UHRMS has both high mass resolving power and high mass accuracy. UHRMS analysers used in atmospheric chemistry include the Fourier Transform Ion Cyclotron (FTICR), the Orbitrap and the high-resolution Quadrupole Time-of-Flight (HR-Q-TOF) which have resolving powers of ≤ 40,000,000, > 1,000,000 and ≤ 40,000 respectively and mass accuracies of < 0.5 ppm, 1–5 ppm and 1–10 ppm respectively (Noziere et al. 2015, Denisov et al. 2012).

Tandem Mass Spectrometry (MS/MS or MS^n) can be applied on some MS instruments to yield additional structural information on molecular ions. When MS/MS is applied, the molecular ion produced from the first mass analyser is fragmented and the fragmentation pattern is used to provide structural information about the compound. Product ions and fragmentation patterns are often characteristic to specific compounds so MS/MS allows detection of specific compounds in complex mixtures which makes it widely applicable to SOA composition analysis. MS/MS techniques used with high resolution FTICR, Q-TOF and Orbitrap instruments and coupled with LC, are very advanced analytical techniques for achieving detailed molecular characterisation of organic aerosol (Noziere et al. 2015).

The Aerodyne Aerosol Mass Spectrometer (AMS), developed for the online measurement of organic and inorganic aerosol, uses thermal desorption followed by EI techniques, to produce bulk mass concentrations of non-refractory species such as suphate, nitrate, organics and ammonium on a timescale of a few seconds to minutes (Pratt and Prather 2012, Ulbrich et al. 2009). The system works by focussing the aerosol particles into a narrow beam that transports them into the MS detector where the particles are flash vapourised at 600°C under high vacuum (Jayne et al. 2000, Canagaratna et al. 2007, Pratt and Prather 2012).

AMS is highly sensitive and can acquire elemental ratios in real time. The extensive fragmentation produced from the EI technique can be used to identify different

functional groups and structures but it is difficult to identify individual compounds (Johnston and Kerecman 2019). AMS has successfully classified OA as hydrocarbon-like OA (HOA), biomass burning OA (BBOA) and oxygenated OA (OOA) which is further classified as low-volatility OOA (LV-OOA) and semi-volatile OOA (SV-OOA) (Ng et al. 2010). However, the complexity of the ion fragmentation in complex organic aerosol can result in biases occurring that must be corrected and accounted for. Potential interferences from other compounds when analysing complex organic aerosol can cause further problems and lead to inaccuracies (Kroll et al. 2011, Aiken et al. 2008, Glasius and Goldstein 2016). As a result, AMS is often not as accurate as soft ionisation techniques like ESI which do not produce extensive fragmentation (Aiken et al. 2008).

The Aerosol Time-of-Flight MS (ATOFMS) is a single particle MS technique that uses the time of flight of a particle between two lasers to determine the aerodynamic diameter of that particle to within 1% and LDI provides composition analysis (Gard et al. 1997). Unlike the AMS, ATOFMS measures the chemistry of individual particles and can provide the size-resolved number fractions or concentrations, the mixing state of individual particles and the distribution of secondary organics on primary particles, for both refractory and non-refractory species (Pratt and Prather 2012). However, AMS instruments complete with TOF MS (TOF-AMS) (Drewnick et al. 2005) and high resolution MS (HR-TOF-AMS) (DeCarlo et al. 2006) can successfully provide both quantitative single particle composition and information about internal and external mixtures of particle components, as well as average particle composition and chemically resolved size distribution measurements.

The coupling of UHRMS with separation techniques like GC and LC can greatly improve identification of compounds in complex organic aerosol because it can separate isomers, unlike direct infusion UHRMS. Gas Chromatography Mass Spectrometry (GC-MS) has high sensitivity, high separation efficiency and is relatively immune to ion signal-quenching effects, making it suitable for atmospheric aerosol. However, many polar, non-volatile compounds such as di- and tri-carboxylic acids and terpenoic acids, require Liquid Chromatography Mass Spectrometry (LC-MS) because LC separation uses the polarity strength of organic compounds so LC-ESI-MS is very useful for detecting polar compounds and organosulphates in aerosol (Johnston and Kerecman 2019). One of the challenges faced with using LC-ESI-MS is the lack of availability of authentic standards for certain organic compounds, including organosulphates (Noziere

et al. 2015). LC-ESI-MS is one of the analytical tools used in the study in Chapter 9 of this thesis and is described in more detail in section 9.1.

1.4.3.2 Ion Trap and Orbitrap

The UHRMS analysis of ambient aerosol and rainwater samples described in Chapters 1.1–9 in this thesis is performed on a Linear Trap Quadrupole (LTQ) Orbitrap Velos™ MS. An Orbitrap is a hybrid instrument comprising two mass analysers that can independently detect ions and record mass spectra; the linear ion trap and the Orbitrap. Ion traps are also now used as high performance mass spectrometers (ITMS) and can produce MS and MS/MS spectra with high sensitivity but relatively low resolution and mass accuracy (de Hoffmann and Stroobant 2002, Warscheid and Hoffmann 2002, Scigelova and Makarov 2006). An LTQ Ion Trap MS is used for the EESI source characterisation study in Chapter 0 of this thesis.

A schematic of the Orbitrap is provided in Figure 1.7. After ions are introduced into the MS via the ESI (or EESI) source, they enter the ion trap (green box in Figure 1.7) where a resonant frequency (RF) voltage is applied and the ions are expelled from the trap according to their mass (de Hoffmann and Stroobant 2002). The ions then pass into an RF-only quadrupole called a 'C-Trap' (yellow box in Figure 1.7) where they are accumulated, stored and have their energy dampened by residual N_2 gas. The C-trap also facilitates higher energy collision fragmentations. Finally, the ions enter the Orbitrap mass analyser (pink box in Figure 1.7) which is filled with a pulse of ions from the C-trap and the MS signals are detected for each ion.

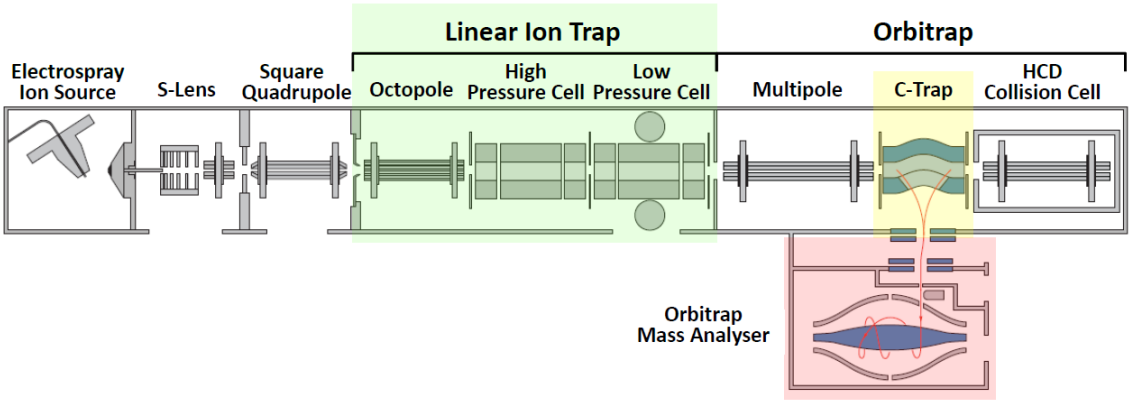

Figure 1.7. The LTQ Orbitrap hybrid instrument. Ions enter the LTQ linear ion trap via the ESI source and are expelled according to their mass. The ions then pass into the C-trap where they are stored and accumulated before being injected into the Orbitrap which produces their MS signals. Schematic adapted from Scigelova and Makarov, 2006 and the Thermo Fisher Scientific LTQ Orbitrap Velos™ Hardware Manual (Scientific 2009b).

2 AIMS AND STRUCTURE OF THIS THESIS

There are many soft ionisation techniques available for analysing the composition of organic compounds in atmospheric aerosol. However, many of these techniques do not allow online measurements of aerosol composition, they require time consuming sample preparation prior to analysis and they are susceptible to matrix effects when ionising complex samples. There is therefore, a need for robust soft ionisation techniques capable of providing real time measurements of organic aerosol oxidation and ageing within complex ambient samples.

Chapter 0 presents research findings from the characterisation of one of these newly developed online soft ionisation techniques; Extractive Electrospray Ionisation (EESI). The study assesses the efficiency of a newly developed EESI source at analysing complex aerosol of mixed organic and inorganic composition. It also includes the first study to date of the application of EESI-MS to analysing complex SOA generated by the oxidation of mixed biogenic and anthropogenic VOCs using the Cambridge Atmospheric Simulation Chamber (CASC). Specific objectives of the work are described in Chapter 0.

In addition to appropriate ionisation techniques, analysis of ambient aerosol using mass spectrometry requires efficient sample preparation to extract target compounds, remove impurities and concentrate samples. It is uncommon for published studies to include

optimisation experiments for sample preparation method development which means there are few protocols available for comparison when developing new methods. It is also rare for studies of aerosol composition to include details of data processing methods for mass spectra. Individual research groups and organisations often use their own "in house" methods for data processing and quality control so it can be difficult to compare new composition analysis with existing analysis for samples of a similar type and from similar environments.

Chapter 1.1 of this thesis serves to remedy these two issues by presenting a detailed Solid Phase Extraction (SPE) method development study suitable for preparing rainwater and aerosol samples collected during the same rain event. The chapter also includes details of the data processing method for the subsequent analysis of multiple rainwater and aerosol samples, including a comparison of three different blank subtraction methods for processing the sample mass spectra which is not readily available in the current literature.

To date, few studies have directly compared the composition of precipitation and ambient aerosol collected during the same rain event. Chapters 5–9 of this thesis present a detailed molecular characterisation of the composition of rainwater and aerosol samples collected during the recent AERORAIN campaign in León, Spain (June 2015–2017), using a combination of direct infusion Nano-ESI-MS and LC-ESI-MS. Chapter 5 provides an overview of the seasonal distribution of organic compounds during the campaign and Chapter 6 focuses on the aromaticity of compounds in the samples. The influence of air mass origin on the sample composition will be investigated in Chapter 7 and Chapter 8 presents a study on aerosol scavenging by the rainwater collected during the same rain event, which to our knowledge is the first study to do so. Chapter 9 uses Liquid Chromatography (LC) coupled to UHRMS to identify specific organic compounds in the rainwater and aerosol, including organosulphates and organonitrates.

Conclusions of the research findings from Chapters 0–9 in this thesis and future work are presented in Chapter 1.1 and supporting material is provided in Appendices A–N in Chapter 0.

3 CHEMICAL CHARACTERISATION OF EXTRACTIVE ELECTROSPRAY IONISATION MS (EESI-MS) USING ORGANIC AND INORGANIC AEROSOL

3.1 Introduction

ESI techniques have been used extensively to characterise aerosol composition (Kourtchev et al. 2014a, Claeys et al. 2009, Bateman et al. 2008, Claeys et al. 2012, Dzepina et al. 2015, Gómez-González et al. 2008, Kampf, Bonn and Hoffmann 2011, Mazzoleni et al. 2012a, Putman et al. 2012, Thorsten Reemtsma et al. 2006, Surratt et al. 2007, Tong et al. 2016, Wozniak et al. 2008, Yasmeen et al. 2011, Yassine et al. 2014). A study of α-pinene ozonolysis by Doezema et al., 2012, found that EESI-MS produced similar mass spectra of the SOA products to those produced by APCI-MS for the same reaction.

The mechanisms of ion production in ESI are not fully understood and are even less so in EESI. ESI signals can be affected by many factors including background noise, the presence of salts in complex samples, and flow instability (Mallet, Lu and Mazzeo 2004). Competing species in the sample matrix which co-elute can increase or

decrease the efficiency of charged droplet formation or droplet evaporation and can result in competitive ionisation whereby some less volatile organic species may not be ionised at all (Fu, Woolf and Matuszewski 1998).

Ion suppression is a major concern for ESI techniques since ESI has a low tolerance to matrix effects due to the dissolved analytes being infused directly to generate ions. This can sometimes lead to a reduction in solvent evaporation in the source due to high concentrations of matrix interferences (King et al. 2000). Ion suppression can affect MS analysis of compounds even when additional separation techniques like HPLC are used in conjunction (Matuszewski, Constanzer and Chavez-Eng 2003, Sangster et al. 2004).

It is expected that EESI spectra are susceptible to similar matrix effects as ESI techniques because the ionisation mechanisms are similar and examples of ion suppression when using EESI have been observed in previous studies (Jackson et al. 2008, Fu et al. 1998, Doezema et al. 2012). However, because the analytes are nebulised first and then ionised separately via collision with charged solvent droplets in EESI and the sample matrix is dispersed over a much larger volume than in ESI, ion suppression effects are expected to be reduced (Chen and Zenobi 2008, Law et al. 2010). The lack of studies on EESI-MS being applied to ambient aerosol analysis means that the full extent of potential ion suppression effects and the impacts of these on the characterisation of complex aerosol composition are unknown, and further investigation is required.

An Extractive Electrospray Ionisation (EESI) source has been developed in the Kalberer research group, by Dr Peter Gallimore, using a commercially available Thermo Scientific Ion Max S Atmospheric Pressure Ionisation Source from an Ion Trap MS. Figure 3.1 shows a schematic of the EESI source. A custom-built aerosol injector was fitted to the commercial source (indicated by the dashed line in Figure 3.1) to allow real-time measurements of aerosol composition. A user-defined solvent is introduced into a heated electrospray probe (Thermo Scientific HESI-II), using a syringe, to provide the charged solvent droplets required to extract the target analytes from the aerosol. A full description of the operational parameters of the source is provided in Gallimore and Kalberer, 2013.

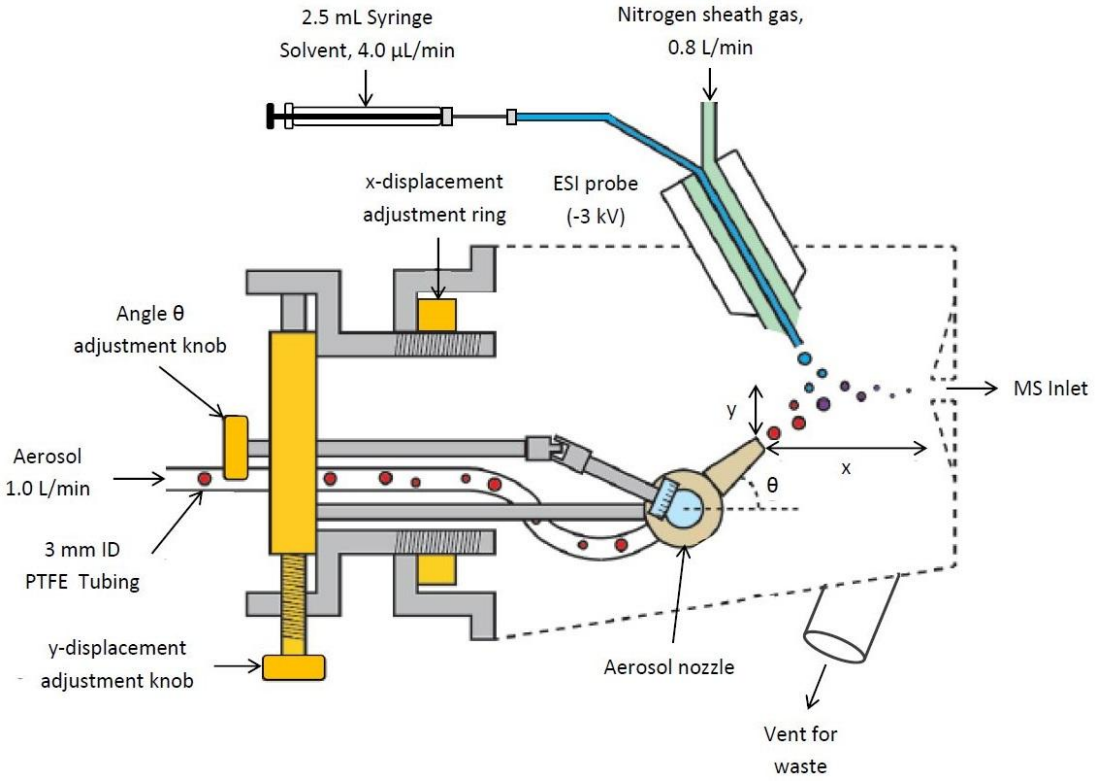

Figure 3.1. The EESI source for use with MS. The source was adapted from a commercially available ESI source (dashed line) with a custom-built aerosol injector and housing. Charged solvent droplets (blue) introduced via a heated electrospray probe, collide with aerosol (red) introduced using an adjustable aerosol nozzle. The analytes (purple) are extracted and pass into the Mass Spectrometer (MS) inlet where they are detected by the Thermo Scientific LTQ Velos Ion Trap Mass Spectrometer. Schematic adapted from Gallimore and Kalberer (2013). (*ID* = Inner Diameter).

Initial experiments performed by Dr Gallimore, showed that the EESI source, when coupled with MS, can produce stable, reproducible signal intensities for dry, solid and aqueous organic particles, and for oxidation products of oleic acid ozonolysis. The technique can also quantify particle composition in the mass concentration range of 0.2–600 µg/m^3 (Gallimore and Kalberer 2013). The EESI source has also been used to characterise chamber-generated SOA formed from the ozonolysis of α-pinene, and laboratory-generated aerosol with a simple mixed tartaric acid and ammonium sulphate (AS) composition, up to 50% AS (Gallimore et al. 2017a) and also SOA produced from the oxidation of limonene (Gallimore et al. 2017b).

The characterisation experiments described in this chapter, build on the previous experiments by using more complex mixtures of organic and inorganic aerosol which are much more representative of ambient aerosol. Urban aerosol in the Northern

Hemisphere, particularly in the USA and China, has been shown to contain mixed aerosol with complex OA and high inorganic fractions and has been successfully quantified using other MS techniques (Jimenez et al. 2009). Using laboratory-generated complex organic aerosol with higher inorganic content than previously tested, these characterisation experiments allow the EESI source to be tested for suppression of organic MS signals caused by inorganic salts and susceptibilities to competitive ionisation which could result in some compounds failing to ionise in the EESI source, which are often a problem for MS soft ionisation techniques (Noziere et al. 2015).

For the simple mixed organic and inorganic aerosol characterisation experiments, c*is*-pinonic acid was chosen as a representative organic compound because it is an atmospherically-relevant carboxylic acid SOA product from the oxidation of biogenic monoterpenes such as *α*-pinene, and ammonium sulphate was used as the representative inorganic compound to create the mixed aerosol. A selection of Water Soluble Organic Carbon (WSOC) compounds were also used to generate complex organic aerosol mixtures. WSOCs were chosen because the WSOC fraction contributes up to 60% of organic carbon in tropospheric aerosol and are often formed through SOA formation pathways (Brooks et al. 2003).

This chapter also includes characterisation experiments using aerosol generated in the new Cambridge Atmospheric Simulation chamber (CASC). Prior to these experiments, the chamber had been used for ozonolysis and oxidation of common atmospheric monoterpenes and analysis of the SOA products using Proton Transfer Reaction Mass Spectrometry (PTR-MS) and ultra-high resolution ESI-MS (Kourtchev et al. 2016a). The EESI source, as previously mentioned, has been used to detect SOA formation from single biogenic VOC experiments (α-pinene ozonolysis and limonene oxidation) but has not been tested with complex organic aerosol or anthropogenic compounds which readily oxidise in the atmosphere to produce SOA. The chamber experiments described in this study will use mixtures of anthropogenic and biogenic VOCs to provide more atmospherically-relevant complex SOA to test the EESI source.

3.2 Aims

The overall aim of this characterisation study was to assess the efficiency of the newly developed EESI source in ionising and detecting organic compounds within complex mixed organic and inorganic aerosol.

There were three different areas of experimental focus:

- To investigate the susceptibility of the EESI source to suppression of organic MS signal from the presence of inorganic salts.
- To assess EESI-MS organic signal detection within complex mixtures of organic and inorganic aerosol and determine the extent of competitive ionisation.
- To test the ability of the EESI source to detect SOA products produced via ozonolysis and OH radical-initiated oxidation of mixed BVOCs and AVOCs in the Cambridge Atmospheric Simulation Chamber (CASC).

3.3 Methodology

3.3.1 Mixed organic and inorganic aerosol characterisation experiments

A stock solution of 1 mM *cis*-pinonic acid (CPA) in ethanol (99.8% (GLC) absolute, Fisher Scientific UK Ltd) was prepared. Stock solutions of ammonium sulphate (AS) (≥ 99.5% BioUltra, Sigma Aldrich) in deionised water (HPLC, Rathburn Chemicals Ltd.) of the following concentrations were also prepared; 0 mM (deionised water), 0.3 mM, 0.5 mM, 1 mM, 2 mM, 5 mM, 8 mM and 10 mM. Eight different mixed organic and inorganic solutions were then prepared in 100 ml volumetric flasks using 50 ml of each of the AS solutions, added to 50 ml of the CPA solution. The resulting mixed solutions comprised the following percentages of ammonium sulphate; 0%, 23%, 33%, 50%, 67%, 83%, 89% and 91%, and equal 0.5 mM concentrations of *cis*-pinonic acid. The concentrations of *cis*-pinonic acid and ammonium sulphate and the molar percentage of AS in each solution are summarised in Table 3.1.

To create the complex organic aerosol mixtures, the four water-soluble carboxylic acids and two alcohols shown in Table 3.2 were mixed together with the same AS solutions

used for the simple organic aerosol mixtures. 1 mM solutions of each of the four carboxylic acids; oxalic acid (99.0%, Sigma Aldrich), salicyclic acid, maleic acid (Analytical Reagent Grade, Fisher Scientific Ltd.) and glutaric acid (99.0%, Sigma Aldrich); and the two alcohols; arabitol (99.0%, Alfar Aesar) and erythritol (≥ 99.0%, Sigma Aldrich), were prepared in deionised water (HPLC, Rathburn Chemicals Ltd.). 10 ml aliquots of each these WSOC solutions were then mixed together in eight separate volumetric flasks. 60 ml of the same eight AS solutions described above were then added to the mixed WSOCs so that the final volume for each mixed WSOC and AS solutions in each flask was 120 ml and the total concentration of WSOCs in each mixed solution was 0.5 mM. Table 3.1 summarises the concentrations of ammonium sulphate and each WSOC and the molar percentage of AS in each mixed solution.

Table 3.1. Concentrations of *cis*-pinonic acid (CPA), water-soluble organic compounds (WSOCs) and ammonium sulphate (AS) used to generate the simple and complex mixed aerosol.

Simple mixed organic and inorganic solution			**Complex mixed organic and inorganic solution**		
AS concentration (mM)	**CPA concentration (mM)**	**AS molar percentage (%)**	**AS concentration (mM)**	**Individual WSOC concentration (mM)***	**AS molar percentage (%)**
0.00	0.50	0	0.00	0.08	0
0.15	0.50	23	0.15	0.08	23
0.25	0.50	33	0.25	0.08	33
0.50	0.50	50	0.50	0.08	50
1.00	0.50	67	1.00	0.08	67
2.50	0.50	83	2.50	0.08	83
4.00	0.50	89	4.00	0.08	89
5.00	0.50	91	5.00	0.08	91

*Total WSOC concentration = 0.5 mM

Table 3.2. Water soluble organic compounds (WSOCs) used for the simple and complex mixed organic and inorganic aerosol. The organic concentration remained constant while the ammonium sulphate (AS) concentration was varied.

WSOC	Structure	$[M-H]^-$ *m/z*	Precursors
Oxalic acid ($C_2H_2O_4$)	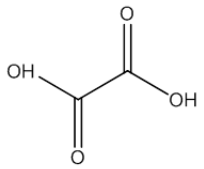	88.9880	Toluene, *p*-xylene, 1,3,5-trimethylbenzene (Kleindienst et al. 1999), ethene, isoprene (Sorooshian et al. 2006), cyclohexene (Kalberer et al. 2000)
Maleic acid ($C_4H_4O_4$)	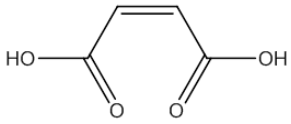	115.0037	Toluene (Kleindienst et al. 1999, Röhrl and Lammel 2002), benzene (Sorooshian et al. 2007)
Erythritol ($C_4H_{10}O_4$)	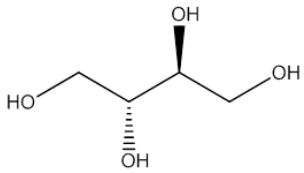	121.0506	Lichens, soil biota (Caseiro et al. 2007). (Analog of 2-methylerythritol; formed via isoprene oxidation and tracer for isoprene SOA (Claeys et al. 2004, Kessler et al. 2010))
Glutaric acid ($C_5H_8O_4$)	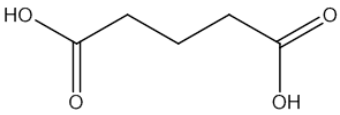	131.0350	Cyclohexene (Kalberer et al. 2000), cyclopentane and glutardialdehyde (Winterhalter et al. 2009)
Salicylic acid ($C_7H_6O_3$)	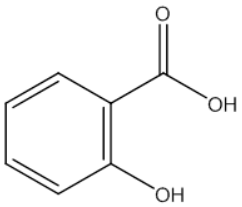	137.0244	Lignin pyrolysis, tracer for smoke from gramineae combustion (Wang et al. 2011, Hyder and Jönsson 2012)
Arabitol ($C_5H_{12}O_5$)	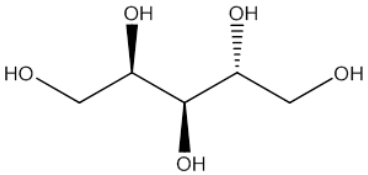	151.0612	Fungal spores and lichens (Bauer et al. 2008, Caseiro et al. 2007)
cis-pinonic acid ($C_{10}H_{16}O_3$)	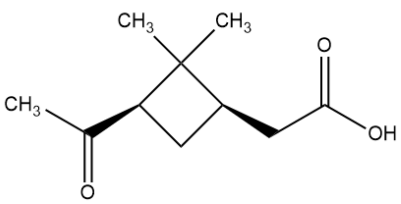	183.1016	α-pinene and β-pinene (Yasmeen et al. 2011)

The experimental set up shown in Figure 3.2 was used for all of the characterisation experiments using aerosol with mixed organic and inorganic composition. 80 ml of each of the mixed CPA/AS and WSOC/AS solutions were transferred to the constant output nebuliser (or atomiser) shown in box A in Figure 3.2. A magnetic stirrer was used in the nebuliser flask throughout the experiments to ensure the organic and inorganic solutes remained suspended and well-mixed. The custom built nebuliser design is shown in Figure 3.3. The nebuliser produced a fine spray of aerosol under 5 bar of nitrogen. Two dreschel bottles were used immediately downstream of the nebuliser to remove any excess water droplets exiting the nebuliser which could have disrupted the aerosol flow through the tubing. Vents were connected downstream of the dreschel bottles to direct excess flow away to provide the required flow rate through the set-up. The aerosol then passed through a charcoal denuder to remove the organic vapours (from the ethanol in the CPA/AS experiments) and through a silica diffusion dryer which removed any water vapour, to produce a dry aerosol. A relative humidity (RH) sensor was used to monitor the RH throughout the experiments. The aerosol flow then split between a Scanning Mobility Particle Sizer (SMPS) spectrometer (box B in Figure 3.2); used with *Aerosol Instrument Manager*® software to measure the particle size distribution; and the EESI-MS to measure the organic signal intensity. More detailed descriptions of the nebuliser, SMPS and EESI source are provided in 3.3.1.1, 3.3.1.2, and 3.3.1.3 respectively.

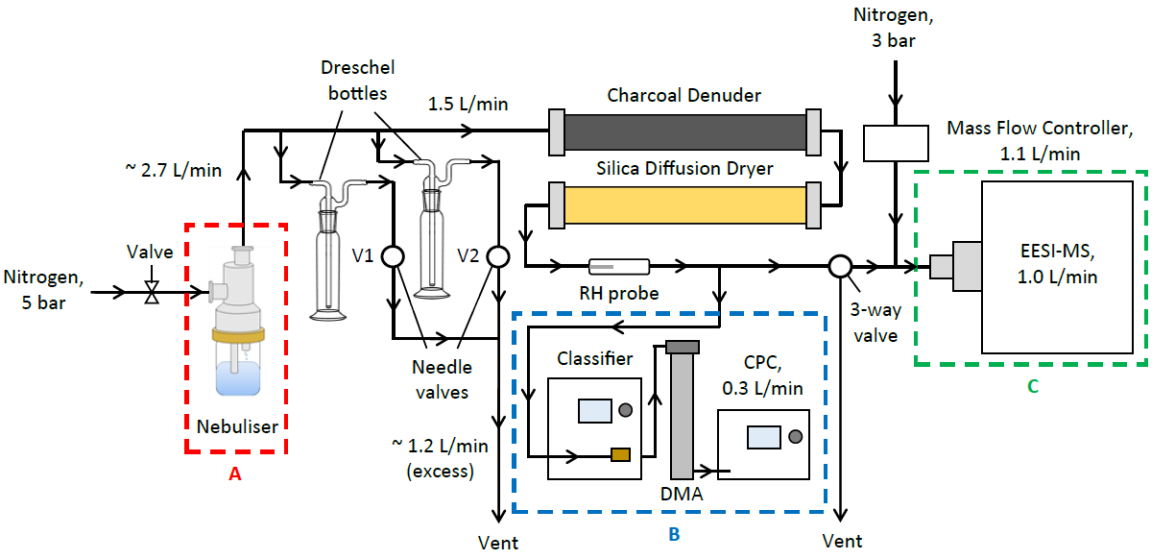

Figure 3.2. Experimental set-up used for chemical characterisation of mixed organic (*cis*-pinonic acid and WSOCs) and ammonium sulphate aerosol. A custom built constant output atomiser (A) was used to produce the aerosol. The Scanning Mobility Particle Sizer (SMPS) (B) measured the aerosol mass concentration and size distribution and the Extractive Electrospray Ionisation (EESI) MS source measured the organic signal intensity (C).

The following experimental procedure was carried out for each CPA/AS and WSOC/AS solution. Signal intensity and aerosol size distribution measurements were made in parallel for 45 minutes. For the first 15 minutes of the experiment, nitrogen from a separate source (see Figure 3.2), set at 3 bar, was injected into the EESI-MS for 15 minutes, at a flow rate of 1.1 L/min, using a mass flow controller. This provided a 'clean air' source to allow stabilisation of the EESI source and equilibration of the MS background ion intensities and to provide a background comparison for the subsequent organic ion intensities. During this period, the aerosol flow was 'off' i.e. was not injected into the EESI-MS and instead, was directed away from the EESI-MS, to a vent, using a three way valve. After the 15 minute equilibrium period and background measurement, the clean air was switched off and the nitrogen source to the nebuliser was switched on. The aerosol was directed towards the SMPS and EESI-MS at a flow rate of 1.5 L/min for five minutes. A second five minute 'aerosol off' (clean air 'on') period occurred, followed by another 'aerosol on' period. A final 'aerosol off' and 'aerosol on' cycle occurred so that in total, there were three five minute periods of aerosol injection, separated by periods of clean air injection.

A compressed nitrogen cylinder, set at 5 bar, was used to supply the 1.5 L/min flow rate during the 'aerosol on' periods as shown in Figure 3.2. The EESI-MS and SMPS required 1.0 L/min and 0.3 L/min respectively and the extra 0.2 L/min ensured there was sufficient flow rate throughout the set-up. Excess flow was directed to the vent, controlled by needle valves *V1* and *V2*. Tests on the nebuliser also showed that a critical threshold of $\geq$ 2 bar of nitrogen was required in order to produce a constant aerosol spray and any pressures lower than this became a limiting factor for the resulting aerosol flow. The combination of 5 bar of nitrogen and a flow rate of 1.5 L/min through the set up was found to produce the largest EESI-MS signal intensities and the smoothest aerosol size distribution measurements compared with other flow rates and nitrogen pressures tested.

3.3.1.1 Constant output nebuliser used for aerosol generation

The custom built constant output nebuliser (or atomiser) used to produce the fine aerosol for the mixed organic and inorganic aerosol experiments is shown in Figure 3.3. Compressed nitrogen set at 5 bar entered the nebuliser inlet and passed through a critical orifice of 0.4 mm diameter which caused it to expand and produce a high velocity jet.

This caused the solution in the nebuliser reservoir to be drawn up into the nebuliser through the vertical inlet. The solution was then atomised by the jet, producing a fine aerosol spray. Any large droplets produced were removed via impaction on the opposite wall of the nebuliser and the finer aerosol spray droplets left the nebuliser via an outlet at the top (TSI 2005). Different diameters of critical orifice were made and tested but 0.4 mm was found to produce the most stable spray.

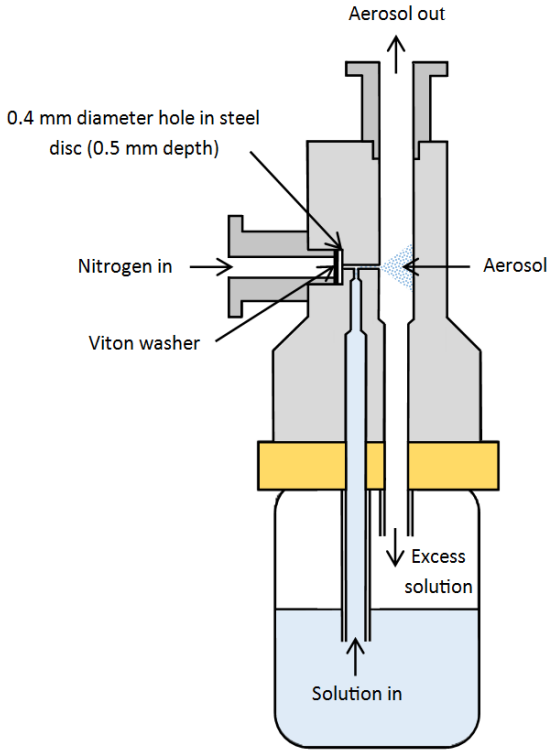

Figure 3.3. Constant output nebuliser used to generate the mixed organic and inorganic aerosol. The solution is drawn up from the flask through a vertical inlet. Compressed nitrogen at 5 bar passes through a critical orifice of 0.4 mm and atomises the solution, producing an aerosol spray which leaves the nebuliser via an outlet at the top. Any excess droplets fall back into the flask.

3.3.1.2 Scanning Mobility Particle Sizer (SMPS) Spectrometer

The aerosol size distribution and concentration measurements for the mixed organic and inorganic aerosol were obtained using a TSI® Scanning Mobility Particle Sizer (SMPS™) Spectrometer. This instrument accurately measures the distribution and concentration of particles in the size range of 10 nm to 1µm, in real time, using the principle of Differential Mobility Analysis (DMA) which separates particles according

to their ability to traverse an electric field. The aerosol measurement process is illustrated in Figure 3.4 and is described as follows.

The dry aerosol produced by the nebuliser set up in Figure 3.3 enters an Electrostatic Classifier (TSI Model 3080) where it first passes through a single stage inertial impactor to remove any large particles outside the measurement range which could cause multiple charging and data inversion errors. This polydisperse aerosol then passes through a bipolar ion neutraliser which uses a Kr-85 source to produce positive and negative ions and creates a steady state charge distribution across the aerosol.

The aerosol then leaves the Classifier and enters the Differential Mobility Analyser (DMA) (TSI model 3081). The charged particles enter the sheath gas stream as shown in Figure 3.4 and flow through a region with an applied electric field, following specific trajectories according to their electrical mobility. Samples are extracted from the aerosol stream via the DMA outlet and the particles are separated according to their mobility (de la Mora et al. 1998).

Monodisperse aerosol particles exit the DMA and enter the Condensation Particle Counter (CPC) (TSI Model 3775) which can detect particles as small as 4 nm over a concentration range of 0 to 10^7 particles/cm^3. The aerosol is drawn continuously at 0.3 L/min through a heated saturator which vapourises butanol. The butanol vapour diffuses into the aerosol sample stream and the mixture passes into a condenser where the vapour condenses onto the aerosol particles which serve as condensation nuclei, producing larger droplets. These droplets then pass through a laser-diode light source and their scattered light is detected using a diode photodetector and this is used to determine the concentration of particles. The data is logged using *Aerosol Instrument Manager*® software which uses TSI's data inversion to transform electrical mobility measurements into particle diameter. The mass concentration is then calculated and exported, along with the aerosol diameter, into Microsoft® Office Excel for data analysis (TSI 2012, Incorporated 2011, TSI 2011).

The size distribution measurements were made starting at time, t = 0 and then every three minutes throughout the experiments. The sampling period used was 135 seconds and 15 samples were acquired for each simple and complex aerosol mixture.

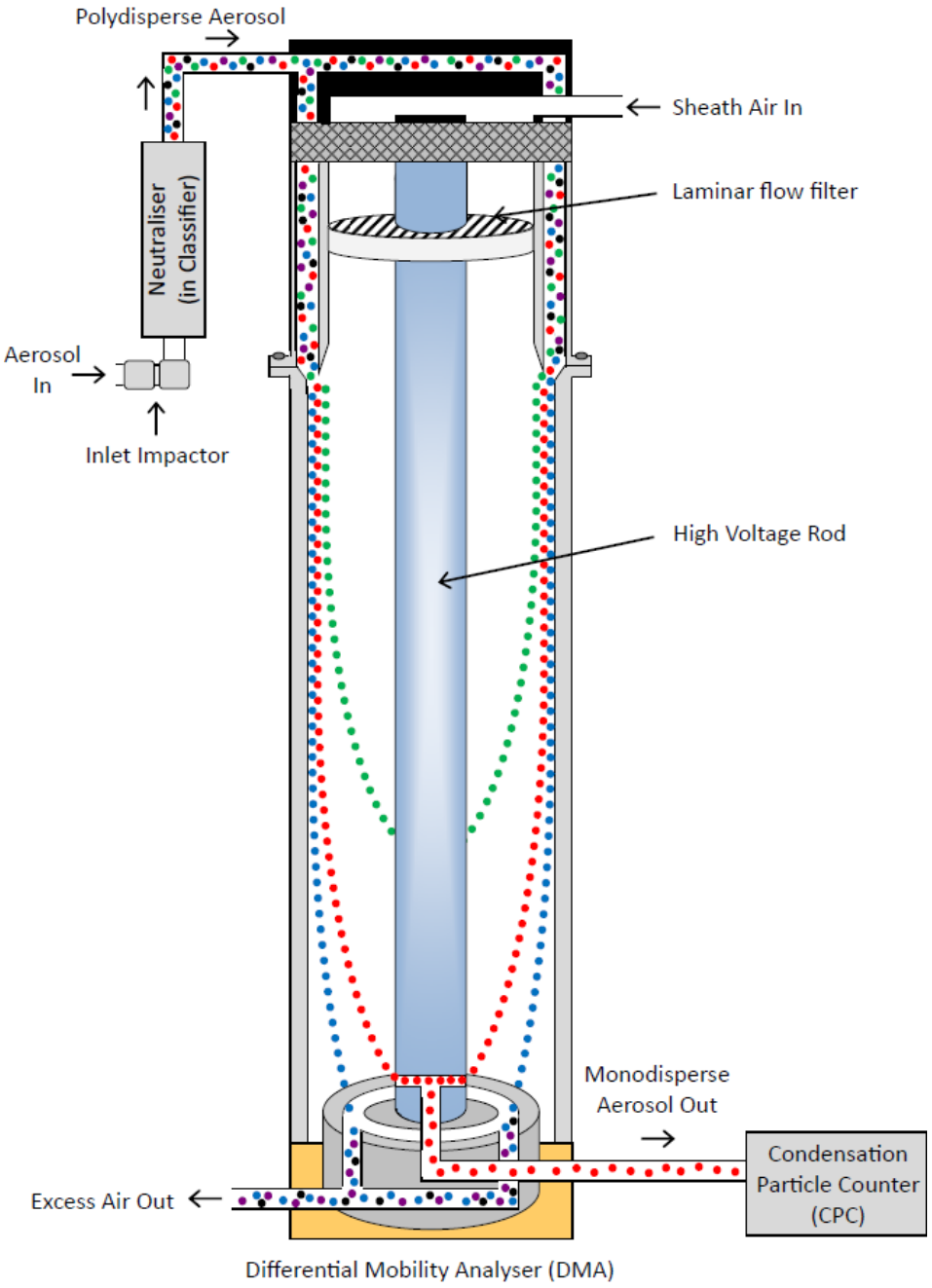

Figure 3.4. Aerosol mass concentration and size distribution determination using a Scanning Mobility Particle Sizer (SMPS) Spectrometer consisting of an Aerosol Neutraliser, Differential Mobility Analyser (DMA) and Condensation Particle Counter (CPC). Schematic adapted from TSI SMPS Model 3936 Manual (TSI 2011).

3.3.1.3 Extractive Electrospray Ionisation (EESI)

The electrospray was created using a 1:1 solvent mixture of ethanol (99.8% (GLC) absolute) and water (HPLC grade, Rathburn Chemicals Ltd.) with 0.1% formic acid (90%, Breckland Scientific) which was infused into the HESI-II probe (Thermo Scientific) using a 2.5 ml syringe (Hamilton, USA) in a syringe pump with a flow rate

of 4.0 µl/min. (Note for the smog chamber experiments described later in this chapter, the solvent used was water containing 0.1% formic acid and methanol (LC-MS grade, Fisher Scientific), in a 1:1 ratio). A spray voltage of −3.0 kV and a N_2 sheath gas flow rate of 0.8 L/min was used to produce the charged solvent droplets.

The aerosol from the experimental set up in Figure 3.2 entered the EESI source via the aerosol inlet using 3 mm inner diameter PTFE tubing, under 1.0 L/min. The aerosol flow then passed through a custom made, adjustable, aerosol nozzle where it intercepted the charged solvent droplets.

A Thermo Scientific LTQ Velos Ion trap Mass Spectrometer was used, in negative ionisation mode, to detect the peak intensities for the organic and inorganic aerosol mixtures. For the CPA/AS aerosol experiments, *cis*-pinonic acid, the main peak of interest, has a *m*/*z* $[M-H]^-$ value of 183.08. The mass spectra were acquired over a scan range of *m*/*z* 150–300. For the mixed WSOC and AS aerosol experiments, a scan range of *m*/*z* 80–200 was used to ensure that all of the WSOC *m*/*z* $[M-H]^-$ values (Table 3.2) were detected.

3.3.2 Cambridge Atmospheric Simulation Chamber (CASC) study using biogenic and anthropogenic Volatile Organic Compounds (VOCs).

Another set of experiments was conducted to test the ability of the EESI-MS source to detect SOA oxidation products formed through gas phase oxidation and ozonolysis of BVOCs and AVOCs. Chamber-generated organic aerosol is more complex and allows for oxidative ageing so is more representative of ambient aerosol. The newly developed Cambridge Atmospheric Simulation Chamber (CASC) was used to produce SOA from the ozonolysis and oxidation, via OH radical, of a mixture of BVOCs and AVOCs. The chamber is a 5.4 m^3 in volume (1.5 m × 1.8 m × 2.0 m) collapsible bag made from Teflon fluorocarbon film and is suspended in an aluminium frame which allows inflation and deflation of the chamber at ambient pressure. Twenty 160 W ultraviolet (UV) tanning lamps (Philips Body Tone, > 300 nm) are situated under the bag for use in photochemical ageing experiments, along with four 75 W “hard” UV lamps (Philips TUV75, 242 nm) used for cleaning the chamber. Two stainless steel bulkhead ports at either end of the chamber, allow introduction of reagents and sampling of air from the

chamber. The chamber is otherwise isolated from the surrounding atmosphere, allowing accurate simulation of different atmospheric conditions to investigate aerosol oxidation and ageing. A full description of the chamber operation is available in (Gallimore et al. 2017b).

3.3.2.1 Generation of SOA in the Cambridge Atmospheric Simulation Chamber (CASC)

Four VOC oxidation experiments were conducted in the CASC to investigate the OH radical-initiated oxidation of mixed BVOCs and AVOCs and the ozonolysis of BVOCs, and the subsequent ageing of the SOA oxidation products. The method of SOA generation in these four experiments was designed and conducted by Brendan Mahon in the Kalberer research group as part of a larger study aimed at investigating the oxidation of simulated urban aerosol. It is noted therefore that the experimental method for the SOA production in the CASC was not designed primarily for characterising the EESI source. However, these chamber experiments provided sufficient SOA for the purpose of testing the ability of the EESI source to detect SOA oxidation products. Aspects of the chamber operation and SOA generation which are relevant to the results of the EESI characterisation covered in this work are described as follows.

Two of the experiments were designed to simulate oxidation of compounds in urban atmospheres using OH• as the oxidant. A mixture of BVOCs and AVOCs was used and the OH• was produced via the photolysis of hydrogen peroxide (H_2O_2). The BVOCs used were α-pinene, β-pinene, Δ_3-carene and isoprene and the AVOCs were octane, toluene, *m*-xylene, 2,3-dimethyl pentane and naphthalene. The structures of these compounds and initial concentrations used are provided in Table 3.3. The other experiments focussed on the ozonolysis of BVOCs only. The BVOCs used were α-pinene, β-pinene, Δ_3-carene and isoprene and the concentrations are shown in Table 3.3.

The method used to produce the SOA in the CASC was as follows. The CASC was filled with dry air using a zero air generator (Parker Hannifin KA-MT2) supplied with air from the Chemistry Department's central supply. Water vapour was introduced into the chamber to achieve approximately 60% RH by bubbling the air at 8 L/min through a heated round-bottomed flask containing water (HPLC grade, Rathbone Chemicals Ltd.). For each experiment, the VOCs were injected into a glass impinger as a mixture and evaporated using air flow from the zero air generator, controlled by a Mass Flow

Controller (247D, MKS Instruments Inc.), and gently heated using a heat gun (PHG 2, Bosch, Germany) to introduce the vapours into the chamber.

For the OH• oxidation experiments, aqueous H_2O_2 was introduced into the chamber via evaporation from a glass impinger and was photolysed by the UV lamps to produce OH•. For the ozonolysis experiments, ozone was introduced using a commercial ozone generator (LABOZONE09, ESCO International Ltd, UK).

Once the VOCs and ozone or H_2O_2 had been introduced into the chamber, the chamber contents were mixed using an 'air sprinkler' system, consisting of two Teflon tubes with perforated holes, in the bottom of the chamber. The experiments were operated in batch mode whereby reactants were introduced into the chamber at the start of the experiment and were allowed to evolve over 6-8 hours. The CASC was cleaned between each experiment by flushing 200 L/min of air, using the clean air generator and mass flow controller, into one end of the chamber, and simultaneously pumping 200 L/min of air out from the opposite end of the chamber. It should be noted that no NO_x was added into the chamber for any of these experiments.

Table 3.3. Initial concentrations of the biogenic and anthropogenic VOCs used in the OH radical-initiated oxidation and ozonolysis experiments in the Cambridge Atmospheric Simulation Chamber (CASC) to generate SOA for detection by EESI-MS.

VOC	Structure	Initial concentration (ppb)	
		OH• oxidation of mixed BVOCs and AVOCs	Ozonolysis of BVOCs
α-pinene	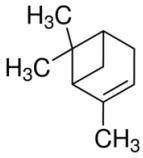	4.63	4.63
β-pinene	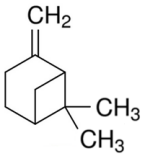	1.39	1.39
Δ_3-carene	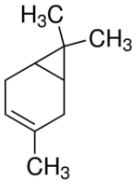	4.63	4.63
isoprene	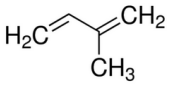	0.93	0.93
octane	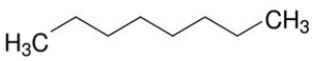	0.07	-
toluene	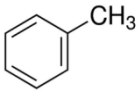	5.93	-
napthalene	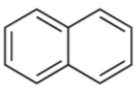	3.33	-
m-xylene	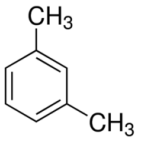	0.09	-
2,3-dimethyl pentane	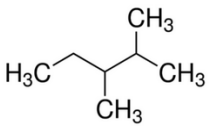	0.07	-

3.3.2.2 Detection of SOA composition from the CASC using EESI-MS

The EESI-MS requires the air from the chamber to enter the EESI source under a flow rate of 1.0 L/min. The EESI-MS source was not leak tight meaning that the aerosol had to be injected into the source and could not enter the source under atmospheric pressure. The design of the CASC allowed extraction of the chamber air under a flow rate of approximately 14.5 L/min, using a pump. In order to pump the aerosol into the EESI source at the required flow rate, reservoir vessels temporarily stored the SOA from the chamber and then pumped it into the EESI at 1.0 L/min. The method used to extract the chamber contents and direct them into the EESI-MS is described as follows and depicted in Figure 3.5.

A similar alternating 'aerosol on' and 'aerosol off' sampling system used for the mixed organic and inorganic and WSOC solutions described in 3.3.1 was used for analysing the SOA from the chamber. To begin with, a vacuum pump was used to draw the air from the chamber at a flow rate of ~14.5 L/min, into a ~10 L reservoir as indicated by the red line in Figure 3.5. This 'aerosol off' period lasted for five minutes and during this period, 1 bar of nitrogen was directed into the EESI-MS as a clean air source, using valve *A* in Figure 3.5, to provide a measurement of background ion intensities. Aerosol size distribution measurements were also made during this period and throughout the experiment. After the five minute period, the pump and nitrogen were switched off at valve *A* and the mass flow controller (MFC) was switched on, pushing the aerosol from the reservoir, into the EESI source and the SMPS, at a flow rate of 1.3 L/min (blue line in Figure 3.5) for five minutes, providing an 'aerosol on' period. This process was repeated twice to produce three cycles of five minute clean air injection ('aerosol off') periods and five minute aerosol injection ('aerosol on') periods to highlight the change in the intensity of the SOA compounds.

EESI-MS measurements were made continuously throughout the 30 minute experiment, during both the 'aerosol on' and 'aerosol off' periods. SOA peak intensities were acquired using the EESI-MS in negative ionisation mode using the same LTQ Velos MS and MS parameters described in 3.3.1.3, except a different solvent was used for the electrospray; water containing 0.1% formic acid, and methanol in a 1:1 ratio. Based on the reagents in the CASC, some of the SOA products could be predicted. However, the exact range of compounds was not known. Therefore, a large scan range of *m*/*z* 150–650 was used to allow for the detection of monomer, dimer and trimer SOA products. The

batch sampling method used allowed the EESI-MS to sample the chamber SOA with a time resolution of approximately 5 minutes. Aerosol size distribution measurements were also made continuously from the first clean air injection period to the last aerosol injection period, using the SMPS. Measurements were taken every three minutes, with a sampling period of 135 seconds.

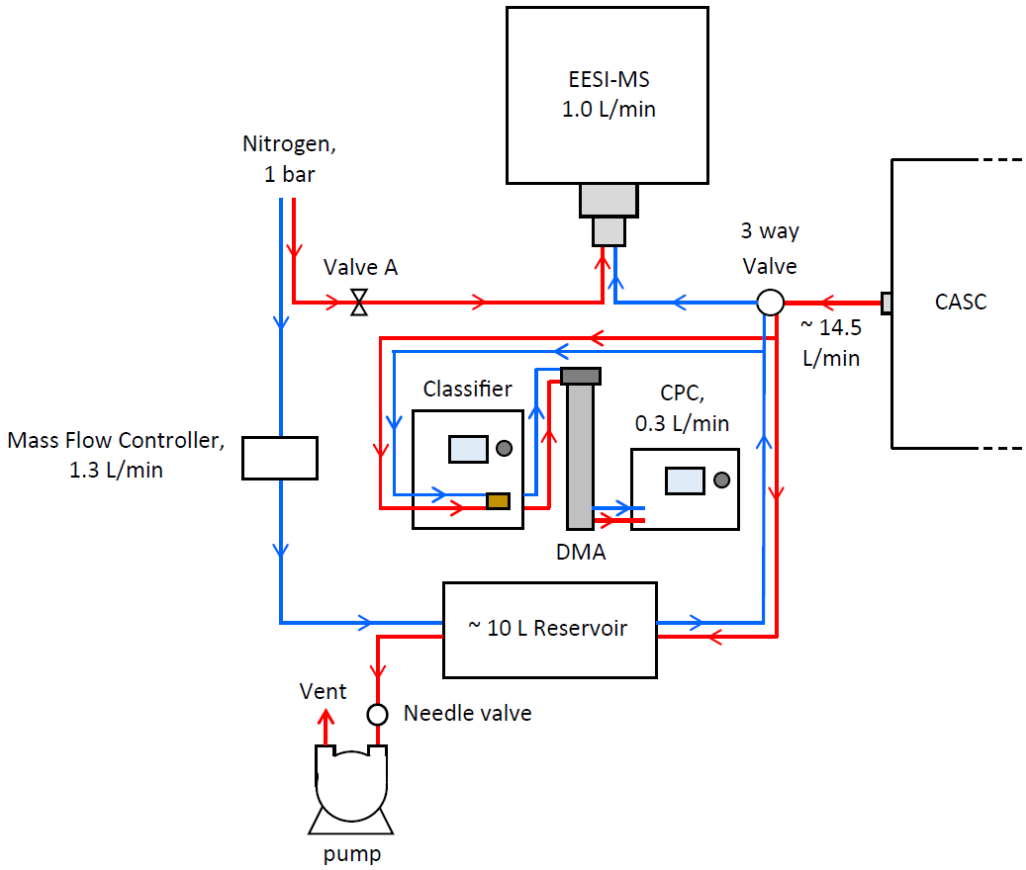

Figure 3.5. Experimental set-up used for EESI-MS measurements of the organic signal intensities of the SOA oxidation products from the ozonolysis and OH radical-initiated oxidation of mixed AVOCs and BVOCs in the CASC. Red line = 'aerosol off' period where air from the chamber was extracted under ~14.5 L/min and held in a 10 L reservoir and nitrogen was pumped into the EESI-MS to acquire a blank mass spectra. Blue line = 'aerosol on' period where air from reservoir was pumped into EESI-MS using Mass Flow Controller (MFC) at 1.3 L/min. Simultaneous aerosol concentration and particle diameter measurements were made using an SMPS. (*DMA* = Differential Mass Analyser, *CPC* = Condensation Particle Counter).

3.4 Results and Discussion

3.4.1 Simple organic and inorganic aerosol mixture

In order to determine if suppression of the organic MS signal occurs in aerosol with mixed organic and inorganic composition when using the EESI source, simple mixed aerosol comprising *cis*-pinonic acid with increasing concentrations of ammonium sulphate were tested.

Figure 3.6 shows the aerosol mass concentration for each particle diameter, determined for the different *cis*-pinonic acid (CPA) and ammonium sulphate (AS) solutions, using the SMPS. There is a clear increase in the modal diameter from ~40 nm to ~140 nm between the 0% AS solution and the 91% AS solution. Since the total AS solute concentration in the nebuliser is increasing from 0 mM AS to 5 mM AS, it is reasonable to expect an increase in particle diameter through the initial generation of more concentrated droplets from the nebuliser.

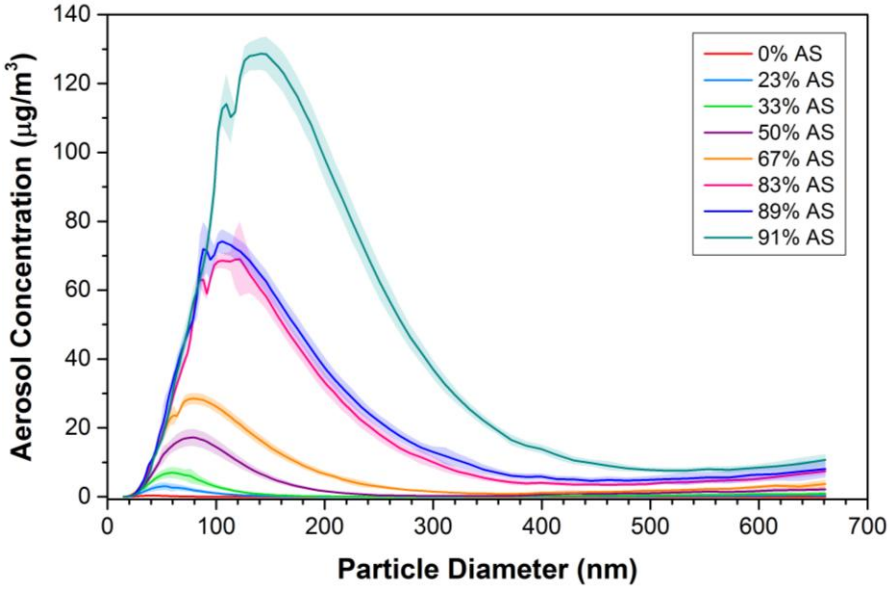

Figure 3.6. Size distribution of the aerosol produced from the CPA/AS solutions, measured using the SMPS. Particle diameters between 14.6 and 661.2 nm were separated into 106 size bins by the DMA and the aerosol mass concentrations recorded for each bin via the CPC. The thick lines represent the average concentration in that size bin for the duration of the experiment and ± 1 standard deviation is represented as shading.

Time series of the aerosol mass concentrations calculated for each CPA/AS solution, using the SMPS, are shown in Figure 3.7. The total concentration was the sum of all of the particles apportioned to each of the 106 size bins in the SMPS, with diameters ranging from 14.6 nm to 661.2 nm. The total aerosol concentration increases as the total solute concentration increases in the nebuliser solution, which produces more aerosol in the nebuliser. The concentration is relatively constant throughout the duration of the experiment, as expected, since a constant flow rate was used to produce the aerosol in the nebuliser. The nebuliser was operated in recirculation mode whereby any solution that was not atomised, was returned to the nebuliser flask. A risk of this method is that over time, the solute concentration changes which could affect the aerosol concentration and size distribution. However, none of the solutions showed a significant increase in aerosol concentration over time, perhaps due to the relatively short duration of the experiments (45 minutes) so this was not an issue.

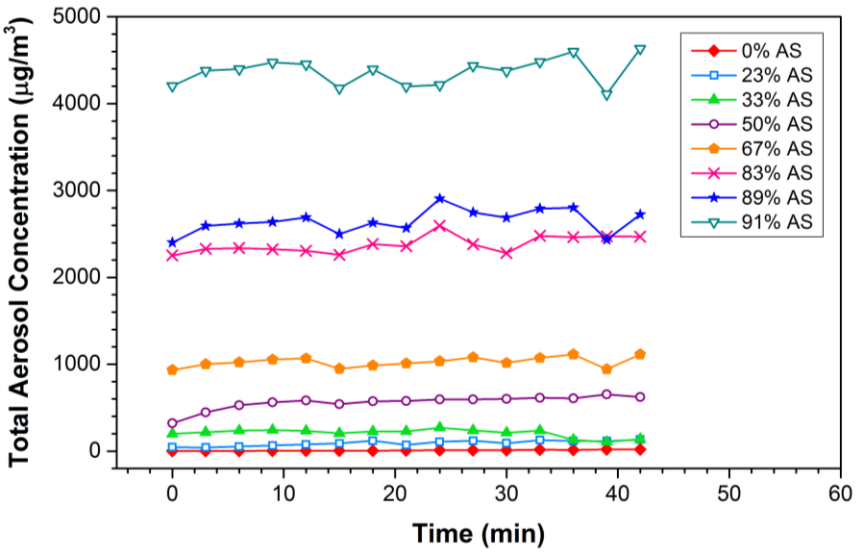

Figure 3.7. Time series of the total aerosol concentration for each CPA/AS solution. Data points shown are averaged over two separate experiments for each solution.

Figure 3.8 shows an example of the change in peak intensity detected by the EESI-MS for the *cis*-pinonic acid ion ($[M-H]^-$ *m/z* value 183.2507) in the 0.5 mM CPA and 0.25 mM AS (33% AS) solution. There was a clear distinction in the CPA peak intensity in the mass spectra between the 'aerosol off' and 'aerosol on' periods. Across all eight solutions, the organic signal increased rapidly at the point of aerosol injection, and then decreased rapidly during the clean air injection periods. The total aerosol concentration

measured by the SMPS during the experiment for the 33% AS solution is also shown in Figure 3.8.

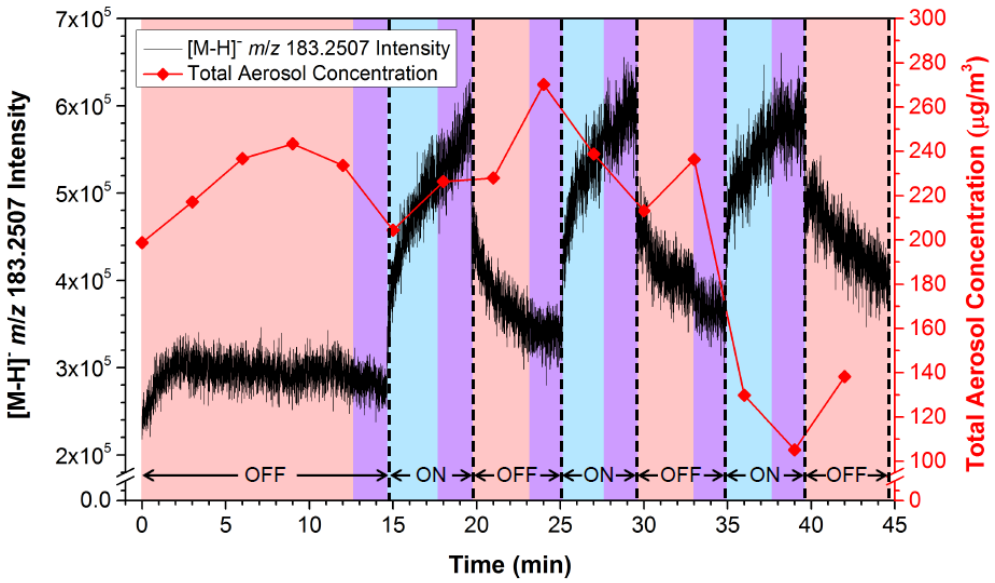

Figure 3.8. The change in (−)EESI-MS peak intensity for *cis*-pinonic acid (CPA) ($[M-H]^-$ *m/z* value 183.2507) in the 0.5 mM CPA and 0.25 mM AS (33% AS) solution (black) during the aerosol injection periods (blue shading) and clean air injection periods (red shading). The total aerosol mass concentration for the 33% AS solution, measured using the SMPS during the experiment, is also shown (red). The purple shaded regions denote the last two minutes of the acquired MS intensities for each 'aerosol on' ("ON") and 'aerosol off' ("OFF") period used to calculate the average background-corrected CPA intensity, Δ *m/z*, in Equation

Figure 3.9 shows the raw peak intensities (not background-corrected) for the 'aerosol on' and 'aerosol off' (background) periods, averaged for the whole experiment, for each of the different CPA/AS solutions. (The intensity value for the 50% AS solution was not included in Figure 3.9 due to it being anomalously high). It is evident from Figure 3.9 that there is little difference in the magnitude of the organic peak intensity change as the inorganic solute concentration in the nebuliser increases. This is expected because the organic solute concentration in the nebuliser (0.5 mM CPA) was conserved in all of the solutions so the organic signal should therefore not change. Some of the solutions did show a drift in the organic signal to larger intensities during the experiment. This is due to a memory effect caused by accumulation of the CPA in the MS inlet which prevents the organic signal returning the initial background level within the subsequent five minute clean air injection period, as seen in Figure 3.8.

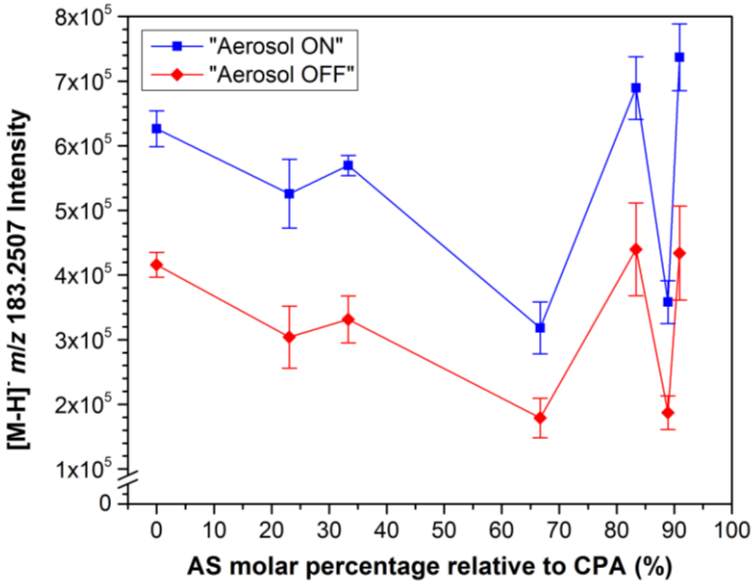

Figure 3.9. The change in (−)EESI-MS peak intensity (raw, not background-corrected) for CPA ($[M-H]^-$ *m/z* value 183.2507) with increasing AS fraction during the aerosol injection periods ("aerosol on", blue squares) and clean air injection periods ("aerosol off", red diamonds). Values shown are averaged over three aerosol injection cycles and error bars denote ± 1 standard deviation.

Figure 3.10 shows the average background-corrected CPA intensities as a function of increasing AS molar percentage relative to CPA, and the average total aerosol concentration for each CPA/AS solution. The background-corrected intensity, Δ *m/z*, was calculated for each 'aerosol off'/'aerosol on' cycle using the average of the last two minutes of the acquired MS intensities for CPA during each 'aerosol off' period, $\overline{I_{A-OFF}}$, subtracted from the average of the last two minutes of the CPA intensities for the next 'aerosol on' period, $\overline{I_{A-ON}}$. This is shown in Equation 3.1. The last two minutes of each 'on' and 'off' period were used for this calculation because this was when the intensities were most stable.

$$\Delta\, m/z = \overline{\mathrm{I_{A-ON}}} - \overline{\mathrm{I_{A-OFF}}}\ . \tag{3.1}$$

The error bars in Figure 3.10 are ± 1 standard deviation (SD) for Δ *m/z* for each cycle. This was calculated from the square root of the sum of the variances for the 'aerosol off' intensity (averaged over the last two minutes) and the 'aerosol on' intensity, as shown in Equation 3.2:

$$\mathrm{SD}_{\Delta m/z} = \sqrt{\left(\mathrm{SD}_{\mathrm{I_{A-ON}}}\right)^2 + \left(\mathrm{SD}_{\mathrm{I_{A-OFF}}}\right)^2}\,. \tag{3.2}$$

As previously mentioned, the average CPA intensity for the 50% AS solution was significantly higher (8×10^5) compared with the other solutions. There was no obvious reason for this significantly high intensity and the result is deemed to be anomalous. The total aerosol concentration measured by the SMPS and averaged across the whole experiment for each CPA/AS solution, is also shown. The increase in total aerosol concentration is very dramatic after ~70% AS. This somewhat exponential increase is unexpected and may be due to changes in the spray generation in the nebuliser occurring once a certain molar percentage of inorganic threshold is reached.

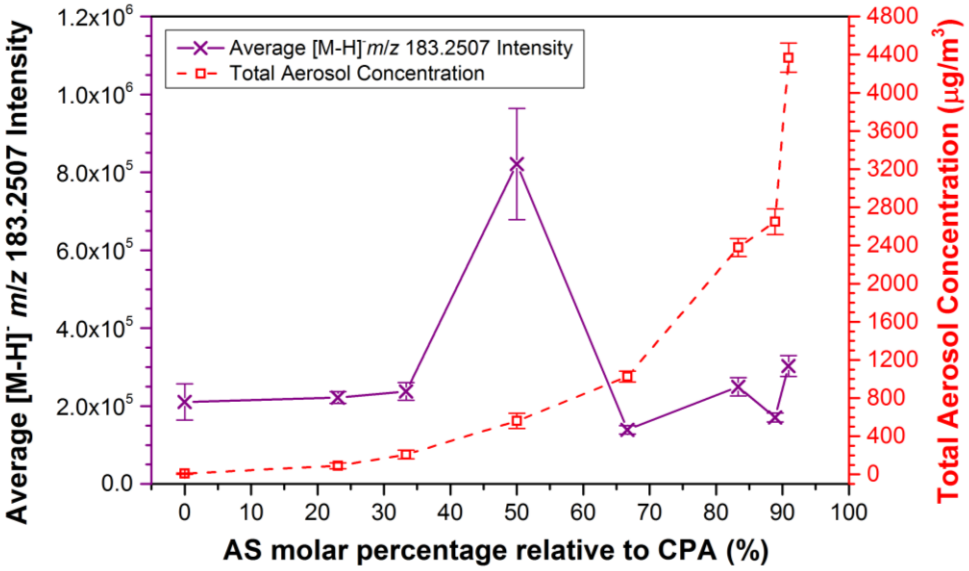

Figure 3.10. Average background-corrected (−)EESI-MS peak intensities for CPA (purple) and average total aerosol concentration (red) as a function of increasing AS concentration. Error bars denote ± 1 standard deviation.

Since the organic solute concentration in the solutions was constant, theoretically, the organic signal detected by the MS should be constant, regardless of the inorganic solute concentration, assuming that the solute composition in the nebuliser is conserved in the aerosol phase. However, normal ESI techniques are prone to artefacts if there are compounds present that have very different ionisation efficiencies such as AS and organic compounds. Figure 3.10 shows that the peak intensities varied between ~140,000 and ~310,000 (excluding the anomalous intensity value for the 50% AS

solution) but remained within a factor of two despite the strongly increasing AS solute concentration. There is no overall decrease in the organic signal with increasing inorganic concentration in the mixture, within the error bars of individual solutions.

Figure 3.11 shows the average CPA intensity detected by the EESI-MS as a function of total aerosol concentration. F-test linear regression analysis, using a significance level of 0.05 was applied to the data (for further details on F-test analysis, see Appendix A). The analysis showed no significant correlation between the average organic signal intensity and aerosol concentration which was mostly inorganic at the higher inorganic fractions. These experiments, therefore, strongly suggest that no significant suppression of the organic signal has occurred as a result of increasing the inorganic solute concentration of the mixed aerosol, and that the CPA signal detected by the EESI-MS was relatively stable over the tested range of mixed organic and inorganic solutions.

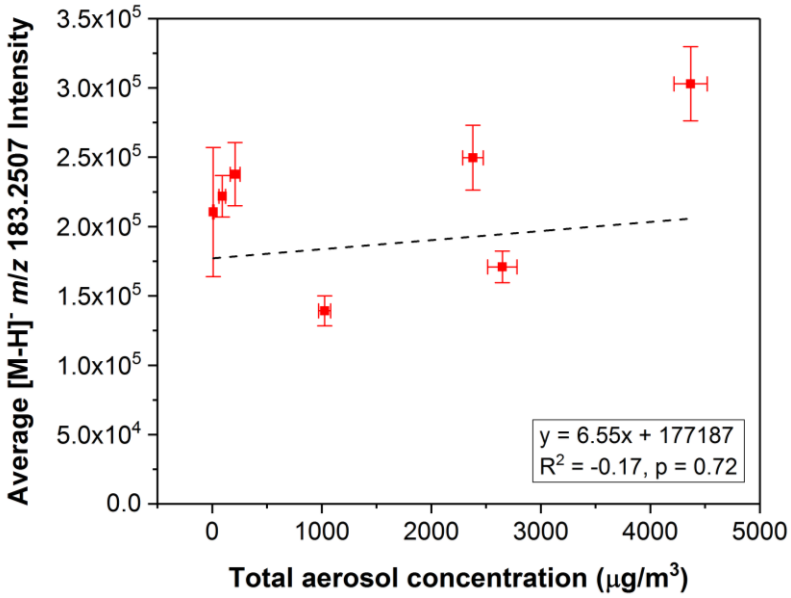

Figure 3.11. Background-corrected (−)EESI-MS peak intensities for *cis*-pinonic acid (CPA) ($[M-H]^-$ *m*/*z* value 183.2507) as a function of the total aerosol mass concentration, measured by the SMPS. Values shown are averaged over the experiment for each solution and error bars denote ± 1 standard deviation.

An example of the mass spectra observed for the 0% AS solution is shown in Figure 3.12. The deprotonated ion for *cis*-pinonic acid *(m*/*z* 183.2507) in negative ionisation mode is highlighted in bold. Other peaks present at *m*/*z* 187.1674, 225.1681, 229.1683, 243.0019 and 263.0023 in Figure 3.12 were observed which were present during both the aerosol injection periods and the clean air injection period. The intensities of all of the peaks were slightly higher during the aerosol injection periods than during the clean

air injection periods but overall the intensities remained within a factor of two throughout the experiments. These peaks were also all present regardless of the concentration of the AS used in the solution. This suggests that these are contaminant peaks in the MS produced from previous experiments and are not salt adducts.

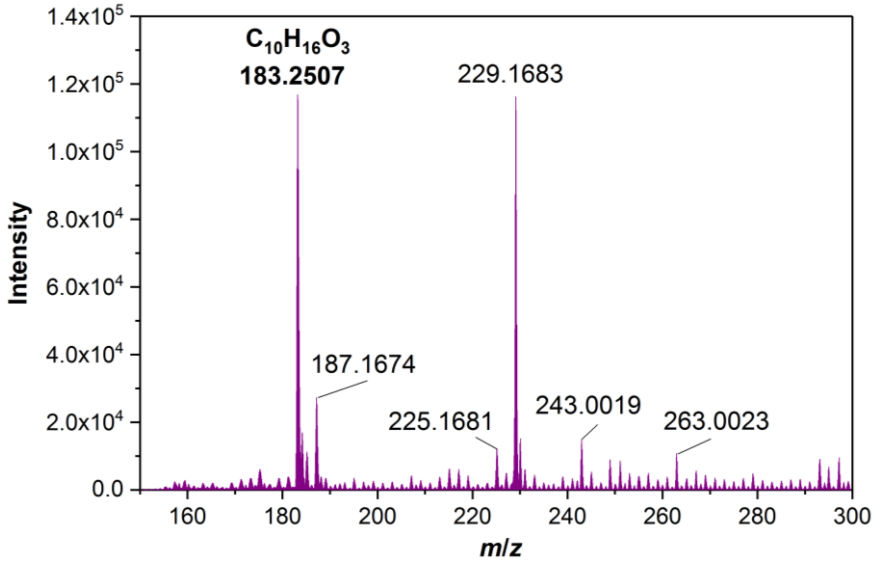

Figure 3.12. (−)EESI-MS spectra for the purely organic CPA (0% AS) solution. The *m*/*z* $[M-H]^-$ value 183.2507 corresponds to the deprotonated ion for *cis*-pinonic acid (CPA).

These simple mixed organic and inorganic experiments suggest that the organic signal detected by the EESI source is not strongly affected by salt suppression since the CPA intensity varied within a factor of two, even in mixed aerosol with very high inorganic concentrations. There was also no significant correlation between the organic signal intensity and total aerosol concentration. However, the mass spectra show that contamination may be a problem in the EESI which highlights the need for regular cleaning of the EESI source between experiments, to minimise persistent contaminants. Increasing the inorganic concentration in mixed aerosol increased both the concentration and the modal diameter of the aerosol. Overall, this is a very positive result for the use of EESI-MS as an absolute quantification method for future experiments analysing ambient and laboratory-generated aerosol with mixed organic and inorganic composition.

3.4.2 Complex organic and inorganic aerosol mixtures

3.4.2.1 WSOC/AS (−)EESI mass spectra

Figure 3.13 shows the intensities of the WSOCs observed in the 67% AS solution. This mass spectrum is representative of all of the solutions tested. Maleic acid (*m*/*z* 115.0037), glutaric acid (*m*/*z* 131.0010) and salicylic acid (*m*/*z* 137.0012) all ionised effectively. Oxalic acid was detected in all of the solutions (*m*/*z* 88.7502) but at very low intensities as indicated in Figure 3.13. The fact that it did not ionise as well as the other carboxylic acids may suggest competitive ionisation was a factor. However, oxalic acid has been observed to have low ionisation efficiencies in other MS studies (Jaitz et al. 2011, Rellán-Álvarez et al. 2011), perhaps due to poor proton transfer in the gas phase reaction (Gao, Zhang and Karnes 2005).

The two WSOC alcohols; arabitol and erythritol did ionise although not as efficiently as the carboxylic acids. This is because the carboxylate ion (COO^-) formed following deprotonation of a carboxylic acid is delocalised and stabilised by resonance. However, when an alcohol is deprotonated, the resulting alkoxide ion (O^-) has a strong negative charge on the oxygen atom due to greater steric hindrance from the carbon chain which pushes electron density towards the already negative ion. This means the ion is more likely to attract another proton and reform the neutral alcohol molecule before it is detected by the MS (Fox and Whitesell 1997). Higher ionisation efficiencies have been observed for ions with more efficient charge delocalisation in previous MS studies (Kruve et al. 2014, Bandu et al. 2004). Erythritol could be detected in most of the solutions but not above the noise level in the MS spectra. This is consistent with previous WSOC experiments conducted in the Kalberer research group using Nano-ESI and Heated Electrospray Ionisation (HESI) MS to analyse complex organic mixtures (Szeto 2014).

In addition to the known WSOCs detected in the spectra, high intensity peaks were detected with *m*/*z* values of 90.5835 and 91.1669. Singly charged ions (z = 1) in mass spectra are separated by 1 atomic mass unit (amu) or Dalton (Da). In ESI, multiply charged ions, ($[M-nH]^{n-}$ in negative ionisation mode), can also occur. Peaks separated by 0.5 Da are indicative of doubly charged ions. The peak at *m*/*z* 90.5835 in Figure 3.13 could have been produced by a doubly charged deprotonated ion ($[M-2H]^{2-}$) corresponding to keto-pinic acid ($C_{10}H_{14}O_3$, *m*/*z* 182.22); the singly charged

deprotonated ion for which has an *m/z* value of 181.0870. This ion was also present in the mass spectra for the WSOC/AS solutions. Keto-pinic acid is regularly used as a standard for carboxylic acids so it is possible that residues from this compound were present in the EESI source or MS inlet which again highlights the need for thorough cleaning of the source and flushing of the solvent lines after experiments. Peaks at *m/z* 91 have been previously observed in a ESI-MS study of organic and inorganic species in topiramate tablets (Xiang, Ko and Guh 1996) which suggested the peaks arose from the dimer ion of formic acid, $[HCOOH + HCOO]^-$. Formic acid is frequently used to aid protonation and separation of compounds when using ESI-MS so it is likely that residues of formic acid were in the EESI source from previous experiments and have produced the peak at *m/z* 91.1669 in Figure 3.13.

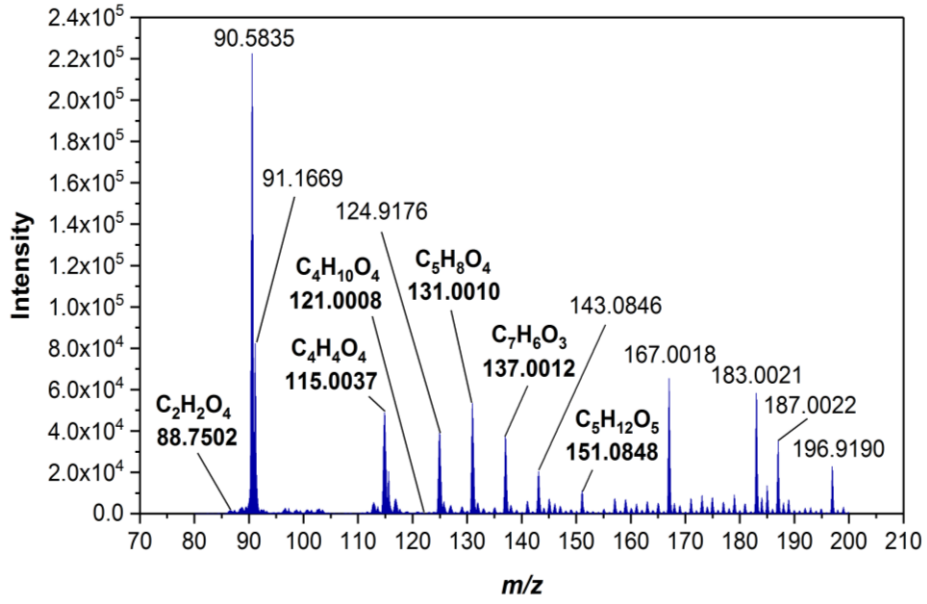

Figure 3.13. (−)EESI-MS spectra showing deprotonated ions detected for oxalic acid ($[M-H]^-$ *m/z* 88.7502), maleic acid ($[M-H]^-$ *m/z* 115.0037), glutaric acid ($[M-H]^-$ *m/z* 131.0010), salicylic acid ($[M-H]^-$ *m/z*137.0012) and arabitol ($[M-H]^-$ *m/z* 151.0848), in bold, in the 67% ammonium sulphate (AS) solution. The deprotonated ion for erythritol ($[M-H]^-$ *m/z* 121.0008) was detected in most of the solutions but not at intensities above the noise level.

There are also some contamination peaks present in the mass spectra corresponding to *m/z* values 124.8342 and 187.0022 which were present during both the aerosol injection and clean air injection periods. There was also a peak at *m/z* 183.0021 which corresponds to CPA despite it not being included in the nebuliser with the WSOC solutions. The apparatus used to direct the aerosol into the EESI-MS for the WSOC/AS

experiments was cleaned thoroughly following the previously described CPA/AS experiments. This means that the CPA signal is arising from accumulation in the MS inlet or in the EESI housing and reiterates the importance of cleaning the EESI source thoroughly to remove residues.

3.4.2.2 WSOC MS intensities and total aerosol concentration

The intensities of the deprotonated WSOC ions detected by the MS are provided in Figure 3.14 as a function of the molar percentage of AS in the total solute concentration of the nebuliser solution. Each intensity value was calculated using Equation 3.1 and was averaged over six aerosol injection periods from two experiments using the same WSOC/AS solution concentration. The error bars represent ±1 standard deviation and were calculated using Equation 3.2.

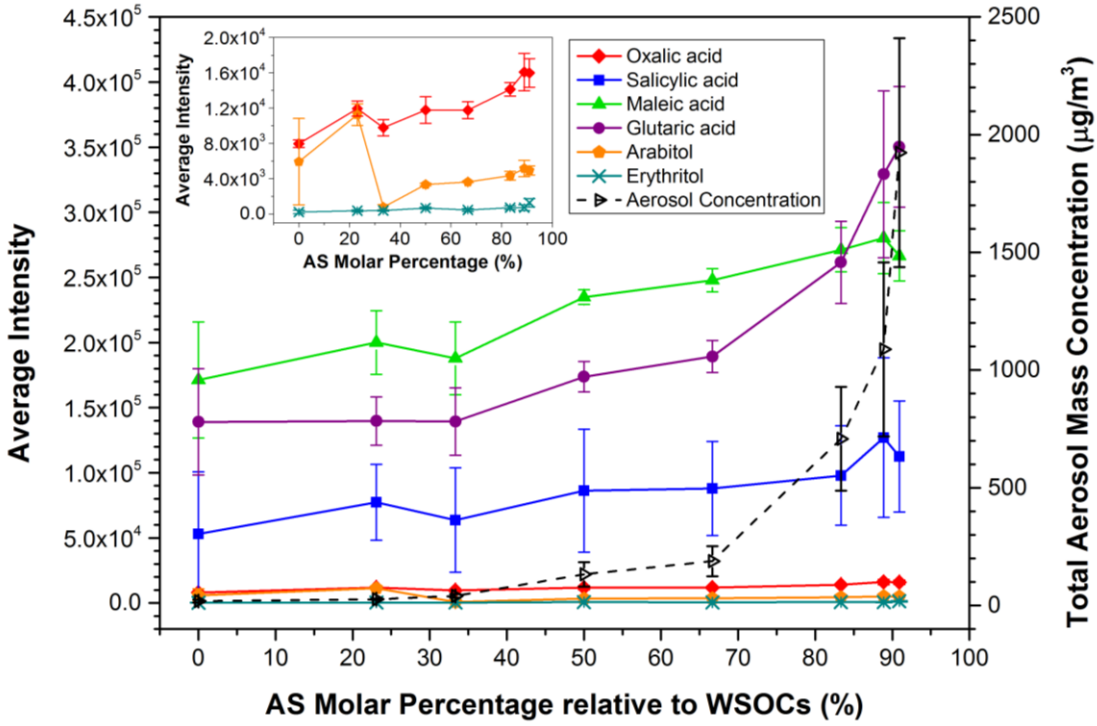

Figure 3.14. Intensities for the WSOC deprotonated ions detected by the EESI-MS in negative ion mode, as a function of ammonium sulphate concentration in the aerosol mixture (closed symbols, solid lines). The total WSOC concentration is constant in all eight measured solutions. The intensity values are averaged over six aerosol injection periods from two experiments using each WSOC/AS solution and ± 1 standard deviation are represented as error bars. Total aerosol concentration averaged for the duration of two experiments per WSOC/AS solution included (open symbols, dashed line) and ± 1 standard deviation is denoted as error bars.

Since the total WSOC solute concentration in the nebuliser is constant in all of the solutions, theoretically, the WSOC signal intensity should be constant. However, Figure 3.14 shows a general increase in MS intensity for the four tested carboxylic acids. F-test linear regression analysis with a significance level of 0.05 revealed that all of the WSOC compounds, except for arabitol, showed a statistically significant increase in intensity ($p = < 0.05$) between 0 and 90% AS molar percentages. This observation contrasts with the simple mixed organic and inorganic solutions which showed variability but no significant increase in intensity as the inorganic fraction increased (Figure 3.10).

Figure 3.14, again shows higher intensities for the carboxylic acids than the alcohols. There are also slight differences in the intensity trend between the four tested carboxylic acids. Acidity, polarity, molecular structure, charge delocalisation, solvation energy and surface activity have all been shown to influence the ionisation efficiency of analytes in ESI (Kostiainen and Kauppila 2009, Oss et al. 2010, Kruve et al. 2014). A study by Henriksen et al. 2005 observed a decrease in ESI-MS response of carboxylic acids at lower pKa values. This may explain why the most acidic carboxylic acid in the current study; oxalic acid ($pKa_1 = 1.23$, $pKa_2 = 4.19$ (Faria, Órfão and Pereira 2008)) had the poorest ionisation efficiency. However, the least acidic carboxylic acid; glutaric acid ($pKa_1 = 4.31$, $pKa_2 = 5.41$ (Piccolo et al. 2003)) showed the highest MS intensity and there was no overall significant correlation observed between the pKa values and average MS intensities of the carboxylic acids. Acidity, therefore, is not the primary influence on ionisation efficiency in this study.

Analyte polarity is believed to have an important influence on ionisation efficiency when aqueous solvents are used (Oss et al. 2010). A study by Huffman, Poltash and Hughey 2012 observed that for C_6–C_{18} carboxylic acids with similar pKa values, ionised in a purely organic solvent, the ESI response doubled with each addition of two CH_2 groups. This is partially due to the surface activity of ions which increases with carbon chain length. Non-polar analytes are more surface-active and have higher ionisation efficiencies than more polar analytes. This is because they reside on the surface of the electrospray droplet where there is excess charge, produced during the ESI process, so are more easily ionised unlike their more polar counterparts which reside in the predominantly electrically neutral interior of the electrospray droplet (Cech and Enke 2000). However, in this study, maleic acid (C_4), has a higher MS intensity

than glutaric acid (C_5) which has a higher intensity than salicylic acid (C_7). It appears that the presence of ammonium sulphate in this complex organic aerosol mixture is disrupting the expected trend in ionisation efficiency of the WSOC compounds, according to polarity.

The increase in intensity for the carboxylic acids observed in Figure 3.14 is within a factor of 2.5 across the 0–91% tested inorganic range. Ambient aerosol rarely exceeds inorganic fractions of 80%, except in highly polluted urban areas (Jimenez et al. 2009). The variation in intensity for the laboratory-generated aerosol in this study is within a factor of ~1.5 in solutions with ≤ 70% AS molar percentages. This small variability over an atmospherically-relevant range suggests that the organic signal intensities in most ambient aerosol will not be significantly affected by the presence of inorganics in the sample. EESI-MS is, therefore, a suitable method for analysing complex organic and inorganic mixtures. However, it is noted that oxalic acid and the two alcohols did not ionise efficiently compared with the carboxylic acids (although alcohols do not generally ionise as well as carboxylic acids) which suggests that competitive ionisation could still be an issue for the EESI source (as with all other ESI techniques) when using this method to analyse the complex organic aerosol.

At very high inorganic fractions (≥ 70% AS), glutaric acid increases significantly and maleic acid and oxalic acid also show clear increases. The total aerosol concentration is also shown in Figure 3.14 and was averaged over two experiments, for each WSOC/AS solution. The total aerosol concentration increases strongly after ~70% AS when the total aerosol concentration is mostly inorganic. This trend is similar to that observed for the CPA/AS solutions (Figure 3.10). The time series of the total aerosol concentration in increasingly inorganic solutions is provided in Appendix B (Figure B.1). A similar trend to the CPA/AS solutions was observed (Figure 3.7); increasing aerosol concentrations at higher ammonium sulphate concentrations although the concentrations were more variable. The size distribution of the WSOC/AS aerosol as a function of increasing ammonium sulphate concentration showed a clear increase in the modal diameter of the aerosol, from ~62 nm in the purely organic (0% AS) solution to ~141 nm in the 91% AS solution. This was a very similar trend to that observed in the CPA/AS solutions (Figure 3.6) and has also been provided in Appendix B (Figure B.2).

It does appear from Figure 3.14 that there is a significant exponential increase in total aerosol concentration from ~200 μg/m^3 to ~1900 μg/m^3 in this study. The intensity for glutaric acid shows a similar increase after ~200 μg/m^3. Aerosol concentrations in field

experiments do not often exceed a few hundred μg/m^3 so it is possible that no significant increase in MS intensity would be observed if the EESI source was to be used for analysing ambient aerosol. However, in future laboratory experiments, where much higher aerosol concentrations can be generated, the aerosol may need to be diluted to concentrations of approximately ≤ 200 μg/m^3, to limit the uncertainties of the data.

A reason why WSOC intensities are not independent of the inorganic fraction in Figure 3.14 at masses higher than ~200 μg/m^3 could be that it is more difficult for EESI to extract and ionise the total aerosol mass at these high total particle concentrations. This could be due to insufficient charges available in the EESI solvent when the aerosol mass reaches a certain threshold. This might explain why the MS intensities in Figure 3.14 decrease for most of the WSOC compounds at 91% AS solute concentration.

The observed correlation between total aerosol concentration and MS intensity observed in Figure 3.14 was investigated further. All of the individual WSOC MS intensities, except arabitol, showed positive correlation with the total aerosol concentration, as shown in Figure 3.15 and F-test linear regression analysis, using a significance level of 0.05, revealed that this linear relationship was statistically-significant for oxalic acid, glutaric acid and erythritol. This clearly shows that the very high total aerosol concentrations observed in Figure 3.14 are having a significant impact on the organic signal intensity in the complex aerosol.

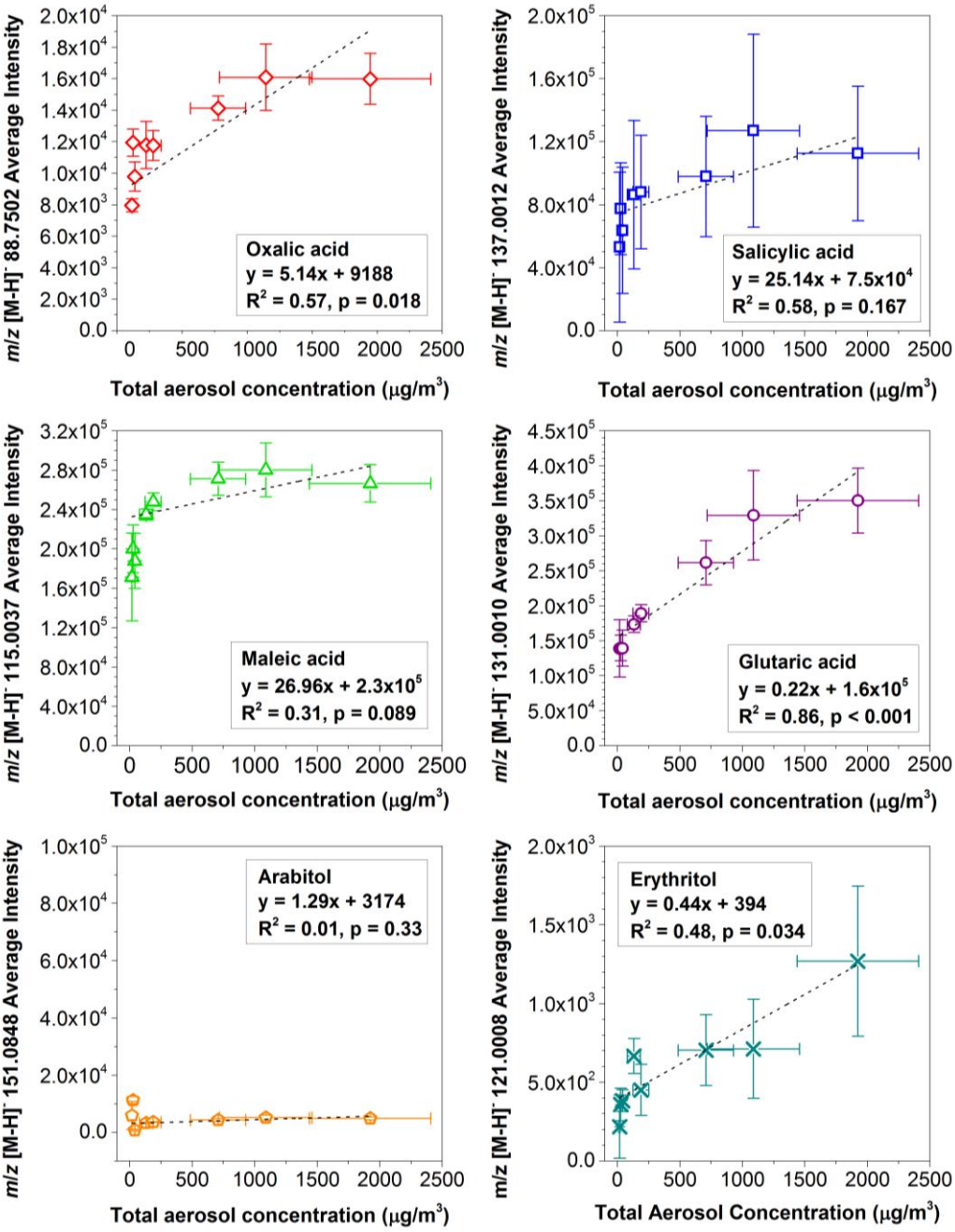

Figure 3.15. The average background-corrected MS signal intensity for each WSOC deprotonated ion, detected by the EESI-MS, as a function of the total aerosol mass concentration, measured by the SMPS. Error bars denote ± 1 standard deviation over the three cycles in two sets of experiments. F-test linear regression analysis included, using a significance level of 0.05.

3.4.2.3 Calculation of theoretical WSOC aerosol mass concentration

To further investigate the increase in WSOC signal intensity, it is assumed in the analysis below that the amount of WSOC in the complex mixed aerosol does not remain constant with increasing AS solute concentration in the nebulised solution and total particle concentration. The individual WSOC-weighted aerosol concentrations were calculated to see if there were any changes in the organic aerosol concentrations which could be causing the increasing MS intensities in Figure 3.14. Each WSOC aerosol mass concentration was calculated independently for the two experiments conducted for each WSOC/AS solution and then averaged. Firstly, the mass fraction for each WSOC (w_{WSOC}), shown in Equation 3.3 was calculated. The values for m_{WSOC}, $m_{TotalWSOC,}$ and m_{AS} which are the masses of each individual WSOC, the total WSOC component, and AS in each solution, respectively, are provided in Table C.1 and Table C.2 in Appendix C. c_{WSOC} and c_{AS} are the concentrations of each WSOC and AS, V, is the volume of the total solution in the nebuliser (120 ml), and M_{WSOC} and M_{AS} are the molar masses of each WSOC (Table C.1, Appendix C) and AS (132.14 g/mol) respectively.

$$w_{\mathrm{WSOC}} = \frac{m_{\mathrm{WSOC}}}{(m_{\mathrm{Total\ WSOC}} + m_{\mathrm{AS}})} = \frac{\mathrm{c_{WSOC}} \times \mathrm{V} \times \mathrm{M_{WSOC}}}{(m_{\mathrm{WSOC\ 1}} + m_{\mathrm{WSOC\ 2}} + \cdots + m_{\mathrm{WSOC\ 6}}) + (\mathrm{c_{AS}} \times \mathrm{V} \times \mathrm{M_{AS}})}. \quad (3.3)$$

Each WSOC mass fraction for each solution was then multiplied by the total aerosol concentrations, A_T, measured by the SMPS for the two experiments, as shown in Equation 3.4, and averaged to produce the WSOC-weighted aerosol concentration, $[A_{WSOC}]$, for each WSOC.

$$[\mathrm{A_{WSOC}}] = w_{\mathrm{WSOC}} \times \mathrm{A_T}\ . \quad (3.4)$$

The WSOC aerosol concentrations are plotted as a function of the molar percentage of AS in Figure D in Appendix D. The WSOC aerosol concentrations range from ~2 to ~34 µg/m^3 and show a general increase with increasing inorganic fraction. The change in WSOC aerosol concentrations are unexpected because the individual WSOC solute concentrations in the nebuliser remained constant (0.08 mol/L) so assuming that the solute amount is conserved in the aerosol phase, there should be no increase in organic aerosol concentration despite the increase in inorganic solute concentration.

To test the relationship between WSOC mass spectra intensities and their calculated mass concentrations in the mixed aerosol, the intensity for each WSOC was plotted as a function of the calculated respective WSOC aerosol concentration Equation 3.4, as shown in Figure 3.16. F-test linear regression analysis, using a significance level of 0.05, revealed a statistically-significant positive correlation for all six WSOCs except arabitol which had an anomalously high intensity value in the 23% AS solution. These positive correlations show very clearly that the increase in organic aerosol concentration is causing the increase in MS intensity observed in Figure 3.14.

The CPA-weighted aerosol concentrations for the simple organic and inorganic aerosol characterisation experiments in this chapter were also calculated using Equations 3.3 and 3.4 for comparison. They range from ~9 to ~535 $\mu g/m^3$; much higher than the WSOC aerosol concentrations (< 40 $\mu g/m^3$), and show a general increase with increasing inorganic fraction, as shown in Figure E.1, Appendix E. When plotted against the CPA MS intensity, as shown in Figure E.2, Appendix E, there is a significant positive linear relationship ($R^2 = 0.99$, $p = 0.03$) up to approximately 150 $\mu g/m^3$. A similar strong, positive linear trend was observed in Gallimore et al 2017a for tartaric acid and AS mixed aerosol, up to 100 $\mu g/m^3$.

It is noted, however, that in the simple CPA/AS mixture in this study, the linear relationship between MS intensity and CPA aerosol concentration is lost at higher CPA aerosol concentrations which could suggest that at higher aerosol concentrations, there are changes in the aerosol formation or composition, resulting in different MS organic signals, or that ionisation limitations may become a factor and the entire aerosol mass can no longer be extracted at such high particle mass concentrations. Further research at higher concentrations is required to understand this fully.

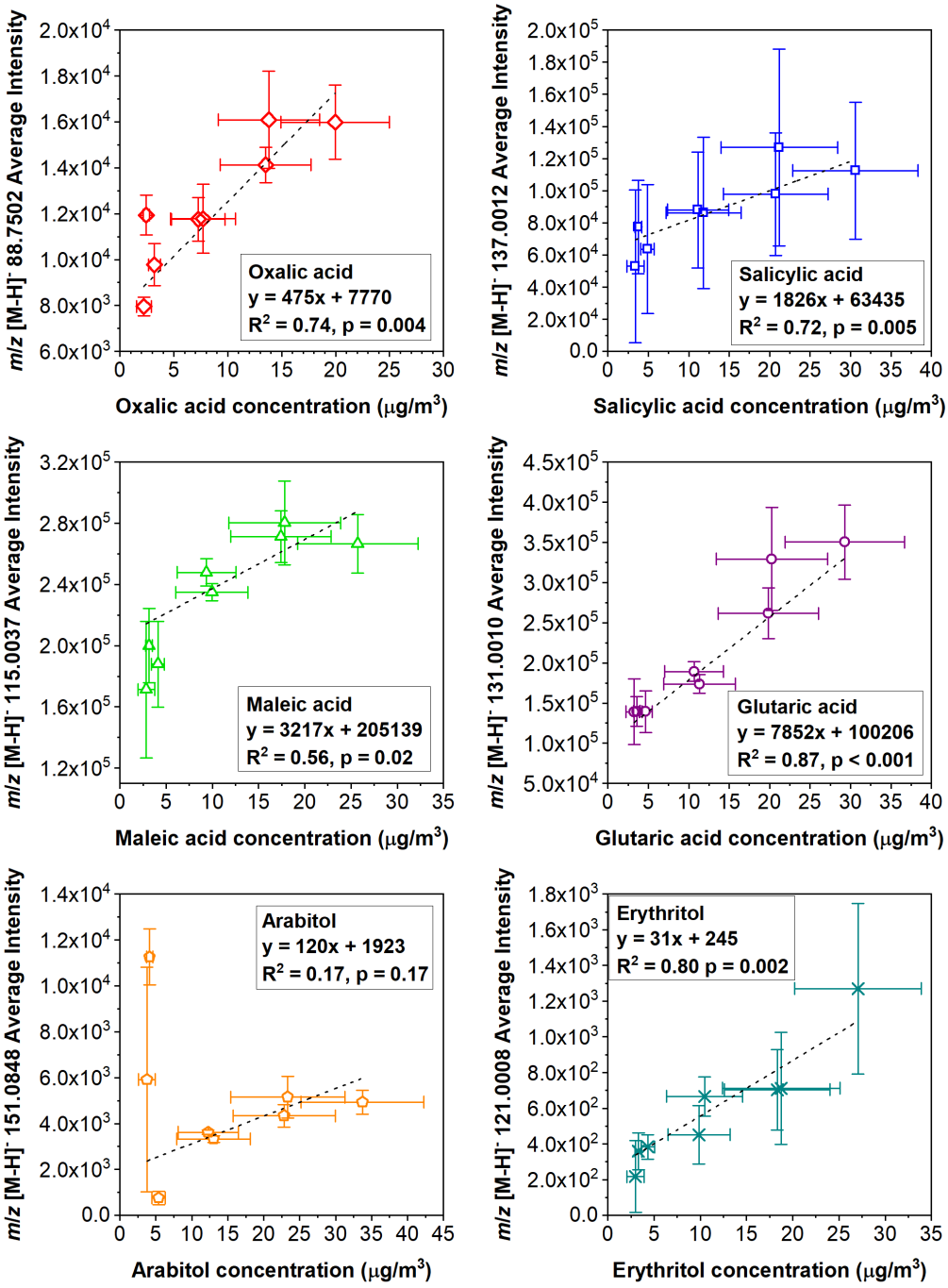

Figure 3.16. WSOC aerosol concentrations; derived from the total aerosol concentration and the WSOC and AS molar masses, as a function of the average background-corrected MS signal intensity for each WSOC deprotonated ion, detected by the EESI-MS. Error bars denote ± 1 standard deviation over the three cycles in two sets of experiments. F-test linear regression analysis included, using a significance level of 0.05.

The extraction efficiency for each WSOC was calculated by dividing the background-corrected EESI-MS intensity (calculated using Equation 3.1) by the WSOC aerosol concentration (calculated using Equation 3.4) and the total aerosol concentration estimated by the CPC during that cycle). The extraction efficiencies were averaged over six cycles (three for each of the two experiments) for all of the WSOCs except erythritol; for which one set of experimental data was used. The extraction efficiencies are plotted as a function of increasing AS molar percentage (% AS) in Figure 3.17 with the error bars denoting ± 1 standard deviation. Ideally, if there is no impact on the organic MS signal from increasing the inorganic solute concentration while keeping the organic solute concentration constant, there should be a horizontal line. However, as indicated by the increase in intensities in Figure 3.14 and the positive linear relationship in Figure 3.15, there is an overall decrease in the extraction efficiency with increasing inorganic fraction. Despite the large uncertainties for the arabitol, erythritol and salicylic acid extraction efficiencies in Figure 3.17, the higher inorganic solute concentrations are having an impact on the organic signal for all of the WSOCs. This, again, suggests that the EESI source is less able to extract the total particle mass at high total aerosol mass concentrations and this is affecting the organic MS signal intensity.

A potential explanation for the observed decrease in extraction efficiencies may be that some of the WSOCs are forming an organic shell around a predominantly inorganic, ammonium sulphate core. A recent study by Kumbhani et al., (2018) suggested that such aerosol particles with a core-shell structure may not completely dissolve and ionise using EESI. Also, the salting-out effect has been observed to be more significant for larger, more non-polar organic compounds in the presence of salts (Endo, Pfennigsdorff and Goss 2012), including ammonium sulphate (Wang et al. 2014). The efficiency of the extraction is dependent on the solubility of the material forming the outer layer in the EESI solvent and also how much the surface material spreads over the core which may inhibit total particle extraction (Kumbhani et al. 2018). Their study also used aerosol mass concentrations of ~6500 $\mu g/m^3$ which despite being three times as high as the concentrations used in this study, could still indicate that EESI is less efficient at extracting total particle mass at high concentrations. Furthermore, the highest aerosol concentrations in this study have the highest ammonium sulphate content and it is possible that the ‘salting-out’ effect, defined as when the solubility of a non-electrolyte substance in water decreases in increasing salt concentrations (Hyde et al. 2017), may be occurring at the highest concentrations. The salting-out effect could be accentuating

the core-shell structure of the aerosol at the higher total aerosol concentrations, which are mostly AS, compared with the solutions with the lower salt concentrations which may be producing a more mixed aerosol. The hypothesis of the WSOC compounds forming an organic layer around the ammonium sulphate core is explored further in the next sub-section.

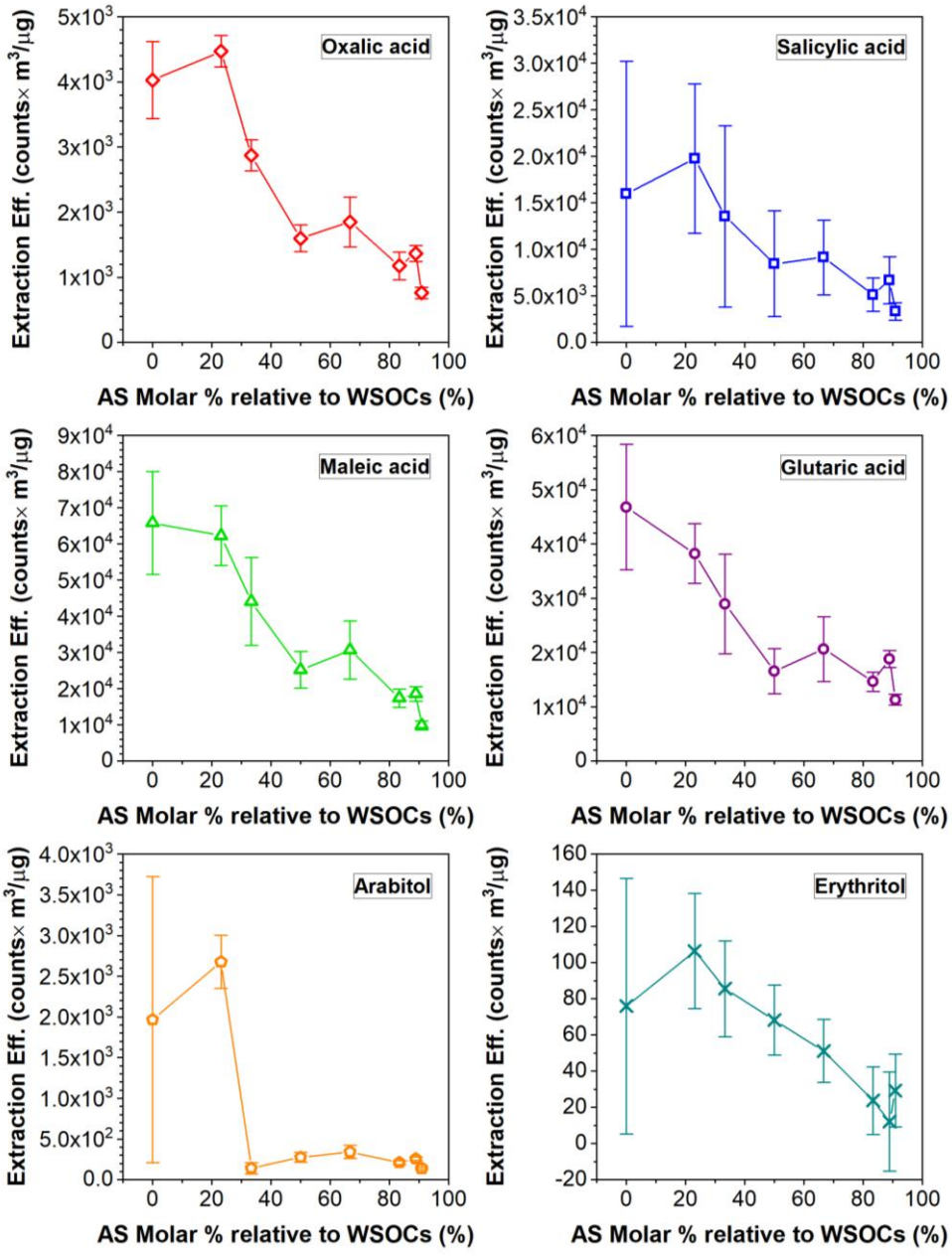

Figure 3.17. WSOC extraction efficiencies calculated by dividing the EESI-MS signal intensities by the respective WSOC aerosol concentrations. Values were averaged over 6 cycles (three cycles in two experiments) for all of the WSOCs except erythritol; for which one set of experimental data was used. Error bars denote ± 1 standard deviation.

3.4.2.4 Scanning and Transmission Electron Microscopy of mixed organic and inorganic aerosol particles to identify core-shell structure

Carboxylic acids with longer carbon chains are more able to act as organic surfactants (Andrews and Larson 1993). Glutaric acid, maleic acid and oxalic acid have been shown to demonstrate surface activity in mixed organic and inorganic aerosol (Topping et al. 2007). Thus, there may be a degree of surface activity happening in the mixed WSOC/AS solutions in this study. This could be occurring for the C_5 glutaric acid solutions in particular which shows the unexpected increase in MS intensity at the highest inorganic concentrations. Given that the increase in WSOC MS intensity coincides with the large increase in aerosol with larger diameters when the inorganic solute concentration is ≥ 67% (Figure B.2, Appendix B), and larger particles tend to have larger surface tensions (Tolman 1949), the larger, more inorganic particles, produced could have a thicker (or more complete if a partial coating-core model is more likely) WSOC coating which could result in a higher WSOC intensity being detected by the EESI-MS.

To test the hypothesis of a WSOC coating surrounding a predominantly inorganic AS core, a Scanning Electron Microscope (JSM-551OLV, JEOL Ltd.) with Energy Dispersive X-ray analysis (SEM-EDX) was used to obtain electron images of aerosol samples from some of the WSOC/AS solutions. SEM-EDX has been previously used to investigate organic coatings on ambient aerosol (Tervahattu et al. 2002, Dzepina et al. 2015) and laboratory-generated aerosol (McNeill, Wolfe and Thornton 2007, Karagulian et al. 2008) and also for providing information on aerosol morphology and elemental composition in urban aerosol (Ault et al. 2012, Liu et al. 2005, Pósfai et al. 1998) and biomass burning aerosol (Dzepina et al. 2015).

A few examples of the WSOC/AS aerosol mixtures were produced using a simplified version of the apparatus set up in Figure 3.2. The aerosol was collected using a custom designed Microelectromechanical systems (MEMS) Impactor Stage (MIS). A full description of the MIS is provided in (Zielinski et al. 2016). Briefly, the MIS is a highly-modular single stage impactor which uses a nozzle to collect particles onto a MEMS resonator. A steel disk (1.4 mm diameter, 0.03 thickness) was placed on the resonator, inside the MIS enclosure, and the nozzle accelerated the particles towards the surface of the disk via inertial impaction. A vacuum pump was used to control the flow through the MIS at 0.87 L/min. The RH was kept below 10% inside the MIS to keep the

aerosol dry and monitored during the aerosol collection using a humidity sensor (Sensirion SHT21).

Prior to the SEM-EDX analysis, the samples were vacuum coated in gold using an Agar sputter coater to ensure even conduction across the sample surface, prevent charging of the sample, promote emission of secondary electrons and also to provide a homogenous surface for analysis and imaging (Leslie and Mitchell 2007).

The results from the EDX analysis varied according to the different WSOCs analysed. The SEM-EDX analysis could provide the atomic percentages for larger individual aerosol particles observed such as the ~400 nm particle in Figure 3.18 (A), produced from 1 mM glutaric acid and 1 mM AS (50% inorganic). This particle contained carbon and no sulphate, indicating that it was pure glutaric acid which may suggest that not all aerosol particles were internally mixed for this solution. The SEM-EDX analysis could also provide the atomic percentages of carbon, oxygen, sulphur and nitrogen in agglomerated particles such as those shown in Figure 3.18 (B) which were produced from 1 mM oxalic acid and 0.3 mM AS (23% inorganic). The modal diameter of the WSOC/AS aerosol particles in this study was ~100 nm and in general, SEM-EDX cannot probe areas smaller than 1 μm^3 and the electron scattering from smaller particles is difficult to differentiate from the background X-ray signal from the substrate (Laskin and Cowin 2001). This meant that for most of the particles, it was not possible to determine if there was a difference in the elemental percentages of carbon; indicative of organic composition, and nitrogen and sulphur; indicative of inorganic composition, within the same particle. Thus, the SEM-EDX analysis was inconclusive in determining whether the WSOCs were forming organic coatings on the individual aerosol particles.

A Transmission Electron Microscope (TEM), which has much higher sensitivities than the SEM was also used to try and determine if there was an organic shell-inorganic core structure in the aerosol. However, the ammonium sulphate is very sensitive to the electron beam (Pósfai et al. 1998) and degraded rapidly upon contact with the beam which made it very difficult to obtain a reliable signal and to determine the percentage of the elements within the sample.

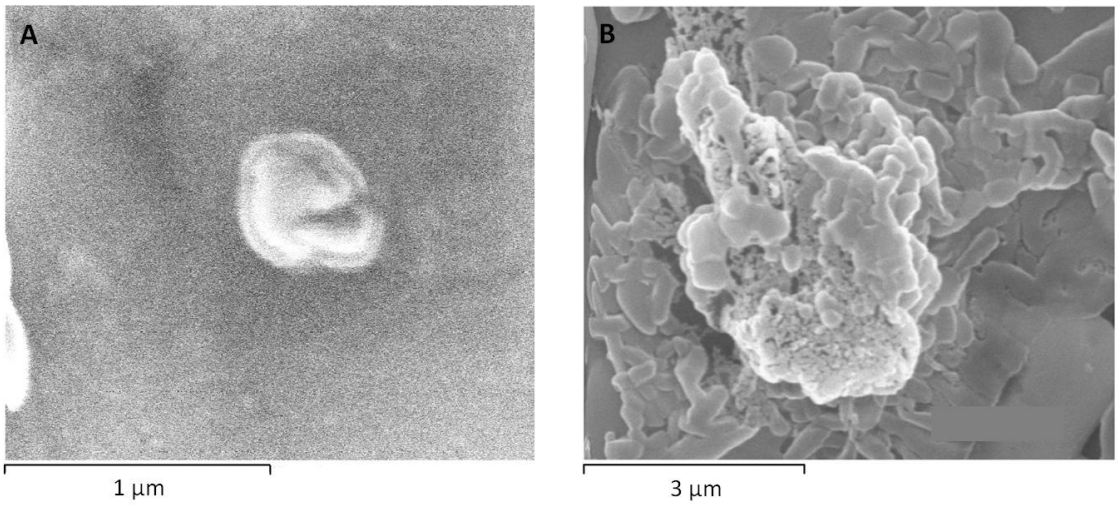

Figure 3.18. SEM images of (A) an individual ~400 nm diameter particle nebulised from 1 mM glutaric acid and 1 mM ammonium sulphate (50% inorganic) solution (× 45,000 magnification, 50 kV) and (B) agglomerated particles nebulised using 1 mM oxalic acid and 0.3 mM ammonium sulphate (23% inorganic) solution (× 17,000 magnification, 2 kV).

The SEM micrographs did provide some information on the aerosol morphology. Figure 3.19 shows an SEM image of the aerosol generated from a 1 mM maleic acid and 1 mM AS (50% inorganic) solution. Two clearly distinct aerosol structures were observed in different areas on the disk. Small, globular-shaped agglomerated particles stacked on top of one another were observed around the perimeter of the impact locations, as shown in Figure 3.19 and in the close-up SEM image in Figure 3.20 (B). It was assumed that the aerosol produced by the nebuliser was well mixed and the SEM-EDX analysis conducted on these particles revealed that these globular particles contained 28 ± 4.2% carbon, 44 ± 8.7% oxygen and 8 ± 3.5% sulphur atomic mass which suggests the aerosol is well mixed. However, these are average values for the agglomerates and it was not possible to conclude from these images whether the individual particles had the same elemental mass ratios. The aerosol morphology also looked very similar to those of the individual, dry particles from another study (Brooks et al. 2003) which observed internally mixed maleic acid and ammonium sulphate aerosol. Therefore, it is likely that the globular-shaped maleic acid and ammonium sulphate in this study is internally mixed and the observed stacked formation may have been produced by the impaction of multiple dry aerosol particles on top of one another.

There are also longer, platelet-like crystal structures towards the centre of the impaction zones as shown in Figure 3.20 (A). The SEM-EDX analysis on these particles also indicates that they are internally mixed since they contained 36 ± 7.2% carbon, 40 ± 2.3% oxygen and 1.3 ± 0.5% sulphur. However there is significantly less sulphur present than was expected for a nebulised solution with 50% inorganic solute concentration. Maleic acid aerosol has been reported to form a crystalline solid during the process of efflorescence (Pope et al. 2010); that is the drying and solidification of aqueous aerosol (Colberg, Krieger and Peter 2004). These platelet-like crystals are too large to be individual aerosol particles and they are likely to be the product of delayed crystallisation of the impacted aerosol particles, perhaps due to the presence of water. It is possible that the crystallisation processes observed in this aerosol may have caused a separation of organics and AS which makes it more difficult to use SEM for reliable composition analysis.

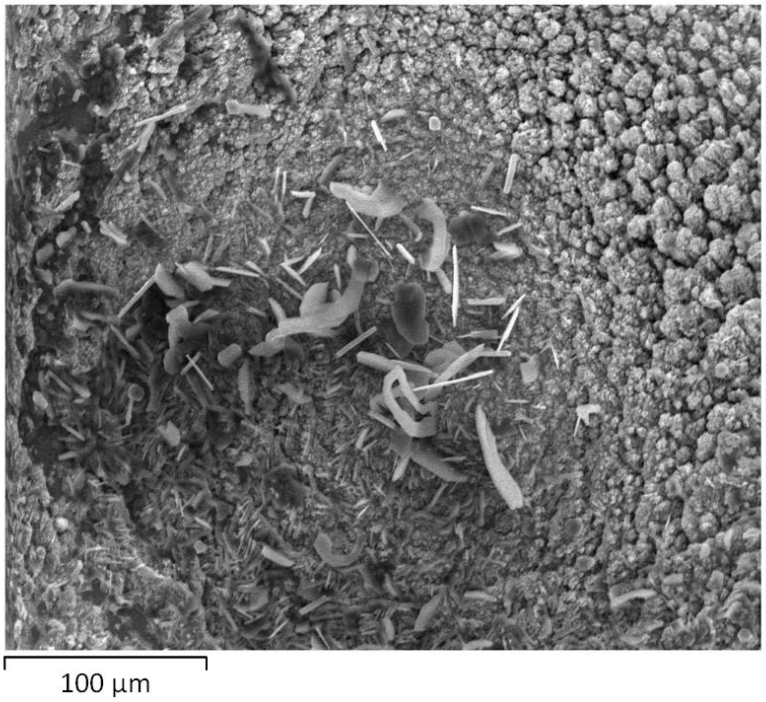

Figure 3.19. SEM image (× 330 magnification) showing relative locations of two distinct structures of aerosol particles nebulised from a solution of 1 mM maleic acid and 1 mM ammonium sulphate (50% inorganic). Long, platelet-like crystals lie towards the centre of the nozzle impaction zones and smaller, globular-like agglomerated particles towards the perimeter of the impaction zones.

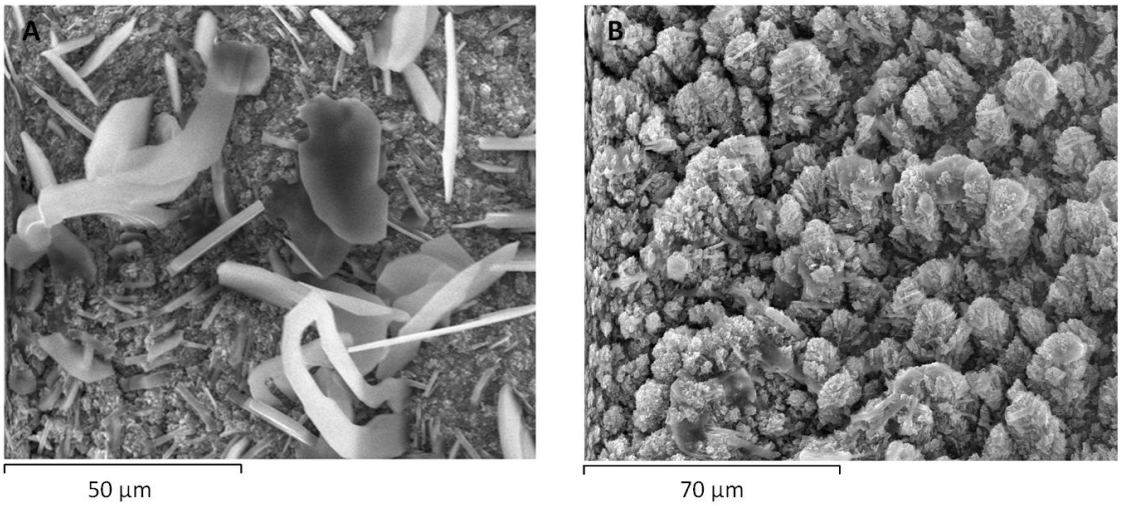

Figure 3.20. Close-up (× 1,100 magnification) SEM images showing (A) long platelet-like crystals on the impactor stage during efflorescence and (B) globular-like agglomerated particles consisting of multiple stacked dry aerosol particles. Both were produced from 1 mM maleic acid and 1 mM ammonium sulphate (50% inorganic) solution.

3.4.3 Chamber-generated SOA

The (−)EESI-MS spectrum during one of the aerosol injection periods of OH• oxidation of mixed AVOCs and BVOCs (A) and ozonolysis of mixed BVOCS (B) are shown in Figure 3.21. A number of SOA products were tentatively identified in both the OH• oxidation and ozonolysis experiments based on literature values in previous studies (Tolocka et al. 2004, Kourtchev et al. 2015, Claeys et al. 2009, Lee et al. 2006a, Jenkin 2004). Most of the ions detected were SOA products of α-pinene ozonolysis. Terpenes with internal double bonds, including α-pinene and Δ_3-carene studied in this work (Table 3.3), produce higher SOA yields than terpenes with external double bonds only, such as β-pinene. This is because oxidation of internal double bonds leads to ring opening and the formation of multifunctional, condensable, first generation oxidation products with no loss of carbon. Contrastingly, oxidation of external double bonds typically leads to fragmentation, a reduction in the number of carbons in the molecule and addition of only one single polar group. This explains why the majority of the SOA products observed from α-pinene oxidation are first generation products (Lee et al. 2006b, Ng et al. 2006).

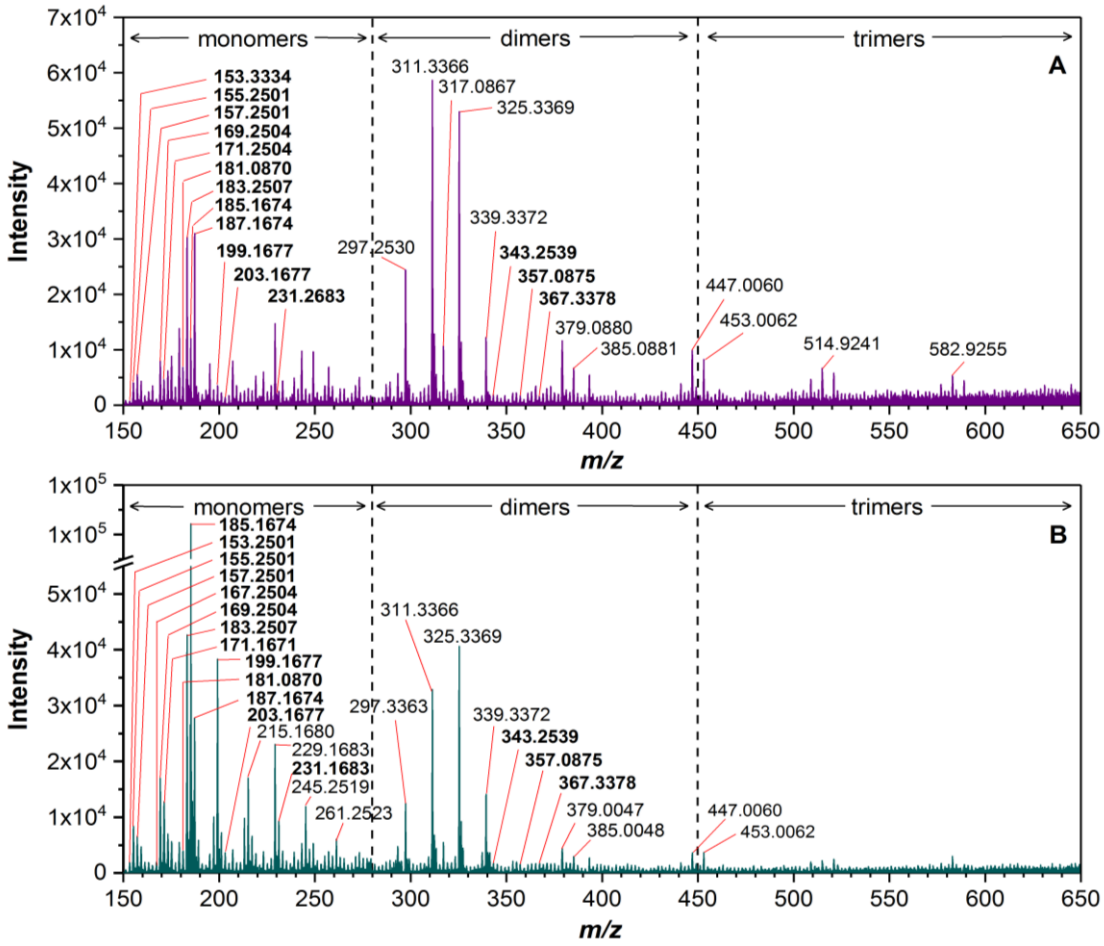

Figure 3.21. (−)EESI-MS spectrum for the (A) oxidation of mixed BVOCs and AVOCs via OH radical and (B) ozonolysis of mixed BVOCs, during aerosol injection periods into the EESI-MS from the CASC. SOA oxidation monomer products,and dimer and trimer products were detected in the oligomeric mass region (*m*/*z* > 280). Tentatively identified compounds are highlighted in bold.

All of the major ions with *m*/*z* values > 150 detected using EESI-MS and PTR-MS in a previous *α*-pinene ozonolysis study in the CASC (Gallimore et al. 2017a) were also detected in both the ozonolysis and OH• oxidation experiments by the EESI-MS in this work. These $[M-H]^-$ ions corresponding to known first generation *α*-pinene ozonolysis products included; 2,2-dimethyl-3-formyl-acyclobutylmethanoic acid (*m*/*z* 157.2501), terpenylic acid (*m*/*z* 171.2504), oxopinonaldehyde (*m*/*z* 181.0870), (CPA (*m*/*z* 183.2507), *cis*-pinic acid (*m*/*z* 185.1674), 2-hydroxyterpenylic acid (*m*/*z* 187.1674), OH-pinonic acid (*m*/*z* 199.1677) and diaterpenylic acid acetate (*m*/*z* 231.1683). Norpinaldehyde (*m*/*z* 153.3334) may also have been present but the absolute intensities were very low. These assignments are tentative, based on previous studies, because

EESI-MS alone, without LC-MS or a similar separation technique, cannot distinguish between isomeric compounds with the same molecular weight. For example, the peak at *m*/*z* 183.2507 may also be *cis*-caronic acid; an isomer of *cis*-pinonic acid and both an ozonolysis and photooxidation product of Δ_3-carene.

Similarly, the deprotonated peaks with *m*/*z* values of 185.1674 observed in the MS spectra for both the ozonolysis and OH• oxidation experiments in this study; correspond to different isomers with a molecular weight of 186 g/mol and molecular formula $C_9H_{13}O_4$. Ambient forest aerosol studies have reported many compounds produced from photooxidation and ozonolysis of *α*-pinene, *β*-pinene and Δ_3-carene with MW 186 including homoterpenylic acid, *cis*-pinic acid and *cis*-caric acid. *Cis*-caric acid has been reported in Δ_3-carene SOA and homoterpenylic acid and *cis*-pinic acid have been reported in *α*-pinene and *β*-pinene SOA (Yasmeen et al. 2011, Docherty and Ziemann 2003). Conducting further ozonolysis and photooxidation experiments of the individual VOCs, coupled with LC-MS or MS/MS, would separate the isomers and allow identification of the compounds.

The later generation oxidation C_8 tricarboxylic acid product 1,2,3-butanetricarboxylic acid (MBTCA) was also observed (*m/z* 203.1677). It is a product of *α*-pinene OH• oxidation but it was observed in the ozonolysis experiments in this study. This is because ozone generates OH• and if no OH• scavenger such as cyclohexane or 2-butanol is used to remove the OH•, they can oxidise a significant fraction of the parent BVOCs and first generation oxidation products. MBTCA has been previously observed in BVOC ozonolysis experiments using ESI-MS and is indicative of aerosol ageing (Kourtchev et al. 2015, Yasmeen et al. 2011).

Peaks were detected at *m*/*z* 169.2504 and *m*/*z* 169.3337 which could correspond to the *α*-pinene ozonolysis product *cis*-norpinonic acid or the major *β*-pinene carboxylic acid ozonolysis product pinalic-3-acid. These ions have previously been identified in other *α*-pinene and *β*-pinene ozonolysis studies using Capillary Electrophoresis Electrospray Ionisation MS (CE-ESI-MS) (Iinuma et al. 2004) and PTR-MS (Lee et al. 2006a) respectively. Pinonaldehyde (*m*/*z* 167.1670) may also be present; previously identified in a terpene ozonolysis studies using PTR-MS (Lee et al. 2006a) and APCI-MS and LC-ESI-MS (Glasius, Duane and Larsen 1999). A deprotonated peak at *m*/*z* 155.1668 was observed in the ozonolysis experiments that was also observed in a previous *β*-pinene ozonolysis study (Lee et al. 2006a). The fact that EESI-MS is able to detect these ions

in a mixed terpene ozonolysis chamber experiment strongly recommends EESI-MS as a suitable technique for complex laboratory-generated aerosol.

Monoterpenes like α-pinene, β-pinene and Δ_3-carene account for approximately 11% of the total global BVOC emissions and the reactions of biogenic terpenes with ozone and OH• contribute the most to the global SOA burden (Wisthaler et al. 2001). Despite isoprene emissions being much higher than terpene emissions, the SOA contribution from isoprene is much lower because the oxidation products are more volatile and unable to partition significantly into the aerosol phase. It is therefore not surprising that no isoprene oxidation products were clearly detected by the EESI-MS in the ozonolysis or OH• oxidation experiments in this study (Kroll et al. 2006).

Also, isoprene SOA has been suggested to mainly occur from the oxidation of first generation products (Ng et al. 2006) and many of these suggested oxidation products reported in the literature have *m*/*z* values < 150 and so were outside of the mass range used for this EESI-MS study. These SOA products include first generation oxidation products methacrolein and methyl vinyl ketone (*m*/*z* 71), and secondary/tertiary oxidation products; isomers 2-methylthreitol and 2-methylerythritol (*m*/*z* 135), 2-methylglyceric acid (*m*/*z* 119), glyceric acid (*m*/*z* 104) and the C_5 alkene triol derivatives of isoprene; 2-methyl-1,3,4-trihydroxy-1-butene (*cis* and *trans*) and 3-methyl-2,3,4-trihydroxy-1-butene (*m*/*z* 118) (Jardine et al. 2012, Kourtchev et al. 2005, Wang et al. 2005).

It is evident from Figure 3.21 that both the OH• oxidation and ozonolysis experiments show clear distinct sets of monomer products (*m*/*z* 150–280) and oligomeric dimer (*m*/*z* 280–450) and trimer (*m*/*z* > 450) SOA compounds. It is characteristic of laboratory-generated SOA to show distinct dimers, trimers and higher oligomeric compounds compared with ambient aerosol which is highly variable and often shows no highly oligomeric SOA products (Kourtchev et al. 2016a). Previous α-pinene ozonolysis studies using APCI-MS (Müller et al. 2008, Tolocka et al. 2004) and ESI-QTOF (Tolocka et al. 2004) have observed similar dimer regions. This presents EESI-MS as a credible alternative to these ionisation techniques for analysing complex chamber-generated aerosol.

The presence of OH• in the ozonolysis experiments, produced by the ozone, due to no OH• scavenger being used, has resulted in many OH• oxidation products also being present in the ozonolysis SOA. However, there are some differences between the OH•

oxidation and ozonolysis MS spectra in this study. The OH• oxidation appears to show more oligomerisation than the ozonolysis experiments which was also observed in a previous study comparing both types of oxidation (Kourtchev et al. 2015). This is due to different reaction pathways occurring in the two mechanisms producing different oxidation products. Also, the presence of the AVOCs in the OH• oxidation experiments may have contributed to the oligmerisation although AVOCs make a much smaller contribution to the global SOA burden than BVOCs (Kroll et al. 2006).

The intensities of some of the monomers are significantly higher in the ozonolysis experiments than the OH• oxidation experiments which may be consistent with less oligmomerisation occurring via ozonolysis than via OH• oxidation. The fact that more SOA peaks were identified from the OH• oxidation experiments may potentially mean there is a higher risk of competitive ionisation which the previous experiments in this chapter have demonstrated to be an issue for EESI-MS. If this is the case then one might expect to see lower intensities for the OH• experiments than the ozonolysis experiments which is what is observed in Figure 3.21.

The use of isoprene in this study may have affected the distribution of monomers and oligomeric products produced in the CASC. Recent studies have shown isoprene suppresses monoterpene dimer formation and subsequently, the overall SOA yield from OH• oxidation, when present in mixtures of atmospheric vapours, by competing for OH• and preventing it from reacting with the monoterpenes (McFiggans et al. 2019, Lee et al. 2016). Further chamber experiments comparing OH• oxidation and ozonolysis, over different timescales, are required to determine the extent of competitive ionisation in chamber experiments.

Signals at *m*/*z* 357.0875 and *m*/*z* 367.3378 were observed, corresponding to the dimer species pinyl-diaterpenyl ester ($C_{17}H_{26}O_8$, MW 358) and pinonyl-pinyl ester ($C_{19}H_{28}O_7$, MW 368) respectively. A signal at *m*/*z* 343.2539 was also observed, corresponding to either the pinyl-diaterebyl ester or diaterpenyl-terpenyl ester; both of which have the $C_{16}H_{24}O_8$ formula and MW of 344). (Using LC-MS or MS/MS would allow one to identify which ester is present). These dimers have all previously been identified in other *α*-pinene ozonolysis studies (Kristensen et al. 2013, Yasmeen et al. 2010, Müller et al. 2008, Glasius et al. 1999, Kourtchev et al. 2015, Kristensen et al. 2014). Suggested structures for these dimers are provided in Figure 3.22.

Yasmeen et al. 2010 suggested an esterification reaction between *cis*-pinic acid and diaterpenylic acid was responsible for MW 358 dimer, with two possible isomeric disaster structures given that *cis*-pinic acid has two carboxyl groups. An esterification reaction of *cis*-pinic acid and 10-hydroxy-pinonic acid has been hypothesised to produce the MW 368 pinonyl-pinyl dimer (Müller et al. 2008). Formation of the MW 344 dimers is suggested to arise from the esterification of terpenylic acid and diaterpenylic acid (producing the diaterpenyl-terpenyl ester) (Yasmeen et al. 2010) and from diaterebic acid and *cis*-pinic acid (producing the pinyl-diaterebyl ester) (Kristensen et al. 2014).

Many of these dimers have only previously been observed in ozonolysis studies and not via OH• initiated-oxidation. The suggested reason for this is the dimers are produced via the gas phase reaction of a stabilised CI formed through the ozonolysis of α-pinene and are not products of particle phase esterification (Kristensen et al. 2014, Zhang et al. 2015). Recently, however, highly oxygenated molecules (HOMs) have been identified as oxidation products from AVOC and BVOC OH• initiated-oxidation (Ehn et al. 2014, Molteni et al. 2018) and have been found to initiate early particle growth and be major contributors to particle formation (Tröstl et al. 2016). The presence of these dimers in the OH• initiated oxidation experiments, therefore, is very interesting and further experiments are required to determine the formation pathways for these compounds.

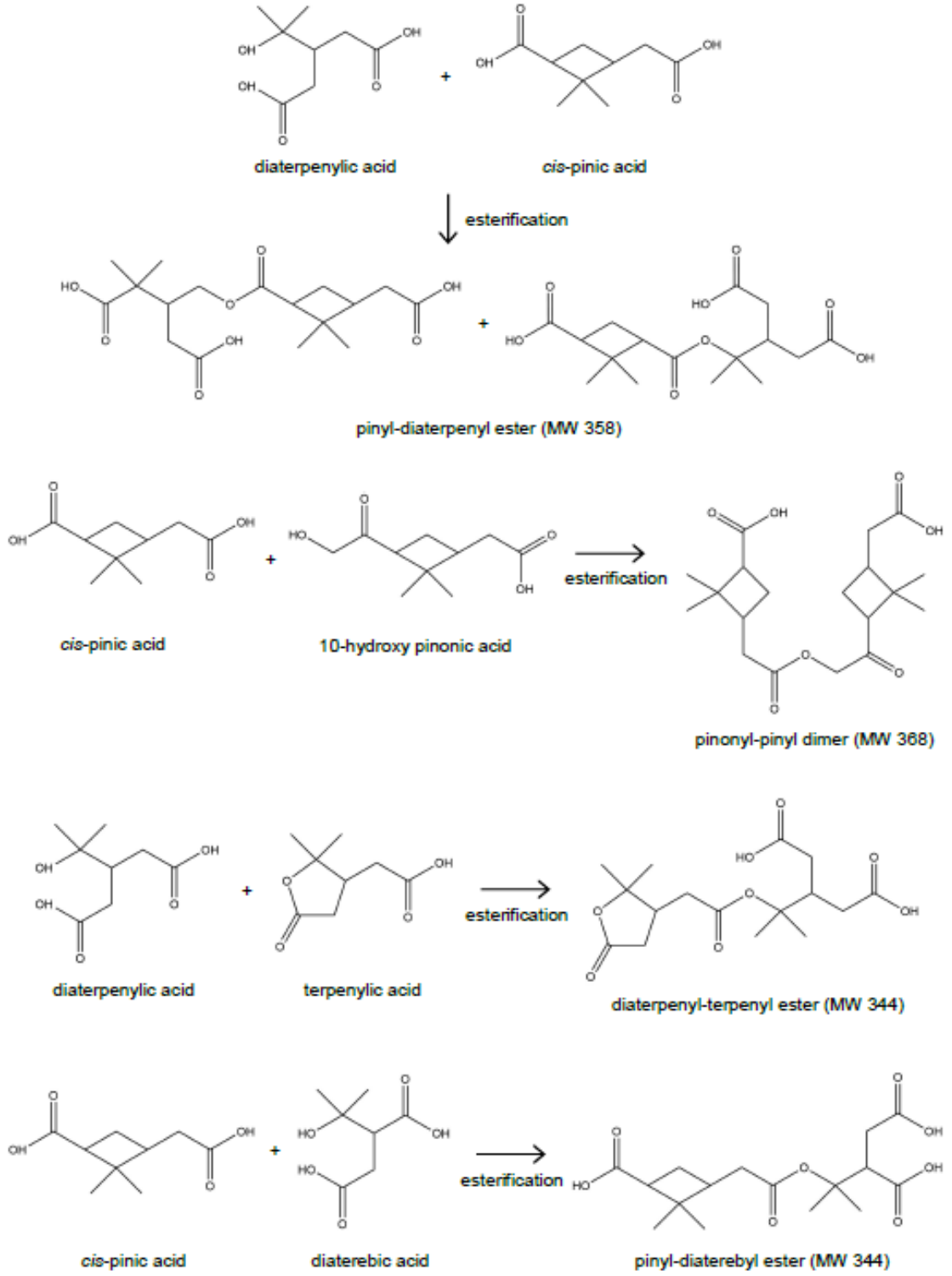

Figure 3.22. Suggested formation pathways and structures for the pinyl-diaterpenyl ester (MW 358) (Yasmeen et al. 2010), pinonyl-pinyl dimer (MW 368) (Müller et al. 2008), diaterpenyl-terpenyl ester (MW 344) (Yasmeen et al. 2010) and pinyl-diaterebyl ester (MW 344) (Kristensen et al. 2014); all observed in the OH-initiated oxidation and ozonolysis CASC experiments.

Figure 3.23 shows the change in MS peak intensity observed from the total ion current (TIC) (A), and for three of the deprotonated peaks; *m*/*z* 183.2507 (CPA) in the monomer region (B), *m*/*z* 311.3366 in the dimer region (C), and *m*/*z* 447.0060 in the trimer region (D), monitored during one of the OH• oxidation of mixed AVOC and BVOC chamber experiments. All of the monitored peaks showed clear, defined changes in intensity that were consistent throughout the experiment. The higher peak intensities in the TIC correspond to periods of aerosol injection into the EESI-MS (blue shading in Figure 3.23 (A)). This trend was observed for many of the monitored dimer and trimer peaks as shown in Figure 3.23 (C) and (D).

However, for many of the monomer peaks including CPA (*m*/*z* 183.2507) in Figure 3.23 (B) and also *cis*-pinic acid (*m*/*z* 185.2507) and *cis*-norpinonic acid (*m*/*z* 169.2504), the intensities were higher during the clean air injection periods than the aerosol injection periods. The higher MS intensity for CPA and other monomers during the clean air injection period suggests that CPA concentrations in the EESI source were higher than what was being extracted from the chamber. CPA residues in the EESI source from previous experiments may be responsible for this and could have influenced the intensities of the CPA during the aerosol injection periods in the chamber experiments. This, again, highlights the need for thorough cleaning of the EESI source between experiments. The decrease in SOA concentration measured using the SMPS during the 65 minute chamber experiment (from ~1900 to ~100 μg/m^3, Figure 3.23 (A)) also contributed to the decrease in intensity difference between the clean air and aerosol injection periods observed for the dimer in Figure 3.23 (C), assuming the same linear relationship between intensity and organic aerosol concentration which was shown in the previous characterisation experiments in this chapter.

The two BVOC ozonolysis experiments used different ozone concentrations. The difference in MS signal intensity between the aerosol injection period and clean air injection period, averaged over the six aerosol injection cycles, was 217% lower for the 183 monomer peak and 10% lower for the dimer peak when lower concentrations of ozone were used. This suggests that the EESI-MS is capable of detecting the changes in SOA MS signal associated with changing concentrations of oxidant, which is useful for longer chamber studies.

Also shown in Figure 3.23 (A) is the total aerosol concentration, measured using the SMPS, during the OH• oxidation of mixed AVOC and BVOC experiment, which

decreased over time due to the wall losses occurring in the chamber. The SMPS measurements made during the chamber experiments showed higher aerosol mass concentrations for the ozonolysis experiments (~1500 µg/m^3 on average) than the OH• oxidation experiments (~1200 µg/m^3 on average). There was also a smaller SOA mass concentration for the ozonolysis experiment which used less ozone (≤ 495 µg/m^3) compared with ≤ 2570 µg/m^3 for the ozonolysis experiment which used more ozone. The chamber experiments lasted for between six and eight hours and the SOA was extracted from the chamber approximately three hours after injection of the H_2O_2 or ozone. By this time, the SOA was more aged and was also being removed via wall losses in the chamber. This may be the cause of the slight decrease in MS signal intensity observed during the chamber experiment for the dimer peak in Figure 3.23 (C).

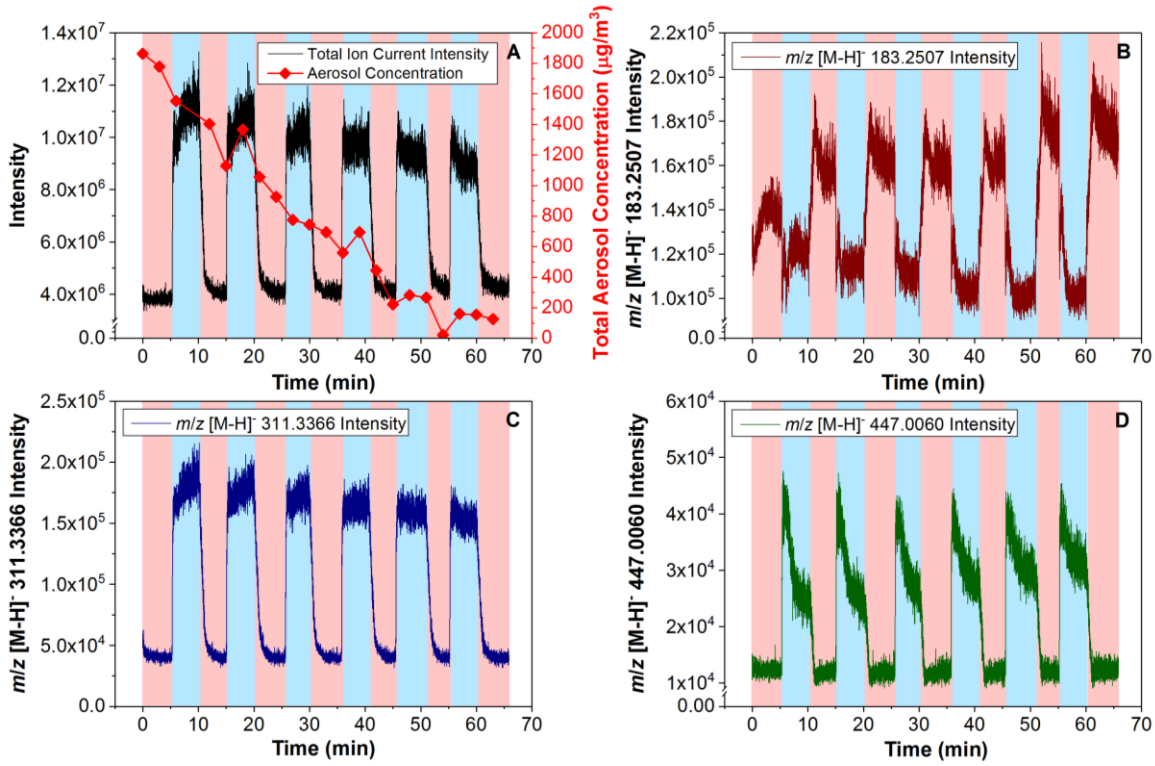

Figure 3.23. (A) Change in (−)EESI-MS Total Ion Current intensity during the six aerosol injection periods (blue shading) compared with the clean air injection periods (red shading) from OH radical oxidation of mixed BVOCs and AVOCs in the CASC. The total aerosol concentration monitored throughout the experiment using the SMPS is also shown (red diamonds). Also included are the peak intensity changes for a (B) monomer ($[M-H]^-$ *m/z* 183.2507), (C) dimer ($[M-H]^-$ *m/z* 311.3366) and (D) trimer ($[M-H]^-$ *m/z* 447.0060) compound detected during the same six aerosol injection cycles in the same chamber experiment.

3.5 Conclusions and Outlook

In the simple mixed organic and inorganic aerosol characterisation experiments, the organic MS signal intensity did not change significantly between inorganic molar percentages of 0–91% AS; with variation remaining within a factor of two. This suggests that salt suppression effects are not significant for EESI when analysing simple mixed organic and inorganic aerosol and that EESI-MS performs better than ESI-MS at analysing aerosol mixtures with high inorganic concentrations. There was also no significant change in the MS intensity for the six tested WSOCs in the complex organic and inorganic characterisation experiments in solutions with ≤ 70% ammonium sulphate solute concentration and at total aerosol concentrations below 200 μg/m^3. At inorganic fractions > 80% and at high total aerosol loadings (> 200 μg/m^3), the ion intensity did increase for some of the WSOCs including glutaric acid although this variability remained within a factor of 2.5. This may indicate that the efficiency of the EESI to extract the total particle mass is reduced at very high aerosol mass loadings which has been suggested in other recent EESI studies. Since these very high inorganic fractions rarely occur in the atmosphere, it can be concluded that the EESI-MS is suitable for detecting organic compounds in complex ambient aerosol from a range of different environments and will not be significantly affected by salt suppression effects.

The increase in organic MS intensity in the WSOC/AS experiments showed a significant positive correlation with the total aerosol concentration measured during the experiments and also with the theoretically calculated organic-weighted aerosol concentrations (up to ~200 μg/m^3 for CPA) which increased unexpectedly during both the CPA/AS and WSOC/AS experiments.

SEM-EDX was used to investigate whether the WSOCs formed an outer coating around an ammonium sulphate inner core but the individual particles were too small for the SEM-EDX to provide accurate enough elemental composition and confirm if this was the case. The SEM did indicate some delayed crystallisation in the aerosol which may have been due to water still being present during aerosol collection. TEM also failed to confirm the presence of an organic coating due to almost instantaneous degradation of the AS in the samples when in contact with the electron beam. This difference in behaviour between organic compounds in simple and complex mixtures highlights the

need for further experiments to understand fully the impact of inorganic compounds on complex organic aerosol.

Another aim of this work was to assess if competitive ionisation was an issue for the EESI source. The complex mixed organic and inorganic aerosol experiments showed that oxalic acid, arabitol and erythritol ionised less effectively than the other carboxylic acids. This suggests some organic compounds are not ionised effectively in complex organic mixtures using EESI when other organic compounds with more ionisable functional groups are present. Competitive ionisation could therefore be a problem for EESI-MS. However, alcohols do not generally ionise as well as carboxylic acids due to their inability to lose a proton as easily so it is not possible to say with certainty if competitive ionisation caused the lower MS intensities for some of the organic compounds. This study highlights some fundamental limitations of using this type of ionisation source to attempt to quantify organic compounds on an absolute level when no suitable calibration standards are available.

The characterisation experiments also show the need for efficient cleaning of the EESI source to avoid residues from sticky organic compounds including CPA which can affect the organic signal intensity of the compounds detected by the EESI-MS. To reduce contaminants in future experiments using this EESI technique, the source must be cleaned thoroughly between experiments.

The results from the CASC experiments are the first to show that EESI-MS can detect complex chamber-generated SOA produced from the ozonolysis and OH• oxidation of mixed BVOCs and AVOCs. Oligomerisation products previously observed in chamber experiments were successfully identified. The EESI-MS also detected changes in organic signal intensity in response to different concentrations of ozone. The EESI-MS chamber measurements in this study took place a few hours after injection of the VOCs into the CASC. It would be interesting to compare these results with the variability of the organic signal detected by the EESI-MS at the start of the chamber experiment, immediately after the injection of ozone or H_2O_2 when there are fewer SOA products and the SOA is less aged.

4 Development of a Solid Phase Extraction (SPE) Method for Extracting Organic Compounds from Ambient Rainwater and Aerosol Samples

4.1 Introduction

4.1.1 The AERORAIN Campaign, León, Spain (June 2015-March 2017)

Researchers at the Department of Applied Chemistry and Physics at the University of León, Spain, sent a selection of rainwater and aerosol filter samples from the AERORAIN Campaign to Cambridge for organic composition analysis using UHRMS. The sampling location in León meant that the ambient samples were exposed to various biogenic and anthropogenic sources and were expected to contain a mixture of organic and inorganic compounds.

The AERORAIN Campaign took place between June 2015 and March 2017 in León in northern Spain. The ground-based project had two main objectives. The first was to

assess the impact of rain on aerosols in the region, and the impact of the aerosol on human health and climate. The second was to assess whether there is a direct link between the presence of allergenic proteins in the atmosphere, and rain or other specific meteorological parameters or physiological characteristics of plants.

The sampling location was the terrace of the Veterinary Faculty at the University of León, Spain (42° 36' 50" N, 5° 33' 38" W) and is shown in Figure 4.1.

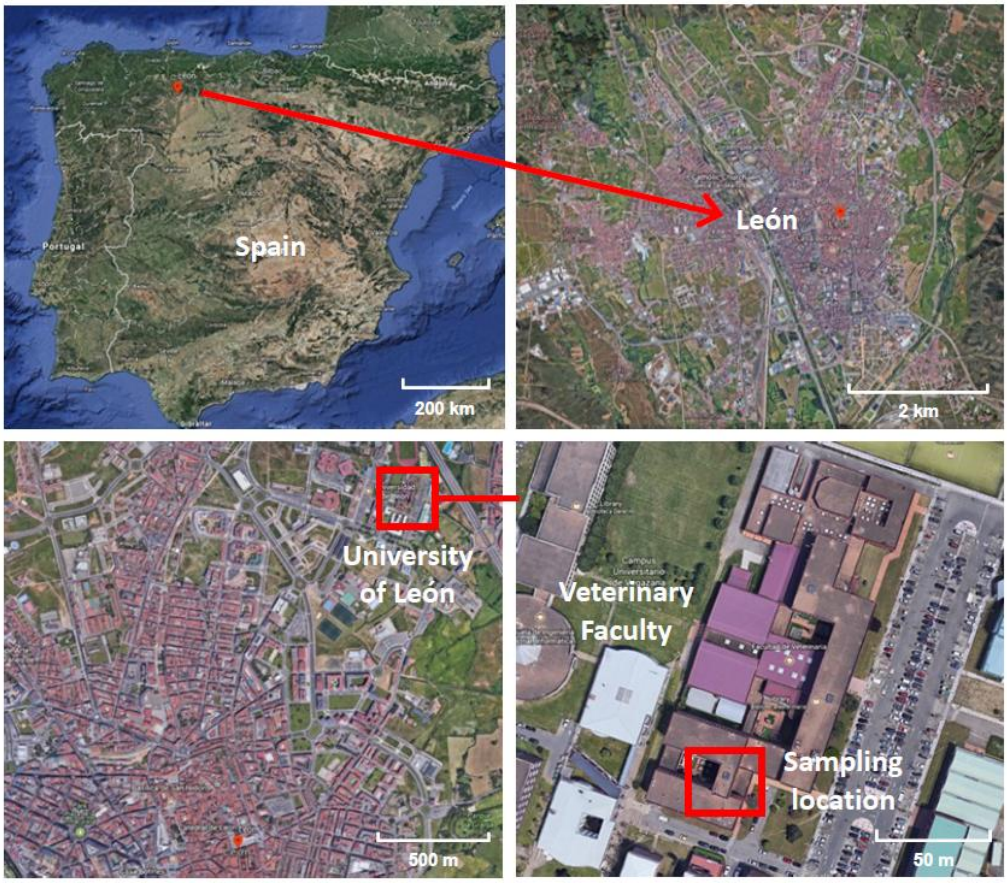

Figure 4.1. AERORAIN campaign sampling location on the roof terrace of the Veterinary Faculty on the campus of the University of León.

A precipitation collector with an automatic open/close system (Laser Disdrometer, Thies) was used to collect rainwater samples when rain events occurred. The vessel used for rainwater collection was a 3.5 L glass bottle which had been previously washed with milli-Q water, and was washed between each different sample collection. After the rain was collected, it was filtered in a sonicated device and frozen for later analysis.

Aerosol was also collected on quartz, teflon and polycarbonate filters before, during, and after rain events. Filters collected during the rain events were collected using a GENT Stacked Filter Unit (SFU) PM_{10} sampler (description of the instrument available

from (Maenhaut, Francois and Cafmeyer 1992) and a Tecora $PM_{2.5}$ mean volume sampling head, only during the period of precipitation. A high volume air sampler (Model CAV-A/mb, MCV, description available at mcvsa.com) was used to collect aerosol every day during the campaign, regardless of whether a rain event occurred that day. These latter filters collected daily aerosol samples for 23.5 hours with a new filter being replaced at 10:00 UTC every day. Once each filter had been removed from the sampler, it was frozen for later analysis.

4.1.2 Solid Phase Extraction (SPE)

Solid Phase Extraction (SPE) is a widely used sample preparation technique for concentrating specific analytes in complex solutions and removing any inorganic salts and other compounds that could suppress the MS ionisation of the organic compounds of interest (Majors 2010). SPE has been used in many previous studies of ambient aerosol composition prior to ESI-MS analysis (Lin et al. 2012b, Thorsten Reemtsma et al. 2006, Schmitt-Kopplin et al. 2010, Wozniak et al. 2008), and LC-MS (Gao et al. 2006). It has also been used to prepare cloud water and fog samples (Mazzoleni et al. 2010b, Zhao, Hallar and Mazzoleni 2013, Cook et al. 2017) and river and coastal waters (Louchouarn, Opsahl and Benner 2000) prior to analysis using ESI coupled with Fourier transform ion cyclotron resonance mass spectrometry (FTICR-MS) and GC-MS.

The most commonly used SPE method for treating environmental samples is disposable plastic cartridges shaped like syringe barrels. They contain sorbent-packing material, designed to retain selected analytes which can then be eluted from the sorbent using a specific elution solvent. The SPE cartridges are available in various sizes, with packing weights between approximately 30 mg to 2 g, and different loading capacities for solvents of different volumes, to suit a range of matrices (Majors 2010).

The principle of Solid Phase Extraction (SPE) is similar to that of HPLC; a stationary phase sorbent material is used to selectively retain analytes of interest from the loaded sample. Chemically bonded silica and polymeric resins such as porous polystyrene are the most commonly used SPE sorbent materials for the stationary phase. Polymer-based sorbents have some advantages over bonded silica. Their packing has a higher surface area, they don’t need to be conditioned as thoroughly, they can be used over an entire

pH range and less eluting solvent and packing is required compared with silica (Huck and Bonn 2000). This also means that the final eluted volumes are smaller with shorter evaporation times. Polymer-based sorbents are also more tolerant to partial drying after the conditioning step without reducing the analyte recovery or reproducibility, and they do not contain silanol (Si-O-H) functional groups so there is less chance of irreversible adsorption of very basic compounds which would then be difficult to recover (Majors 2010).

Once the sorbent type has been selected, an analyte retention mechanism is chosen. There are three different SPE retention mechanisms; *Reversed Phase*, *Normal Phase* and *Ion-Exchange*, each targeting different analyte functional groups. Reversed Phase uses a non-polar stationary phase and is suitable for neutral, non-polar and moderately polar compounds which exhibit hydrophobic interactions, including hydrocarbons and aromatic compounds. Normal Phase uses a polar stationary phase and is suited to polar analytes with hydroxyl (R-OH) and amino ($R\text{-}NH_2$) functional groups. Ion-Exchange is used for compounds that are charged when in solution such as positively charged cations like quaternary ammonium cations (NR_4^+) and amines (RNH_3^+), and negatively charged anions like sulfonate ions (RSO_3^-) and carboxylate ions (RCO_2^-). Analytes are extracted based on electrostatic attraction between the charged functional group on the compound and the charged group on the sorbent surface (Supelco 1998). A typical Reversed Phase SPE method using cartridges is illustrated in Figure 4.2.

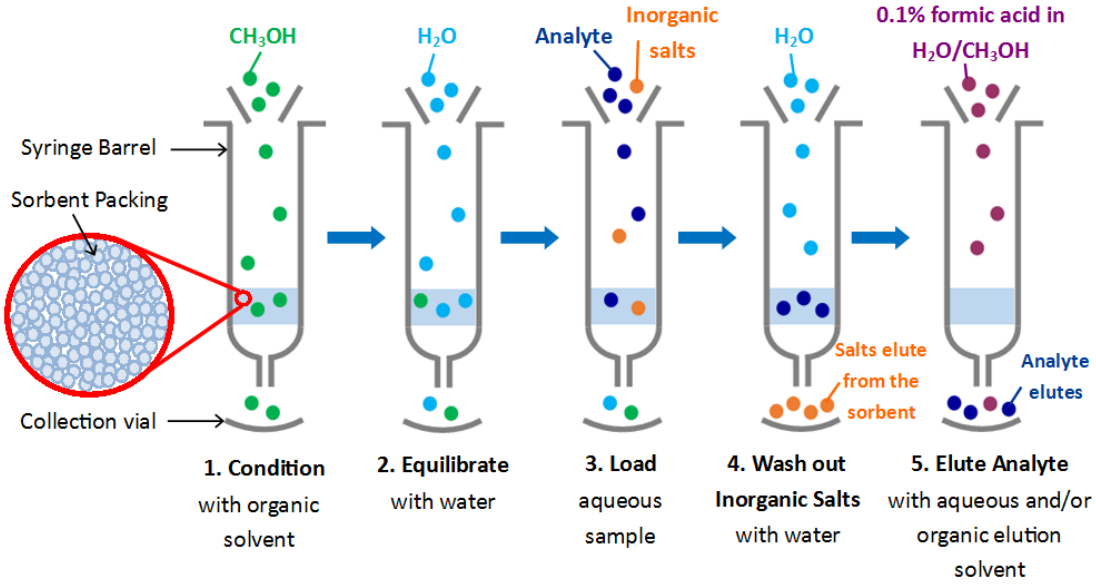

Figure 4.2. An example of a typical Reversed Phase Solid Phase Extraction (SPE) method, using single-use cartridges with polymer-based sorbent, for concentrating analytes in ambient samples. Step 1 is *Conditioning* where a solvent (e.g. methanol or acetonitrile) is applied to remove any contaminants from the cartridge. Step 2 is *Equilibration* where water is added to the cartridge to prepare the sorbent for interaction with an aqueous sample. Step 3 is the *loading* of the sample onto the cartridge at a flow rate of 2-4 ml/min and the analyte functional groups bind with the sorbent functional groups, followed by Step 4 where the sorbent is *washed* with water to remove any inorganic salts. Step 5 is the addition of an elution solvent and the subsequent *elution* and collection of the target analytes for further analysis.

SPE targets specific compounds which ultimately results in the removal of some compounds from the samples. The exact composition of ambient samples is often unknown and they contain many different functional groups so there is a risk of compounds of interest being removed when SPE is applied. To minimise this risk, SPE methods are developed and optimised to ensure they are suitable to be applied to the samples of interest.

There are currently few SPE optimisation studies available detailing the testing of different sorbents and assessing their impacts on the samples they are applied to. Different SPE methods have been compared for preparing surface water (Van De Steene, Mortier and Lambert 2006), wastewater (Balakrishnan, Terry and Toito 2006) and seawater (Komjarova and Blust 2006), primary organic aerosol (Parshintsev et al. 2010) and atmospheric aerosol (Vidal et al. 2012). However, these studies do not discuss the preferential retention and removal of different classes of organic

compounds. The work in this chapter aims to address this shortfall by providing a detailed comparison of the number and type of organic compounds retained using reversed-phase SPE sorbents with different retention mechanisms.

4.2 Aims

A pre-campaign selection of test rainwater samples and aerosol collected on Quartz filters in León, in June 2015, were sent to Cambridge to allow method development for the subsequent analysis of the samples from the main campaign in 2016. The collection dates of the samples analysed in this work are provided in Table 4.1 and Table 4.4.

The specific objectives of this work were to:

- Use the pre-campaign test samples to see if SPE would be an appropriate method for use with the main set of ambient AERORAIN campaign samples.
- Test three different Reversed Phase SPE polymer-based sorbent types and determine which would yield the highest number of analytes from the samples following analysis using UHRMS.
- Develop a suitable SPE method which can be applied to both the rainwater and aerosol samples to ensure identical sample preparation and that the rainwater and aerosol MS analysis results are comparable.

4.3 Methodology

4.3.1 Filter Extraction Method

Before the aerosol samples could have SPE applied, they needed to be extracted from the filters. The following extraction method was used for the test filter samples (Q7, Q9 and Q Blank, details provided in Table 4.1), and later for the 2016 aerosol filter samples.

4.3.1.1 Filter Preparation

Three 21 ml dram glass vials and caps per sample were cleaned thoroughly with methanol (Optima® LC/MS grade, Fisher Scientific or UHPLC/MS grade, Sigma Aldrich) and labelled '*A*', '*B*' and '*C*'. Tweezers and scissors used for handling the filters were also cleaned with methanol and water (Fisher Scientific LC/MS grade) and were left to dry in a fume hood. The filters were trimmed 1-2 mm from the edge to remove any contamination from the filter case or from the impactor during sampling. The filters were then cut into strips, approximately 1 cm in width and no taller than one third of the height of the vial, and were placed in the vials labelled *A*.

4.3.1.2 Filter Sonication

The *A* vials containing filter strips were filled with water (Optima® LC/MS grade, Fisher Scientific) so that the water level just covered the filters (6-7 ml). Water was chosen over methanol as an extraction solvent for the filters to prevent any reactions between the organic compounds in the filters and methanol. Carboynl functional groups have been shown to react with methanol to produce acetal compounds and carboxylic acids specifically have been observed to produce esters upon reaction with methanol (Bateman et al. 2008). Similarly, acetonitrile was not used in the extraction because it often contains more contamination ions than methanol which can reduce the ionisation efficiency of the sample ions in direct infusion analysis (Kourtchev et al. 2014b). Water was, therefore, a more appropriate extraction solvent for these rainwater and aerosol samples and water was also more compatible with the SPE method which followed.

The vials containing the filters were agitated in an ultrasonication bath (MXB6, Grant Instruments Ltd), filled with iced water to prevent the temperature rising above 10 °C. After the vials were sonicated for 30 minutes, the liquid was decanted into the vials labelled *B* and the *A* vials were refilled with 6-7 ml of water, sonicated for a further 30 minutes and the liquid decanted into the *B* vials. This was repeated so each sample underwent three rounds of sonication. To ensure as much sample was extracted from the filters as possible, a syringe (5 ml Luer Lock, Supelco) was used to press the filter pieces against the sides of the vials and transfer the remaining extract from vial *A* into vial *B*. Finally the filter pieces in the *A* vials were vortexed (TopMix FB15024, Fisher Scientific) in short bursts for a few seconds, using 1 ml of water, to extract any

remaining sample, but not for so long that the filters started to disintegrate. This final extract volume was transferred into the *B* vials using the syringe.

4.3.1.3 Filtration

The extracts in the *B* vials were filtered using a 0.45 µm pore sized PTFE filter (Supelco Iso-Disc 4 mm) filter on a 5 ml syringe (Supelco Gas Tight Luer Lock). Each filter was cleaned before use with the samples using water (Optima LC/MS, Fisher Scientific). Starting with the blank filter, the filtrates were deposited directly from the syringe into the clean *C* vials and a different filter was used for each sample. Once all of the extracts had been filtered, 1 ml of water was added to the *B* vials and they were vortexed to remove any filtrate on the inside wall of the vial. This remaining filtrate was transferred to the *C* vials.

The filtrates in the *C* vials were split into four equal, approximately 5 ml sub-samples. Three of the sub-samples underwent different SPE methods described in 4.3.2 and the fourth sub-sample had no SPE applied, as shown in Table 4.1, in order to assess the impact of SPE on the samples. Once the 'SPE' extracts had been collected, they were evaporated down to 1 ml using a custom built evaporation unit which gently passed nitrogen over the samples while they were heated at 30 °C on a hot plate. The 'No SPE' samples were also evaporated to 1 ml. All of the concentrated filtrates were then vortexed for a few seconds to re-suspend the solution. The samples were then filtered a second time using a PTFE filter with a 0.20 µm pore size (Supelco Iso-Disc 4 mm) attached to a 1 ml syringe (Supelco Gas Tight Luer Lock) and they were filtered directly into 2 ml LC vials which were cleaned beforehand with methanol and water. 500 µl of water (Optima LC/MS, Fisher Scientific) was then added to the *C* vials and vortexed to collect any remaining sample on the inner vial walls and was transferred to the LC vial. The filtrates were then evaporated further to 200 µl and transferred into 350 µl glass inserts (29441-U, Supelco), which were cleaned with methanol beforehand, to make it easier to collect the sample during the direct infusion MS analysis. The whole filtration process is summarised in Figure 4.3.

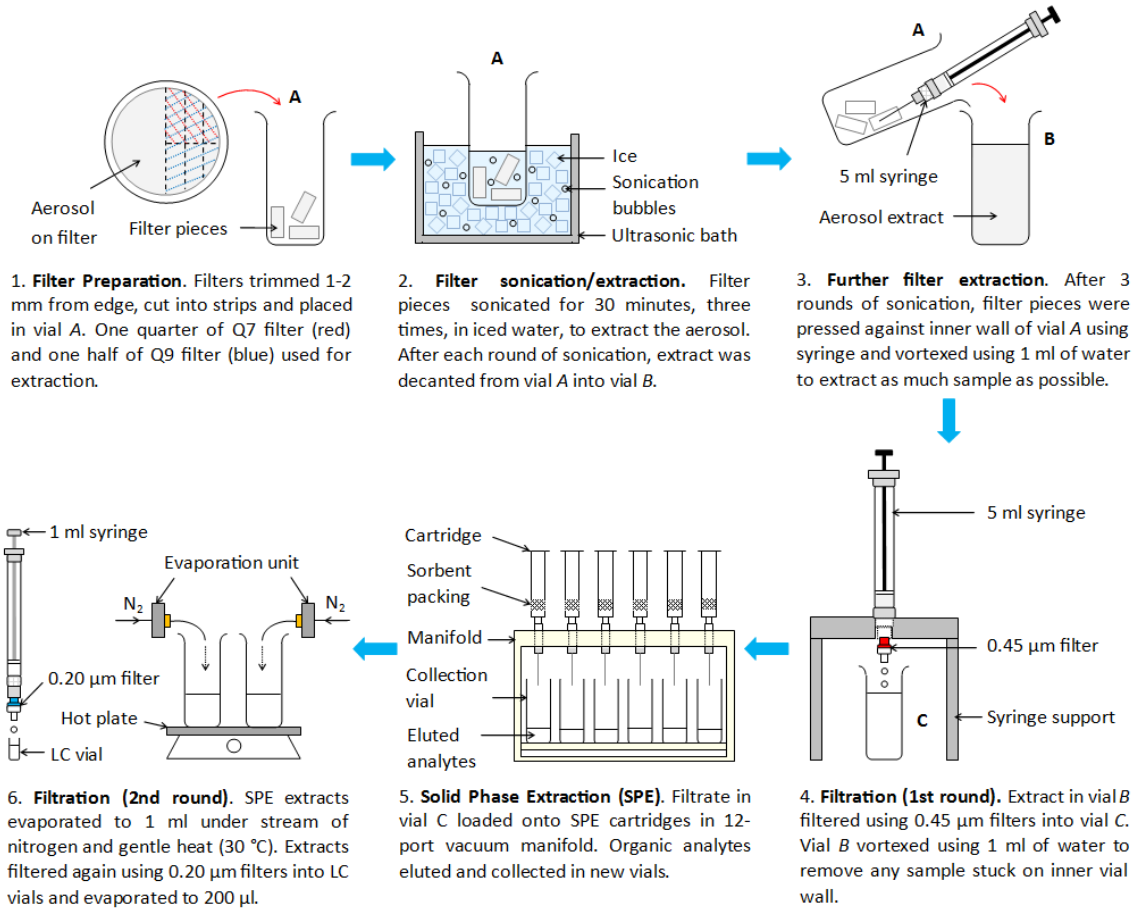

Figure 4.3. Filter extraction method used for the test aerosol samples. Filters were cut into pieces and transferred into a vial (Step 1) and underwent three rounds of sonication, each lasting 30 mins (Step 2). A syringe was used to press the filter pieces against the vial inner wall after sonication to yield as much extract as possible (Step 3). After the first round of filtration (Step 4), the filtrates were split into four ~ 5 ml sub-samples. Three sub-samples underwent SPE and the fourth 'No SPE' samples skipped Step 5 and were evaporated and filtered a second time (Step 6). (*A*, *B* and *C* refer to the vials used during the procedure. *LC* = Liquid Chromatography).

4.3.2 SPE Method Development

4.3.2.1 Comparison of different SPE sorbents

SPE needed to be applied to the rainwater samples to reduce the sample volume from approximately 20 ml to 200 µl prior to direct infusion Nano-ESI-MS analysis, and also to increase the concentrations of the analytes. Since one of the aims of this work is to

develop a sample preparation method which will allow the rainwater and aerosol samples to be directly comparable, the same method must be applied to both the rainwater and aerosol samples. The exact composition of the ambient samples from León was unknown but they were likely to have been influenced by forest, marine and urban sources. Carboxylic acids, organosulphate and nitrate functional groups were predicted to be present due to the presence of monoterpenes and industrial emissions surrounding the sampling site.

Three different polymer-based SPE sorbents were tested using the test aerosol samples in Table 4.1 to see which sorbent retained the highest number of compounds. The total aerosol mass loadings and collection dates for the PM_{10} test aerosol samples used are provided in Table 4.1. Organic aerosol has been estimated to contribute between 20-90% of total aerosol and specifically, 40–60%, for European urban-influenced areas like León (Jimenez et al. 2009, Dzepina et al. 2015). Therefore a conservative estimate of 50 % was made for the contribution of organic aerosol within the total aerosol mass loading on the León filters.

It was estimated in a previous study of ambient aerosol (Kourtchev et al. 2016a) that a concentration of 0.2 µg/µl in the final sample extract was the minimum organic carbon (OC) concentration necessary to obtain a reliable MS signal in the LTQ Orbitrap Velos MS instrument which was to be used for the analysis of the rain and aerosol samples in this study. The target final volume for both the rainwater and aerosol samples was 200 µl; a manageable volume for use with LC-MS. To obtain at least 0.2 µg/µl of organic carbon in 200 µl, ¼ of the Q7 filter was used for extraction which was calculated to produce 0.30 µg/µl of organic carbon. For the Q9 filter which contained approximately 50% less OC than Q7, half of the Q9 filter was used for extraction which was calculated to produce 0.34 µg/µl. The Q Blank filter was slightly smaller in diameter and the whole filter was used for extraction. The remaining parts of the Q7 and Q9 filters were returned to the freezer for later analysis.

Table 4.1. Two aerosol PM_{10} samples and a blank sample collected on quartz filters in June 2015 were used for Solid Phase Extraction (SPE) method development. (OC = Organic Carbon). Three different Strata-X™ sorbent types were tested.

Sample Name	Collection Date(s)	Total aerosol mass loading (mg)	Estimated OC mass loading (mg)	SPE - 100 mg / 6 ml tubes			No SPE
				Strata-X	Strata-X-A	Strata-X-AW	
Q7	09.06.15	0.48	0.24	✓	✓	✓	✓
Q9	14.06.15	0.27	0.135	✓	✓	✓	✓
Q Blank	-	-	-	✓	✓	✓	✓

Once the Q7, Q9 and Blank filters had been filtered the first time using the 0.45 µm filters, the filtrates in vial *C* were split into four sub-samples. Three of these sub-samples had SPE applied, each with 100 mg of a different polymer-based Strata-X™ sorbent in a 6 ml SPE tube (Phenomenex®), and the fourth sub-sample was prepared without SPE. The SPE tube manufacturer (Phenomenex 2011) recommended polymer-based sorbents for aqueous samples. A comparison of the structures of the different Strata-X sorbents is provided in Table 4.2. The Strata-X sorbent uses reversed phase retention and is suitable for neutral, non-polar to mildly polar compounds which exhibit hydrophobic interactions. This includes most carboxylic acids excluding very short carbon chained acids like oxalic acid. The Strata-X-A sorbent uses strong anion exchange and reversed phase retention mechanisms and is suitable for strong acids. Strata-X-AW uses weak anion exchange and reversed phase retention and is suitable for weak acids. Both of these latter sorbents are suitable for charged compounds including potential organosulphates present in the León samples. However, it was unknown if either of these would be more effective for the ambient samples than Strata-X so they were both tested.

The SPE methods used for the three different SPE sorbents are shown in Table 4.3. The SPE methods for the samples were developed using the Phenonenex® Solid Phase Extraction Method Development Guide (Phenomenex 2015) as a starting point. They were then adapted using the SPE methods described in other studies which used Strata-X sorbent to analyse organic aerosol (Dzepina et al. 2015) and (Mazzoleni et al. 2012a), fog samples (Mazzoleni et al. 2010b), and cloud water samples (Zhao et al. 2013). The main changes made to the recommended Phenomenex general method were that water

replaced methanol as the wash solvent and the elution solvent was a mixture of water and methanol in a 1:9 ratio as opposed to methanol.

The recommended wash and elution volume for the 100 mg sorbent mass was 2 ml (Phenomenex 2011) and all of the methanol and water used in the methods were of Optima LC/MS or UHPLC/MS grade. The SPE cartridges were used with a 12-port Vacuum Manifold (Visiprep™) so that the different SPE methods could be run simultaneously and the eluent from the SPE was allowed to flow under gravity at a flow rate of 1–2 ml/min. Disposable flow control valve liners (Visiprep-DL 57059, Supelco) were used in the manifold to transfer the eluent from the SPE tube to the collection vial and prevent any contamination occurring within the manifold.

The SPE methods in Table 4.3 yielded approximately 2 ml of eluted analytes per sample. These were evaporated to 1 ml which took approximately 1 hour and filtered a second time into LC vials. Finally, the samples were evaporated to 200 µl which took another hour due to the small surface area of sample in the LC vial. All of the aerosol samples were then placed in the freezer until required for MS analysis.

Table 4.2. Three different Solid Phase Extraction (SPE) polymer-based sorbent types tested to see which yielded the highest number of analytes from the extracted aerosol test samples, collected prior to the main AERORAIN campaign, in June 2015. 6 ml Phenomenex® Strata-X™ tubes with 100 mg of each sorbent were used.

Sorbent	Functional Group	Mode	Analyte
Strata-X	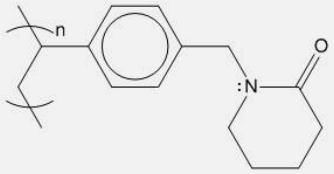	Reversed Phase	Polar and Non-Polar
Strata-X-A	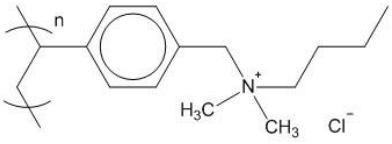	Reversed Phase and Strong Anion-Exchange: di-methylbutyl quaternary amine ligand	Strong acids
Strata-X-AW	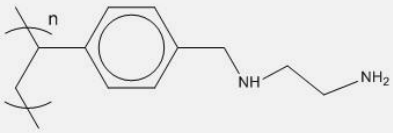	Reversed Phase and Weak Anion-Exchange: di-amino ligand	Weak acids (including sulphonic acids)

Table 4.3. SPE methods used with 6 ml 100 mg SPE tubes for each of the Strata-X, Strata-X-A and Strata-X-AW polymer-based sorbents.

	Step	Strata-X	Strata-X-A	Strata-X-AW
1	Condition	2 ml methanol	2 ml methanol	2 ml methanol
2	Equilibrate	2 ml water	2 ml water	2 ml water
3	Load	Dluted sample	Dluted sample	Dluted sample
4	Wash	2 ml water	25 mM ammonium acetate buffered, pH 6-7 2 ml water	25 mM ammonium acetate buffered, pH 6-7 2 ml water
5	Elute	2 ml of [2% formic acid in 1:9 ratio of water : methanol]	2 ml of [5% formic acid in 1:9 ratio of water : methanol]	2 ml of [5% formic acid in 1:9 ratio of water : methanol]

4.3.2.2 Comparison of sample preparation with and without SPE.

Previous studies had indicated that SPE may result in the removal of very small compounds including oxalic acid and also specific functional groups (Surratt et al. 2008, Gao et al. 2006). To test if this would be the case for the León samples, part of each test aerosol sample (Q7, Q9 and the Blank) were prepared using SPE and part were prepared without SPE but were otherwise prepared identically to allow a direct assessment of the impact of SPE on the number and distribution of organic functional groups in the samples.

The method for this comparison was as follows. When the samples were split into four following the first round of filtration, three of the sub-filtrates had SPE applied with the three different sorbents, while the fourth sub-filtrate from each sample did not have SPE applied. These 5 ml 'No SPE' sub-filtrates were evaporated down to 1 ml which took approximately 1 day; much longer than the 'SPE' filtrates from the same sample because they were aqueous based and not methanol based. The 'No SPE' filtrates were then filtered a second time, using the 0.20 µm filters, into a LC vial, and were evaporated, again, down to 200 µl.

A limitation of the method for testing the different SPE sorbents was that the two test aerosol samples were split into four, which diluted the sample concentration. This may have resulted in fewer compounds being detected by the MS and a potentially altered compound class distribution compared with an un-split sample. This in turn may have made the comparison between the different SPE sorbents and the comparison between the 'No SPE' and the SPE sorbent sub-samples more difficult.

To see if this was the case, the remaining ¾ of the Q7 filter and ½ of the Q9 filter which were not extracted for the SPE sorbent comparison, were extracted using the method in 4.3.1 and had no SPE applied to see how many compounds were detected without splitting the sample. The results from this un-split 'No SPE' sample would then be directly comparable with the split 'No SPE' sub-sample.

The test rainwater samples were also used to provide a "SPE versus No SPE" comparison. The rainwater sample volumes ranged from 9 ml to 24 ml as shown in Table 4.4. The test rainwater samples were tested in two batches. The first batch of rainwater samples; R1–R6, Blank 1 and Blank 2, were pre-campaign samples collected in June/July 2015. The Dissolved Organic Carbon (DOC) measurements made in León indicated that the organic carbon content was quite low in some of these samples. These

samples were used as a fundamental test to see if the Strata-X SPE sorbent would yield sufficient organic compounds in the rainwater samples following MS analysis. The samples in Batch 1 were not split in case this diluted the organic content too much and resulted in too few compounds being detected by the MS.

12 ml SPE tubes containing 1 g of Strata-X sorbent (Phenomenex®) were used for Batch 1 of the rainwater samples. These tubes had a larger volume and higher sorbent mass than the 6 ml tubes used for the aerosol samples because the rainwater sample volumes were much larger. Eight bed volumes of conditioning, equilibration and elution solvents were recommended for these tubes (Phenomenex 2011) which was 20 ml. The SPE tubes were used with the same Vacuum Manifold which was used for the test aerosol samples and the flow rate did not exceed 5 ml/min. Each SPE tube was conditioned with 20 ml of methanol (UHPLC/MS grade, Sigma Aldrich) and then equilibrated with 20 ml of water (LC/MS grade, Fisher Scientific). The sample was loaded into the tubes directly from the original sample bottles to avoid contamination, having first been vortexed briefly to ensure the sample was well mixed. The SPE tubes were then washed with 20 ml of water to wash out inorganic salts and 20 ml of 0.1 % formic acid in a 1:9 solution of water and methanol was used to elute the analytes which yielded approximately 20 ml of extracted analytes. This SPE method was very similar to that recommended for the Strata-X sorbent (Phenomenex 2015). Water was used to wash the sorbent instead of methanol and less formic acid was used to elute the rainwater analytes compared with the Strata-X method used for the aerosol samples in Table 4.3. These changes were made to align this method to previous studies using Strata-X to elute organic compounds (Dzepina et al. 2015, Mazzoleni et al. 2012b, Zhao et al. 2013) which used less formic acid than the Phenomenex recommendation.

Table 4.4. Test Rainwater samples from 2015 used for the Solid Phase Extraction (SPE) method development. Batch 1 were tested to determine if SPE would retain sufficient organic compounds which could be detected by the MS. Batch 2 samples were split into two with one half being prepared with SPE and the other half without to determine how SPE influenced the number and distribution of organic compounds detected by the MS. (*DOC* = Dissolved Organic Carbon).

	Sample Name	Collection Date(s)	Sample Volume (ml)	DOC (mg/l)	SPE with Strata-X		No SPE
					1 g/ 12 ml	100 mg/ 6 ml	
Batch 1	R1	04.06.15	22	5.73	✓		
	R3	05.06.15	9	9.23	✓		
	R4	10.06.15	24	4.56	✓		
	R5	14.06.15	23	1.33	✓		
	R6	31.07.15	20	8.32	✓		
	Blank 1	-	20	-	✓		
	Blank 2	-	21	-	✓		
Batch 2	R47	05.07.16 – 06.07.16	9*	3.07		✓	✓
	R50	25.08.16 – 26.08.16	11*	11.02		✓	✓
	Blank R37	-	10*	-		✓	✓
	Blank R38	-	11.5*	-		✓	✓

*Volume of sub-sample after splitting

The second batch of rainwater samples; R47, R50 and blanks R37 and R38, were collected in summer 2016 during the main AERORAIN campaign. R47 and R50 were approximately double the volume of other rain samples collected during this period so these two samples, and the two blanks, were split into two sub-samples of equal volume. One sub-sample had SPE applied and the other one did not to provide a "SPE versus no SPE" comparison for the rainwater samples, like the aerosol samples. Note the sample volumes for R47, R50 and blanks R37 and R38 in Table 4.4 are the volumes following splitting and these are the volumes which were loaded onto the SPE tubes. Since these volumes were smaller than Batch 1, smaller Strata-X SPE tubes were used (100 mg / 6 ml**,** Phenomenex) and the method was changed slightly to increase the amount of formic acid in the elution solvent to make sure the analytes would be acidified sufficiently to be ionised in negative mode $[M-H]^-$ in the MS. The SPE method for the 'SPE' sub-samples of Batch 2 was the same as the Strata-X method used for the aerosol samples in Table 4.3.

The eluted analytes for both batches were then evaporated to 1 ml. The evaporation time was approximately eight hours for Batch 1 of the SPE-eluted rainwater analytes and approximately one hour for Batch 2. The 'No SPE' sub-samples from batch 2 were evaporated from their initial volumes in Table 4.4 down to 1 ml which took approximately three days and the samples had to be frozen overnight between the evaporation periods. This significant difference in evaporation time highlighted why SPE was necessary because evaporating multiple aqueous samples for the main AERORAIN campaign without applying SPE, would have extended the sample preparation time by many weeks. The use of SPE greatly reduced the evaporation time because the eluted analytes were in a predominantly methanol-based solvent which was much more volatile than the aqueous sample and also because the final eluted extract volume was much smaller so took less time to evaporate than the initial sample volume. Once the eluted analytes were evaporated, they were filtered a second time as described in 4.3.1.3 and evaporated further to 200 µl ready for MS analysis.

4.4 Analysis via nanoelectrospray ionisation (Nano-ESI) using Advion TriVersa NanoMate®

The rainwater and aerosol samples were analysed using an UHR LTQ Orbitrap Velos Mass Spectrometer (Thermo Fisher, Bremen, Germany) equipped with a TriVersa NanoMate® chip-based ESI source (Advion Biosciences, Ithaca NY, USA). The ESI chip® consists of 400 nanoelectrospray nozzles in a silicon chip. A robotic arm takes an aliquot of a sample from a sample plate using a fresh pipette tip. The tip engages with the back of the ESI chip, positioned in front of the MS inlet, and a high voltage is applied to the tip. Nanoelectrospray ionisation (Nano-ESI) is initiated and the ions are sprayed into the MS (Advion 2017). Figure 4.4 illustrates the coupling between the ESI chip and MS inlet. For this work, 16 µl of each sample was loaded onto the sampling plate. The sample volume injected onto the chip was set at 5 µl and the gas pressure and voltage were set at 0.7 psi and 1.4 kV respectively.

When using negative ionisation mode, it is necessary for the sample to have a minimum proportion of organic solvent to achieve a stable spray (Advion 2009). Since the 100 µl rainwater and aerosol samples were effectively entirely aqueous, 233 µl of methanol

(UHPLC/MS grade) was added to them to obtain a final solvent ratio of 30% aqueous and 70% methanol. This solvent composition was found to achieve a good stable spray.

A *m*/*z* calibration was carried out on the NanoMate in negative mode using Pierce™ ESI Negative Ion Calibration Solution (Thermo Scientific, UK) and the spray was optimised using a solution of 20 ng/µl glutaric acid (99%, Sigma-Aldrich), 20 ng/µl deuterated succinic acid (Succinic acid-2,2,3,3-d_4, 98%, Sigma-Aldrich) and 20 ng/µl salicylic acid (ACS reagent, ≥ 99%, Sigma Aldrich). To ensure ions at the upper or lower end of the large mass range (*m*/*z* 50–1000) were detected precisely, two *m*/*z* scan ranges were used for each sample and blank; 60–550 and 150–900 (Ranninger et al. 2016). Three MS measurements, each of one minute duration, were acquired for each scan range. This provided six spectra and approximately 240 mass spectral scans in total per sample and blank.

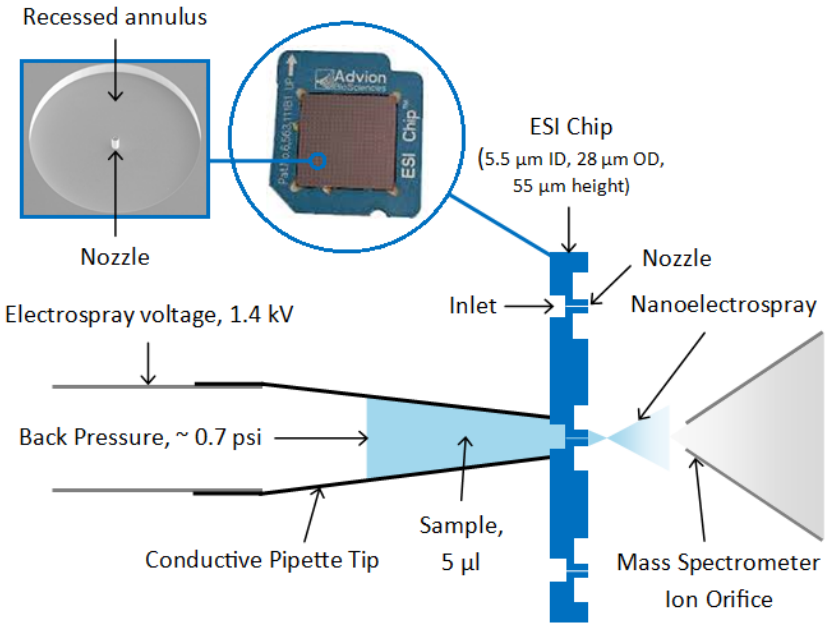

Figure 4.4. Coupling between an ESI chip and Mass Spectrometer inlet on a TriVersa NanoMate in chip-based infusion mode. *ID* = inner diameter, *OD* = outer diameter. Schematic adapted from (2010).

4.5 Data Processing for ESI-MS data

Analysing the León samples with soft ionisation like ESI coupled with high resolution mass spectrometry allows molecular assignment of compounds based on their *m/z* ratio and identification of functional groups within the sample. To achieve this, however, requires substantial data processing of a large amount of raw MS data.

The processing method used for the rainwater and aerosol MS data was conducted using *Xcalibur* software followed by a series of Mathematica 10 (Wolfram Research Inc., UK) codes. The process is outlined below, in three stages, and is described in full in (Zielinski et al. 2018). This processing technique, in both its entirety or aspects of it, has been applied and adapted for processing various complex atmospheric samples (Kourtchev et al. 2013, Kourtchev et al. 2016b, Kourtchev et al. 2015, Kourtchev et al. 2014a, Kourtchev et al. 2014b) and with the use of different ionisation techniques including Liquid Extractive Surface Analysis (LESA) of aerosol (Fuller et al. 2012) and flower petals (Giorio et al. 2015).

4.5.1 Data Pre-treatment

Xcalibur software was used for pre-treating the rainwater and aerosol raw data from the Orbitrap MS. For each MS measurement, approximately 80 scans were averaged into one mass spectrum and a maximum of 40 different potential formulae assignments per single *m*/*z* value were allowed. The maximum mass error was set to ± 5 ppm. The following constraints on the maximum number of elements allowed for each formula assignment were applied; $1 \geq {}^{12}C \leq 100$; $0 \geq {}^{13}C \leq 1$; $1 \geq {}^{1}H \leq 200$; $1 \geq {}^{16}O \leq 50$; $0 \geq {}^{14}N \leq 20$; $0 \geq {}^{32}S \leq 2$; $0 \geq {}^{34}S \leq 1$. The list of formulae assignments and their associated intensities for each MS measurement were exported as a *.csv* file for further data processing.

4.5.2 Main Processing of data

4.5.2.1 Noise and mass shift

The first processing code estimated the noise level in the mass spectra based on the fit of the mean, plus three standard deviations, of the lowest intensity peaks in each MS spectrum. The noise intensity is often characterised by a bimodal distribution as shown in Figure 4.5 from (Zielinski et al. 2018), with the first and dominant mode corresponding to peaks associated with thermal noise and the second mode corresponding to chemical noise including shoulder ion peaks next to high intensity peaks. It is difficult to discriminate between high intensity noise and sample analyte peaks with low intensities and as such, the first mode is used to estimate the noise level as indicated by the red line in Figure 4.5.

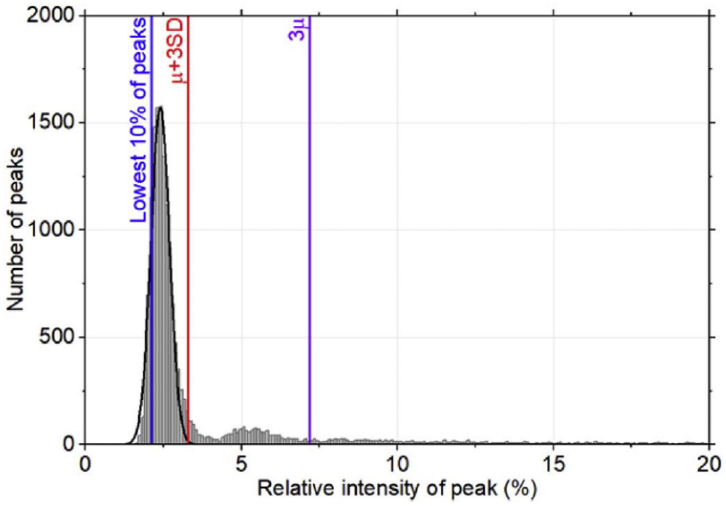

Figure 4.5. Schematic taken from Zielinksi et al., 2018 showing an example of a sample intensity histogram used for noise level estimation. A bimodal distribution is observed for the noise intensity; the first mode is associated with thermal noise and the second mode is associated with chemical noise. The noise level (red line) is set to the mean plus three standard deviations of the fitted curve (black) for the first mode. The purple line is three times the mean in samples with insufficient replicates for common ion comparisons and the blue line is an additional noise level, below which 10% of all peaks reside.

An estimation of the overall mass shift for each spectrum was made based on the measured mass errors calculated using Xcalibur, for a list of 20 reference compounds (provided in Table F, Appendix F) which were expected to appear in the sample or solvent. The mass shift calculation provided an upper and lower mass shift limit and an

additional 0.5 ppm was added to the upper and lower limits to provide a more conservative approach. Any formulae assignment proposed for a sample peak in the Xcalibur software which had mass errors lying outside of these mass shift limits was not assigned to that peak. The second Mathematica data processing code used the identified noise levels and mass shift to remove formulae assignments from the sample dataset which did not lie within the defined lower and upper limits.

4.5.2.2 Blank Subtraction and element ratio filters

The purpose of blank subtraction is to remove any peaks from the sample spectra that are also present in the blank spectra. The second processing code uses a sample to blank ratio to assess if the sample and blank peaks are statistically equivalent. Two checks are performed to establish if this is the case. The first check determines if the sample and blank are within one standard deviation of one another using the mass shift parameters calculated previously and a two sample *t*-test. If they are within one standard deviation, like the blank peaks 1 and 2 in Figure 4.6, taken from Zielinski et al. 2018, a second check determines if the sample peak intensity to blank peak intensity ratio is above a certain sample to blank intensity limit as indicated by the dashed line in Figure 4.6. For the León samples and for other studies using this data processing method, the sample to blank ratio was set as 10. If the blank peak is above this level (like blank peak 1 in Figure 4.6) then the sample peak will be removed from the dataset as it is deemed to be the same compound that is present in the blank. Conversely, if the blank peak is below the sample to blank ratio, the sample peak is believed to represent a different compound from that in the blank and is left in the dataset. Similarly, if the sample contains significantly more of the particular peak than the blank does, then the peak remains in the dataset (like blank peak 2 in Figure 4.6).

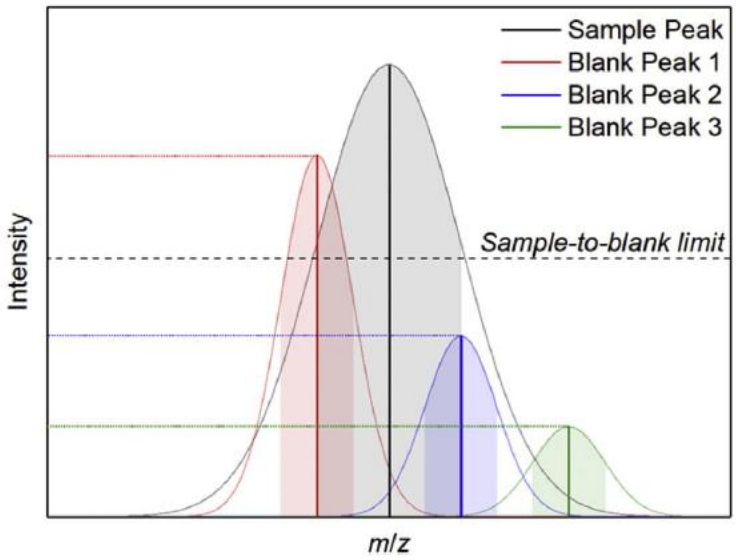

Figure 4.6. Schematic taken from Zielinski et al., 2018 illustrating the blank subtraction process. The sample peak (black) is compared to nearby blank peaks (red, blue, green). If the sample peak and blank peak are within one standard deviation of each other (shaded region) like blank peaks 1 and 2, a second check determines if the sample intensity to blank intensity ratio is above a certain limit. If it is, as is the case for blank peak 1 (red), the sample peak is removed from the dataset. If the blank peak is below the sample to blank ratio or if the sample contains significantly more of the peak than the blank does, like blank peak 2 (blue), then the sample peak remains in the dataset.

In addition to the blank subtraction, the second processing code also applies filters for ratios of particular elements, excluding those which are unlikely to occur naturally in the environment. Any ratios falling outside of these criteria were excluded; $0 \geq O/C \leq 2$, $0.3 \geq H/C \leq 2.5$, $N/C \geq 1.3$ and $S/C \geq 0.8$. The formulae were also checked for the presence of ^{13}C and ^{34}S isotopes. Any formulae containing these heavy isotopes were checked for matching compositions containing the ^{12}C and ^{32}S counterparts. If the $^{12}C/^{13}C$ ratio exceeds 1.1% or the $^{32}S/^{34}S$ ratio exceeds 4.5%, the assignment is deemed to be incorrect and is removed but the peak remains and the assignment with the next smallest mass error is used.

Any molecular assignments with negative or non-integer Double Bond Equivalence (DBE) values were removed from the dataset. DBE represents the sum of rings and double bonds in a molecule and is a measure of the degree of unsaturation in the compound (Wozniak et al. 2008). Neutral molecules have integer DBE values (Koch et al. 2006). Charged molecules and radicals have non-integer values. DBE is calculated using the following equation:

$$\mathrm{DBE} = 1 + \frac{\mathrm{H}}{2} + \frac{\mathrm{N}}{2} + \frac{\mathrm{S}}{2} + \mathrm{C}\,, \tag{4.1}$$

where *C, H, N* and *S* correspond to the number of carbon, hydrogen, nitrogen and sulphur atoms in any given formula assignment (Kourtchev et al. 2013). The formulae assignments were also checked using the nitrogen rule which states that neutral compounds with odd nominal molecular masses have odd numbers of nitrogen (Kind and Fiehn 2007). Any compounds which did not follow this rule were removed from the list of peaks.

4.5.2.3 Common Ions, Shoulder Peaks and combining of spectra

Once the sample spectra have been processed, the three MS measurements for each scan range are compared for common ions. Any peaks which do not exist in all three of the replicate mass spectra are removed and the intensities of the remaining peaks, present in all of the replicates, are averaged into one spectrum output. At this point there are now two spectra per sample; one for each scan range. Any shoulder peaks, which are low intensity peaks bordering a high intensity peak, are removed from these spectra. Shoulder peaks are noise signals produced by mass spectrometers as artefacts from the Fourier transform function calculation. Their intensity is usually less than 5% of the intensity of the main *m*/*z* peak (Pluskal et al. 2010). After shoulder peak removal, the two spectra from the two different scan ranges are joined together to produce one combined spectrum per sample and any duplicate formulae assignments are removed. This produces the final spectrum.

4.6 Different approaches for blank subtraction

At the blank subtraction stage of the data processing, the Mathematica code requires one blank MS spectra to be subtracted from each sample MS spectra of the same scan range. Different research groups have their own “in house” data processing methods for MS data and details of these methods are rarely included in published studies. There is currently no standard protocol for blank subtraction regarding the quality of the blank used or number of blank spectra replicates subtracted from each sample spectra. This

also applies to the data processing method described in 4.5. Previous users of this method have used various blank subtraction options, from choosing a single blank spectrum of sufficiently good quality and subtracting it from all sample spectra, to combining all blank replicates into a single blank and using that to subtract assignments from the sample spectra. Other published studies rarely go into details of their blank selection and blank subtraction methodologies. Therefore, as part of the data processing of the test rainwater and aerosol samples used in this study, three different blank subtraction methods were compared to see how they affected the yield of formulae assignments.

The first approach subtracted each of three *m*/*z* 100–550 blank MS spectra individually from each of the three *m*/*z* 100–550 sample MS spectra. The same was done for the *m*/*z* 150–900 blank MS spectra and sample MS spectra. This resulted in nine different blank subtracted spectra for each scan range. The common ions present across all nine averaged spectra were kept and the rest were removed. The averaged spectra from the two scan ranges were then combined into one spectra and any duplicate formulae were removed. The accuracy of this approach relied on the quality of the three blank spectra available for each scan range. During the MS measurements, multiple blank spectra were acquired for each scan range to ensure that there were at least three blank spectra of high enough quality; defined by peak intensities $\geq 10^5$ and stable spray ionisations throughout the acquisition time, for blank subtraction. A disadvantage of this approach is the extra run time required by the Mathematica code to produce the blank-subtracted spectra. Each sample spectra took on average 1.5 hours to undergo blank subtraction (the spectra acquired over the larger *m*/*z* 150–900 scan range took longer to process than the *m*/*z* 100–550 scan range). To produce nine different blank-subtracted spectra for one scan range took approximately 14 hours, as opposed to ~5 hours if one blank was being subtracted from each sample spectra.

The second approach used a ‘master blank’ for each scan range. The master blanks were created by combining all three individual blank spectra *.csv* files into one *.csv* file. The data entries in the combined file were then sorted according to intensity from largest to smallest, and any duplicate formulae assignments were removed so that the highest intensity for each formulae assignment was retained and any lower intensities were removed. The *m*/*z* 100–550 master blank was then subtracted from each of the three *m*/*z* 100–550 sample spectra and the same was done for the *m*/*z* 150–900 master blank and *m*/*z* 150–900 sample spectra. The common ions present in all three blank subtracted

sample spectra were kept for each scan range. The two resulting *m*/*z* 100–550 and *m*/*z* 150–900 spectra were then combined and any duplicate formulae were removed.

The third approach used one single, 'good' blank replicate for each scan range. The chosen blank had the highest peak intensities ($\geq 10^5$) and the most stable spray conditions of all of the blank replicates measured. This single blank was subtracted from all of the sample replicates of the same scan range. The common ions were then selected across the three blank subtracted sample spectra for each scan range. The two final spectra were then combined and the duplicate formulae were removed. A potential limitation of this approach is the quality of the blanks available to choose from. However, as mentioned previously, enough blank spectra were obtained to ensure blanks of sufficient quality were available to choose one single blank per scan range.

The three approaches were tested on the Q7 and Q9 'No SPE' sub-samples. Table 4.5 shows the number of formulae assignments in the raw data files exported from the *Xcalibur* software and the number of assignments remaining once the blank subtraction and ratio filtering had taken place, using the three different blank subtraction approaches. All three methods decreased the number of formulae assignments in the raw sample data, prior to blank subtraction, by > 99%. More assignments were removed in the MS measurements acquired over the *m*/*z* l50–900 scan range than the *m*/*z* 100–550 scan range in both samples.

Table 4.6 shows the number of formulae assignments remaining following common ion selection i.e. only the peaks present in all of the chosen replicates were kept. The approach using all three of the blank replicates for each scan range, referred to as the 'All Blanks' approach in Table 4.5, resulted in the greatest number of peaks being removed following common ion selection and was, thus, the most conservative approach. This method took much longer to process the test samples which would be an issue for the large number of samples to be analysed from the main campaign. Another disadvantage of this method is that subtracting three different blank spectra and only retaining the common ions in all nine of the blank-subtracted sample spectra may have 'cleaned' the samples too much and some genuine sample compounds may have been lost. This approach was therefore considered unsuitable for use with the main sample analysis. The 'Single Blank' approach where one blank was chosen, removed the fewest assignments overall, although compared with the 'Master Blank' approach, there was little difference in the final number of formulae assignments in the combined spectra.

The single blank method relied strongly on the quality of one single blank. A poor quality blank which contained a lot of noise could have produced inaccurate blank subtraction of the sample spectra. Using a master blank, however, allowed validation of the blank spectra since only the common ions that were present in all of the three blank spectra used were subtracted from the sample replicates. The master blank approach was therefore considered the most suitable for the 2016 rainwater and aerosol samples.

Table 4.5. Number of formulae assignments in the test aerosol samples before and after blank subtraction and removal of formulae assignments with unrealistic elemental ratio, using three different blank subtraction approaches.

Sample, *m/z* scan range, (replicate #)	Number of formulae assignments in raw data	Number of formulae assignments after blank subtraction		
		All Blanks	Master Blank	Single Blank
Q7 *m/z* 100–550 rep 1	165131	1400	1237	1388
Q7 *m/z* 100–550 rep 2	163135	1384	1224	1376
Q7 *m/z* 100–550 rep 3	166189	1220	1061	1211
Q7 *m/z* 150–900 rep 1	442412	1383	1479	1425
Q7 *m/z* 150–900 rep 2	442507	1756	1876	1800
Q7 *m/z* 150–900 rep 3	432525	1589	1707	1622
Q9 *m/z* 100–550 rep 1	130194	492	436	524
Q9 *m/z* 100–550 rep 2	100663	361	318	386
Q9 *m/z* 100–550 rep 3	137278	767	703	802
Q9 *m/z* 150–900 rep 1	175748	445	478	464
Q9 *m/z* 150–900 rep 2	407687	1239	1336	1258
Q9 *m/z* 150–900 rep 3	402563	1253	1358	1275

Table 4.6. Number of formulae assignments remaining in the test aerosol samples after common ion selection, after three different blank subtraction approaches were applied.

Sample, *m/z* scan range	Number of formulae assignments after common ion selection		
	All Blanks	Master Blank	Single Blank
Q7100–550	60	78	115
Q7 150–900	40	106	71
Q7 Combined Spectra	83	164	160
Q9 100–550	50	71	95
Q9 150–900	52	117	83
Q9 Combined Spectra	87	164	152

Figure 4.7 shows a breakdown of the removal of formulae assignments which occurred at different stages of processing the test aerosol samples, using the 'Master Blank' approach. It is clear that for both scan ranges, the stages of the processing where the majority of formulae assignments are removed are firstly the noise removal stage and secondly the removal of assignments lying outside the defined upper and lower mass shift limits. Both the 'All Blanks' and 'Single Blank' blank subtraction methods showed very similar trends to those shown in Figure 4.7.

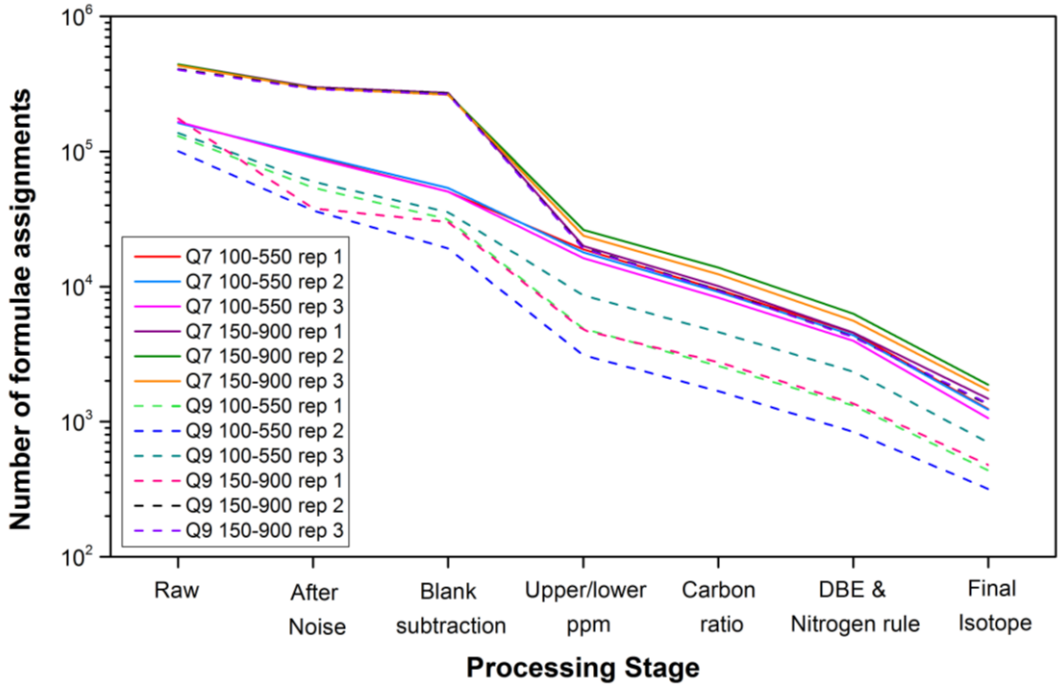

Figure 4.7. Removal of formulae assignments in the test aerosol 'No SPE' sub-samples Q7 (solid lines) and Q9 (dashed lines), using the 'master blank' method for blank subtraction. '100–550' and '150–900'are the two *m*/*z* scan ranges and 'rep #' refers to each *m*/*z* scan replicate.

4.7 Results and Discussion

4.7.1 Nano-ESI-MS direct infusion analysis of rainwater samples

Following MS analysis, the data from the test rainwater samples was treated as described in Section 4.5, using the master blank approach for the blank subtraction of the MS spectra. The resulting number of formulae assignments across both *m*/*z* scan ranges in the first batch of samples (R1–R6) are provided in Figure 4.8. It is clear from these high numbers that many compounds were successfully ionised by the nanoelectrospray and detected by the MS. This means that the SPE sorbent was successful in extracting analytes in the rainwater samples, both in the lower *m*/*z* 100–550 scan range and higher *m*/*z* 150–900 scan range.

Figure 4.9 shows the negative ion mode ultra-high resolution mass spectra for Batch 1 of the test rainwater samples. The peak intensities are high and there is clear variation in the detected *m*/*z* values between the different samples. This suggests that identifying potential seasonal and other variations within the 2016 rainwater and aerosol samples will be possible. Sample R6 has much lower intensities than some of the other samples which may be due to different meteorology in July 2015 when R6 was collected, from the meteorology in June 2015 when the other samples were collected. The oxygen/carbon (O/C) and hydrogen/carbon (H/C) ratios for these samples are shown as a Van Krevelen plot in Figure 4.10. Most atmospheric organic compounds have H/C ratios between 0.5 and 2.0 (Kind and Fiehn 2007). The H/C ratios for the first batch of samples lie predominantly within these boundaries. Van Krevelen plots can be used to detect the presence of different classes of compounds which have their own characteristic H/C or O/C ratios. For example, H/C ratios of 2.0 normally correspond to long chain alkanes and H/C ratios of 0.5 are associated with polycyclic aromatic hydrocarbons (PAHs) (Sunghwan Kim, Robert W. Kramer and Hatcher 2003, Kourtchev et al. 2013). Aliphatic compounds have low O/C ratios (≤ 0.5) and high H/C ratios (≥ 1.5) as indicated by the boxed areas labelled *A* in Figure 4.10. Aromatic compounds have lower H/C ratios (≤ 1.0) and O/C ratios of ≤ 0.5 as indicated by the boxed areas labelled *B* in Figure 4.10. Both aromatic and aliphatic hydrocarbon regions have been tentatively assigned in every sample in the first batch of test rainwater samples.

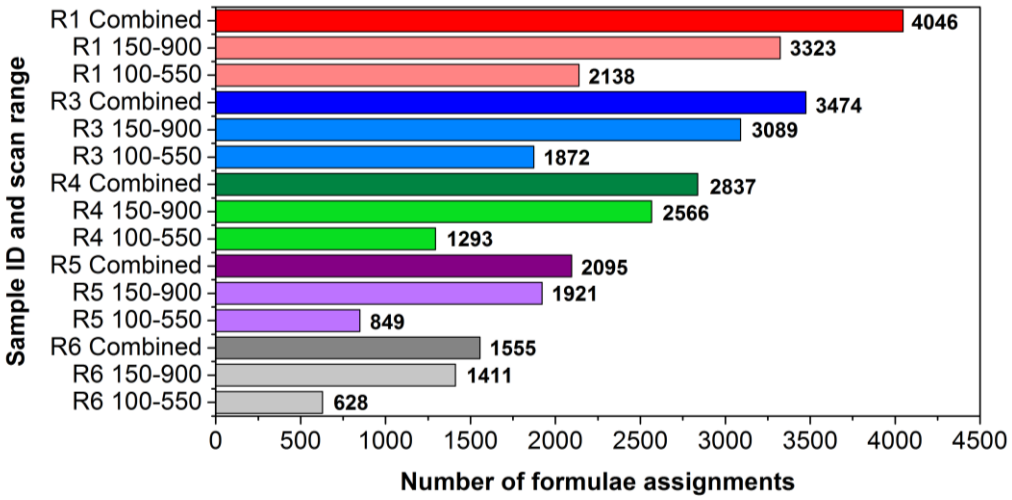

Figure 4.8. Number of formulae assignments in batch 1 of test rainwater samples (R1–R6) after SPE had been applied using Strata-X sorbent and the data had been processed. The total number of formulae assignments are shown separately for the two scan ranges; *m*/*z* 100–550 and *m*/*z* 150–900 and the combined figure with duplicate assignments removed.

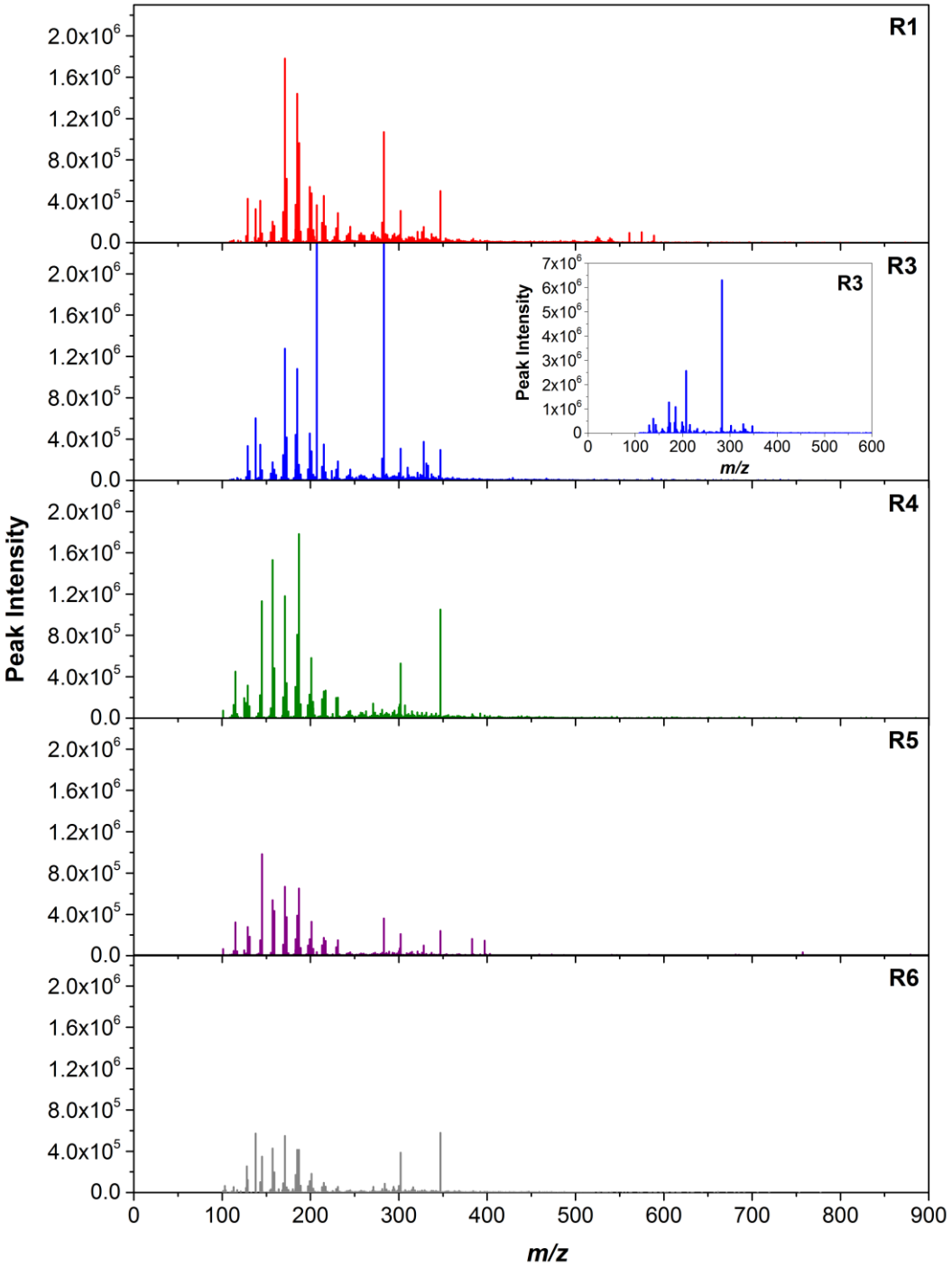

Figure 4.9. Reconstructed (−)Nano-ESI ultrahigh resolution mass spectra for batch 1 of the test rainwater samples following SPE, using Strata-X sorbent. The spectrum shown for each sample is the result of separate processing of the two datasets acquired over scan ranges *m*/*z* 100–550 and *m*/*z* 150–900, and subsequent combination and removal of duplicates. Inset for sample R3 shows full range of peak intensities.

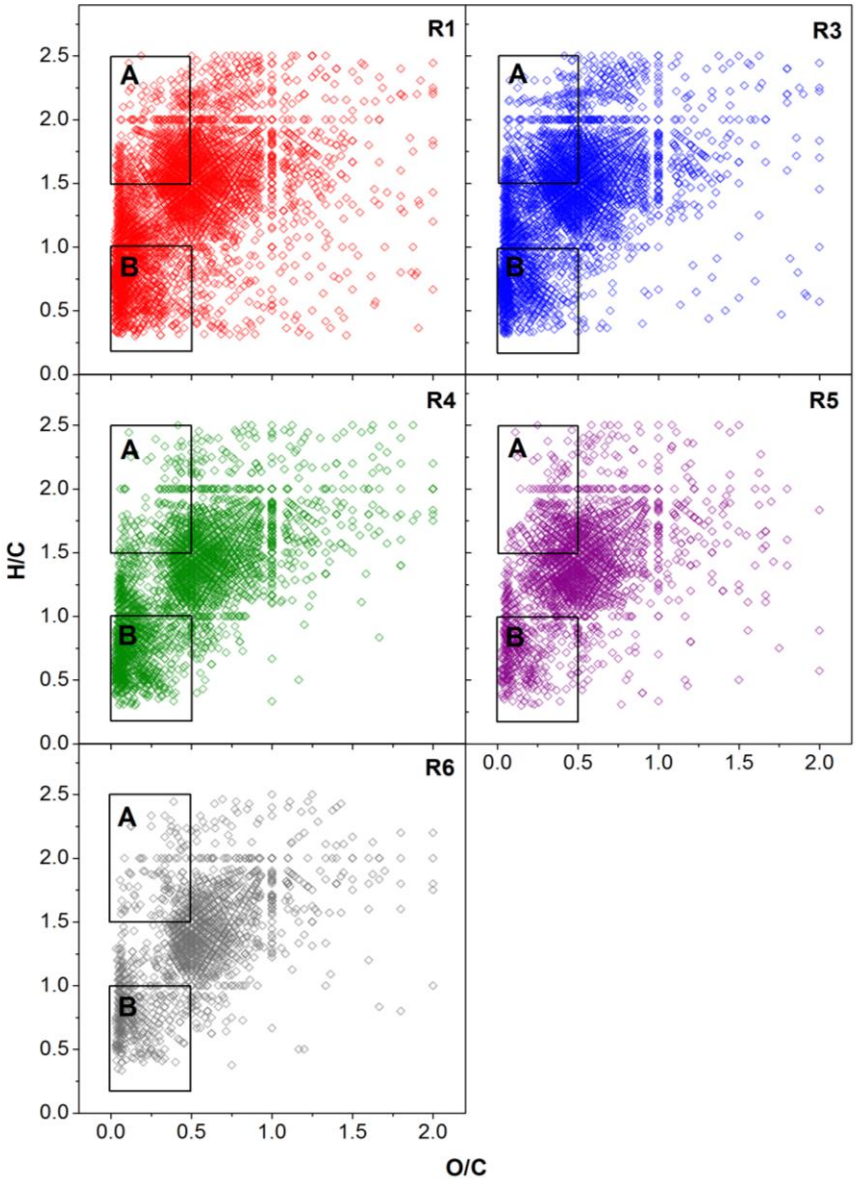

Figure 4.10. Van Krevelen plots showing O/C and H/C ratios for batch 1 of the test rainwater samples under Strata-X SPE conditions. Box *A* indicates aliphatic compounds characterised by low O/C ratios (≤ 0.5) and high H/C ratios (≥ 1.5). Box *B* indicates aromatic compounds with lower H/C ratios (≤ 1.0) and O/C ratios of ≤ 0.5.

Figure 4.11 shows the number of formulae assignments for R47 and R50; Batch 2 of the rainwater samples which were used to assess the impact of using SPE on the number of compounds detected using Nano-ESI-MS. Both samples were split into two; half of which had SPE applied using Strata-X sorbent and half had no SPE applied. There were far fewer formulae detected in sample R47 compared with R50 which may be due to R47 having a much lower DOC (3.07 mg/l) than R50 (11.02 mg/l), caused by different VOC sources and meteorology affecting the rain events. Since R50 contained almost

four times as much organic carbon as R47, it is likely that there were far more analytes in the sample available for extraction with SPE. For sample R47, SPE did not have much of an effect on the number of assignments whereas for R50, the 'SPE' sub-sample had a factor of three more formulae assignments than the 'No SPE' sub-sample.

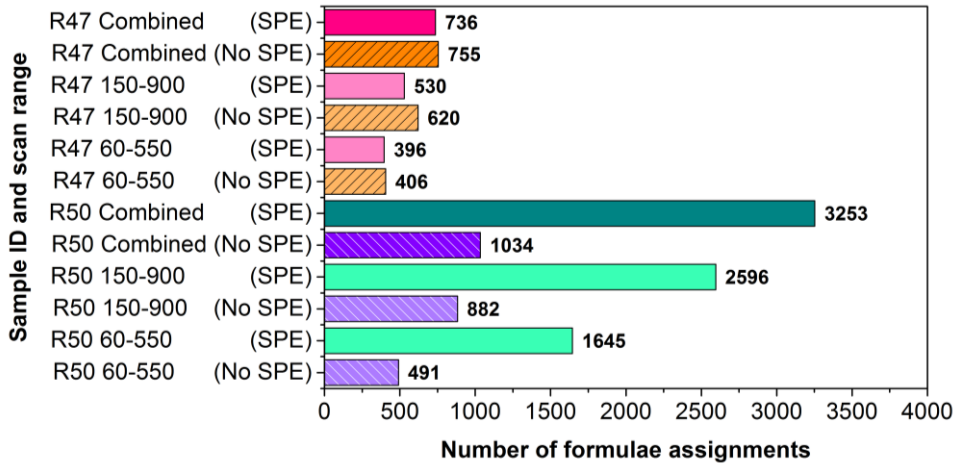

Figure 4.11. Number of formulae assignments in Batch 2 of the test rainwater samples; R47 and R50, following data processing. The samples were split into two with half undergoing SPE with Strata-X sorbent and the other half having no SPE applied. The total number of formulae assignments are shown separately for the two scan ranges; *m*/*z* 100–550 and *m*/*z* 150–900, and the combined figure with duplicate assignments removed.

The difference in the number of assignments between the 'Strata-X' and 'No SPE' sub-samples for R47 and R50, and also the large difference in the number of assignments between R47 and R50, can partially be explained by examining the formulae assignment removal during the different stages of data processing, shown in Figure 4.12. The removal trends for both scan ranges in the 'No SPE' sub-samples for R47 and R50 (shown as the orange and purple lines respectively in Figure 4.12) are very similar and this is the likely reason why the R47 and R50 'No SPE' sub-samples have similar numbers of formulae assignments after the common ion selection (Figure 4.11). However, the assignment removal patterns for the 'Strata-X' R47 and R50 sub-samples (pink and green lines respectively in Figure 4.12), for the *m*/*z* 150–900 scan range in particular, are very different. The removal of assignments due to noise and upper and lower mass shift limits is larger for the 'No SPE' sub-samples than for the 'SPE' sub-samples. Also, the blank subtraction is more significant for the 'Strata-X' sub-samples than the 'No SPE' sub-samples because the SPE-treated blank subtracted a higher

percentage of compounds from the 'Strata-X' sub-sample than the 'No SPE' blank subtracted from the 'No SPE' sub-samples.

The large difference in formula assignments removed during the data processing for the R47 and R50 'Strata-X' sub-samples, in Figure 4.11, is primarily driven by the noise removal and blank subtraction which is larger for the R47 sample. The R47 sample contained fewer compounds so it is likely that a higher percentage of those compounds were blank-subtracted and removed from the sample. After the final isotope removal, the R50 'Strata-X' sub-sample had approximately 7000 more assignments in the *m*/*z* 150–900 scan range and 2000 more assignments in the *m*/*z* 100–550 scan range than the respective R50 'No SPE' sub-sample scan ranges. The R47 'Strata-X' sub-sample however, had ~1500 more assignments in the *m*/*z* 150–900 scan range and 170 more assignments in the *m*/*z* 60–550 scan range than the respective R47 'No SPE' sub-sample scan ranges. This smaller difference in the number of assignments between 'No SPE' and 'Strata-X' in the R47 sample prior to common ion selection then translated to the final values in Figure 4.11 after the rest of the data processing.

Since the use of SPE results in the removal of certain compounds in the sample, it was expected that the 'Strata-X' sub-samples would contain fewer compounds than the 'No SPE' sub-samples. This is observed for the R47 sample (although the difference is very small), but not for the R50 sample. A reason for this difference could be that the R50 rainwater sample contained higher concentrations of inorganic ions than the R47 sample. These inorganic salts could have suppressed the ionisation of some of the organic ions in the R50 sample which were then not detected by the MS. The reconstructed Nano-ESI mass spectra for the R50 sub-samples in Figure 4.13 show that more compounds with *m*/*z* values 60–160 and *m*/*z* values > 500 were detected in the 'Strata-X' sub-sample than the 'No SPE' sub-sample for the R50 sample. This suggests that the application of SPE removed the inorganic salts and allowed more organic analytes to be ionised and detected by the MS, which would explain why the 'Strata-X' sub-sample contained many more formulae assignments than the 'No SPE' sub-sample, after data processing.

The R50 sample does suggest using SPE is advantageous over not using SPE because it yields a higher number of analytes but this is not evident from the R47 sample. More rainwater samples would need to have been analysed to know for certain if SPE yielded significantly more compounds in the rainwater samples. However, regardless of

whether SPE yielded more compounds or resulted in target organic compounds being removed from the samples, using SPE was essential for the rainwater samples because the evaporation times were too long for the ~20 ml samples if no SPE was used.

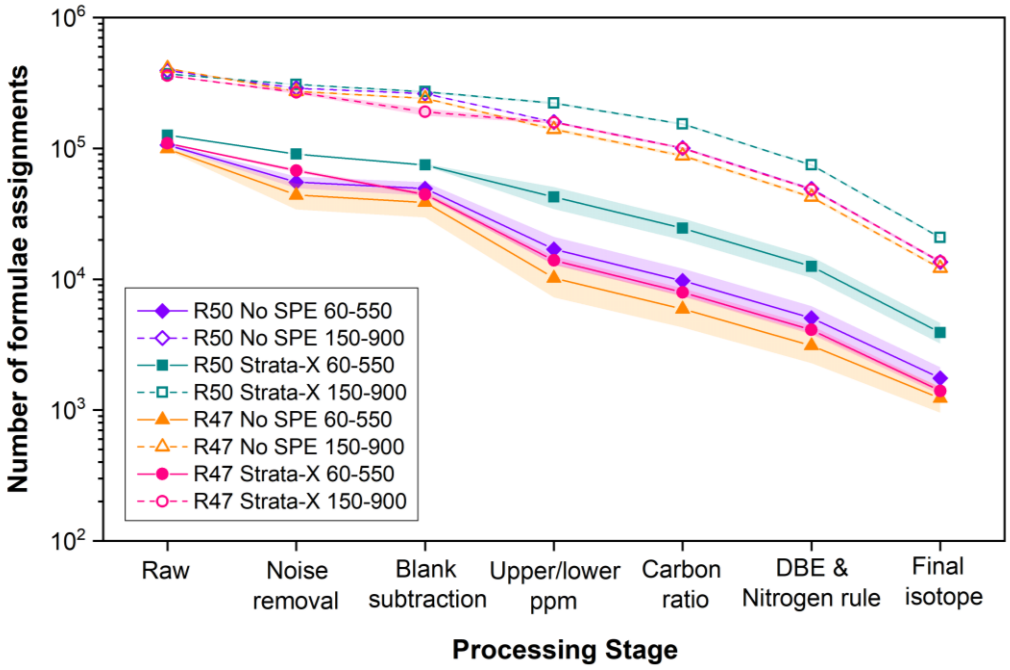

Figure 4.12. Removal of formulae assignments during the main data processing stages (prior to common ion selection) for the second batch of test rainwater samples; R47 and R50. Each sample was split into two sub-samples; one had SPE applied using Strata-X sorbent and the other had no SPE applied. The two scan ranges; *m*/*z* 60–550 (solid lines) and *m*/*z* 150–900 (dashed lines) are averages of three MS measurements for each scan range with shading denoting ± 1 standard deviation.

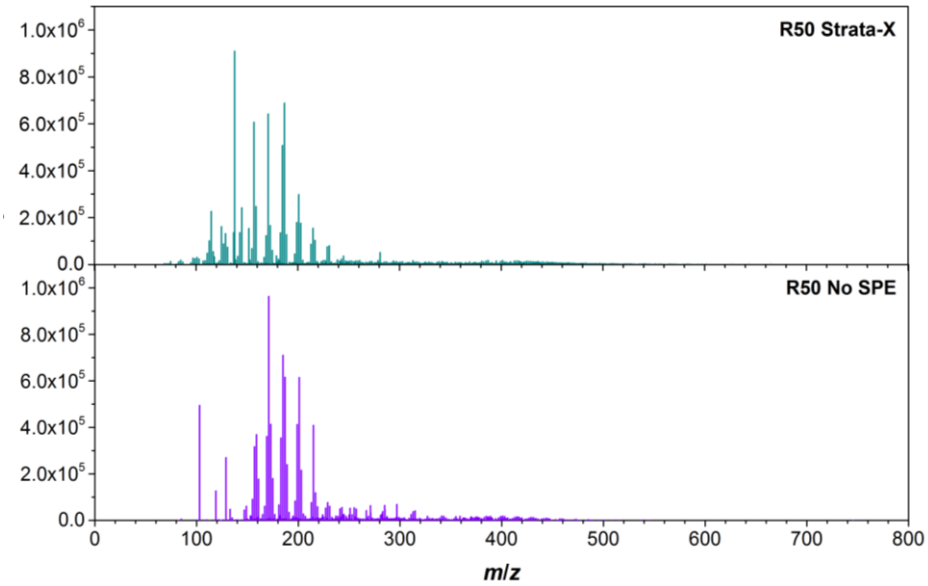

Figure 4.13. Reconstructed (−)Nano-ESI ultra-high resolution mass spectra showing the peak intensities in the combined *m*/*z* 60–550 and *m*/*z* 150–900 scan ranges, after blank subtraction and common ion selection, for batch 2 test rainwater sample R50. 'R50 Strata-X' had SPE applied using Strata-X sorbent and 'R50 No SPE' had no SPE applied.

Figure 4.14 shows the van Krevelen diagrams for both R47 and R50 samples, with and without SPE. Like the first batch of test rainwater samples, there appear to be both aliphatic and aromatic compounds present in the second batch of samples. The SPE ('Strata-X') sub-samples for both R47 and R50 appear to have more aromatic compounds than their 'No SPE' counterparts, as indicated by boxed region *B*. The R50 sample in particular also shows more aliphatic compounds in the 'Strata-X' sample than in the 'No SPE' sample (boxed region *A* in Figure 4.10). There is a slight decrease in the number of aliphatic compounds in region *A*, for the R47 'Strata-X' sub-sample compared with 'No SPE' which could imply that the Strata-X sorbent might be losing some functional groups.

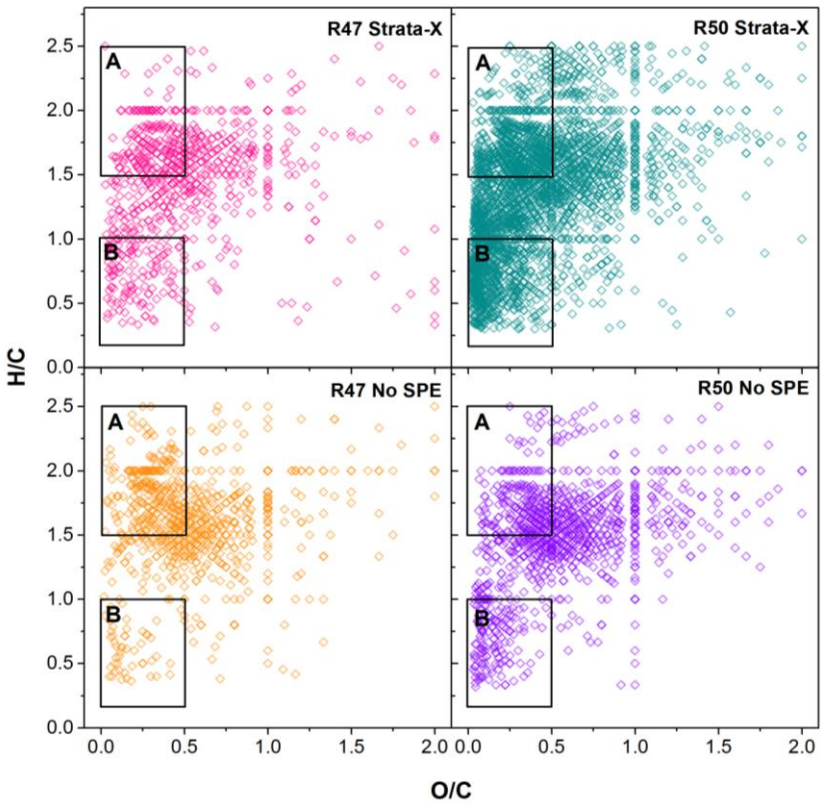

Figure 4.14. Van Krevelen plots showing O/C and H/C ratios for batch 2 of test rainwater samples under no SPE and Strata-X SPE conditions. Box *A* indicates low O/C ratios (≤ 0.5) and high H/C ratios (≥ 1.5); associated with aliphatic compounds and Box *B* indicates aromatic compounds with lower H/C ratios (≤ 1.0) and O/C ratios of ≤ 0.5.

4.7.2 Nano-ESI-MS direct infusion analysis of aerosol samples

The three quarters of the Q7 test aerosol filter and half of the Q9 test aerosol filter which were not used to compare the three SPE sorbent types, were extracted and evaporated as described in 4.3.2 without the use of SPE. These samples were analysed using the direct infusion Nano-ESI-MS and processed using the method with the master blank approach described in 4.5. Between 600 and 1000 compounds were detected using the Nano-ESI-MS in negative ionisation mode in both aerosol samples as shown in Figure 4.15. Q7 had a much higher aerosol mass loading than Q9 and also three quarters of the Q7 filter was used for extraction compared with half of the Q9 filter. These are the likely reasons why approximately 30% more compounds were detected in Q7 and why the peak intensities were much higher in Q7 than in Q9. The combined mass spectra for these samples, following data processing, are shown in Figure 4.16.

The peak intensities are much higher in Q7 than in Q9 due to the higher concentration of organic compounds in Q7. Compared with the test rainwater samples, the aerosol samples contain more compounds with *m*/*z* values > 500 and fewer compounds with *m*/*z* values < 140. The van Krevelen plots for these samples are provided in Figure 4.17. Compared with the test rainwater samples, the test aerosol samples have a broader distribution of organic compound classes with less obvious clustering in the aliphatic regions (Box *A*) and aromatic regions (Box *B*). In particular, there are more compounds with O/C ratios ≥ 1.0 and H/C ratios ≤ 1.0 in the aerosol samples than in the rainwater.

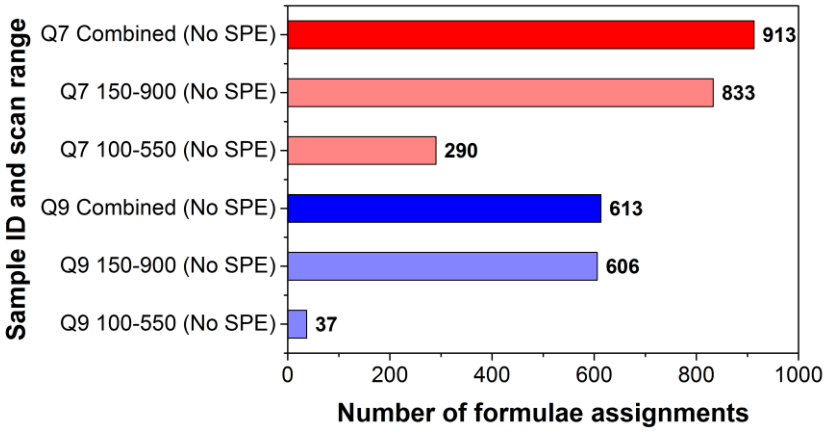

Figure 4.15. Number of formulae assignments in the test aerosol samples Q7 and Q9. Three quarters of the Q7 filter and half of the Q9 filter were used for extraction and no SPE was applied. The number of assignments in the two independently acquired *m*/*z* scan ranges are provided (light red/blue) as well as in the combined spectra with duplicate formulae assignments removed (dark red/blue).

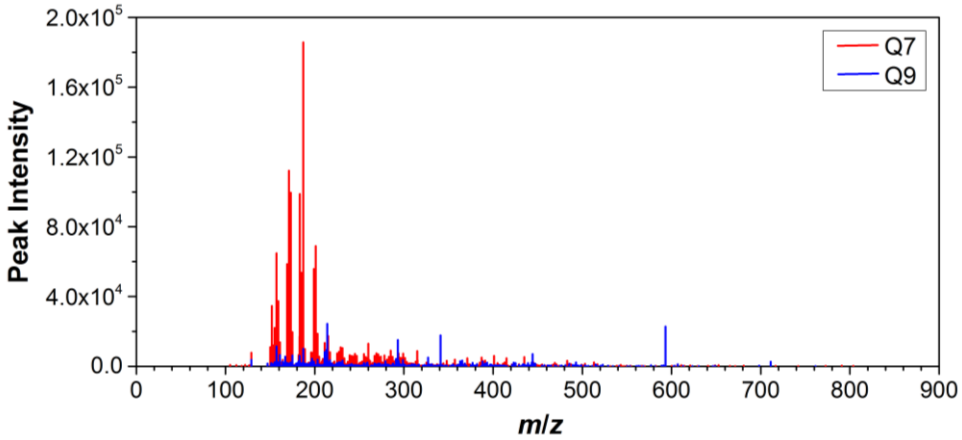

Figure 4.16. Reconstructed (−)Nano-ESI ultra-high resolution mass spectra showing the peak intensities in the combined *m*/*z* 100–550 and *m*/*z* 150–900 scan ranges after blank subtraction and common ion removal, for the test aerosol samples; Q7 and Q9, with no SPE applied.

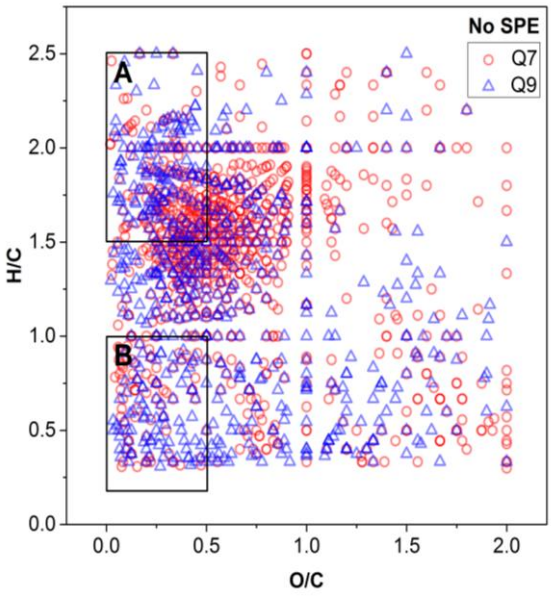

Figure 4.17. Van Krevelen plots showing O/C and H/C ratios for direct infusion Nano-ESI-MS analysis of filter samples; Q7 (red circles) and Q9 (blue triangles) with no SPE applied. Box *A* indicates low O/C ratios (≤ 0.5) and high H/C ratios (≥ 1.5); associated with aliphatic compounds and Box *B* indicates aromatic compounds with lower H/C ratios (≤ 1.0) and O/C ratios of ≤ 0.5.

The remaining quarter of the Q7 filter and half of the Q9 filter were used to compare the three different SPE sorbents. After the first round of filtration, the Q7 and Q9 filtrates were split into four sub-samples; three of the sub-samples had SPE applied using a different type of sorbent and the fourth sub-sample had no SPE applied to provide a direct comparison of "SPE versus no SPE" on the number and distribution of compounds in these samples. Using the data treatment method with the master blank approach, described in section 4.6, the numbers of formulae assignments remaining after applying the three different Strata-X SPE sorbent types are shown in Figure 4.18. It is clear that both the Q7 and Q9 'No SPE' sub-samples did contain more formulae assignments than any of the 'SPE' sub-samples. However, SPE must be used for the 2016 aerosol samples to enable a direct comparison between the rainwater and aerosol samples, as outlined in the initial aims.

Strata-X-AW yielded the highest number of compounds for the Q7 sample but yielded very few compounds in Q9. This difference may be the result of the samples being collected during different rain events and therefore having different compositions influenced by the air mass origin and meteorology on the sampling days. Closer inspection of the two scan ranges revealed that all of the compounds eluted using Strata-

X-AW were in the *m*/*z* 100–550 scan range and none were eluted with *m*/*z* values between 550 and 900, in both Q7 and Q9. This is illustrated in Figure G in Appendix G. More analytes were eluted using Strata-X-AW than Strata-X-A which suggests that either the samples contained sulphate functional groups that formed strong ionic bonds with the Strata-X-A sorbent which then could not be broken by the elution solvent, or that most of the analytes were not retained on the Strata-X-A sorbent at all. The Strata-X-AW sorbent used weak anion exchange so any ionic bonds which formed could have been broken by the elution solvent and more analytes were eluted. Strata-X-A sorbent was consistently poor across both samples, yielding fewer than 10 compounds in each sample, making it unsuitable for use with these samples. Strata-X sorbent yielded similar numbers of compounds in both samples and had an even distribution across both scan ranges (see Appendix G).

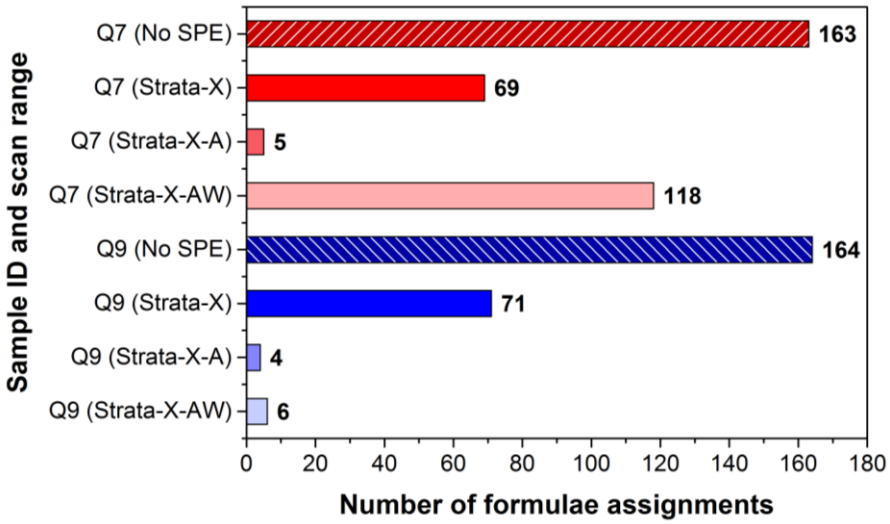

Figure 4.18. Number of formulae assignments in the Q7 and Q9 test aerosol samples, combined across *m*/*z* 100–550 and *m*/*z* 150–900 scan ranges. Each sample was split into four sub-samples after the first round of filtration. Three sub-samples had SPE applied with three different SPE sorbent types and the fourth sub-sample had no SPE applied for comparison.

Figure 4.19 shows the van Krevelen plots for Q7 and Q9. As previously observed, the Strata-X-A sorbent retained very few compounds in both samples. Accounting for the difference in the total number of formulae assignments, the distribution of compound classes in Q7 is similar in the ‘Strata-X’, ‘Strata-X-AW’ and ‘No SPE’ van Krevelen diagrams. There is slightly greater clustering of aliphatic compounds in the ‘No SPE’ sample but generally, the Strata-X sorbent successfully eluted the compounds with

higher H/C ratios. Since the Strata-X sorbent is suited to extracting both polar and non-polar neutral compounds with hydrophobic interactions, it is likely that the Q7 sample contains compounds with long hydrocarbon chains which have stronger hydrophobic interactions. Many compounds with lower H/C ratios of varying degrees of oxidation were also detected in Q7 with no SPE, including in the aromatic region, and most of these compounds were also retained after Strata-X, and to a lesser extent, after Strata-X-AW. There is a clear difference in composition between the Q7 and Q9 samples because the 'No SPE' and 'Strata-X' distributions look very different for Q9. Many more compounds with H/C ratios < 1.0 were observed in the 'Strata-X' sub-sample than in the 'No SPE' sub-sample, although they were present in the un-split Q9 sample van Krevelen diagram in Figure 4.17 which indicates that the Strata-X sorbent was efficient at extracting aromatic compounds and highly oxidised compounds. The Strata-X-AW sorbent did not effectively retain many compounds from Q9 and provides no useful information on the compound classes within this sample.

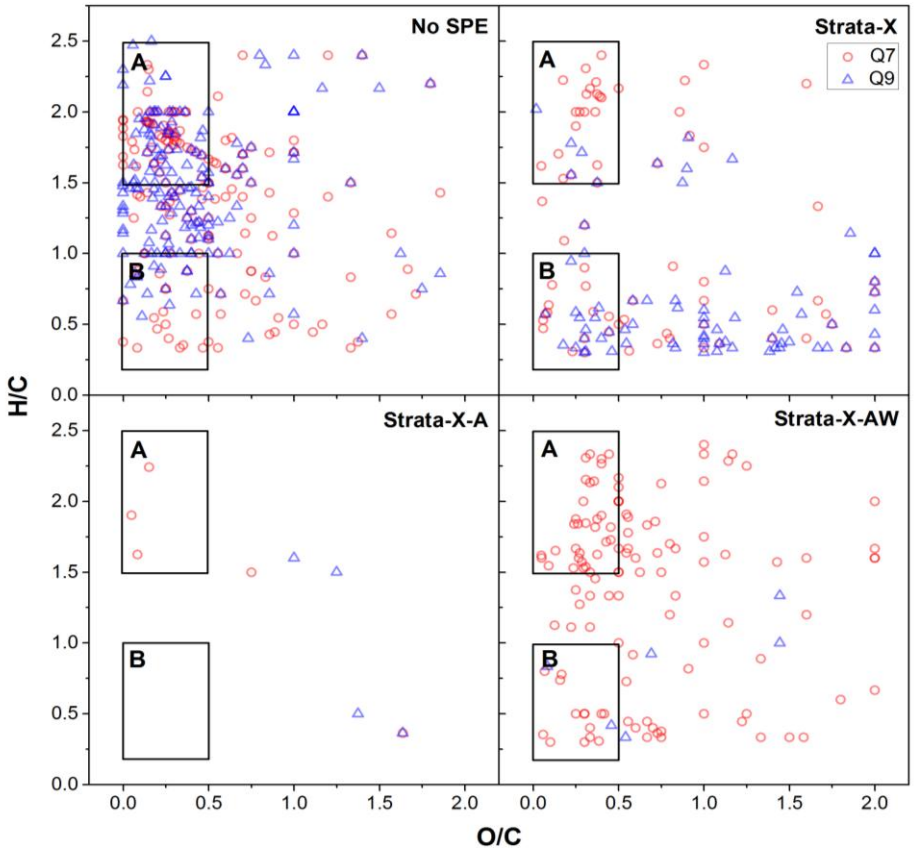

Figure 4.19. Van Krevelen plots showing O/C and H/C ratios for the filter samples; Q7 (red circles) and Q9 (blue triangles) under no SPE and different SPE sorbent conditions. Box *A* indicates low O/C ratios (≤ 0.5) and high H/C ratios (≥ 1.5); associated with aliphatic compounds and Box *B* indicates aromatic compounds with lower H/C ratios (≤ 1.0) and O/C ratios of ≤ 0.5.

These results have shown that two of the SPE sorbents tested; Strata-X and Strata-X-AW, were able to successfully retain compounds with different functional groups. However, Strata-X-AW sorbent was only able to extract a sufficiently high number of analytes from Q7 and not from Q9 whereas Strata-X sorbent did successfully extract a similar number of compounds from both samples, some of which were not detected when no SPE was used but were present in the un-split sample van Krevelen diagram in Figure 4.17. Since the samples from the AERORAIN campaign are likely to be influenced by different pollution sources, air masses and meteorology, the required sorbent needs to be applicable for a wide range of different compounds. Therefore, of the three tested SPE sorbents, Strata-X is the most appropriate and will be used for the 2016 AERORAIN samples.

A limitation of the method used for testing the SPE sorbents is that the samples were split into four sub-samples which greatly diluted the concentrations in the samples. As a result, the 'No SPE' sub-samples contained almost six times fewer formulae assignments in Q7 and four times fewer formulae assignments in Q9 compared with the respective un-split samples which also had no SPE applied. This means that the distribution of compounds is not entirely representative of the distributions expected in the 2016 samples. This dilution of the sub-samples also means that it is not possible to quantify how much of an impact SPE will have on the number and distribution of compounds in the 2016 samples, although its use is essential as previously stated.

4.8 Conclusions

Analysis of the test rainwater samples shows that SPE with Strata-X sorbent recovers a high number of compounds from the rainwater and, in most cases, produces high intensity peaks from the nanoelectrospray ionisation. A comparison of 'SPE versus no SPE' on the same rainwater samples showed that SPE yielded a larger range of detectable organic compounds, especially those with m/z values of 60–160 and m/z > 500, and also potentially more aliphatic and aromatic compounds. This may be due to the removal of inorganic salts which were suppressing the ionisation of organic ions but this is a tentative conclusion as it was only observed for one of the two tested rainwater samples.

The filter extraction method used in this work successfully extracted between 600 and 1000 compounds from both of the test aerosol samples. Fewer compounds were extracted from the aerosol samples than from the rainwater samples but the total number of assignments was more consistent across the different aerosol samples than the rainwater samples. The aerosol samples did appear to contain more compounds with higher O/C ratios (≥ 1.0) and lower H/C ratios (≤ 1.0) and less clustering in the aliphatic and aromatic regions of the van Krevelen diagrams.

Three different blank subtraction approaches were tested as part of the data processing method for the samples. Using a 'master blank', comprised of three MS blank spectra combined into one blank spectrum for each scan range, was found to yield a high number of formulae assignments while still sufficiently validating the quality of the chosen blank spectrum and allowing multiple samples to be processed within a suitable period of time.

Comparison of the three polymer-based SPE sorbents revealed that both Strata-X and Strata-X-AW eluted several compounds from the aerosol samples, while Strata-X-A recovered very few and as such is unsuitable for these samples. Strata-X was able to recover a similar number of compounds from the two scan ranges in both tested aerosol samples whereas Strata-X-AW could only recover a significant number of compounds in one sample and only compounds with m/z values ≤ 550.

It was evident from the two test aerosol samples and one of the test rainwater samples that using SPE results in some compounds being removed. However, SPE must be used to ensure that the rainwater samples are sufficiently reduced in volume and concentrated for the MS analysis. Without the use of SPE, the evaporation times for the ~20 ml rainwater samples are too long. The Strata-X sorbent was consistent across both test aerosol samples despite their differences in composition and did appear to recover some compounds with low H/C ratios which were not detected when no SPE was used. Strata-X also appears to be capable of recovering significant numbers of both the aliphatic and aromatic compounds which were observed in the un-split 'No SPE' test aerosol samples and are likely to be present in the 2016 AERORAIN samples. Therefore, the Strata-X sorbent will be used in the SPE application for the 2016 rainwater and aerosol samples.

The results from the SPE sorbent comparison highlighted that splitting the test aerosol samples into sub-samples greatly diluted the sample concentrations and thus, the

number of compounds detected by the Nano-ESI-MS. To ensure there is a sufficient enough initial filter volume for SPE extraction of the 2016 samples, all of the 47 mm diameter filter provided per sample will be extracted.

Comparing the impact of SPE sorbents with different retention mechanisms on the number of total formulae assignments and the distribution of compounds successfully eluted from the test samples, allowed the most suitable SPE sorbent to be chosen for the AERORAIN samples. Comparing the use of SPE with not using SPE was also useful to see how much of an impact SPE had on the sample composition and should be accounted for in future studies involving SPE. Optimising the SPE method formed an important part of the sample preparation protocol for the ambient samples and it is important that details of SPE optimisation are included in future studies to aid analysis of ambient environmental samples and improve sample preparation protocols for MS analysis.

5 Analysis of Organic Composition of Rainwater and Aerosol Samples from the AERORAIN Campaign using Ultra-High Resolution Mass Spectrometry (UHRMS)

The work covered in the previous chapter concluded that Strata-X™ SPE sorbent was the most suitable sorbent for extracting the organic compounds from the rainwater and aerosol samples prior to composition analysis using UHRMS. Pre-campaign test samples from the AERORAIN campaign were used to reach this conclusion.

This chapter focusses on the rainwater and aerosol samples collected during the main stage of the campaign in 2016. These samples have the developed SPE method applied to extract the organic compounds and a discussion of the subsequent analysis is provided.

5.1 Introduction

Currently, less than 50% of rainwater Dissolved Organic Matter (DOM) is believed to be characterised and much of the uncharacterised rainwater DOM is found in aerosol (Altieri et al. 2009, Kawamura, Steinberg and Kaplan 1996). Dissolved Organic Carbon (DOC) is an important component of both marine and continental rainwater and can be present in higher concentrations than inorganic species (Willey et al. 2000).

Organic acids such as formic acid and acetic acid account for up to 36% of DOC while other monocarboxylic acids including propionic acid and aldehydes, dicarboxylic acids, alkanes, fatty acids and polycyclic aromatic compounds make a smaller contribution to rainwater DOC (Avery et al. 2006, Peña et al. 2002, Durana et al. 1992, Avery Jr et al. 2001, Gill, Graedel and Weschler 1983). Organic acids have been found to contribute significantly to rainwater acidity in urban areas (Peña et al. 2002, Kawamura et al. 1996) and up to 80-90% of rainwater acidity in remote areas (Andreae et al. 1988). More recently, organic nitrogen has been found to contribute 30% of total nitrogen in continental rainwater content and is largely attributed to anthropogenic industrial and agricultural sources (Zhang et al. 2008, Mace, Duce and Tindale 2003).

Many studies have used ultra-high resolution ESI-MS to characterise the composition of organic species in rainwater (Altieri et al. 2012), (Altieri et al. 2009) cloud and fog water (Boone et al. 2015, Mazzoleni et al. 2010b, Zhao et al. 2013, Pratt et al. 2013) and ambient aerosol (Mazzoleni et al. 2012b, Wozniak et al. 2008, Kourtchev et al. 2013, Tong et al. 2016). Observations have shown that while some rainwater organic species do have primary sources, most are produced by secondary mechanisms and are incorporated into rainwater via cloud droplets or as SOA following gas phase, aerosol phase and in-cloud reactions (Altieri et al. 2009).

Organosulphates, organonitrates and nitrooxy-organosulphates have also been detected in SOA (Altieri et al. 2009, Thorsten Reemtsma et al. 2006, Boone et al. 2015, Cook et al. 2017, Pratt et al. 2013, Surratt et al. 2007). They are formed when sulphur and nitrate reacts with oxidation products of biogenic precursors such as isoprene, α-pinene and limonene (Hamilton et al. 2013).

5.2 Aims

The purpose of this chapter is to use direct infusion Nano-ESI-MS to provide an overview of the molecular composition of organic compounds in the rainwater and aerosol samples collected during the AERORAIN campaign, as a function of season.

The specific objectives of this analysis were to:

- Identify, broadly, the different types of organic compounds present in the rainwater and aerosol samples, according to functional group.
- Investigate any seasonality within the rain and aerosol samples from Spring, Summer and Winter of 2016 and any associated shifts in compound distribution.

5.3 Methodology

5.3.1 Sample Description and Preparation

The selection of rainwater and aerosol samples shown in Table 5.1–Table 5.3 were delivered, frozen, from León to Cambridge, where they were analysed. Table 5.1 shows the dates of collection for the 10 rainwater samples and 9 aerosol samples from Spring (April–May), Table 5.2 shows details for the 4 rainwater samples and 9 aerosol samples from Summer (July–August) and Table 5.3 shows the details for 12 rainwater samples and 9 aerosol samples from Winter (October–December). The alternating shading in all three tables indicates which rain and aerosol samples were collected during the same rain event. For all rainwater samples, the pH values were recorded in León prior to arrival in Cambridge and the volumes of the samples were recorded in Cambridge prior to the sample preparation. Dissolved Organic Carbon (DOC) and meteorological measurements were also measured and recorded during the AERORAIN campaign by Dr A. I. Calvo at the University of León, and fellow researchers participating in the campaign, prior to the composition analysis in Cambridge.

The aerosol samples were either collected during rain events and are denoted as ‘RE’ in Table 5.1–Table 5.3 or they were collected every 24 hours regardless of whether a rain event had occurred, as described in 4.1 in the previous chapter. The ‘RE’ samples listed

in the tables were all collected on quartz filters, 47 mm in diameter using a low volume sampling head. The '24 hr' samples were originally collected on a 150 mm quartz filter using a high volume sampling head and 47 mm diameter punches were taken from these larger filters and sent to Cambridge. Blank aerosol samples collected using the low volume sampling head and high volume sampling head are referred to as 'Low vol' and 'High vol' respectively in Table 5.1–Table 5.3. Both types of filters were therefore of the same diameter and were treated equally in terms of sample preparation.

Table 5.1. Rainwater and aerosol samples from Spring 2016. Collection dates are shown for both rainwater and aerosol samples and shading indicates different rain events. pH values recorded in León and volumes of the samples received are provided for the rainwater samples. Aerosol samples received were either collected during rain events ('RE') or every 24 hours regardless of whether rain occurred ('24 hr'). Blank aerosol samples were collected using either a low volume sampling head ('Low vol') or high volume sampling head ('High vol').

Rainwater					Filters			
Sample ID	**Collection Start Date**	**Collection End Date**	**Volume (ml)**	**pH**	**Sample ID**	**Collection Start Date**	**Collection End Date**	**24 hour / RE**
R19	14.04.16	15.04.16	20	6.98	Q53	12.04.16	14.04.16	24 hr
R20	15.04.16	16.04.16	20	6.20	Q154	14.04.16	16.04.16	RE
R21	16.04.16	17.04.16	18	5.56	Q155	16.04.16	18.04.16	RE
R27	05.05.16	06.05.16	20	6.96	Q74	03.05.16	04.05.16	24 hr
R28	06.05.16	06.05.16	22	6.31	Q200	05.05.16	07.05.16	RE
R29	07.05.16	08.05.16	21	6.51	Q201	07.05.16	09.05.16	RE
R30	08.05.16	09.05.16	22	6.87	Q202	09.05.16	11.05.16	RE
R31	09.05.16	10.05.16	19	6.79	Q203	11.05.16	12.05.16	RE
R32	10.05.16	11.05.16	25	7.30	Q84	12.05.16	13.05.16	24 hr
R33	11.05.16	12.05.16	22	6.82				
Blank R35	-	-	21	-	Blank Q157	-	-	Low vol
Blank R36	-	-	15	-	Blank Q207	-	-	Low vol
					Blank Q208	-	-	Low vol

Table 5.2. Rainwater and aerosol samples from Summer 2016. Collection dates are shown for both rainwater and aerosol samples and alternated shading indicates different rain events. pH values recorded in León and volumes of the samples received are provided for the rainwater samples. Aerosol samples received were either collected during rain events (RE) or every 24 hours regardless of whether rain occurred (24 hr). Blank aerosol samples were collected using either a low volume sampling head ('Low vol') or high volume sampling head ('High vol').

Rainwater					Filters			
Sample ID	**Collection Start Date**	**Collection End Date**	**Volume (ml)**	**pH**	**Sample ID**	**Collection Start Date**	**Collection End Date**	**24 hour / RE**
R47	05.07.16	06.07.16	9	6.49	Q169	04.07.16	05.07.16	24 hr
R48	06.07.16	07.07.16	5	5.41	Q170	05.07.16	06.07.16	24 hr
					Q206	05.07.16	05.07.16	RE
					Q172	06.07.16	07.07.16	24 hr
R49	14.08.16	15.08.16	7	4.76	Q259	13.08.16	14.08.16	24 hr
					Q260	14.08.16	15.08.16	24 hr
R50	25.08.16	26.08.16	11	6.03	Q272	24.08.16	25.08.16	24 hr
					Q273	25.08.16	26.08.16	24 hr
					Q218	26.08.16	26.08.16	RE
Blank R37	-	-	10		Blank Q171	-	-	High vol
Blank R38	-	-	11.5					

Table 5.3. Rainwater and aerosol samples from Winter 2016. Collection dates are shown for both rainwater and aerosol samples and alternated shading indicates different rain events. pH values recorded in León and volumes of the samples received are provided for the rainwater samples. Aerosol samples received were either collected during rain events (RE) or every 24 hours regardless of whether rain occurred (24 hr). Blank aerosol samples were collected using either a low volume sampling head ('Low vol') or high volume sampling head ('High vol').

Rainwater					Filters			
Sample ID	**Collection Start Date**	**Collection End Date**	**Volume (ml)**	**pH**	**Sample ID**	**Collection Start Date**	**Collection End Date**	**24 hour / RE**
R55	11.10.16	12.10.16	20	5.45	Q211	13.10.16	13.10.16	RE
R56	12.10.16	13.10.16	19	5.71				
R57	13.10.16	13.10.16	20	5.48				
R63	04.11.16	04.11.16	15	6.65	Q212	04.11.16	04.11.16	RE
R64	04.11.16	05.11.16	7	5.83				
R65	11.11.16	12.11.16	8	5.53	Q358	10.11.16	11.11.16	24 hr
R69	19.11.16	20.11.16	12	6.73	Q366	18.11.16	19.11.16	24 hr
R70	20.11.16	21.11.16	19	5.61	Q367	19.11.16	20.11.16	24 hr
R71	24.11.16	24.11.16	16	5.82	Q214	24.11.16	24.11.16	RE
R73	14.12.16	14.12.16	14	5.57	Q392	13.12.16	14.12.16	24 hr
R74	14.12.16	15.12.16	21	5.53	Q232	14.12.16	14.12.16	RE
R75	15.12.16	16.12.16	24	6.00	Q393	14.12.16	15.12.16	24 hr
Blank R67	-	-	11	-	Blank Q215	-	-	Low vol
Blank R68	-	-	17.5	-	Blank Q216	-	-	Low vol
					Blank Q401	-	-	High vol

The rainwater and aerosol samples were prepared using the 6 ml SPE tubes with 100 mg Strata-X sorbent (Phenomenex) and the method for Strata-X sorbent described in Table 4.3. The rain samples had SPE applied while the aerosol samples were filtered using 0.45 µm pore sized PTFE filters, then had SPE applied and were filtered again with 0.2 µm pore sized filters post-SPE, using the method outlined in 4.3.1. These filtrates were then evaporated to 200 µl under a gentle nitrogen stream at 28°C and each sample volume was divided in half; one half to be analysed using the Nano-ESI source while

the other half would be analysed using LC-ESI-MS (covered in Chapter 9 of this thesis). These split samples were then evaporated to 100 µl in LC vials.

5.3.2 Analysis using direct infusion Nano-ESI and UHRMS

Each rain and aerosol 100 µl sub-sample was analysed using the TriVersa NanoMate chip-based ESI source, described in section 4.4, coupled to the Orbitrap Velos Mass Spectrometer, in negative ionisation mode. 233 µl of methanol (UHPLC-MS grade) was added to each sub sample to achieve a stable spray. The same parameter settings were used for the 2016 samples as for the test samples; an injection volume of 5 µl from 16 µl loaded onto the sample plate, injected under a pressure of 0.7 psi and voltage of 1.4 kV. Three scan replicates were acquired for two split *m*/*z* scan ranges; 60–550 and 150–900, providing six spectra in total for each sample and blank. It should be noted that some of the rain and aerosol samples did not ionise efficiently and the spectra contained only background intensities. These samples were filtered a second time using the 0.2 µm pore sized filters to remove small, insoluble particles which affect the ESI ionisation and after this second round of filtration, ionised well. The samples were analysed in batches according to season and type to reduce any potential variation between samples of the same season which could have been introduced by different lab atmospheres.

5.3.2.1 Nano-ESI-MS Data treatment

The same elemental constraints were applied to the 2016 rain and aerosol samples in the *Xcalibur* software as detailed in section 4.5, to remove any formulae assignments unlikely to occur in the natural environment.

There were multiple blanks provided for most of the seasonal rain and aerosol samples. Where possible, spectra of the same scan range across different blanks were combined to produce a more reliable and accurate blank. The spring rainwater samples had two blanks; R35 and R36. The *m*/*z* 60–550 mass spectra for both blanks were combined into one file and the duplicates were removed. The mass drift and noise removal processing described in 4.5.2.1 was then applied. The peak intensities from this new combined

Spring rainwater blank were subtracted from all of the Spring rainwater sample spectra and the remaining data treatment occurred as described in 4.5.2.2 and 4.5.2.3.

For the aerosol samples collected during the first Spring rain event, Blank Q157 *m*/*z* intensities were subtracted from the peak intensities of filter samples Q154, Q155 and Q53. It was noted that Blank Q157 was a 'low vol' (hereon denoted as 'LV') filter and therefore collected under different conditions from the Q53 'high vol' (hereon denoted as 'HV') filter sample. However, there were no HV spring blank filters available and since the blank was collected in a similar time period to the Q53 filter, it was the most suitable option. Subtracting the same blank from all the filters during the same rain event also meant that the composition of the LV and HV filters would be directly comparable.

For the second spring rain event, the three *m*/*z* 60–550 spectra MS measurements for the Q207 LV blank filter were combined with the three Q208 LV *m*/*z* 60–550 MS spectra measurements, into one master blank *.csv* file. The assignments were sorted by intensity (highest to lowest) and any duplicate formulae assignments were removed, prior to any code processing. The same was done for the *m*/*z* 150–900 MS spectra in each blank. Combining the blanks in this manner acted as a verification of the blank and increased the accuracy and reliability of the blank for blank subtraction. The peak intensities from the master blanks were then subtracted from the Spring LV filter samples Q200, Q201, Q202, Q203 and the HV filters Q74 and Q84. Again, the LV blank filters were used in the blank subtraction of the HV sample filters Q74 and Q84 because they were collected at similar times and this makes the final composition of the LV and HV filters directly comparable.

There were no blank rainwater samples available for the summer period so some 'spare' rainwater blanks; R37 and R38, which were sent with the Spring rainwater samples were used as substitutes for the summer blanks. These were used for blank subtraction for all of the summer rainwater samples in the same way as for the spring blank rainwater samples. The one summer blank filter; Q171, was a HV filter and this was used in the blank subtraction of all of the summer HV and LV filters in Table 5.2.

Two rainwater blanks; R67 and R68 which were collected during the winter period were used in the blank subtraction of all of the winter rainwater samples in Table 5.3. The winter HV Q401 blank filter was used for the blank subtraction of the winter HV sample filters; Q358, Q366, Q367, Q392 and Q393. The Q215 LV and Q216 LV blank

filters were combined as described for the spring filter samples and the master blank peak intensities for each scan range were subtracted from the winter LV filter samples; Q211, Q212, Q214 and Q232.

It was noted that in preparation of these master blanks, it was not always possible to combine all six complete MS spectra from the two separate blanks because the final output *.csv* file became too large and exceeded the maximum number of rows in Microsoft® Office Excel. This issue occurred for the *m*/*z* 150–900 scan range for the Spring filter Q207/Q208 LV blank, Summer rain R37/R38 blank, Winter rainwater R67/R68 blank and Winter filter Q215/Q216 LV blank. This was not a significant concern because the mass spectra peak intensities from the different blanks looked very similar so it was unlikely that important peaks would be missed from the master blank.

In addition, after shoulder peak removal, any formulae assignments with more than five ^{14}N atoms were removed as compounds with more than five nitrogen atoms in their structure rarely occur naturally in the atmosphere (Kourtchev et al. 2013).

5.4 Results and Discussion

5.4.1 Number of compounds and different formulae groups identified

Figure 5.1 shows the number of formulae assignments, combined across the two scan ranges, for the 26 rainwater samples collected in spring (green), summer (yellow) and winter (blue). On average, the spring rainwater samples contain 244 ± 220 formulae assignments across the two rain events measured, summer rainwater samples contain 1147 ± 713 formulae assignments across the three rain events measured and winter rainwater samples contain 442 ± 188 assignments across the six rain events measured.

The number of formulae assignments in the 27 aerosol samples collected during spring (green), summer (yellow) and winter (blue) are shown in Figure 5.2. The darker shades correspond to the HV filters collected every 24 hours, denoted as ‘24 hr’ in Figure 5.2 and the lighter shades are LV filters collected only during rain events, denoted as ‘RE’ in Figure 5.2. Overall the spring aerosol contained 893 ± 229 formulae assignments, summer aerosol had 1444 ± 543 assignments and winter samples had 691 ± 338

assignments. Across all seasons, the HV aerosol samples contain more compounds than the LV aerosol samples. This is not surprising because the HV filters sampled air for the duration of a rain event plus the rest of the 24 hour period before the filter was replaced whereas the LV filters only sampled air during the rain event so contained fewer compounds. The difference in formulae assignments may also reflect the difference in composition between the 'RE' aerosol and '24 hr' aerosol. The air prior to the rain event may have contained more 'aged' aerosol which had had time to react with sulphate and nitrate emissions from the local urban environment and produce more oxygenated compounds. These compounds would have been included on the '24 hr' filters but would have been missed off the 'RE' filters.

The second spring rain event in May 2016 shows a clear decrease in the number of assignments in the rainwater from approximately 800 on the first day of rain on 5th May (R27) down to fewer than 100 on the last day on 11th May (R33). This is likely to be due to the rain removing aerosol from the atmosphere over the course of the rain event. This trend is mirrored somewhat in the LV filters for the second rain event but not to the same extent. Further discussion of aerosol scavenging by the rainwater will be covered in Chapter 8 of this thesis.

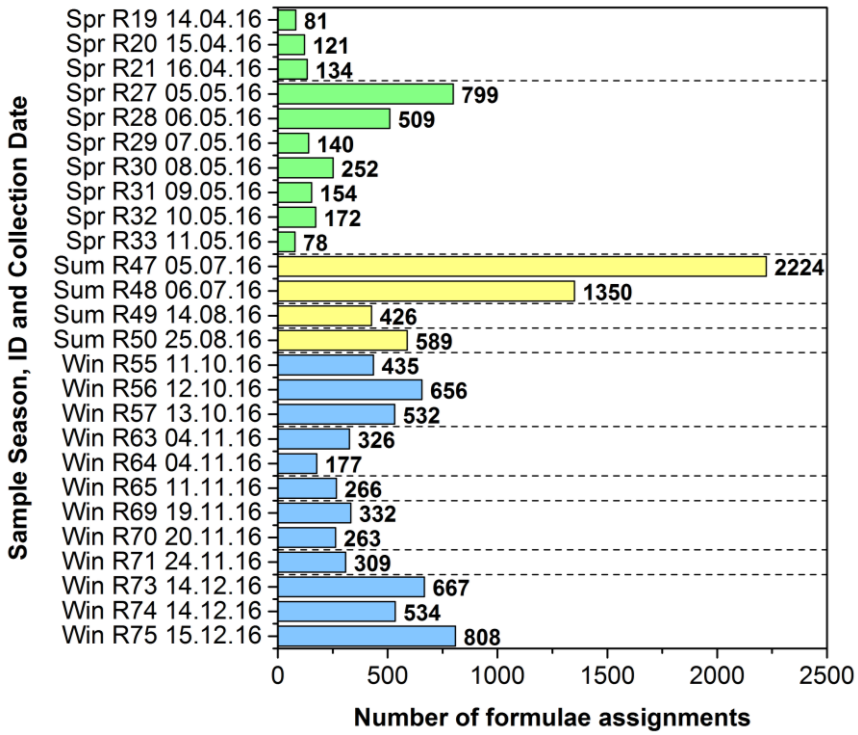

Figure 5.1. Number of formulae assignments in the rainwater samples; Spring (green), Summer (yellow) and Winter (blue). Values shown are combined across both scan ranges; *m*/*z* 60–550 and 150–900. Dashed lines indicate different rain events.

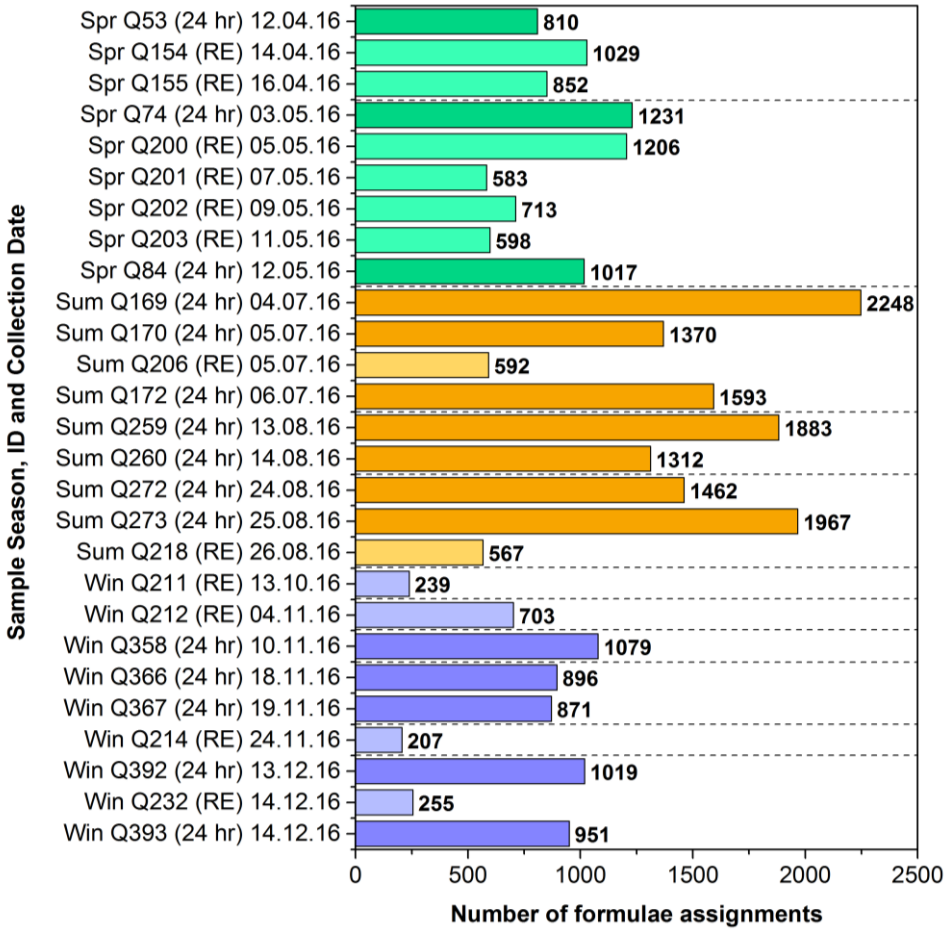

Figure 5.2. Number of formulae assignments in the aerosol samples; Spring (green), Summer (yellow) and Winter (blue). Values shown are combined across both scan ranges; *m*/*z* 60–550 and 150–900. Dashed lines indicate different rain events. Darker shading denotes samples collected every 24 hours ('24 hr'). Lighter shading denotes samples collected during rain events only ('RE').

Four different formulae assignment sub groups were identified in the samples. In all of the spring rainwater and aerosol, formulae containing C, H and O atoms only (CHO sub group) are the dominant sub group. Two sample *t-tests* with a significance level of 0.05 were used to identify any significant changes in the percentage of formulae sub-groups in the samples throughout the year (see Appendix A). Overall, there was a significant 67% decrease ($p = < 0.001$) in the percentage of CHO in the rainwater between spring and winter but no significant trend in the aerosol CHO throughout the year. There were significant increases in both the rainwater nitrogen containing compounds (CHON) (30%, $p = < 0.001$) and aerosol CHON (24%, $p = 0.004$) between the spring and winter samples. CHON compounds become more dominant throughout the year. This is illustrated in Figure 5.3 which shows the absolute number of compounds averaged for

each formulae sub group (A) and the number of compounds expressed as a percentage of the total number of formulae in the rainwater and aerosol samples (B). In the aerosol samples, even though the percentage of CHON compounds does increase throughout the year, there are still many individual samples which contain more CHO compounds so the dominance of CHON compounds in the winter samples is not as strong in the aerosol as it is in the rainwater.

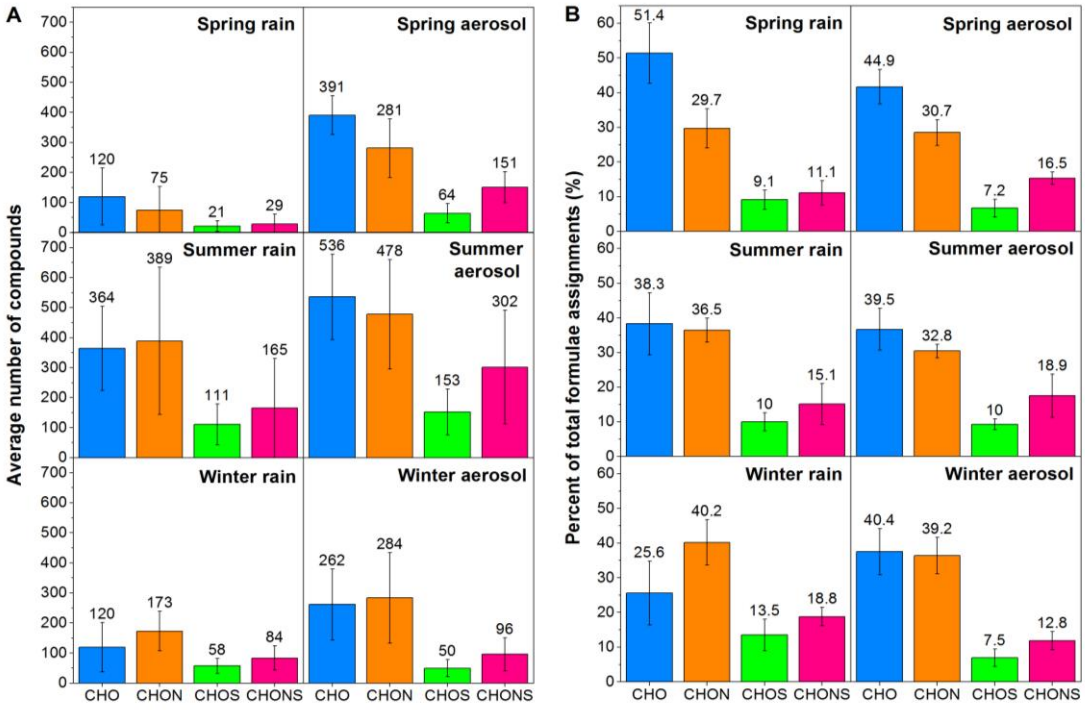

Figure 5.3. Average percentages of each formulae sub group; CHO, CHON, CHOS, CHONS, within the total formulae assignments (A) and average number of compounds in each formulae sub group (B) for rainwater and aerosol samples in each season. Error bars denote ± 1 standard deviation across each formulae sub group for each season.

The increase in the number and percentage of CHON compounds throughout the year is indicative of an extra source of nitrogen in the winter. Increases in organic nitrogen have been observed in polluted regions, both during the day through reaction with NO_x and at night through NO_3 radical-initiated reactions with alkenes (Kourtchev et al. 2014b). In north-west Spain, anthropogenic emission influence from coal combustion used for residential heating in the winter months, observed in a recent study in Madrid (Mirante et al. 2013), could be the source of the increase in CHON compounds in the winter samples. The large increase in the number of CHON compounds in the rainwater

and aerosol observed between spring and summer is likely due to enhanced photochemical production of nitrogen-containing organic compounds in summer.

Sulphur-containing compounds (CHOS) are present in the lowest abundance, across most of the individual rainwater and aerosol samples, in all seasons. In the rainwater samples, the percentage of CHOS compounds increased throughout the year by 39% ($p = 0.02$) with the highest percentage occurring during the winter. Previous studies have suggested that gas-to-particle partitioning of organosulphates is higher at cooler temperatures (Kourtchev et al. 2014b, Surratt et al. 2008) and this could explain why more CHOS and CHONS compounds are observed in the winter samples in this study. However the percentage of CHOS in the aerosol was more variable; there was a statistically significant increase between the spring and summer (34%, $p = 0.02$), followed by a significant decrease between summer and winter (29%, $p = 0.04$). The decrease in the winter could be linked to the increase observed for the rainwater and indicate that the gas to particle partitioning is resulting in more CHOS being removed from the atmosphere by the rainwater during the winter.

Significant increases in the nitrogen and sulphur-containing compounds (CHONS) were also observed in both the rainwater (52%, $p = < 0.001$) and aerosol (25%, $p = 0.008$) between spring and winter but the number of CHONS did decrease significantly (38%, $p = 0.04$) in the aerosol between summer and winter, perhaps for the same reason described above for the CHOS compounds. It should be noted, however, that the percentages of CHOS and CHONS compounds in the individual samples are highly variable.

Figure 5.4 shows the negative ionisation mode ultra-high resolution mass spectra for the common ions in all of the spring, summer and winter rainwater samples respectively. The winter rain samples contain compounds with higher m/z values (> 600) which are almost non-existent in the spring and summer rain mass spectra and these compounds comprise all four formulae sub groups. This indicates different sources are influencing the winter samples from the spring and summer samples. This may be due to the origin of the air mass which will be discussed in Chapter 7.

In Figure 5.5, the mass spectra for the CHO compounds in the rainwater samples are shown and are grouped together according to the rain event they were from. It is clear that different rain events produced different distributions of compounds. For example, the samples from the winter rain event on 14–15 December produced compounds with

very high *m/z* values which were not present in the other winter rain samples and had a wider distribution of CHO compounds than the other winter rain events. This suggests this was a particularly polluted air mass containing many compounds that were scavenged by the rain. The mass spectra for the CHON, CHOS and CHONS compounds detected in the rainwater samples are provided in Figure H.1–H.3 in Appendix H. The spring and summer rainwater samples overall appear to have relatively even distributions of CHO, CHON, CHOS and CHONS compounds. The CHO and CHON compounds detected in all three seasons occupy a slightly lower *m*/*z* value range than the CHOS and CHONS compounds in the same samples. Very few CHOS and CHONS compounds have *m*/*z* values < 200 whereas the majority of detected CHO and CHON compounds in the rainwater with the highest intensities are in the 100–200 *m*/*z* range. The 19–20 November and 14–15 December rain events appeared to contain more compounds in all formulae groups with *m*/*z* values > 580 compared with the other winter rain events.

Figure 5.6 shows the mass spectra for all four formulae sub-groups detected in the aerosol samples. Like the rainwater, the winter samples contain more compounds with *m*/*z* values > 600 than the spring or summer rainwater. However, far fewer compounds with *m*/*z* values > 600 were detected in the aerosol compared with the rainwater samples collected during the same rain events. The mass spectra for the CHO compounds detected in the aerosol samples is shown in Figure 5.7 and the mass spectra for the CHON, CHOS and CHONS compounds are provided in Figure H.4–Figure H.6 in Appendix H. Similar to the spring rainwater samples, the spring aerosol CHO and CHON compounds occupy a lower *m*/*z* range than the CHOS and CHONS compounds.

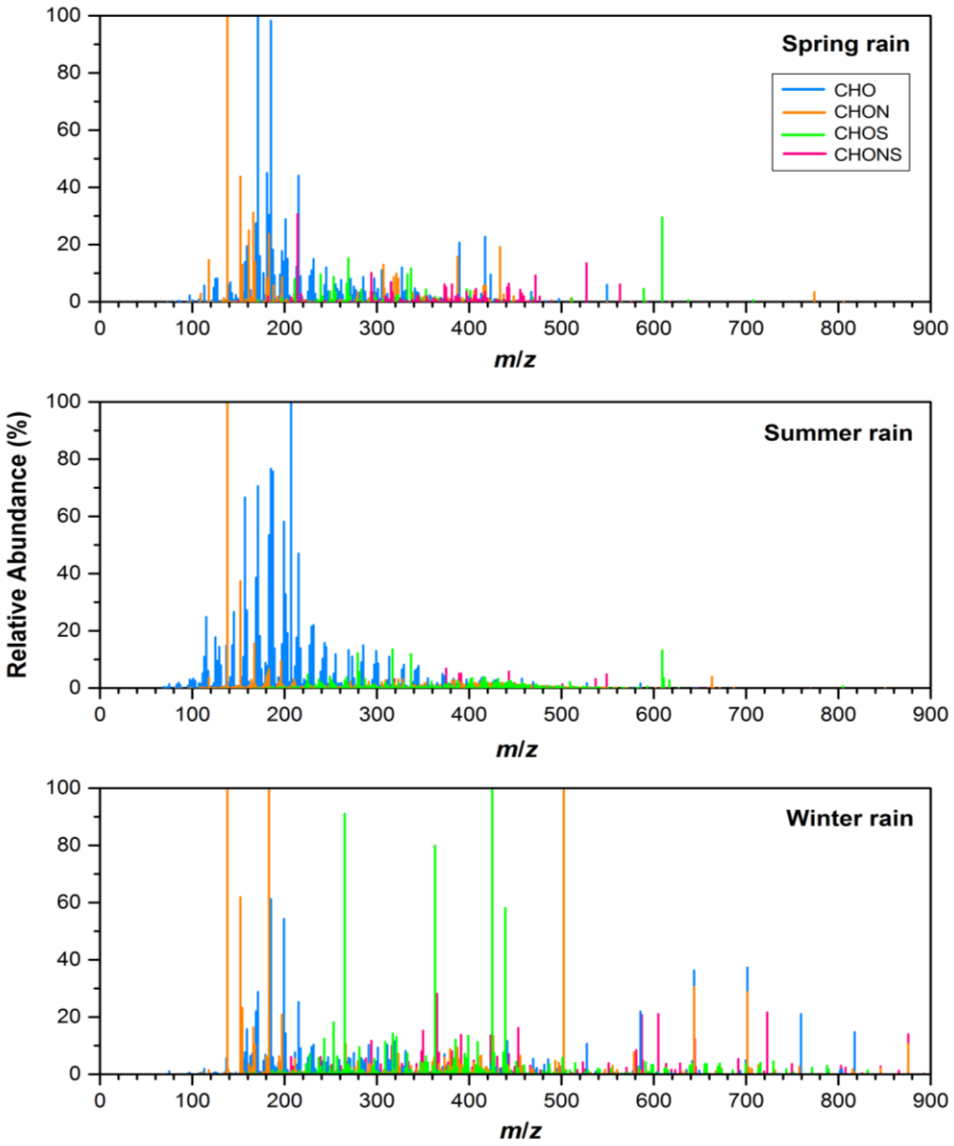

Figure 5.4. Reconstructed (−)ESI mass spectra showing common ions for the four identified formulae sub groups; CHO (blue), CHON (orange), CHOS (green) and CHONS (pink) in the spring, summer and winter rainwater samples.

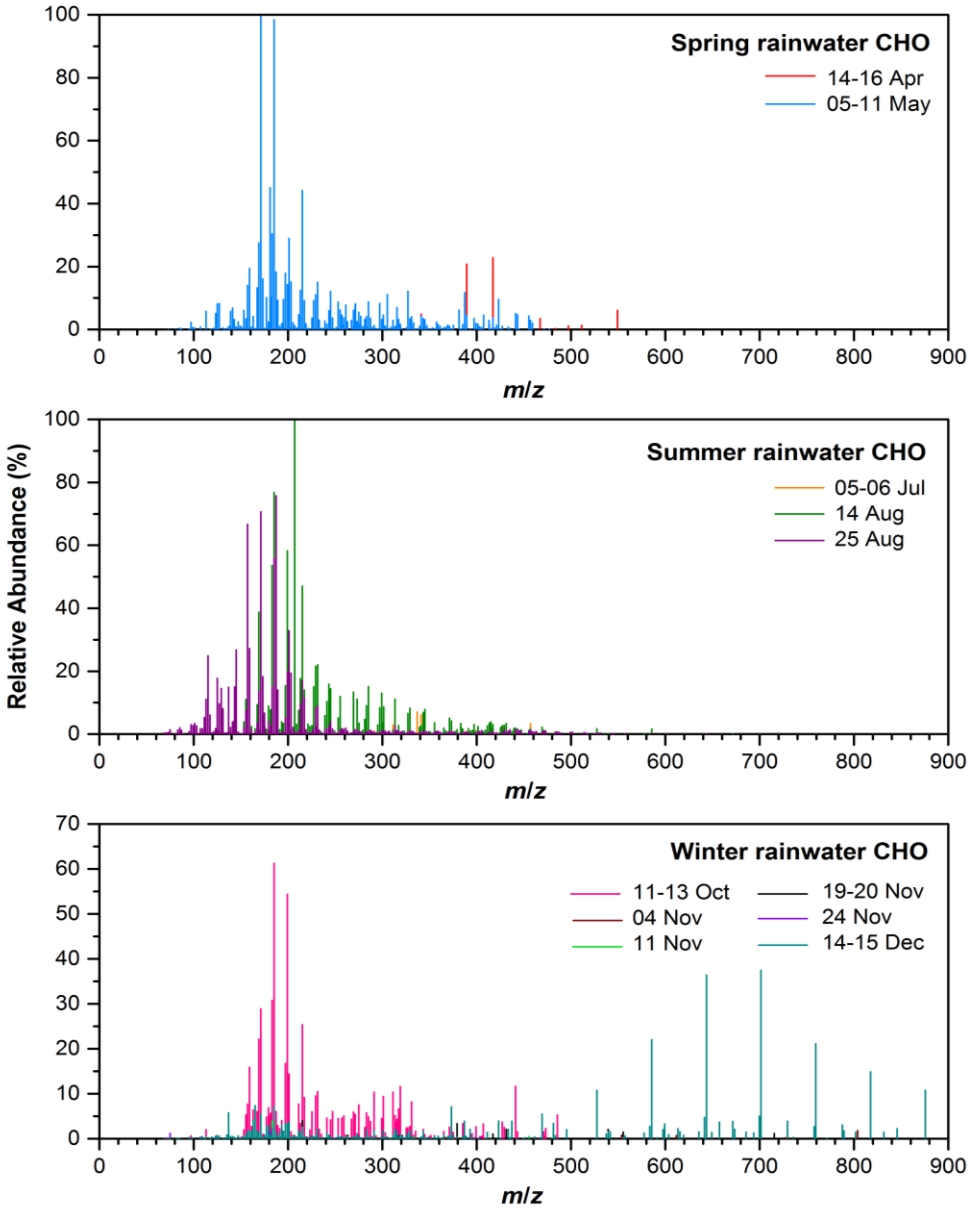

Figure 5.5. Reconstructed (−)ESI mass spectra showing common ions for the CHO compounds only in the rainwater samples across spring, summer and winter 2016. Samples are colour coded according to the rain events they were collected during.

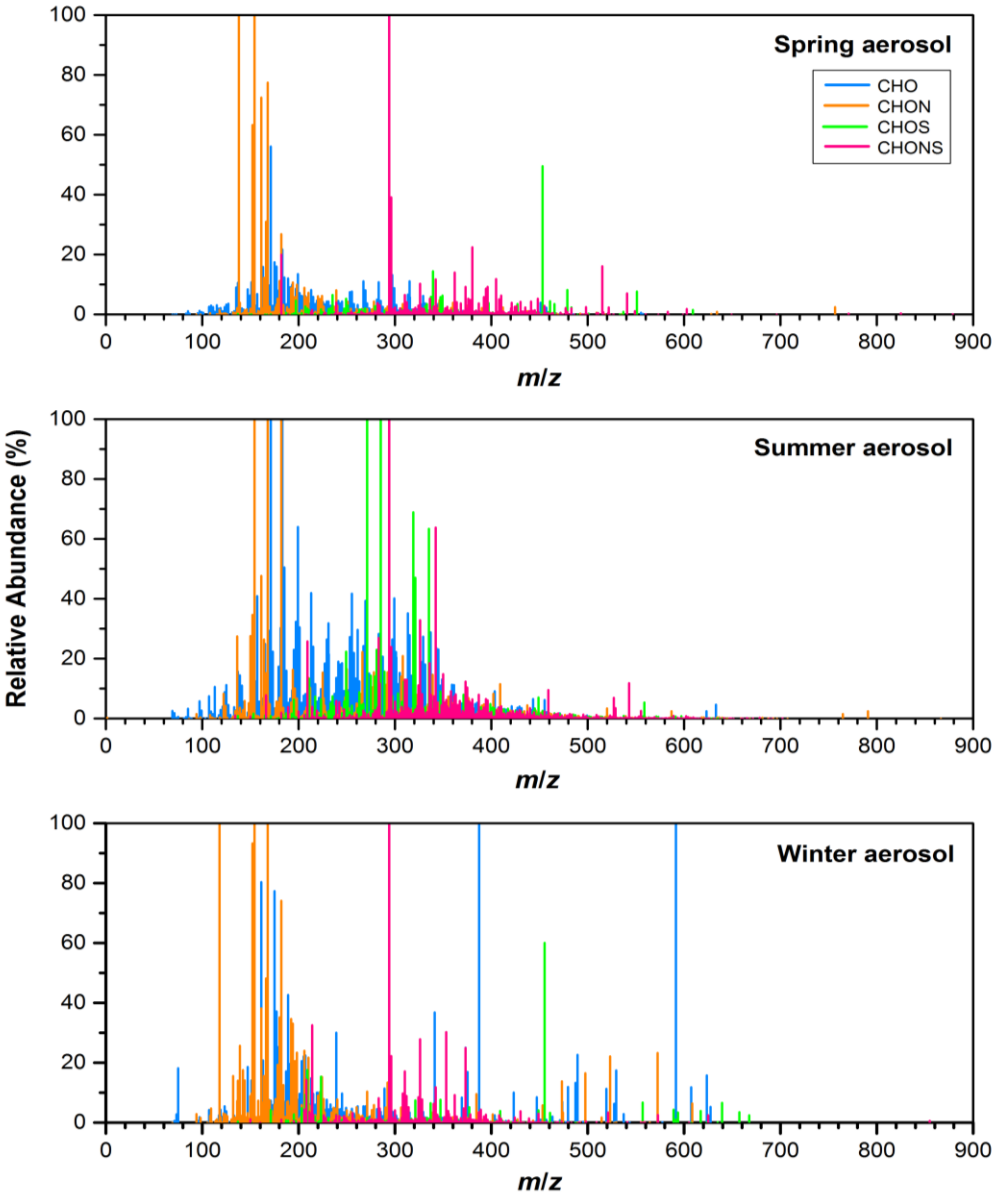

Figure 5.6. Reconstructed (−)ESI mass spectra showing common ions for the four identified formulae sub groups; CHO (blue), CHON (orange), CHOS (green) and CHONS (pink) in the spring, summer and winter aerosol samples.

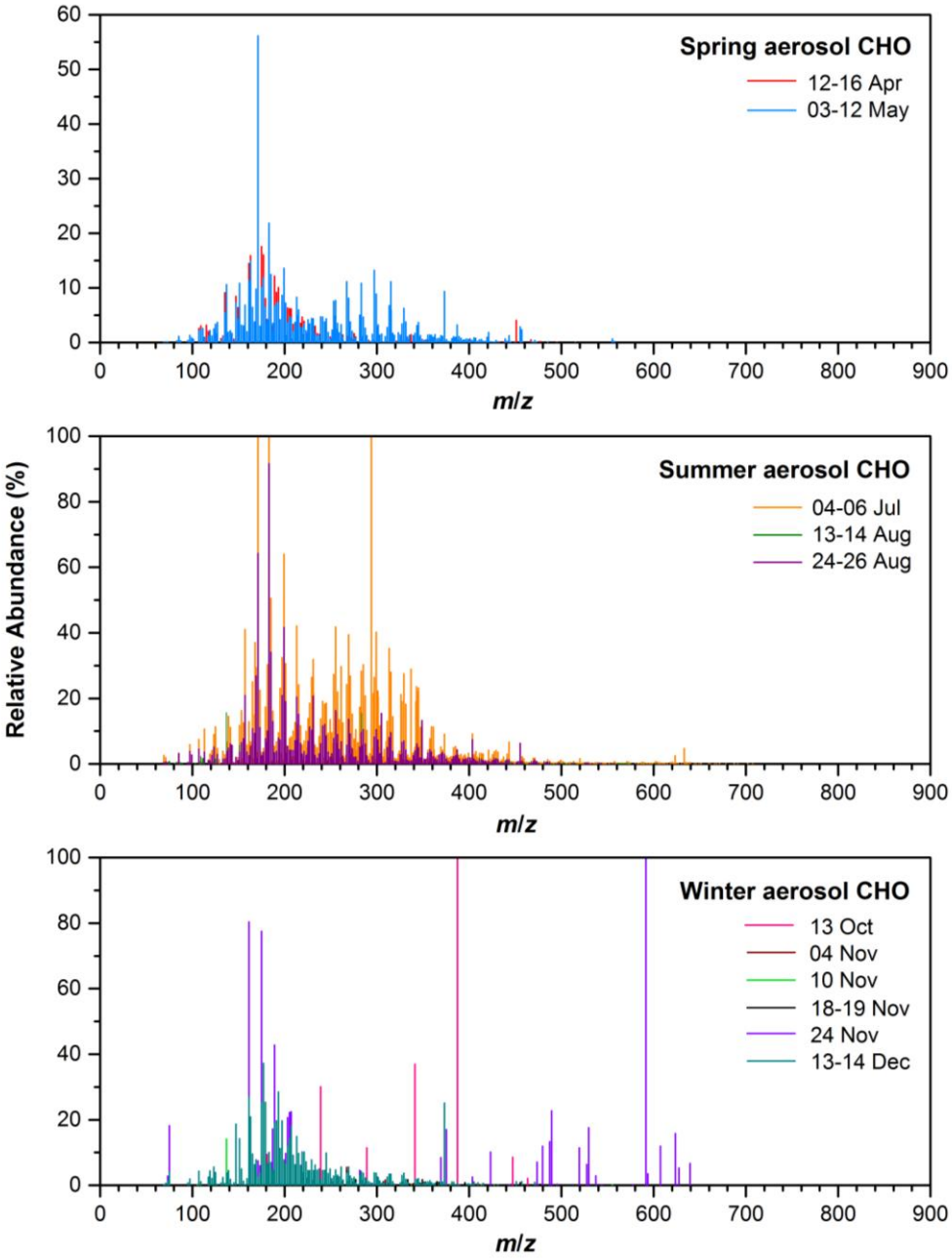

Figure 5.7. Reconstructed (−)ESI mass spectra showing common ions for the CHO compounds only in the aerosol samples across spring, summer and winter 2016. Samples are colour coded according to the rain events they were collected during.

5.4.2 Seasonal and local meteorological influence on sample acidity and composition

The Dissolved Organic Carbon (DOC) measured in the rainwater samples, pH of the rainwater samples and additional meteorological measurements (all measured by Dr A. I. Calvo and fellow researchers during the AERORAIN campaign, prior to the composition analysis in Cambridge) are shown in Figure 5.8. The DOC in the rainwater shows clear seasonal variation with high concentrations in the four summer samples which has also been observed in previous rainwater studies (Willey et al. 2000). This is partly due to phytoplankton blooms over the Atlantic ocean during the late summer (O'dowd et al. 2004) emitting primary organic matter through bubble bursting and oxidised organic species. It is also due to increased natural BVOC emissions from terrestrial sources and biomass burning from forest fires in the summer periods (Durana et al. 1992).

The average pH values for the spring, summer and winter rainwater samples were 6.63 ± 0.47, 5.67 ± 0.65 and 5.83 ± 0.42 respectively. 10% of the spring rainwater samples, 50% of the summer samples and 42% of the winter samples have pH values less than 5.6; the pH of *pure* rainwater in equilibrium with atmospheric CO_2, and thus could potentially be classified as acidic rain. A previous study of rainwater collected in north-west Spain observed a lower average pH value of 5.0 ± 0.7 (Peña et al. 2002). Modelled studies of global pH such as (Tost et al. 2007) have observed pH values between 4 and 5 for western Europe. Field studies have observed lower pH values over continental regions (pH 3.5–5.5) due to higher inorganic nitrogen (NO_3^-, NO_2^- and NH_4^+) concentrations and secondary SO_4^{2-} aerosol from anthropogenic sources including biomass burning (Paerl 1985). Acidic gases like NO_x and SO_2 and basic gases like NH_3 also contribute to rainwater acidity when they dissolve in cloud water and produce nitric and sulphuric acids respectively (Salve et al. 2008). The increased percentage of CHOS and CHONS compounds in the winter rainwater compared with the spring rainwater in Figure 5.3 suggests this could be the case for the samples in this study. However, some continental locations with high emissions of alkaline dust particles, Ca, K, Mg ions from soil, and gaseous NH_3 have more alkaline rainwater pH values due to neutralisation of some of the acidity (Mouli, Mohan and Reddy 2005, Singh et al. 2001). Marine locations have higher pH values (pH 5.5–6.8) than continental regions due to a lack of acidic ions produced from anthropogenic emissions (Paerl 1985). This

could suggest that the León samples have marine influence which is producing a higher pH than previously observed in north-west Spain. Potential influence from rain origin will be investigated in Chapter 7.

There is a slight increase in the acidity of the rainwater samples throughout the year as shown in Figure 5.8. Some of the summer rainwater samples are significantly more acidic than the spring rain samples. There were only four recorded rain events in León during summer 2016 and the pH of the rainwater in these samples corresponds very closely to the relative humidity in the atmosphere. It has been suggested that desert regions in Africa that have small amounts of total cloud and rainwater, have the available acidity in the atmosphere concentrated (Tost et al. 2007). If the summer rain events in León have been influenced by Saharan air masses, the available acidity could have been concentrated in the rainwater, resulting in more acidic samples. The winter samples are clearly more acidic on average than the spring samples which could be due to additional sources of SO_2 and NO_x compounds in the winter months from coal combustion used for residential heating or from the condensation of HNO_3 at the colder temperatures. These compounds then oxidise to sulphuric, nitric or organic acids and are removed from the atmosphere via wet deposition, increasing the acidity of the rainwater.

There are no strong trends attributing the number of compounds in the rainwater samples to the mean wind speed, maximum rain intensity or relative humidity (RH) during the rain events. There is a slight positive correlation between the mean air temperature and average number of compounds, driven mainly by the four summer rain samples which had high compound loadings. The lack of moisture in the air during the summer as shown by the RH trend, coupled with the high DOC loading (and also the increased rates of photochemistry and more sources of BVOCs during the summer) helps to explain why the summer rainwater contains the highest number of compounds on average compared with the spring and winter rainwater.

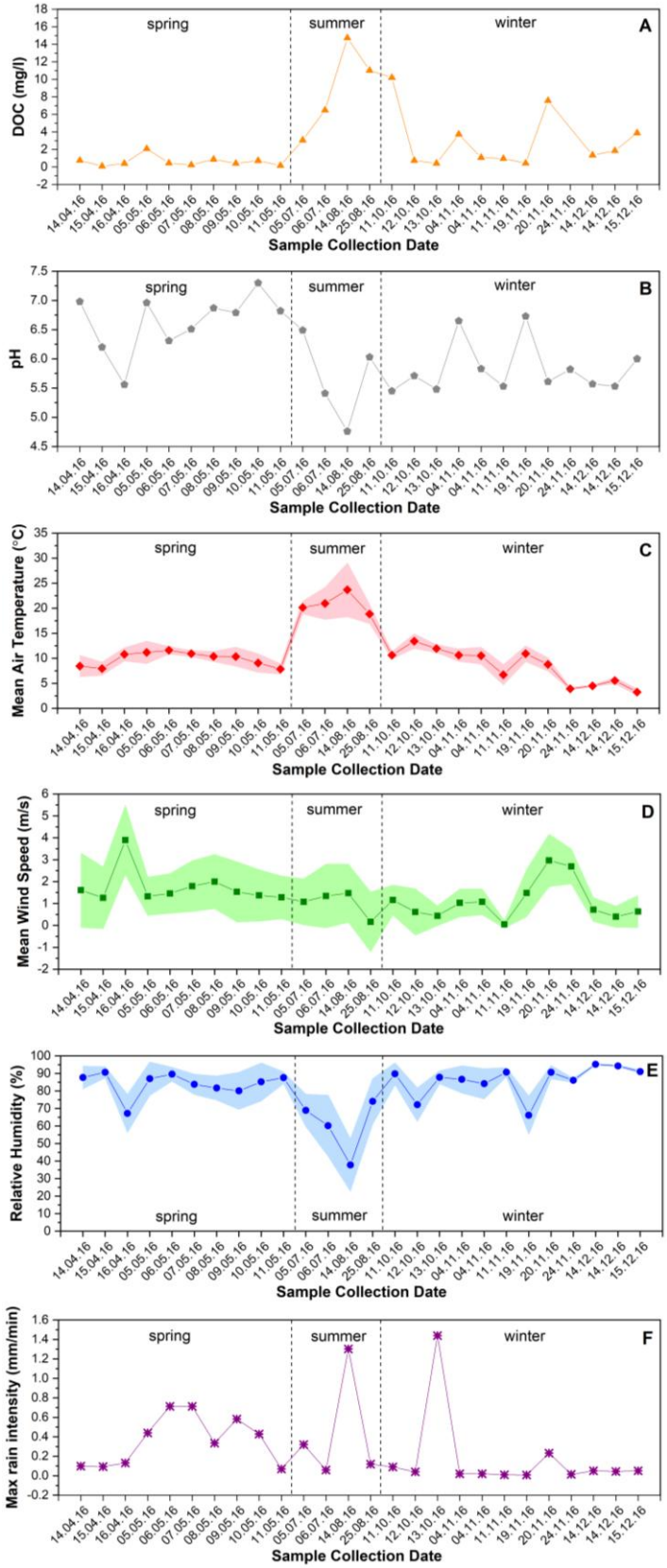

Figure 5.8. Meteorological data collected in León during rain events; measured Dissolved Organic Carbon (DOC) in the rainwater samples (A), pH of rainwater samples (B), mean air temperature (C), mean wind speed (D), relative humidity (E) and maximum rain intensity (F). Shading denotes ± 1 standard deviation.

5.4.3 Concentrations of particulate matter and inorganic ions during AERORAIN campaign

Two different aerosol samplers (Tecora and GENT) were used to collect the 'RE' aerosol samples during the rain events. This resulted in $PM_{2.5}$ concentrations being measured for the spring 'RE' aerosol samples and the summer 'RE' aerosol sample collected on 05.07.16; and PM_{10} concentrations being measured for the 26.08.16 summer 'RE' sample and the winter 'RE' aerosol samples.

To allow a comparison between the two sets of data, PM_{10} concentrations were estimated for the spring and July samples using the ratio of the available $PM_{2.5}$ and PM_{10} concentrations for the '24 hr' aerosol samples collected either on the day before or on the same day as the 'RE' aerosol sample. Four pairs of samples were used to calculate an average ratio of 2.08 ± 1.18 and this was applied to the $PM_{2.5}$ concentrations for the 'RE' aerosol to provide estimates of the PM_{10} concentrations, shown as green diamonds in Figure 5.9 (A). It is noted that this estimated PM_{10} concentration is based on the average of only four samples, and thus the error bars representing ± 1 standard deviation of the average $PM_{10}/PM_{2.5}$ ratio in Figure 5.9 (A) are very large. However, whilst the individual values should be viewed with caution, the temporal trend is conserved from the $PM_{2.5}$ concentrations, and is thus comparable with the measured PM_{10} concentrations for the 'RE' and '24 hr aerosol.

The PM_{10} concentration for the '24 hr' aerosol collected using the CAV high volume sampler along with the organic carbon (OC), elemental carbon (EC) and total carbon (TC) analysis are shown in Figure 5.9 (B). The solid symbols in (B) are the '24 hr' samples that were collected on the day a rain event occurred and the open symbols are the '24 hr' samples that were collected on days either before or after a rain event occurred. All data shown in Figure 5.9 was measured in León by Dr A. I. Calvo and fellow researchers prior to the sample composition analysis in Cambridge.

PM_{10} concentration for the '24 hr' aerosol samples peak during the summer and this corresponds to an increase in TC, driven largely by the increased OC concentration in the summer due to increased photochemical activity. There is little variation in the EC throughout the year. Almost all of the PM_{10} concentration peaks in the '24 hr' aerosol samples correspond to peaks in concentration of SO_4^{2-}, NH_4^+ and NO_3^- ions measured in León prior to the Cambridge analysis. These ion concentrations are provided in

Figure I in Appendix I. The large peak in Figure 5.9 (B) for the PM_{10} and TC concentration, and the SO_4^{2-}, NH_4^+ and NO_3^- concentrations, on 24.08.16 also corresponds to the MS detection of a large number of CHON, CHOS and CHONS compounds for the summer aerosol during the 24.08.16–26.08.16 rain event, shown in Figure H.4–Figure H.6 in Appendix H. The case is the same for the peak in PM_{10} and TC concentration on 13.12.16 which also corresponds to very large peaks in concentration for SO_4^{2-}, NH_4^+ and NO_3^- and the CHON, CHOS and CHONS compounds from the 13.12.16–14.12.16 rain event which dominated the respective MS spectra for the winter aerosol in Appendix H (Figure H.4–Figure H.6).

The estimated PM_{10} concentrations for the spring 'RE' samples are similar to the measured PM_{10} concentrations for the August and winter 'RE' aerosol samples. The high estimated PM_{10} concentration for the July 'RE' sample corresponds to the summer peak shown for the '24 hr' aerosol samples in Figure 5.9 (B) although the error for this one sample is significant due to the average $PM_{10}/PM_{2.5}$ ratio used. The estimated PM_{10} concentration for the long rain event in May decreases over the course of the rain event, similar to the measured $PM_{2.5}$ concentrations which steadily decreased from 3.8 μg/m^3 on the first day of the rain event (03.05.16) to 0.1 μg/m^3 on the last day (11.05.16). It can be said with confidence, therefore, that the estimated PM_{10} concentration does show a genuine decrease in aerosol concentration during the rain event which is indicative of aerosol scavenging by the rain droplets. It may also suggest evaporative loss of aerosol species from gas-to-particle conversion where volatile species have re-equilibrated back into the atmosphere from the filter, which has been proposed to happen during aerosol sampling (Zhang and McMurry 1987, Zhang and McMurry 1991). The more 'aged', volatile species would evaporate, leaving behind the less 'aged' and less volatile species on the filter, making the aerosol collected at the end of the rain event less complex and less aged than the aerosol collected at the beginning of the rain event.

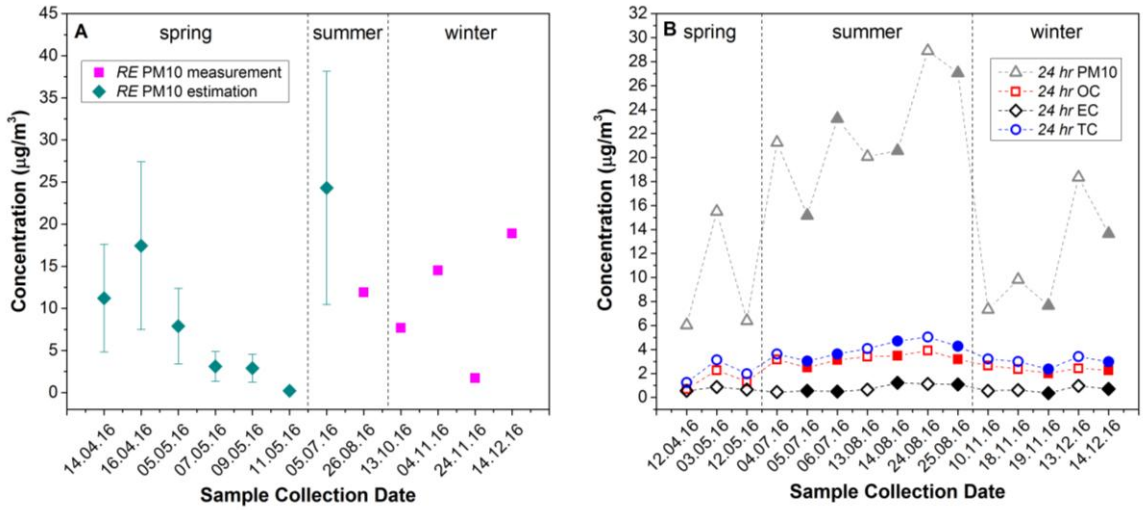

Figure 5.9. (A) Estimated PM_{10} concentrations for the spring and July aerosol samples collected during the rain event only ('RE'), (green diamonds) and measured PM_{10} concentrations for the August and winter 'RE' aerosol (pink squares). (B) PM10 (grey triangles), measured OC (red squares), EC (black diamonds) and TC (blue circles) concentrations for the aerosol collected every 24 hours ('24 hr'). Solid symbols indicate aerosol samples collected on the same day as rain events and open symbols are '24 hr' aerosol samples collected before or after rain events. Estimated PM_{10} concentrations were calculated using the ratio of the measured $PM_{2.5}$ concentrations for those samples and the PM_{10} concentrations of '24 hr' aerosol samples collected on the day before or on the same day as the 'RE' aerosol samples. Error bars denote the ± 1 standard deviation of the average $PM_{10}/PM_{2.5}$ ratio, scaled for each $PM_{2.5}$ concentration. The connecting lines in B are included to aid interpretation of temporal variation only.

5.4.4 Seasonal distribution of different compound classes

UHRMS analysis for ambient samples produces a large amount of data. To aid interpretation, various visualisation techniques can be used to estimate bulk elemental ratios and in doing so, categorise the formulae assignments and identify chemical relationships and potential differences between different data sets (Noziere et al. 2015, Heald et al. 2010).

The van Krevelen (VK) diagram, first defined in (Van Krevelen 1950) uses the oxygen to carbon (O/C) and hydrogen to carbon (H/C) elemental ratios for each formulae assignment and has been used in numerous studies to characterise OA (Ng et al. 2011, Heald et al. 2010, Lambe et al. 2011, Bateman et al. 2009, Tong et al. 2016, Mazzoleni et al. 2010a, Zhao et al. 2013, Kim, Kramer and Hatcher 2003, Lin et al. 2012a,

Kourtchev et al. 2013). O/C ratios are used as a measure of oxidation of compounds, with the most oxidised species lying in the lower right part of the plot. H/C ratios reflect the saturation or degree of reduction of compounds and more highly saturated compounds lie in the upper left part of the plot.

VK diagrams for the rain and aerosol samples, grouped according to season, were plotted using the direct infusion Nano-ESI-MS data and are presented in Figure 5.10. Larger versions of each of the VK plots are available in Figure J1–Figure J6 in Appendix J. The arrows included in Figure 5. indicate potential structural relationships between the molecular formulae. Arrow A has a gradient of +2 and is consistent with hydration reactions. Arrow B represents addition of an alcohol (–OH) group only to a carbon backbone which involves an increase in oxygen but no change in hydrogen so the gradient is zero ($\Delta H/C = 0$). Arrow C represents an intermediate gradient of −1 ($\Delta H/C = -\Delta O/C$), produced by the simultaneous addition of an alcohol and a carbonyl (–C(=O)–) group, forming a carboxylic acid or hydroxycarbonyl compound. Arrow D has a gradient of −2 ($\Delta H/C = -2 \times \Delta O/C$) from the replacement of an aliphatic carbon with a carbonyl group as in the formation of an aldehyde or ketone, corresponding to a loss of 2 hydrogens and a gain of 1 oxygen. Arrow E has a gradient of −4 and represents dehydrogenation (oxidation) reactions of alcohols or amines to produce aldehydes, ketones or imines. The reverse reaction is hydrogenation (reduction) for example, the reduction of a carboxylic acid to an aldehyde (Heald et al. 2010, Lambe et al. 2011). It should be noted that these relationships denoted by the arrows can only be tentatively suggested for ambient aerosol as it is not possible to be certain of these relationships without using Nuclear Magnetic Resonance (NMR), LC-MS, MS/MS or a similar technique to obtain information on the structural changes of the compounds.

Figure 5.10. Van Krevelen plots showing oxygen to carbon (O/C) and hydrogen to carbon (H/C) elemental ratios for CHO (blue), CHON (orange), CHOS (green) and CHONS (pink) compounds in every rainwater and aerosol sample from León. Boxes represent potential sources of molecular classes. Grey boxes: (1) Lipids, (2) Proteins, (3) Aminosugars, (4) Cellulose, (5) Lignin, (6) Tannins, (7) Poly-Aromatic Hydrocarbons. Red box (8) and blue box (9) are monocarboxylic and dicarboxylic acids respectively. Purple box (10) is SOA and dashed boxes (11) and (12) are aliphatic and aromatic compounds respectively. Arrows indicate potential chemical reactions; (A) hydration, gradient = 2, (B) addition of OH group, gradient = 0, (C) simultaneous addition of C=O and OH group, gradient = −1, (D) replacement of CH_2 group with C=O group, gradient = −2, (E) dehydrogenation, gradient = −4.

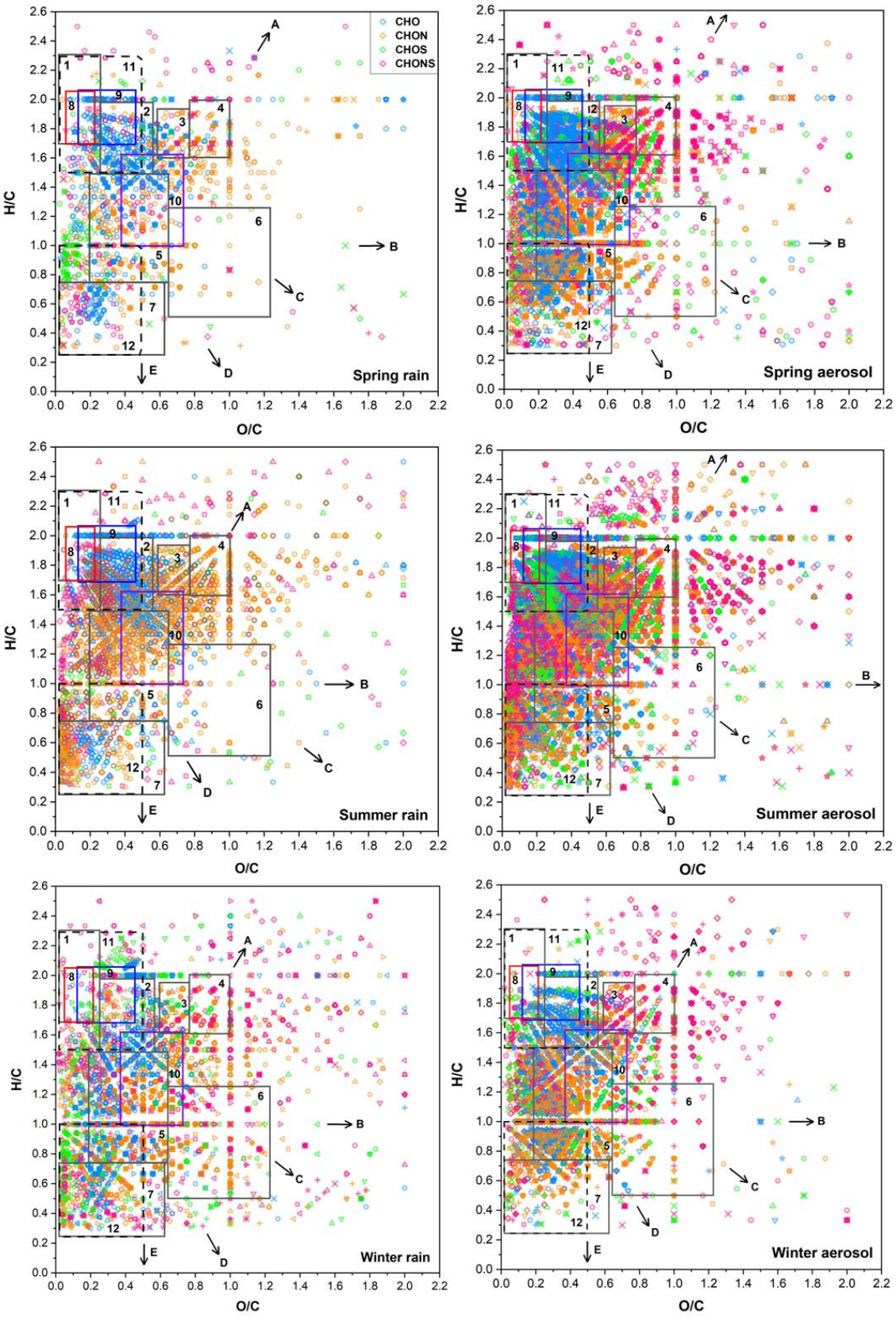
CHO
CHON
CHOS
CHONS
Spring rain
Spring aerosol
Summer rain
Summer aerosol
Winter rain
Winter aerosol
H/C
O/C
A
B
C
D
E
1
2
3
4
5
6
7
8
9
10
11
12

The O/C and H/C ratios are plotted for each of the four identified formulae sub groups; CHO (blue), CHON (orange), CHOS (green) and CHONS (pink) in the rainwater and aerosol samples across the seasons in Figure 5.10. The grey boxes (1–7) in the VK diagrams indicate potential sources of these O/C and H/C ratios which have been determined from swamp dissolved organic matter (DOM) (Sleighter and Hatcher 2007) and are traditionally used as aids for interpreting complex ambient aerosol MS data (Wozniak et al. 2008, Noziere et al. 2015). The monocarboxylic acid (red box, 8) and dicarboxylic acid (blue box, 9) regions are based on WSOC aerosol O/C and H/C measurements from the USA (Wozniak et al. 2008). The area in the purple box, 10, corresponds to laboratory SOA O/C and H/C ratios (Reinhardt et al. 2007, Altieri et al. 2008). Aliphatic compounds which typically have low O/C ratios (≤ 0.5) and high H/C ratios (≥ 1.5) are indicated by dashed box 11 and aromatic hydrocarbons which have low O/C ratios (≤ 0.5) and low H/C ratios (≤ 1.0) are indicated by the dashed box 12 (Kourtchev et al. 2013).

The VK plots show that there are aliphatic and aromatic CHO compounds present in all of the rainwater and aerosol samples, across all seasons. The rainwater CHO compounds are largely clustered in the aliphatic (box 11), aminosugar (3), SOA (10) and Lignin (5) regions with O/C ratios between 0.0 and 0.8 and H/C ratios between 1.3 and 1.9. There is a smaller cluster in the aromatic hydrocarbon region with O/C ratios between 0.0 and 0.5 and H/C ratios between 0.3 and 0.8. Formulae with O/C ratio ≤ 0.5 and H/C ratios ≤ 1.0 are often Polycyclic Aromatic Hydrocarbons (PAHs) (Tong et al. 2016) which have anthropogenic sources including soot from coal combustion, residential heating, industrial emissions, vehicle exhaust and also natural sources such as forest fires (Lin et al. 2012a, Abdel-Shafy and Mansour 2016).

There are a lot of compounds in the aromatic regions of the VK plots, particularly in the summer samples which may suggest anthropogenic sources and forest fires are responsible. However, only oxidised PAHs are observed in this data so the VK plots may be more useful for interpreting the extent of photo-oxidation rather than potential sources of these compounds. The aerosol samples across all seasons generally contain more CHO compounds and more reduced compounds (lower O/C ratios and higher H/C ratios) than their rainwater counterparts. The average O/C ratios for the rainwater compounds were 0.46 ± 0.03 (spring), 0.55 ± 0.08 (summer) and 0.53 ± 0.04 (winter) and the average H/C ratios were 1.37 ± 0.06 (spring), 1.27 ± 0.35 (summer) and 1.20 ±

0.09 (winter). For the aerosol, the average O/C ratios were 0.44 ± 0.01 (spring), 0.48 ± 0.02 (summer) and 0.43 ± 0.02 (winter) and the average H/C ratios were 1.32 ± 0.04 (spring), 1.42 ± 0.02 (summer) and 1.23 ± 0.06 (winter).

The winter rainwater samples appear to contain fewer aliphatic mono- and dicarboxylic acids and more lignin-associated compounds than either the spring or summer rainwater samples. Aliphatic compounds can be of both biogenic and anthropogenic origin (Kourtchev et al. 2014a) but lignin is a prominent component of biomass (Ahmad and Subawi 2013) so this suggests a potential shift from marine sources to biomass burning sources from summer to winter. The summer aerosol contains a much wider distribution of CHO compounds compared with other seasons, including many more highly oxygenated compounds with O/C ratios > 1.0 and hydrogen-rich compounds with H/C ratios > 2.0. There is less clustering of aromatic hydrocarbons (box 7) in the winter aerosol than the other datasets. These two observations suggest that there are more aged particles undergoing photo-oxidation and more gas-to particle partitioning is occurring in the summer whereas there is less photo-oxidation occurring in the winter; meaning fewer oxygenated aromatic compounds (Williams et al. 2007). It is also possible that PAHs are being scavenged by rainwater in the winter samples, since there appear to be more PAHs in the winter rainwater than the winter aerosol.

The distribution of CHON compounds are reasonably similar across the seasons, concentrated in the aminosugar (3), cellulose (4), lignin (5), SOA (10) and in the aromatic (12) regions. Photo-oxidation in the summer may be producing R-NO_2 and R-NO_3 compounds. The summer rainwater and aerosol samples contain more aromatic CHON compounds with O/C ratios between 0.0 and 0.2 and H/C ratios between 0.3 and 0.8, than the spring or winter samples. Biomass burning from forest fires could be influencing the composition in the summer samples because organic aerosol affected by biomass burning is often characterised by large numbers of CHON compounds with O/C ratio < 0.5 and H/C ratios < 1.0 (Kourtchev et al. 2016b).

There are significant clusters of CHOS compounds in the aromatic and aliphatic regions of the VK plots. The spring rainwater samples contain very few CHOS compounds compared with the summer and winter rainwater samples. The summer samples contain a cluster of CHOS compounds with O/C ratios between 0.1 and 0.4 and H/C ratios between 0.9 and 1.3 which are less prominent in the other seasons. This further suggests that the summer samples may have some different meteorological influences from the spring and winter samples.

CHONS compounds are mainly clustered in the aliphatic and aromatic regions and could potentially include monocarboxylic acids. There is a large cluster of CHONS compounds with O/C ratios between 0 and 0.4 and H/C ratios between 0.7 and 1.6 in the aerosol samples, partially in the lignin (box 5) region. The aerosol samples also have many highly oxygenated compounds (O/C ratios > 1.0) because these compounds are likely to contain R–NO_2/NO_3–SO_4 groups, and also highly saturated compounds (H/C ratios > 2.0), in the aminosugar (box 3) and cellulose (box 4) regions. The presence of compounds in the lignin and cellulose regions does suggest that biomass burning has influenced these samples.

5.5 Conclusions

The primary aim of this work was to investigate any seasonal trends in the distribution of compounds within the samples. 26 rainwater samples and 27 aerosol samples collected in León during the AERORAIN campaign, over three different seasons, were analysed using direct infusion Nano-ESI-MS. Summer aerosol contained the highest overall number of compounds due to increased photochemical and biogenic activity producing more SOA components, and also changes to the local meteorology including reduced RH on the days of the summer rain events which concentrated the acidity and available material in the atmosphere, producing higher concentrations of DOC and acidity in the summer rainwater.

CHO compounds dominated the spring rain and aerosol samples. CHON compounds increased throughout the year, becoming the dominant formulae sub-group in winter rain and aerosol. This was probably due to enhanced photochemical activity in the summer and residential heating coal combustion in winter in Spain. CHOS compounds were present in the lowest abundance in most individual samples, across all seasons. The percentage of CHOS and CHONS compounds increased throughout the year overall, perhaps aided by increased gas-to-particle partitioning occurring in the cooler temperatures in the winter. There was a decrease in the percentage of CHOS and CHONS compounds between summer and winter which could be indicative of aerosol scavenging.

PM_{10}, TC and OC concentrations in the '24 hr' aerosol samples were highest during the summer due to higher photochemical activity. The peaks in PM_{10} concentration coincided with peaks in the concentrations of SO_4^{2-}, NH_4^+ and NO_3^- ions in the '24 hr' aerosol. Estimated PM_{10} concentrations in the aerosol collected during the rain events showed a clear decrease throughout the seven day rain event in May 2016. This is indicative of aerosol scavenging by rain droplets and could indicate evaporative loss of aerosol species following gas-to-particle partitioning on the filter and subsequent re-equilibration of volatile species back into the atmosphere. If this is the case, aerosol collected at the end of the rain event is less aged and less complex than aerosol collected at the beginning of the rain event.

Van Krevelen diagrams highlighted aliphatic and aromatic compounds in all of the samples and an increase in lignin-associated compounds in the winter rainwater which suggests biomass burning becomes a stronger source of compounds in the winter. However there were also many CHON compounds in the summer samples compared with the spring and winter samples which suggests biomass burning from forest fires were influencing the summer sample composition. Summer aerosol contained more oxygenated CHO compounds, indicating more photo-oxidation, more aged particles and potentially more gas-to-particle conversion occurring in the summer compared with the winter samples. The VK diagrams also showed more aromatic compounds in the winter rain than the winter aerosol suggesting scavenging of particulates is occurring during the winter. CHOS and CHONS compounds were mainly confined to the aliphatic and aromatic regions of the VK plots and more highly oxygenated CHONS compounds were observed in the aerosol samples than the rainwater.

6 Investigating the Aromaticity of Compounds present in Rainwater and Aerosol during the AERORAIN Campaign

The van Krevelen plots in Chapter 5 identified numerous aromatic compounds in the rainwater and aerosol samples from the AERORAIN campiagn, across all seasons. The same direct infusion Nano-ESI-MS data will now be examined further in this chapter to identify any seasonal distributions of aromatic compounds in the samples, using different aromaticity metrics.

6.1 Introduction

Aromatic compounds including PAHs are considered to be the most important SOA precursors of all anthropogenic hydrocarbons and also important tracer compounds for wood combustion, vehicle emissions and tobacco smoke. Their presence in these sources is of interest because it is now widely known that PAHs can cause mutagenic

and carcinogenic effects and are potent immunosuppressants (Noziere et al. 2015, Abdel-Shafy and Mansour 2016, Henze et al. 2008).

VK plots are very useful for visualising the chemical diversity of complex ambient mixtures but they offer limited structural information and it is not possible to distinguish between compounds with identical O/C and H/C ratios (Yassine et al. 2014). However, various different metrics exist for identifying mono-aromatic and poly-aromatic compounds.

Choosing the most appropriate visualisation tools for classifying aromatic compounds in ambient samples is imperative for efficient interpretation of UHRMS data. The presence of heteroatoms and compounds with long alkyl side chains may make some aromaticity classification metrics more favourable than others. Three of the most common visualisation tools for classifying aromatic compounds in environmental samples will be discussed as they are applied to the direct infusion Nano-ESI-MS data for the AERORAIN rainwater and aerosol samples.

6.2 Aims

The aim of this chapter is to build on the initial characterisation of the AERORAIN rainwater and aerosol samples completed in Chapter 5 by focussing on the distribution of mono-aromatic and poly-aromatic compounds in the samples, using the direct infusion Nano-ESI-MS data.

The specific objectives of this analysis are to:

- Compare distributions of mono-aromatic and poly-aromatic compounds in the rainwater and aerosol samples.
- Investigate any seasonal distributions of mono-aromatic and poly-aromatic compounds in the samples.

6.3 Analysis and Discussion

6.3.1 Double Bond Equivalent (DBE)

Double Bond Equivalent (DBE), or the 'index of hydrogen deficiency', represents the number of rings plus double bonds and, thus, the degree of unsaturation in a compound which is an important structural feature and is a measure of the compound's reactivity (Yassine et al. 2014). When applied to complex ambient samples, DBE is used to remove molecular assignments containing an unreasonably high number of rings and double bonds that would be unlikely to exist in the environment. It can also yield information on aerosol sources and precursors (Noziere et al. 2015, Lin et al. 2012a). The equation for calculating DBE is provided in Equation 6.1:

$$\mathrm{DBE} = 1 + \frac{1}{2}(2\mathrm{C} - \mathrm{H} + \mathrm{N}) \, . \qquad (6.1)$$

The DBE value of formulae assignments is used to classify them as 'mono-aromatic' or 'poly-aromatic'. Benzene is the simplest aromatic compound and has a DBE value of 4 (3 double bonds plus 1 aromatic ring). Therefore, any aromatic compounds with additional aliphatic chains or rings must have at DBE value of ≥ 4. The simplest PAH; Napthalene, has a DBE value of 7 (5 double bonds plus 2 aromatic rings) so any poly-aromatic compounds must have a DBE value of ≥ 7.

A disadvantage of using DBE values alone for indicating aromatic compounds is that they do not account for heteroatoms, e.g. N, O or S which may reduce the number of single C–C bonds in the overall formulae without influencing aromaticity. Divalent atoms like O and S may replace a C–C single bond with a double bond. Trivalent atoms like N may form N–C π bonds which also reduce the potential number of C–C single bonds for that given DBE value and the additional H atom required to fill the extra valence of the N atom to form an uncharged compound will alter the H/C ratio. This means that there could be multiple H/C ratios for particular DBE values and makes classifying formulae based on DBE much more difficult (Koch et al. 2006, Yassine et al. 2014).

6.3.2 Aromaticity Index, AI

The *Aromaticity Index*, AI, introduced by (Koch et al. 2006) is used in conjunction with DBE to better classify aromatic compounds. It accounts for heteroatoms forming double bonds which do not contribute to ring formation, aromaticity or condensation. AI is calculated using the ratio of two parameters; DBE_{AI} and C_{AI}. DBE_{AI} is the minimum number of C–C double bonds plus rings in molecular structures which contain heteroatoms and is defined in the following equation:

$$DBE_{AI} = 1 + C - O - S - 0.5H, \tag{6.2}$$

where *C*, *O*, *S* and *H* are the number of carbon atoms, oxygen atoms, sulphur atoms and hydrogen atoms respectively.

C_{AI} is the number of C atoms reduced by the number of potential double bonds contributed by heteroatoms and is defined by

$$C_{AI} = C - O - N - S. \tag{6.3}$$

The Aromaticity Index is then calculated from the ratio of DBE_{AI} to C_{AI}:

$$AI = \frac{DBE_{AI}}{C_{AI}} = \frac{1 + C - O - S - 0.5H}{C - O - S - N}. \tag{6.4}$$

Compounds with high O/C and high H/C ratios have low AI values. The threshold value of AI > 0.5 is used to assign compounds as aromatic because any unsaturated, conjugated aliphatic compound (excluding cumulated π bond systems such as those in 2,3-hexadiene, and triple bonds, which have additional unsaturation) must include an aromatic structure and these compounds have AI values of 0.5 so > 0.5 is a conservative calculation for aromatic compounds. Any compounds with 0.5 < AI < 0.67 values are likely to be mono-aromatic and an AI value of ≥ 0.67 is used to indicate poly-aromatic compounds (Koch et al. 2006). Compounds with AI values between 0 and 0.5 are termed *olefinic* and are not aromatic (Mazzoleni et al. 2012b).

A limitation of the AI value is that some aromatic compounds with long alkyl side chains may have a reduced AI value below 0.5 and, therefore, can be wrongly assigned as non-aromatic structures (Tong et al. 2016). Such compounds include those associated with lignin degradation. Lignin compounds also may not be classified as being aromatic

because non-aromatic molecules can be constructed using the same formula (Koch et al. 2006).

6.3.3 Aromaticity Equivalent, X_C

To avoid misclassifying aromatic compounds, an *Aromaticity Equivalent*, X_C, parameter, proposed in Yassine et al., 2014, can be used and is calculated in a similar way to the AI, using the following equation:

$$X_C = \frac{3(DBE - mO - nS) - 2}{DBE - mO - S}, \tag{6.5}$$

where DBE is the Double Bond Equivalent, *O* and *S* are the number of oxygen and sulphur atoms respectively and *m* and *n* are parameters accounting for the fraction of oxygen and sulphur atoms respectively which are involved in π bond structures.

Organic compounds have X_C values in the range of 0.0 to 3.0. Formulae containing a benzene ring have X_C values of ≥ 2.5 which are unaffected by additional aliphatic C atoms but are affected by C=O functional groups. Therefore, $X_C \geq 2.5$ is used as the minimum threshold for the presence of aromatic structures in a compound. The minimum threshold value for poly-aromatic compounds is $X_C \geq 2.7143$ which is the value for naphthalene; the smallest poly-aromatic compound.

6.3.4 Application of DBE, AI and X_C to the AERORAIN samples

On average, the CHO formulae sub-group was the most common in the León rain and aerosol samples so the aromaticity classification was focussed on these CHO compounds. Since there are no N or S atoms in CHO compounds, the AI calculation in Equation 6.4 simplifies to the following:

$$AI = \frac{DBE_{AI}}{C_{AI}} = \frac{1 + C - O - 0.5H}{C - O}. \tag{6.6}$$

Figure 6..1 shows the DBE plotted as a function of carbon number for all of the León rain and aerosol samples. DBE alone was not sufficient to efficiently classify the oxidised aromatic compounds due to their heteroatoms affecting the number of C–C single bonds so AI values were calculated using Equation 6.6. Some CHO formulae contained enough oxygen atoms to exceed the carbon number and produce a negative DBE_A or C_{AI} value and subsequent negative AI value. AI was set to zero for any formulae where either the DBE_A or C_{AI} value was less than zero. To minimise misclassification of aromatic compounds, any formulae with DBE values < 4 were not included because as stated previously, aromatic compounds cannot have DBE values < 4. Similarly, when classifying poly-aromatic compounds, any formulae with DBE values < 7 were not included because PAHs cannot have DBE values < 7. Figure 6..1 shows the final result with aromatic compounds (AI values > 0.5) in blue and poly-aromatic compounds (AI values ≥ 0.67) in red.

Using the Aromaticity Index values alone, no compounds with fewer than 6 carbons were classified as being aromatic in any of the rainwater or aerosol samples. The spring and summer rain samples had fewer aromatic compounds with DBE values < 12 than the winter samples.

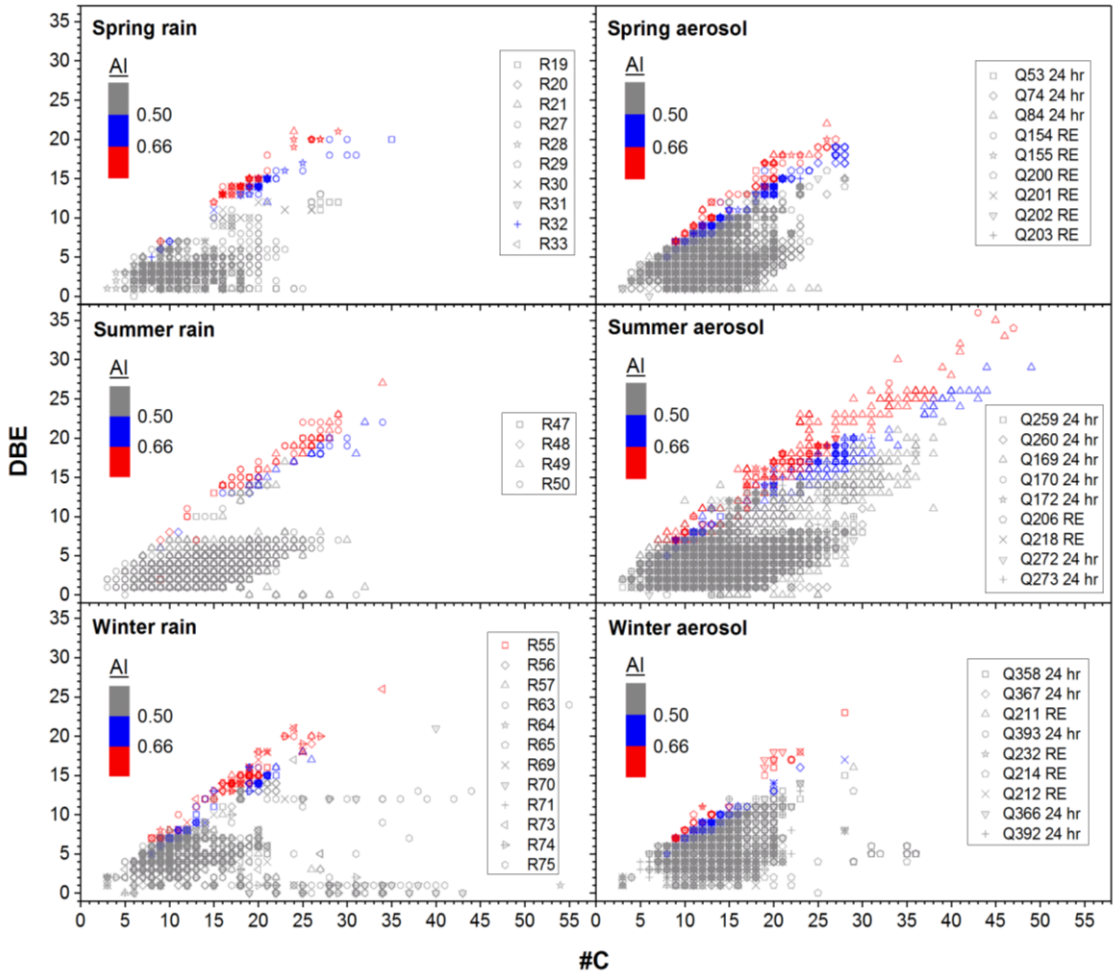

Figure 6.1. Double Bond Equivalent (DBE) as a function of the number of carbon atoms with the Aromaticity Index (AI) values for the rain and aerosol samples. Formulae with AI values > 0.5 are classified as aromatic compounds (blue) and AI ≥ 0.67 are classified as poly-aromatic compounds (red).

There were many potentially lignin-associated compounds in box 5 in the VK plots for the rain and aerosol samples in Figure 5.10 in Chapter 5. There was therefore, a significant chance of misclassifying aromatic species using the Aromatic Index as a result of the long alkyl side chains in the lignin-associated compounds; reducing their AI value to below 0.5, and also because their molecular formulae could be assigned as non-aromatic.

To avoid misclassifying these compounds, the X_C calculation was applied to the same CHO compounds in the rainwater and aerosol samples, simplifying Equation 6.5 to the following equation:

$$X_C = \frac{3(\mathrm{DBE} - m\mathrm{O}) - 2}{\mathrm{DBE} - m\mathrm{O}}. \quad (6.7)$$

For the rain and aerosol samples, parameters *m* and *n* were set to 0.5 which is used for carboxylic acid (R–COOH), ester (R–COOR) and nitro ($R–NO_2$) chemical classes (Yassine et al. 2014). The same additional criteria were used for applying the Aromaticity Equivalent assignments as for the Aromaticity Index values. For assigning aromatic compounds, only formulae with DBE values ≥ 4 were included and for assigning poly-aromatic compounds, only formulae with DBE values ≥ 7 were included. Any formulae with a DBE value < (*m* × O), where *m* is 0.5 and *O* is the number of oxygen atoms, were automatically assigned an X_C value of zero.

Figure 6..2 shows the Aromaticity Equivalent values for the CHO compounds in the rain and aerosol samples, with the aromatic compounds (X_C values ≥ 2.5) in green and the poly-aromatic compounds (X_C values ≥ 2.7143) in orange. Many CHO compounds which were assigned as olefinic using the AI approach, were assigned as aromatic using the X_C approach. The number of poly-aromatic compounds was underestimated using the AI approach which may be due to aromatic compounds with longer alkyl chains not being identified. Similar underestimations were observed for organic aerosol samples in previous studies (Tong et al. 2016, Yassine et al. 2014). The X_C approach also appeared to be more rigorous for the León samples given that the selection criteria removed many more formulae compared with the AI approach.

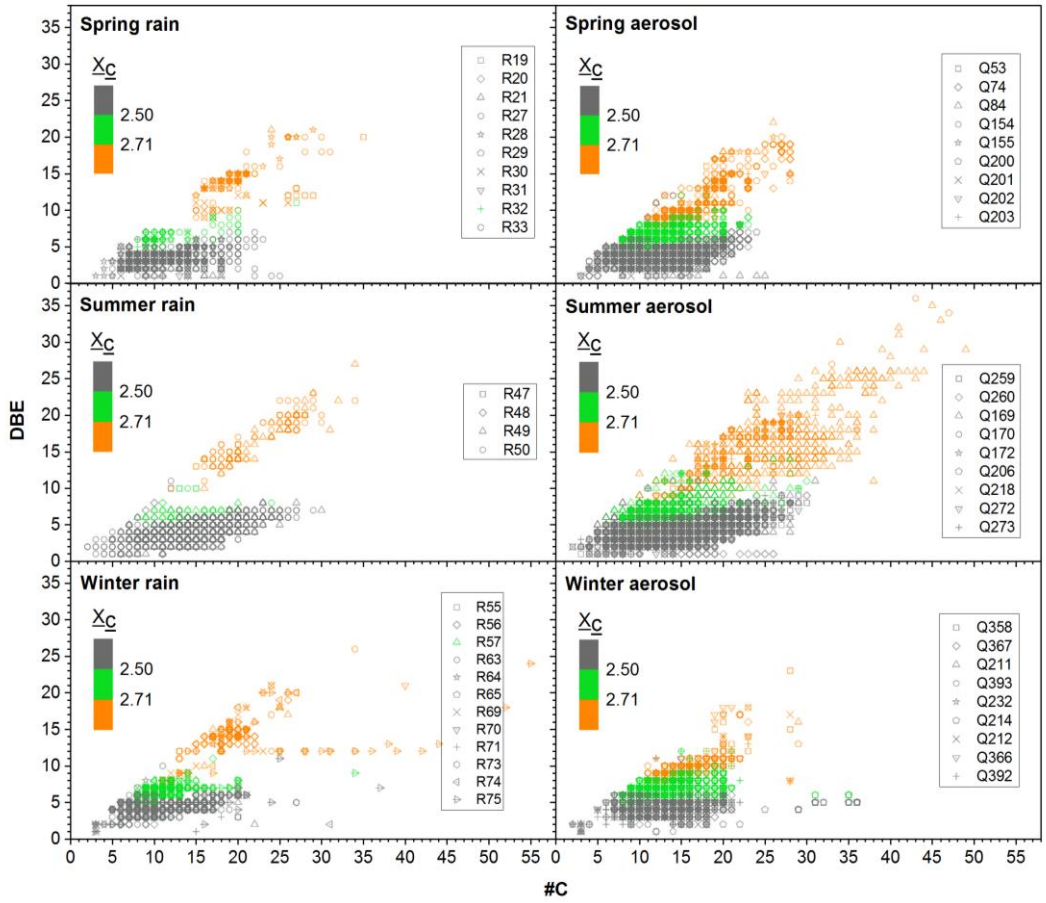

Figure 6.2. Double Bond Equivalent (DBE) as a function of the number of carbon atoms with the Aromaticity Equivalent (X_C) values for the rain and aerosol samples. Formulae with X_C values ≥ 2.5 are classified as aromatic compounds (green) and X_C values ≥ 2.7143 are classified as poly-aromatic compounds (orange).

Figure 6.3 and Figure 6.4 show the average percentages of aromatic compounds classified using the Aromaticity Index (AI) and the Aromaticity Equivalent (X_C) values for the rain and aerosol samples according to season. In every rain and aerosol sample, more formulae were classified as being aromatic and poly-aromatic using the X_C scale than the AI scale. This strongly suggests that the compounds with long alkyl carbon chains caused the number of aromatic compounds in the samples to be underestimated when the AI method was used. The X_C method was therefore deemed to be the most suitable metric for the León samples.

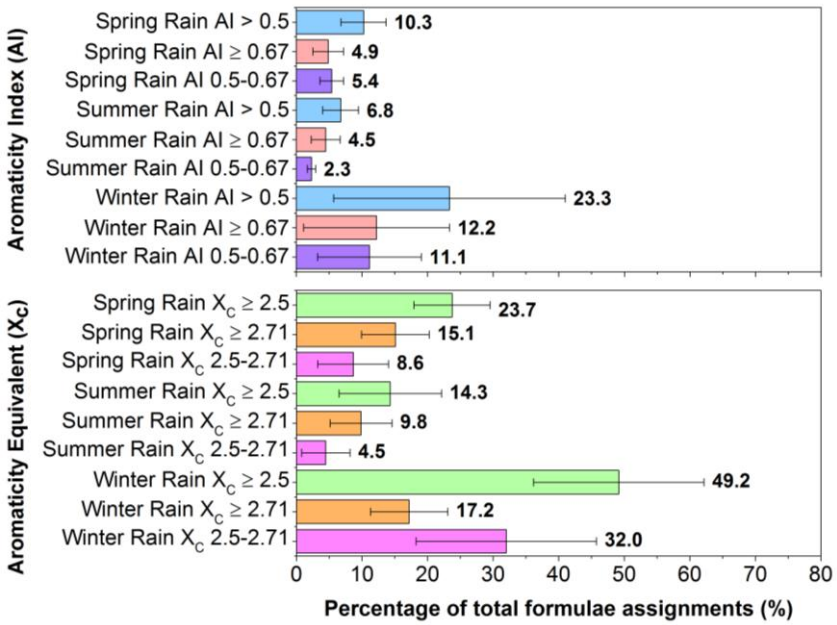

Figure 6.3. Average numbers of Aromaticity Index (AI) and Aromaticity Equivalent (X_C) classified aromatic compounds as percentage of total formulae assignments in rainwater in that season. Aromatic compounds = AI > 0.5 (blue) or $X_C \geq 2.5$ (green), poly-aromatic compounds = AI ≥ 0.67 (light red) or $X_C \geq 2.7143$ (orange) and mono-aromatic compounds = AI 0.5-0.67 (purple) and X_C 2.5-2.7143 (pink). Error bars denote ± 1 standard deviation.

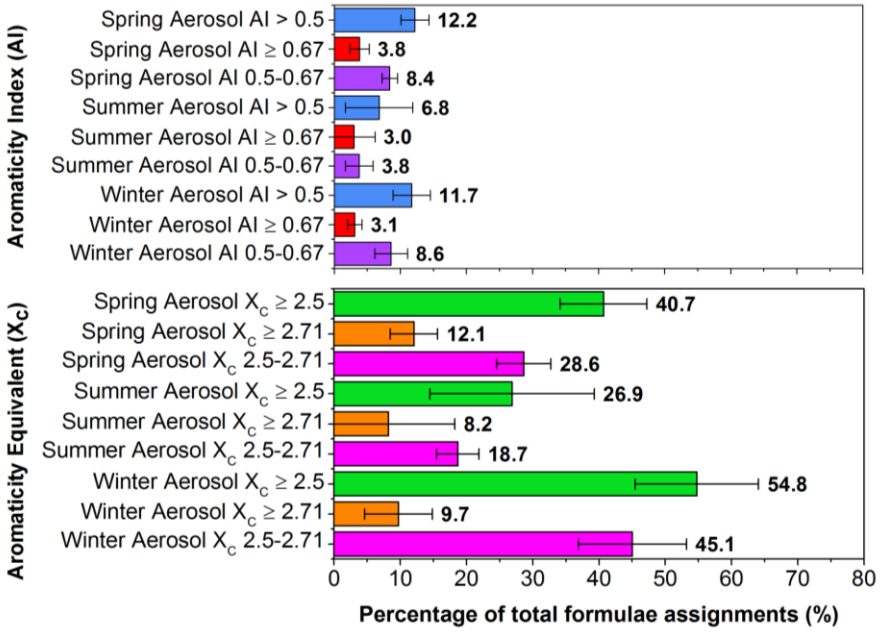

Figure 6.4. Average numbers of Aromaticity Index (AI) and Aromaticity Equivalent (X_C) classified aromatic compounds as percentage of total formulae assignments in aerosol in that season. Aromatic compounds = AI > 0.5 (blue) or $X_C \geq 2.5$ (green), poly-aromatic compounds = AI ≥ 0.67 (light red) or $X_C \geq 2.7143$ (orange) and mono-aromatic compounds = AI 0.5-0.67 (purple) and X_C 2.5-2.7143 (pink). Error bars denote ± 1 standard deviation.

This analysis has shown that the X_C metric was the most appropriate tool for classifying the aromatic compounds in the AERORAIN samples because of the presence of nitrogen and sulphur-containing compounds which alter the number of C–C bonds without affecting the aromaticity, and also compounds with long alkyl side chains which reduce the AI resulting in misclassification of aromaticity. This selection process is illustrated in Figure 6.5 and could be beneficial for future UHRMS studies of ambient sample composition to ensure suitable visualisation tools are selected for effective data interpretation.

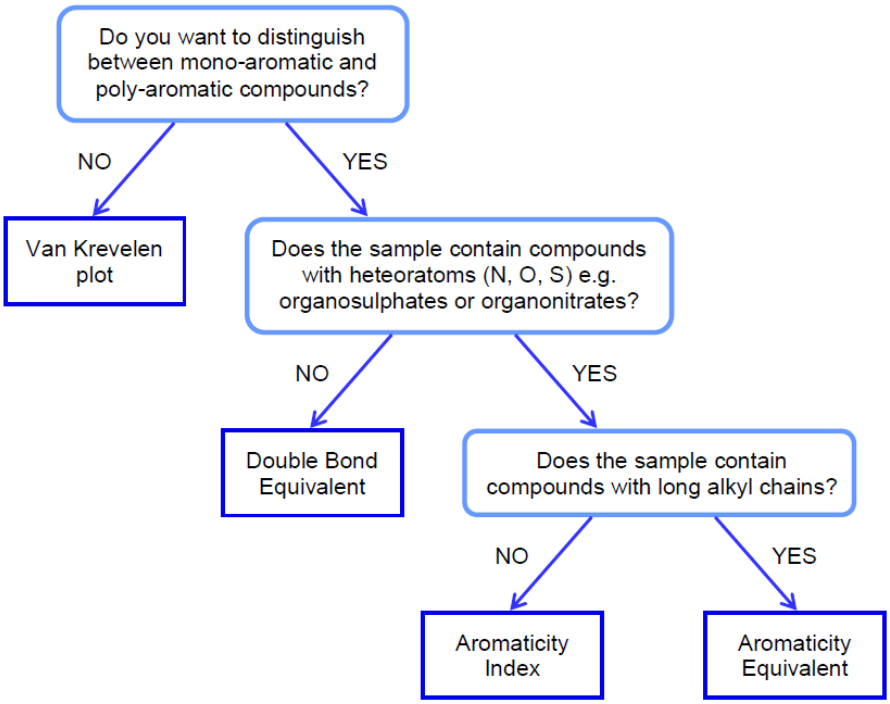

Figure 6.5. Decision-tree for selecting appropriate visualisation tools to classify oxidised aromatic compounds in ambient samples.

6.3.5 Distribution of mono-aromatic and poly-aromatic compounds in the rainwater and aerosol samples

T-test statistical analysis of the X_C approach highlighted some clear differences between the aromatic compounds in the rain and aerosol samples. Figure 6.4 shows a significant increase in the percentage of mono-aromatic compounds in the aerosol between summer and winter (83%, $p = < 0.001$). This may be due to forest fires in summer increasing the production of mono-aromatic compounds and the additional biomass burning for winter

residential heating may account for the maximum number of mono-aromatic compounds observed in the winter period. The percentage of mono-aromatic compounds in the rainwater samples (Figure 6.3) also increased between summer and winter (151%, $p = < 0.001$), likely because of the increased water-soluble mono-aromatic compounds in the aerosol phase which were then scavenged by the rain droplets and incorporated into the rainwater. A significant 42% decrease ($p = < 0.001$) in mono-aromatic compounds in the aerosol samples between spring and summer was observed, indicating a change in source influencing the organics in the samples.

A non-statistically significant 54% increase ($p = 0.07$) in poly-aromatic compounds was observed in the rainwater samples between summer and winter but no such increase was observed in the aerosol samples during this period. Overall, the winter rainwater samples contain the highest percentages of total aromatic compounds. The spring rainwater samples contain slightly higher percentages of aromatic compounds than the summer rainwater although this difference is not statistically significant. The spring and summer rain samples contain 54% ($p = 0.02$) and 75% ($p = 0.17$) more poly-aromatic compounds, respectively, than mono-aromatic compounds whereas the winter rain samples contain 60% ($p = 0.005$) more mono-aromatic compounds than poly-aromatic compounds. It is surprising that some of the rain samples would contain more poly-aromatic compounds than mono-aromatic compounds because mono-aromatics are usually water-soluble whereas PAHs have very low water solubilities. PAHs are often only present in rainwater because they were scavenged by the rain droplets or were incorporated into cloud condensation nuclei (Blando and Turpin 2000). A potential reason is that many more mono-aromatic compounds were being emitted later in the year from biomass burning for residential heating so the winter rainwater was able to dissolve these gas phase organics or scavenge any water-soluble POA emitted and these outnumbered the poly-aromatic compounds.

Regardless of season, the aerosol samples all contained higher percentages of mono-aromatic compounds than poly-aromatic compounds (82% more for spring, 78% for summer and 129% for winter; all $p = < 0.05$). The much larger difference in mono-aromatic compounds and poly-aromatic compounds in the winter aerosol compared with the spring and summer aerosol may be attributed to different sources influencing the air masses during the different seasons.

Comparing the rainwater and aerosol samples, the aerosol samples contained higher percentages of mono-aromatic compounds, on average, than the rainwater, in all

seasons; 107% ($p = < 0.001$) higher in spring, 123% ($p = 0.002$) higher in summer and 34% ($p = 0.02$) higher in winter. The rainwater samples, however, contain slightly higher percentages of poly-aromatic compounds, on average, than the aerosol samples for each season; 22% higher for spring, 18% higher for summer and 55% higher for winter although only the difference for the winter samples was statistically significant ($p = 0.009$). This meant that overall, the spring, summer and winter aerosol samples contained 53% ($p = < 0.001$), 61% ($p = 0.08$) and 11% ($p = 0.29$) more aromatic compounds respectively i.e. more compounds with X_C values ≥ 2.5, than their rainwater counterparts. This could indicate that some aromatic species are not being washed out of the atmosphere effectively.

6.4 Conclusions

Two commonly used metrics for classifying aromatic compounds were compared; Aromaticity Index (AI) and Aromaticity Equivalent (X_C) and the AI method underestimated the number of aromatic compounds in every rainwater and aerosol sample, due to the presence of compounds with long alkyl side chains which lowered the AI value to below the aromaticity threshold. The more rigorous X_C method was therefore pursued to investigate the distribution of aromatic compounds in the samples.

The X_C method identified more mono-aromatic and poly-aromatic compounds in the samples and revealed an increase in the percentage of mono-aromatic compounds in the rain and aerosol samples between summer and winter, likely driven by summer forest fires and winter residential biomass burning, producing more soluble mono-aromatic compounds which were then scavenged by the rain. The winter rainwater samples contained the highest percentage of total aromatic compounds overall and also more mono-aromatic compounds than poly-aromatic compounds whereas the spring and summer rainwater contained more poly-aromatic compounds. The aerosol samples on the other hand, contained higher percentages of mono-aromatic compounds than poly-aromatic compounds, regardless of season. Overall, the aerosol samples contained significantly more aromatic compounds, and mono-aromatic compounds in particular, than the rainwater samples from the same season which could suggest that some aromatic species are not being washed out of the atmosphere efficiently.

7 INVESTIGATING THE INFLUENCE OF AIR MASS ORIGIN ON THE AERORAIN SAMPLE COMPOSITION

It is apparent from the initial analysis of the rainwater and aerosol samples that there is clear seasonal influence on the composition of the samples. However, many of the trends observed between the different seasons hinted at different sources and meteorology influencing the sample composition at different times of the year.

This chapter focuses on analysis of the rainwater and aerosol composition as a function of air mass origin to determine the extent of the influence by marine, terrestrial and anthropogenic sources on the samples.

7.1 Introduction

Meteorological conditions, seasonality and air mass trajectories have been shown to influence concentrations and distributions of organics in precipitation (Blando and Turpin 2000) including rainwater (Zhang et al. 2008, Altieri et al. 2009, Durana et al. 1992, Avery et al. 2006), cloud water (Cook et al. 2017) and aerosol (Tong et al. 2016), as well as the ionic constituents and pH (Safai et al. 2004) of the sample.

The sample collection site in León during the AERORAIN campaign was exposed to urban influence from the city but was also close to the Atlantic Ocean and forested regions which are likely to have had an impact on the composition of the samples. Forest fires are a common occurrence on the Iberian Peninsula and it is highly likely that the sample composition will have been influenced by biomass burning, which is known to be a source of brown carbon and ELVOCs (Di Lorenzo et al. 2017).

In addition, Spain and Portugal have long been exposed to African dust deposition and sporadic *red rain* events (rainwater with a reddish silty content) from the Saharan desert (Àvila i Castells and Roda 1991, Avila et al. 1996). These events are rich in base cations (Ca^{2+}, Mg^{2+}, K^{+}, Na^{+}), and sulphate and occur as a result of low pressure systems in north-west Africa or south-west of the Iberian Peninsula which direct air mass trajectories over Western Europe, and are thought to be an increasing source of nitrate emissions from industry which influence rainwater (Izquierdo, Avila and Alarcón 2012).

Air mass backward trajectories can be used to identify possible source regions and assess the influence of air mass origin and have been used in several previous studies (Altieri et al. 2012, Cook et al. 2017, Avery et al. 2006, Kourtchev et al. 2013). Identifying the air mass origins for the rain events occurring during the AERORAIN campaign would yield important information regarding the influence of meteorology, forest fires and desert dust on the composition of the rainwater and aerosol samples.

7.2 Aims

The overall aim of the analysis in this chapter is to use air mass backward trajectories to investigate the influence of air mass origin and long range transport on the chemical composition of samples at the León site.

Specific objectives of this work were to:

- Investigate the influence of marine, continental and desert dust environments on the composition of the rainwater and aerosol samples.
- Determine the influence of biomass burning from forest fires on the sample composition.

- Assess the impact of air mass origin on the distribution and oxidation of aromatic compounds in the rainwater and aerosol samples.

7.3 Methodology

7.3.1 Generation of backward trajectories

The work described in this sub-section (7.3.1) detailing the production of the air mass backward trajectories was completed by Dr Cameron Rae at the University of Cambridge. The subsequent analysis of the generated air mass trajectories and use of them to aid source attribution and interpretation of the León sample composition was carried out independently. The method used to produce trajectories is described as follows.

The online version of the NOAA Air Resources Laboratory (ARL) Hybrid Single-Particle Lagrangian Integrated Trajectory (HYSPLIT) Model (Stein et al. 2015) was used to plot backward trajectories for the air masses producing the rain events associated with the measured rain and aerosol samples. The Ensemble Trajectory mode was used to run 27 individual back trajectories for 5 days (120 hours) from the starting location (Leon; 42°36.0018' N, 5°34.2192' W) and the set start time. The trajectories were run at three different altitudes; 500 m, 1500 m and 3000 m, using the meteorological dataset 'GDAS (0.5 degree, global, 09/2007-present)'.

For the analysed '24 hr' aerosol samples which were collected every 24 hours regardless of whether a rain event occurred, trajectories were run from the start time 10:00 UTC (the time at which the filter was removed and replaced with a new one), 12 hours from the start time and 24 hours from the start time, and at the three different altitudes stated previously, to ensure that any significant meteorological changes were accounted for. For example, the aerosol sample Q53 was collected between 12.04.16 and 13.04.16 so backward trajectories were run for 120 hours starting from 10:00 UTC on 12.04.16 at 500 m, 1500 m and 3000 m, 22:00 UTC on 12.04.16 at 500 m, 1500 m and 3000 m, and at 10:00 UTC on 13.04.16, at 500 m, 1500 m and 3000 m. This resulted in nine separate trajectory output files.

On the days where the rain and ‘RE’ aerosol sample collection occurred only during the specific rain event, 120 hour backward trajectories were run at 500 m, 1500 m and 3000 m with the start time set as close to the sample collection start time as possible. If the sample collection duration was greater than 22 hours then further trajectories were run from 12 hours after the start time. If the sample collection duration was less than 22 hours then further trajectories were run from 6 hours after the start time.

For each date or set of dates corresponding to each sample, coordinates from the output files of the HYSPLIT backward trajectories from each start time and each altitude were used to plot the Time-Integrated Parcel Density using a National Centre for Atmospheric Research (NCAR) Command Language (NCL) script. This uses the cumulative sum of air parcel density across the whole duration of the backward trajectories and has a unit of “Parcel-hours”. The calculation assumes that each air parcel is equally likely to influence the final sample measured in León, at any time and point along the trajectory. The darker colours indicate a higher density of air and these regions are likely to have a stronger influence on the sampled air at León. Hashing was used in the backward trajectory plots to indicate when the air parcel along its trajectory moved into the planetary boundary layer. All of the calculated backward trajectory plots are provided in Appendix K.

The same meteorological data set used to plot the backward trajectories was used to identify any recent rainfall which may have occurred prior to the air mass arriving at the sampling site. If rainfall had occurred before sampling, this would have removed some compounds from the atmosphere before the sampling took place which results in less accurate composition representation and source attribution. Rainfall occurring prior to collection for each sample was identified by more than 50% of the total 27 ensemble backward trajectories that experienced > 0.02 mm/hr rainfall in up to 48 hours into the backward trajectory from the start time.

7.3.2 Air mass origins

All of the subsequent analysis of the air mass backward trajectories discussed in this sub-section and in the rest of this chapter was conducted and written independently. The air masses responsible for the rain events in León can largely be classified into three categories; examples of which are shown in Figure 7.1.

Air masses which originated mostly from the Atlantic Ocean are hereon referred to as 'Marine'. 90% of the spring and 25% of the winter rainwater samples had air mass backward trajectories of marine origin. There were no summer rain events which had air mass backward trajectories dominated by marine influence. The marine air mass example shown in Figure 7.1 was responsible for the spring samples recorded on 12.04.16. This is representative of the marine trajectories observed overall although some of the other marine classified trajectories did include some minor influence from the UK.

Air masses with significant origins from the African continent specifically and thus potentially influencing the León samples with desert dust are characterised as *Saharan*. The Saharan air mass backward trajectory shown in Figure 7.1 produced the winter rain event on 04.11.16. 10% of the spring, 50% of the summer and 17% of the winter rainwater samples were from rain events influenced by Saharan air mass trajectories.

Air masses originating mostly from mainland Europe and the UK, with more terrestrial influence than marine were classified as 'Continental'. The Continental air mass shown in Figure 7.1 produced the summer rain event on 25.08.16. Backward trajectories of continental-classified air masses varied considerably; many included some marine influence from the Mediterranean and North Seas. There were some Continental trajectories which did contain some Saharan influence. If a significant proportion of the air parcel density (> 25.9 parcel-hours) was over the African continent, then the air mass was deemed to have potentially significant Saharan influence and was classified as being of 'Saharan' origin. 50% of the summer and 59% of the winter rainwater samples were influenced by continental air masses. There were no spring samples classified with continental air mass influence.

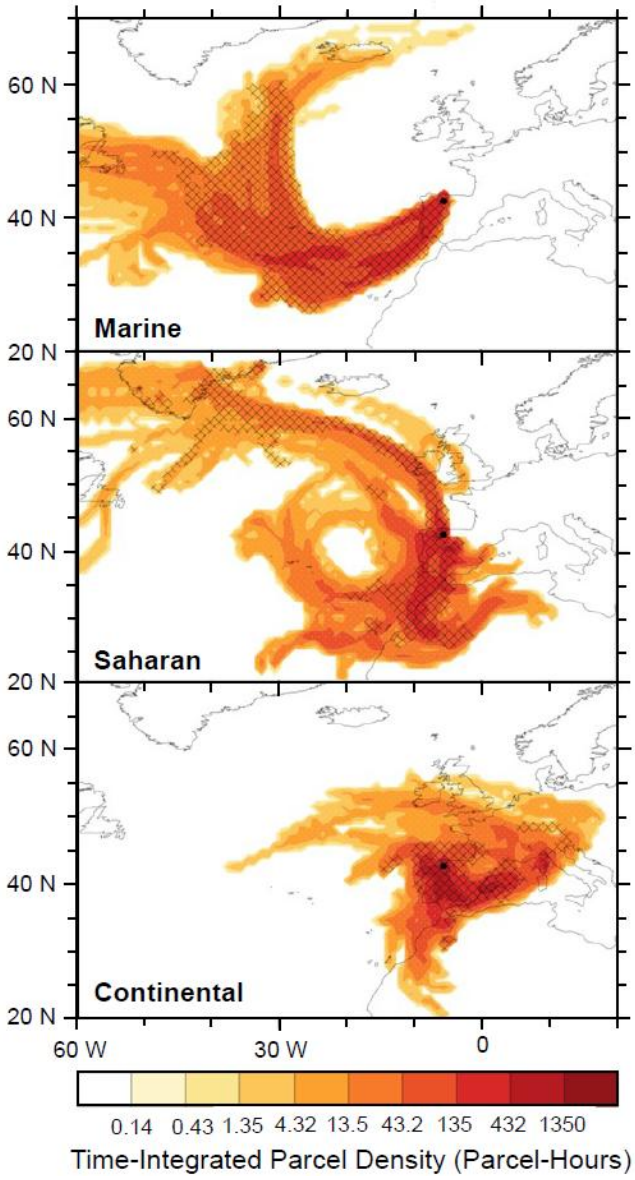

Figure 7.1. Examples of the 120 hour backward trajectories of air masses arriving at the sampling site in León (generated by Dr Cameron Rae, University of Cambridge). Marine (top) samples; R19 and Q154 (14.04.16). Saharan (middle) samples; R64 and Q212 (04.11.16). Continental (bottom) samples; R50 and Q218 (25.08.16). Plots presented as time-integrated parcel density where darker colours indicate higher air parcel density. Hashing indicates air parcels entering the planetary boundary layer.

7.4 Results and Discussion

7.4.1 Aerosol particulate and elemental concentrations

Table 7.1 shows the measured PM_{10}, sulphate (SO_4^{2-}), ammonium (NH_4^+), nitrate (NO_3^-) and nitrite (NO_2^-) concentrations for the aerosol samples every 24 hours regardless of the rain events occurring. The PM_{10} and $PM_{2.5}$ concentrations recorded for the aerosol samples collected during the rain events are also included. There was a change from $PM_{2.5}$ to PM_{10} measurements for the 'RE' aerosol during the campaign due to a change in aerosol sampling unit. The data has been arranged in Table 7.1 according to air mass origin.

Table 7.1. PM_{10}, OC, EC, TC, SO_4^{2-}, NH_4^+, NO_3^- and NO_2^- concentrations for the '24 hr' aerosol and the $PM_{2.5}/PM_{10}$ concentrations for 'RE' aerosol. All data calculated elsewhere prior to sample analysis in Cambridge.

		Marine	Saharan	Continental
24 hr aerosol	PM_{10} (μg/m^3)	8.79 ± 3.24	19.50 ± 3.05	22.06 ± 5.45
	OC (μg/m^3)	1.88 ± 0.67	2.80 ± 0.34	3.25 ± 0.55
	EC (μg/m^3)	0.60 ± 0.15	0.62 ± 0.21	0.96 ± 0.23
	TC (μg/m^3)	2.49 ± 0.71	3.42 ± 0.24	4.21 ± 0.71
	SO_4^{2-} (μg/m^3)	0.0192 ± 0.0100	0.0608 ± 0.0567	0.0424 ± 0.0118
	NH_4^+ (μg/m^3)	0.0474 ± 0.0178	0.1107 ± 0.0321	0.1346 ± 0.0685
	NO_3^- (μg/m^3)	0.0374 ± 0.0136	0.1020 ± 0.0971	0.0615 ± 0.0151
	NO_2^- (μg/m^3)	0.0030 ± 0.0022	0.0068 ± 0.0007	0.0000 ± 0.0000
RE aerosol	$PM_{2.5}$ (μg/m^3)	3.36 ± 3.08	7.75 ± 3.95	-
	PM_{10} (μg/m^3)	-	14.53 ± 0.00*	10.05 ± 6.26

*Based on one value

More than 76% of the total carbon (TC) measured in all of the samples is organic carbon (OC), irrespective of air mass origin. In the marine aerosol, 76% of the TC is OC which is likely to be mostly of biogenic origin but may include some terrestrial and anthropogenic sources over northern Spain. 24% of the marine TC is elemental carbon (EC) which is a higher contribution of EC than in the Saharan and continental aerosol.

There are many operational coal-powered plants in northern Spain and the black carbon emissions from these are likely to have been picked up by the marine-influenced air mass trajectories. The marine aerosol PM_{10} concentration, 8.79 ± 3.24 μg/m^3, and the average SO_4^{2-}, NH_4^+, NO_3^- and NO_2^- concentrations are much lower than the Saharan or Continental-influenced aerosol due to the marine air mass having originated from a cleaner environment. The marine samples collected during winter have slightly higher SO_4^{2-} concentrations than the spring marine samples. Wet deposition of SO_4^{2-} occurs in the vicinity of the emissions sources of SO_2 (Tost et al. 2007) which suggests that coal combustion from the power plants or from winter residential heating could have been picked up by the air mass shortly before sampling at León.

The continental aerosol samples have the highest PM_{10} concentrations (22.06 μg/m^3 on average) because they are exposed to more primary particulate emissions from industry and transport and also more secondary compounds formed via gas-to-particle conversion mechanisms (Seinfeld and Pandis 2006). SO_4^{2-} concentrations are significantly higher (75%, $p = 0.01$) for continental aerosol than marine aerosol due to terrestrial sources including coal combustion which are compounded by air masses incorporating emissions from other European countries. Average NH_4^+ concentrations in the continental aerosol are 96% higher ($p = 0.07$) than in the marine and 19% higher ($p = 0.56$) than in the Saharan aerosol which could be due to agricultural and industrial emissions from Spain, Portugal and other areas of Western Europe. NO_3^- concentrations are 49% higher ($p = 0.04$) in continental aerosol than marine due to NO_x emissions from vehicles and other fossil fuel combustion. Forest fires in Spain during the summer in particular will also have produced NO_x emissions, contributing to the NO_3^- concentrations. OC contributes 77% and EC contributes 22% of TC which is similar to the marine carbon distribution.

The average PM_{10} concentration for the Saharan aerosol is 19.50 μg/m^3 which is consistent for remote continental aerosol (Seinfeld and Pandis 2006). The Saharan aerosol contains 103% ($p = 0.30$) higher SO_4^{2-}, 80% ($p = 0.03$) higher NH_4^+ and 93% ($p = 0.34$) higher NO_3^- concentrations than the marine aerosol. In addition, the Saharan aerosol contains 36% ($p = 0.62$) higher SO_4^{2-} and 50% ($p = 0.53$) higher NO_3^- concentrations than the continental aerosol. The Saharan aerosol will have been exposed to similar fossil fuel combustion and forest fire emissions as the continental aerosol but there must be an extra source to produce these higher concentrations. Desert dust is often mixed with particulate pollutants from industrial emissions from North Africa in

the Saharan Air Layer. The air mass backward trajectories for the Saharan samples indicate air passing over Morocco and Algeria which may have picked up significant SO_2 and NO_x emissions from oil refineries, power plant and fertiliser industry (Rodríguez González et al. 2011). The Saharan aerosol TC has the highest contribution from OC (82%) and the lowest contribution from EC (18%).

7.4.2 Composition analysis of rainwater and aerosol

Figure 7.2 (A) shows the average number of CHO, CHON, CHOS and CHONS compounds in the rain and aerosol samples influenced by each air mass origin and Figure 7.2 (B) shows the average percentage of CHO, CHON, CHOS and CHONS formulae assignments out of the total number of formulae assignments, averaged across the rain and aerosol samples for each air mass origin. These figures are directly comparable with the seasonal formulae sub group distributions in Figure 5.3 (A) and (B). The spring and marine rain and aerosol formulae distributions are very similar because 75% of the marine-influenced rain and 73% of the marine-influenced aerosol samples were spring samples. This shows that marine air mass influence had a direct impact on the composition of the spring samples. Continental rain and winter rain show similar distributions because 78% of the winter rain samples were of continental origin. Saharan aerosol and summer aerosol are also very similar although fewer of the summer aerosol samples were Saharan-influenced (57%). The Saharan rain has a mixture of spring, summer and winter rain samples and the percentage and number distributions reflect this accordingly. Similarly, the continental-influenced aerosol was 56% summer aerosol and 44% winter aerosol and hence the number of compounds in the samples are less than the summer aerosol but higher than the winter aerosol distributions in Figure 5.3. Overall, the clear similarities between the seasonal distributions and specific air mass origins, show that the composition of the samples have been greatly influenced by the air mass origins.

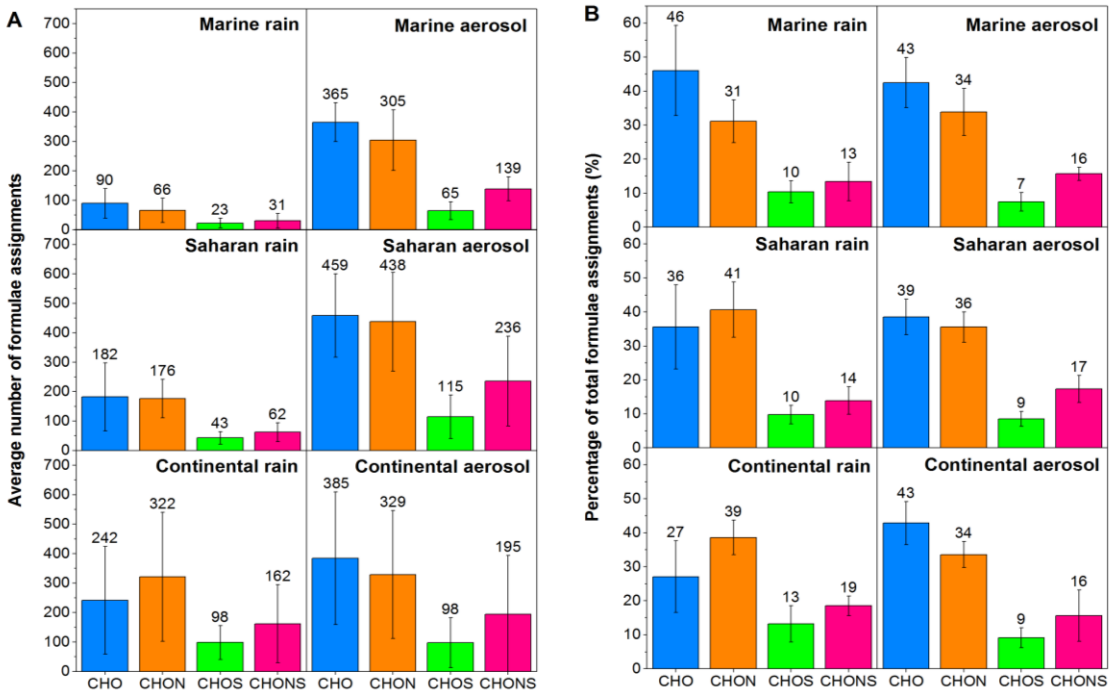

Figure 7.2. Average number of compounds in each formulae sub group; CHO, CHON, CHOS, CHONS (A) and percentages of each formulae sub group within the total formulae assignments (B) for rainwater and aerosol samples from each air mass origin. Error bars depict ± 1 standard deviation across each formulae sub group for each air mass origin.

Table 7.2 summarises the composition analysis for the marine-influenced rainwater samples. The marine samples are the least acidic (average pH; 6.43) compared with the Saharan and continental-influenced samples which is to be expected for samples from more remote origins which have the smallest contributions of acidic inorganic compounds such as H_2SO_4 and HNO_3. All the RE aerosol samples contain more compounds than their rainwater counterparts which clearly shows that not all of the organic aerosol are being removed from the atmosphere by the rain droplets. There is variation in the total number of compounds between the different marine-influenced rain samples. The marine-influenced samples can be broadly divided into two categories; the samples collected in spring which have curved trajectories resembling anti-clockwise cyclonic motion, experiencing influence from the Arctic Ocean, Atlantic Ocean and in some cases, western Europe; and the winter samples which have straighter trajectories, brought to León by westerly winds across the Atlantic Ocean (Appendix K). The difference in composition between these two sets of marine samples is highlighted in Table 7.2. The spring marine samples are dominated by CHO compounds

whereas the winter marine samples have higher percentages of CHON. The winter marine rainwater has significantly higher percentages of CHOS and CHONS than the spring marine rainwater, reflecting the higher anthropogenic emissions of NO_x and SO_2 in winter.

Table 7.2. Composition analysis for the four formulae sub-groups in the marine-influenced rainwater and aerosol as a function of season. Averages are provided ± 1 standard deviation.

		Formula sub group	Average Percentage	Average number	O/C	H/C
Rainwater	Spring	CHO	52 ± 9	94 ± 57	0.41 ± 0.03	1.49 ± 0.08
		CHON	29 ± 6	52 ± 36	0.57 ± 0.04	1.24 ± 0.14
		CHOS	9 ± 3	18 ± 15	0.27 ± 0.14	1.10 ± 0.11
		CHONS	11 ± 4	21 ± 20	0.54 ± 0.06	1.39 ± 0.15
	Winter	CHO	28 ± 4	79 ± 9	0.38 ± 0.04	1.17 ± 0.15
		CHON	38 ± 3	109 ± 21	0.52 ± 0.02	1.01 ± 0.08
		CHOS	14 ± 2	39 ± 3	0.52 ± 0.03	1.32 ± 0.02
		CHONS	21 ± 2	61 ± 9	0.73 ± 0.03	1.20 ± 0.01
Aerosol	Spring	CHO	46 ± 5	379 ± 60	0.34 ± 0.01	1.36 ± 0.04
		CHON	31 ± 4	268 ± 96	0.41 ± 0.09	1.14 ± 0.04
		CHOS	7 ± 3	59 ± 31	0.54 ± 0.04	1.46 ± 0.10
		CHONS	16 ± 2	140 ± 45	0.64 ± 0.05	1.52 ± 0.03
	Winter	CHO	35 ± 6	328 ± 68	0.33 ± 0.01	1.23 ± 0.07
		CHON	43 ± 4	404 ± 28	0.39 ± 0.02	1.08 ± 0.02
		CHOS	8 ± 2	80 ± 23	0.47 ± 0.02	1.29 ± 0.06
		CHONS	14 ± 2	136 ± 25	0.63 ± 0.02	1.49 ± 0.04

Comparing the absolute numbers of compounds; CHO fluctuates depending on each rain event and there is no significant seasonal fluctuation in this data set. This could mean that the source of these CHO compounds is oceanic POA from bubble bursting, or SOA. However, there is an extra source of nitrogen and sulphur producing more CHON, CHOS and CHONS compounds in the winter marine samples. Previous studies have detected high concentrations of organic nitrogen in the Atlantic Ocean SOA in the form of ammonium salts produced by biogenic amines from algae (Facchini et al. 2008) and in aerosol in the western North Pacific Ocean from marine biological sources (Miyazaki, Kawamura and Sawano 2010), emitted from the ocean surface microlayer. It

is possible that marine nitrogen could be influencing the winter marine León samples earlier in the air mass trajectories but it is likely that the terrestrial nitrogen and sulphur is influencing the air mass in the last couple of days before rain deposition. Linear regression analysis (using F-tests, significance level of 0.05) revealed a statistically significant positive correlation between the number of marine CHON compounds and the NH_4^+ concentrations in the 24 hr aerosol ($p = < 0.001$), measured in León, and also between the percentage of CHON compounds and the NO_3^- concentrations ($p = 0.04$) in the 24 hr aerosol. These are shown in Figure L in Appendix L.

There are no statistically significant differences between the spring and winter O/C and H/C ratios for the CHO compounds in the rain and aerosol samples. The following percentage differences are statistically significant ($p = < 0.05$). The spring aerosol average O/C ratio for the CHOS is significantly higher (14%, $p = 0.02$) than in the winter. The relatively low average O/C ratios for the CHOS/CHONS compounds in the spring marine rain, which are 63% lower ($p = < 0.001$) and 30% lower ($p = < 0.001$) respectively than the winter rain CHOS/CHONS, can be explained by the long rain event in May 2016 which removed many soluble oxygenated aerosol species from the atmosphere over the six day rain event. The O/C ratios for the CHOS compounds at the beginning of the long rain event, and the shorter three day rain event beforehand, were 0.54 and 0.51 respectively. (The O/C ratios for the CHO, CHON and CHONS compounds in the aerosol also decreased during this period). These values are far more similar to the winter rain, spring aerosol and winter aerosol O/C ratios. The spring rain CHOS O/C ratios then reduced to 0.27 and 0.22 respectively at the end of the rain events. The trend for the O/C ratios of the spring CHONS compounds in the rain was similar.

Accounting for the removal of oxidised compounds during the long spring rain events, the higher O/C ratios in the winter for the CHOS/CHONS compounds may be partially due to the winter marine trajectories potentially having some boreal forest influence from Canada or the USA. Studies on biogenic aerosol from the northern US, (Mazzoleni et al. 2012b), and boreal forest aerosol from Finland (Kourtchev et al. 2013), have observed significant amounts of CHON, CHOS and CHONS, so it is possible that long range transport of nitrogen and sulphur-containing compounds over the Atlantic Ocean could have influenced the winter samples.

However, it should be noted that all of the air masses producing the marine-influenced samples experienced previous rainfall in the last 48 hours before sampling at León,

which does imply that some of the potential terrestrial compounds produced from Canada or the USA could have been removed over the Atlantic Ocean via wet deposition. Furthermore, other studies that have observed a lack of CHON, CHOS and CHONS compounds in marine rainwater compared with continental rainwater. Altieri et al. 2012 have postulated that organonitrates, nitroxy-organosulphates and organosulphates have insufficient lifetimes to withstand transport from the continental USA to Europe.

In the rainwater, the spring CHOS compounds are less saturated (18%, $p = < 0.001$) than the winter CHOS but in the aerosol, the spring CHOS are 12% more saturated ($p = 0.03$) than the winter CHOS. The CHON H/C ratios are 21% higher ($p = 0.03$) in the spring rain than in the winter rain and the aerosol CHON H/C ratios are 5% higher ($p = 0.02$) in the spring aerosol than in the winter aerosol. Both rain and aerosol CHONS compounds are 15% more saturated ($p = 0.007$) in the spring and the aerosol CHONS are significantly more highly saturated than the rainwater CHONS (9%, $p = 0.04$ for the spring, and 22%, $p = 0.01$, for the winter).

Table 7.3. Composition analysis for the Saharan-influenced rainwater and aerosol. Averages are provided ± 1 standard deviation.

		Formula sub group	Average Percentage	Average number	O/C	H/C
Rainwater	Spring/ Summer	CHO	45 ± 6	268 ± 60	0.43 ± 0.03	1.57 ± 0.06
		CHON	34 ± 2	208 ± 59	0.46 ± 0.21	1.35 ± 0.04
		CHOS	9 ± 3	54 ± 21	0.47 ± 0.19	1.22 ± 0.04
		CHONS	12 ± 4	75 ± 35	0.54 ± 0.10	1.39 ± 0.12
	Winter	CHO	21 ± 1	53 ± 13	0.48 ± 0	1.23 ± 0.25
		CHON	50 ± 2	129 ± 44	0.55 ± 0.01	1.02 ± 0.05
		CHOS	11 ± 1	27 ± 6	0.55 ± 0.02	1.08 ± 0.09
		CHONS	17 ± 0	43 ± 12	0.75 ± 0.02	1.21 ± 0
Aerosol	Spring/ Summer	CHO	39 ± 6	510 ± 129	0.41 ± 0.03	1.46 ± 0.07
		CHON	33 ± 2	468 ± 185	0.51 ± 0.04	1.33 ± 0.04
		CHOS	10 ± 1	142 ± 72	0.50 ± 0.03	1.39 ± 0.14
		CHONS	19 ± 4	281 ± 160	0.54 ± 0.08	1.40 ± 0.06
	Winter	CHO	38 ± 1	329 ± 69	0.38 ± 0.01	1.37 ± 0.02
		CHON	42 ± 0	362 ± 67	0.46 ± 0.01	1.20 ± 0.02
		CHOS	6 ± 0	47 ± 5	0.48 ± 0	1.39 ± 0.03
		CHONS	14 ± 1	123 ± 17	0.71 ± 0.05	1.53 ± 0.02

The Saharan-influenced rainwater is more acidic (average pH; 6.27) than the marine rainwater due to stronger biomass burning and anthropogenic influence and it also contains significantly more compounds than the marine rainwater (Table 7.3). Like the marine samples, all of the Saharan aerosol samples collected during rain events, contain more compounds than their rainwater counterparts. There is an overall decline in the total number of compounds in the Saharan rainwater and to a lesser extent, in the aerosol, throughout the year, with a notable decrease in CHO compounds. The Saharan samples collected during the spring and summer have slightly more marine influence from both the Atlantic Ocean and the Mediterranean Sea compared with the winter samples and they also have more CHO compounds than the winter Saharan samples. This again suggests that a significant fraction of the CHO compounds in the León samples are of oceanic origin. The decrease in CHO in the winter period leads to CHON compounds dominating the rainwater. The higher percentage of CHON compounds in the Saharan rainwater and aerosol compared with the marine and continental samples may be partially due to the increased NO_3^- emissions from North Africa. Linear

regression analysis using F-tests with a significance level of 0.05 showed a statistically significant positive correlation between the NO_3^- concentration and the percentage of CHON compounds in the Saharan 24 hr aerosol (Figure L, Appendix L). Overall, the winter rainwater CHO, CHON, CHOS and CHONS have higher O/C ratios and lower H/C ratios than the spring and summer rain, meaning that the winter rainwater contains more oxidised and less saturated compounds. However, the spring and summer aerosol CHO, CHON and CHOS compounds have higher O/C ratios than the winter aerosol.

Due to the limited sample size of the Saharan rain category, there are few statistically significant differences between the O/C and H/C ratios. The H/C ratios for the rainwater CHON compounds are 29% higher ($p = 0.03$) in the spring/summer compared with the winter. The aerosol CHON H/C ratios are also 11% higher ($p = 0.01$) for the spring/summer samples than the winter samples. The H/C ratios for the CHONS compounds in the aerosol oppose this trend; the spring/summer samples are 8% lower ($p = 0.02$) than the winter samples. The observed O/C ratios in this dataset are higher than observed for ambient and laboratory primary biomass burning (O/C = 0.3–0.4) which indicates highly oxidised compounds in the Saharan rainwater and aerosol (Aiken et al. 2008). The lower H/C ratios observed in the winter coincide with the observation of more aromatic compounds during the winter. PAHs in particular, are less saturated, and could have lowered the average H/C ratio for the winter Saharan samples.

Table 7.4. Composition analysis for the Continental-influenced rainwater and aerosol. Averages are provided ± 1 standard deviation.

		Formula sub group	Average Percentage	Average number	O/C	H/C
Rainwater	Summer	CHO	31 ± 3	542 ± 76	0.42 ± 0.02	1.50 ± 0.02
		CHON	40 ± 2	701 ± 142	0.53 ± 0.03	1.33 ± 0.04
		CHOS	10 ± 2	182 ± 70	0.43 ± 0.05	1.40 ± 0.03
		CHONS	19 ± 4	363 ± 150	0.41 ± 0.03	1.41 ± 0.05
	Winter	CHO	26 ± 12	156 ± 90	0.41 ± 0.03	1.21 ± 0.20
		CHON	38 ± 6	213 ± 53	0.55 ± 0.04	1.17 ± 0.10
		CHOS	14 ± 6	75 ± 18	0.42 ± 0.10	1.21 ± 0.18
		CHONS	18 ± 3	105 ± 40	0.65 ± 0.06	1.38 ± 0.05
Aerosol	Summer	CHO	40 ± 6	550 ± 140	0.40 ± 0.01	1.49 ± 0.02
		CHON	33 ± 2	470 ± 165	0.54 ± 0.08	1.32 ± 0.05
		CHOS	10 ± 2	153 ± 76	0.51 ± 0.04	1.43 ± 0.11
		CHONS	19 ± 8	309 ± 200	0.59 ± 0.13	1.43 ± 0.03
	Winter	CHO	46 ± 5	178 ± 112	0.34 ± 0.03	1.27 ± 0.07
		CHON	35 ± 5	154 ± 132	0.43 ± 0.02	1.06 ± 0.06
		CHOS	8 ± 3	29 ± 18	0.51 ± 0.07	1.17 ± 0.09
		CHONS	11 ± 3	52 ± 52	0.76 ± 0.03	1.29 ± 0.12

Continental rain is the most acidic of the samples (average pH; 5.59) and contains, on average, four times as many compounds as the marine rain and twice as many compounds as the Saharan rain (Table 7.4). In particular, continental rain contains 91% more CHO compounds ($p = 0.048$), 132% more CHON ($p = 0.01$), 124% more CHOS ($p = 0.01$) and 136% more CHONS ($p = 0.02$) compounds than marine rain. It also contains 78% more CHOS compounds ($p = 0.03$) than the Saharan rain, indicating a stronger or different source of sulphate from those which influenced the Saharan rain samples, such as coal combustion emissions from northern Spain. Unlike the marine and Saharan samples, the continental rainwater contains more compounds than the continental aerosol from the same rain event, in most cases. This strongly suggests more scavenging of the aerosol is occurring from the continental air mass than the marine or Saharan air masses. The number of CHON, CHOS and CHONS compounds in the continental aerosol decrease rapidly between the summer and winter period. This decrease may be due to far fewer forest fires occurring in the winter compared with the summer but may also be reflecting the generally higher rates of photochemical activity in the summer, producing more CHON, CHOS and CHONS. This is not observed to the

same extent in the Saharan aerosol because the extra nitrate and sulphur emissions from North Africa are contributing to the CHON and CHONS compounds. There is little difference between the O/C ratios for the CHO, CHON and CHOS compounds in the summer and winter rainwater. However, the summer rain CHONS have 46% lower ($p = 0.01$) O/C ratios than the winter rain CHONS. The H/C ratios for the rainwater and aerosol CHO compounds are 21% higher ($p = 0.01$) and 16% higher ($p = 0.01$) respectively in the summer than in the winter. The O/C ratio for the summer aerosol CHO is 15% higher ($p = 0.04$) than the winter aerosol CHO. H/C ratios for the aerosol are higher in the summer than winter for CHO (16%, $p = 0.01$), CHON (21%, $p = < 0.001$) and CHOS (20%, $p = 0.01$) aerosol.

7.4.3 Biomass burning influence on sample composition

The air mass backward trajectories indicate that all of the air masses will have passed over forested regions of Spain, and thus may have been influenced by forest fires. Aerosol from forest fires is usually dominated by fine organic matter (Kaufman, Tanré and Boucher 2002). The number of forest fires to occur in Spain, on the day each sample was collected, is shown in Table 7.5. The data was taken from the satellite data available from the forest fire alert maps via *Global Forest Watch Fires (2018)*. An example of one of the Global Watch Forest Fire maps is provided in Figure M in Appendix M. It should be noted that data for the number of forest fires in Spain was used for this analysis because it was readily available from *Global Forest Watch Fires*. The area of land covered by each recorded forest fires was not accounted for but it would be useful to know how the total burned area in the local vicinity on the day of sample collection affected the sample composition.

Linear regression analysis, using F-tests with a significance level of 0.05, was completed for the number of forest fires and the number of compounds in the rainwater and aerosol samples. Figure 7.3 shows a positive correlation in most cases, excluding the marine rain total number of compounds and CHO compounds. Statistically significant ($p = < 0.05$) positive correlation between the number of forest fires and the number of compounds in the samples was observed for the total number of compounds and all formulae sub-groups in the continental aerosol, and for the continental rain CHON and total number of compounds.

Table 7.5. Total number of compounds in the rainwater and aerosol samples and the number of forest fires in Spain observed during the day of the sample collection (2018). Highlight colour corresponds to season (green = spring, yellow = summer, winter = blue).

	Rainwater			Aerosol		
		Number of compounds	Number of forest fires in Spain		Number of compounds	Number of forest fires in Spain
Marine	R19	81	41	Q53 24 hr	810	9
	R20	121	23	Q154 RE	1029	52
	R21	134	15	Q155 RE	852	30
	R28	509	0	Q74 24 hr	1231	149
	R29	140	8	Q201 RE	583	12
	R30	252	9	Q202 RE	713	12
	R31	154	4	Q203 RE	598	22
	R32	172	9	Q84 24 hr	1017	25
	R33	78	22	Q358 24 hr	1079	140
	R65	266	79	Q366 24 hr	896	75
	R69	332	43	Q367 24 hr	871	43
	R70	263	26			
Saharan	R27	799	38	Q200 RE	1206	38
	R47	589	53	Q169 24 hr	2248	74
	R48	426	35	Q170 24 hr	1370	53
	R63	326	14	Q206 RE	592	53
	R64	177	14	Q172 24 hr	1593	35
				Q212 RE	703	14
				Q392 24 hr	1019	76
Continental	R49	1350	218	Q259 24 hr	1883	254
	R50	2224	216	Q260 24 hr	1312	218
	R55	435	147	Q272 24 hr	1462	341
	R56	656	2	Q273 24 hr	1967	216
	R57	532	0	Q218 RE	567	79
	R71	309	0	Q211 RE	239	0
	R73	667	29	Q214 RE	207	0
	R74	534	40	Q232 RE	255	29
	R75	808	11	Q393 24 hr	951	40

Visually, positive trends exist for all of the Saharan formulae sub-groups. The Saharan and continental samples show stronger positive correlation overall compared with the marine samples and the molecular composition analysis revealed that Levoglucosan, $C_6H_{10}O_5$; a marker of biomass burning, is potentially identifiable in all of the continental samples. This is partly because the marine air mass trajectories covered less forested area. It is also due to the Saharan and continental selections containing more summer samples which were influenced by many more forest fires than the spring or winter samples.

The marine aerosol showed statistically-significant positive correlation between forest fires and number of compounds, excluding the CHO compounds, but none of the rain samples showed a significant increase in compounds with increasing forest fire frequency. This difference in the marine rainwater and aerosol trends may be due to two of the aerosol samples being collected on days with 149 and 140 forest fires (Table 7.5) which skew the positive correlation slightly for the aerosol samples. The number of forest fires occurring on the days when the rain samples were collected ranges from 0 to 79 which is a much smaller range than for the aerosol and subsequently produces a weaker positive trend.

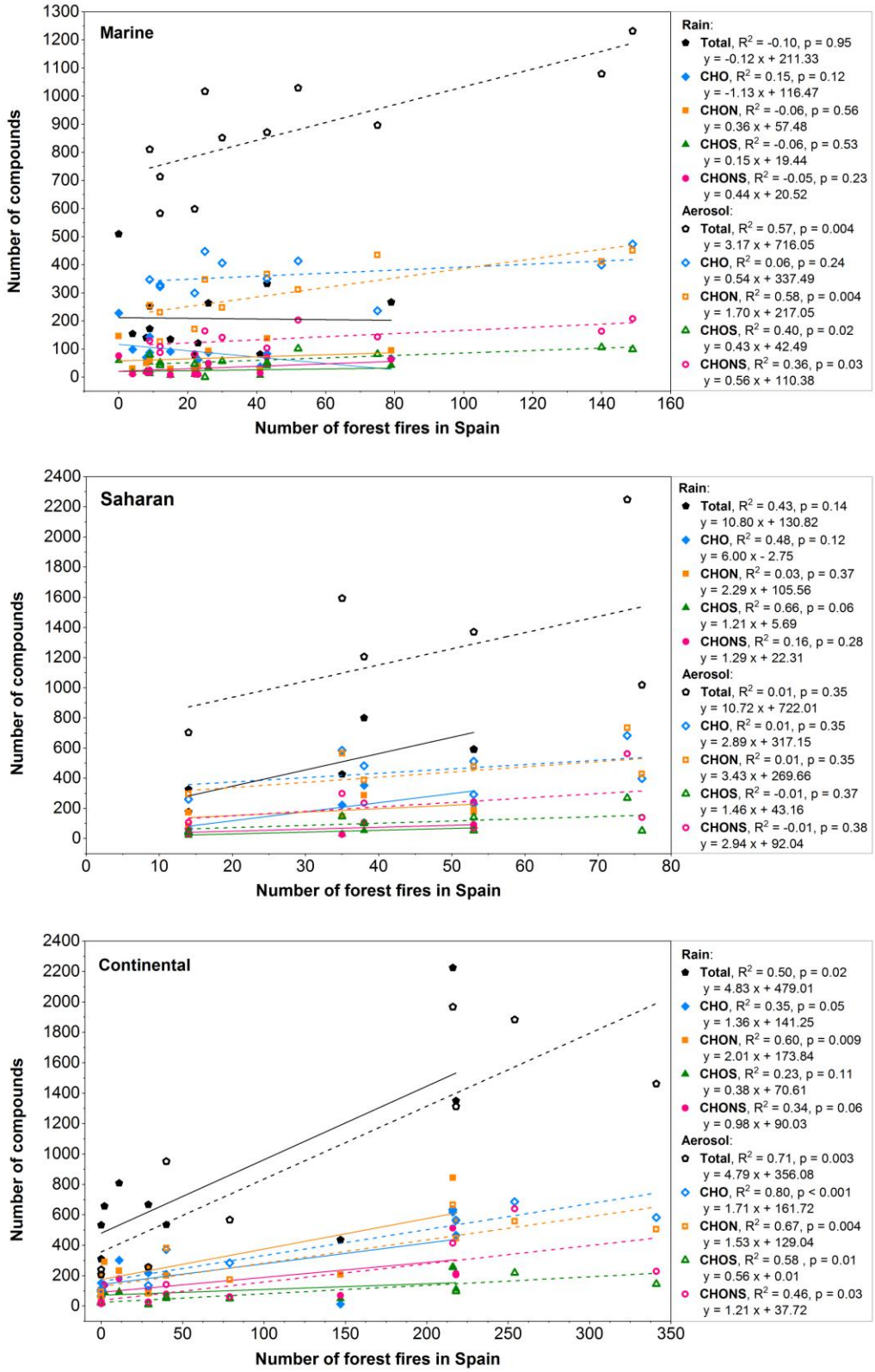

Figure 7.3. The number of compounds in the rain and aerosol samples as a function of the number of forest fires in Spain during the sample collection dates in 2016. Linear regression shown for rainwater (solid symbol, solid line) and aerosol (open symbol, dashed line). Adjusted R-squared values and F-test p-values, using a significance level of 0.05, are included.

Figure 7.4 shows the OC, EC and TC concentrations in the marine, Saharan and continental '24 hr' aerosol (plots A-C). TC and OC show significant positive linear correlation (F-test, $p = < 0.05$) with forest fires in the marine and continental aerosol. Between 30 and 80 forest fires occurred on the days when the Saharan aerosol samples were collected and these samples contained higher OC concentrations (2.8 $\mu g/m^3$ on average) than the marine aerosol (1.9 $\mu g/m^3$ on average) which were influenced by ≤ 149 forest fires. This suggests that emissions from forest fires of Northern Spain picked up in the last few hours of the marine air mass trajectories were a major source of organic matter for the marine samples, even though the majority of the air mass influence was from the Atlantic Ocean. There were many more forest fires on the days when the continental aerosol was collected (≤ 254) which is likely the reason why the OC concentrations are higher (3.25 $\mu g/m^3$ on average) than the Saharan aerosol. However, the OC concentration in the Saharan aerosol was higher than in the continental aerosol on days when there were fewer forest fires occurring. The extra source of organic matter in the Saharan aerosol may be the industrial emissions from Northern Africa as described earlier or from biogenic and anthropogenic SOA from Spain.

Potentially weak, non-statistically-significant, positive correlation is observed between the aerosol EC concentrations and the forest fires (Figure 7.4 (A-C)). The rainwater DOC also showed positive correlation with forest fire frequency (Figure 7.4 (D)) although this was only statistically-significant ($p = < 0.05$) for the continental rainwater. The marine rainwater DOC concentration does not appear to be as strongly influenced by the biomass burning as the marine aerosol OC. This could suggest that most of the organic particular matter produced by the forest fires which is present in the aerosol samples, is not being scavenged by the rainwater samples. The marine and continental PM_{10} concentrations show a positive linear correlation with the number of forest fires ($p = > 0.05$) as shown in Figure 7.4 (E), suggesting that biomass burning is a major source of the particulates. There is no observable trend for the Saharan aerosol which has been omitted from the figure.

Figure 7.4 (F) shows positive linear correlation between the number of forest fires and the ammonium and sulphate concentrations in the marine '24 hr' aerosol. This correlation is not statistically-significant and there may be other factors influencing the sulphate and ammonium concentrations in the marine aerosol such as the active coal-powered plants in Northern Spain and agricultural emissions across the country. The

continental ‘24 hr’ aerosol shows a positive linear correlation between the forest fire frequency and the sulphate ($p = > 0.05$) and ammonium ($p = < 0.05$) concentrations. This suggests that forest fires are a major source of these compounds, particularly ammonium, in the continental aerosol. Such links have been suggested in previous studies of rainwater composition in Spain (Izquierdo et al. 2012). Positive correlations between the sulphate and ammonium concentrations and forest fire frequency in the Saharan ‘24 hr’ aerosol were present but not statistically-significant due to the small sample size so have been omitted from Figure 7.4 (F).

Overall, these results show that the forest fires in Spain have had a large impact on both the composition and number of compounds in the samples. The aerosol OC appears to be more strongly influenced by the biomass burning than the rainwater OC. A significant fraction of continental and marine aerosol OC concentrations can be attributed to forest fires in Spain whereas the Saharan aerosol OC is influenced by other potential sources including the industrial and agricultural emissions from Northern Africa. Marine aerosol which had relatively clean air mass backward trajectories, compared with the continental and Saharan aerosol, appears to be significantly affected by emissions from the forest fires in Northern Spain, in terms of OC, sulphate and ammonium concentrations.

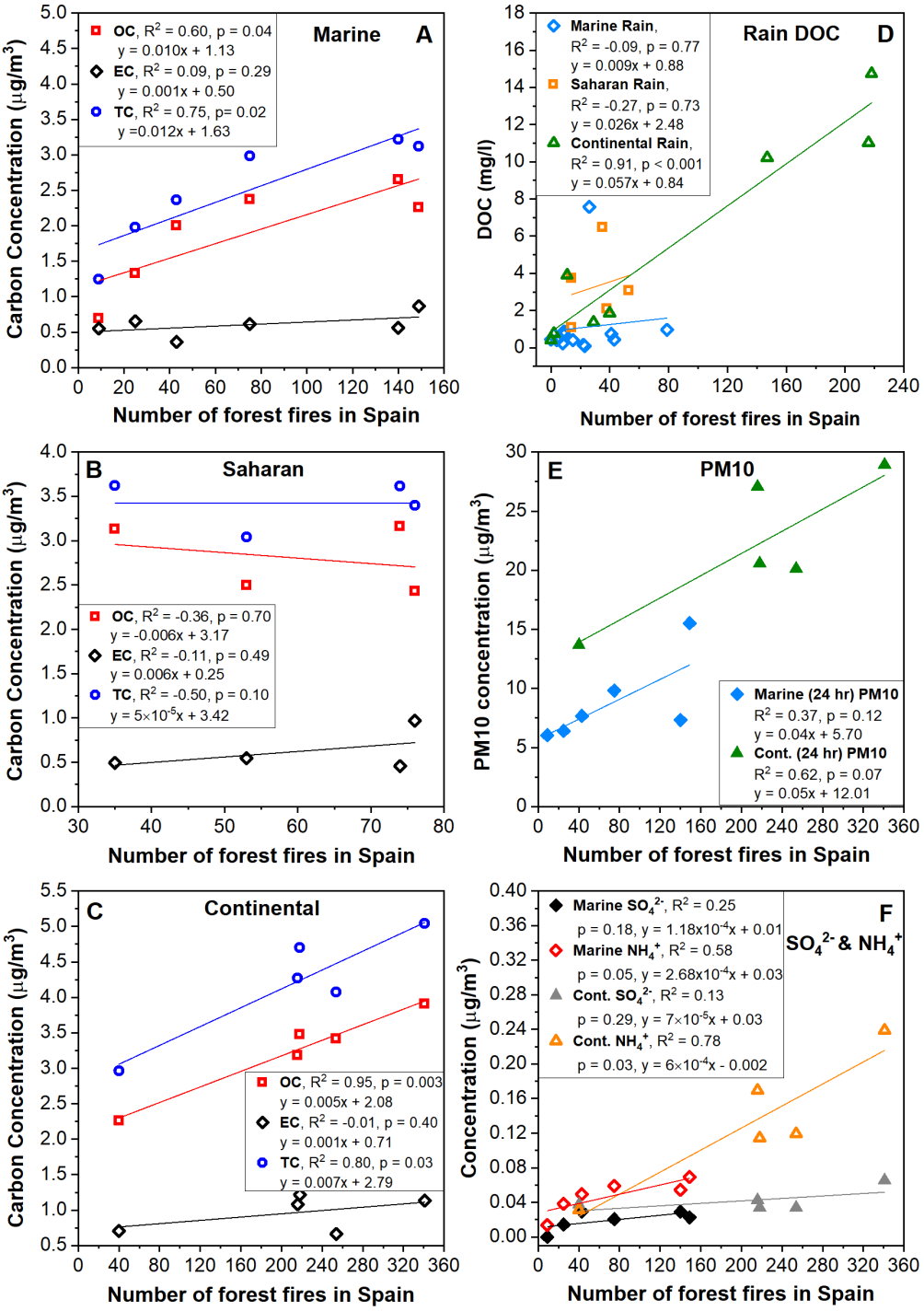

Figure 7.4. The influence from forest fires in Spain on the (A) marine, (B) Saharan and (C) Continental carbon concentrations in the '24 hr' aerosol, (D) Rainwater DOC, (E) PM_{10} concentrations in '24 hr' aerosol and (F) sulphate and ammonium concentrations in '24 hr' aerosol. (*OC* = organic carbon, *EC* = elemental carbon, *TC* = total carbon, *DOC* = dissolved organic carbon, *M* = marine, *C* = continental). Linear regression adjusted R-squared values and F-test p-values, using a significance level of 0.05, are included.

7.4.4 Air mass influence on aromatic compound distribution and oxidation

Previously, the seasonal O/C and H/C ratios for the samples were plotted in the format of van Krevelen diagrams. To determine if air mass origin had influenced the aromaticity of the compounds in the samples, the formulae sub group O/C and H/C ratios from the Nano-ESI-MS data were plotted as a function of the formulae assignment neutral mass in Figure 7.5 and Figure 7.6 for the three representative rainwater and aerosol samples corresponding to the air mass backward trajectories in Figure 7.1. Figure 7.5 and Figure 7.6 also include the mono-aromatic (green diamonds) and poly-aromatic (orange diamonds) CHO compounds identified using the aromaticity equivalent, X_C.

Figure 7.5 and Figure 7.6 show clearly that the marine and Saharan aerosol contain more compounds than their rainwater counterparts whereas the continental rain contains more compounds than its aerosol counterpart from the same rain event, as was observed in Table 7.2–Table 7.4. The marine rain and aerosol, continental rain and aerosol and Saharan aerosol samples contain CHO compounds with H/C ratios ~2.0 and O/C ratios < 1.0. These compounds could be aliphatic (C_2–C_5) aldehydes, alcohols and fatty acids. Marine aerosol is often dominated by lower molecular weight C_{14}–C_{19} fatty acids (Mochida et al. 2002). Formulae consistent with low molecular weight fatty acids and hydroxy-fatty acids e.g. $C_{11}H_{22}O_3$, $C_{16}H_{32}O_3$ and $C_{18}H_{36}O_3$ are observed in both the rain and aerosol marine samples. There are very few of these in the Saharan rainwater. In the marine rain and Saharan rain and aerosol, there are very few highly oxidised compounds (O/C ratios > 1.0). There are some compounds in the marine aerosol, continental rain and continental aerosol with higher O/C ratios (1.0–2.0) and high H/C ratios (~2.0) which could be aliphatic oxygenated compounds. These are mostly CHON and CHONS compounds so could be organonitrates but do include some CHO and CHOS compounds. Most of the aromatic CHO compounds, defined by the aromaticity equivalent, X_C, have O/C ratios between 0.1 and 0.5. This is similar to urban aerosol samples in a previous study (Tong et al. 2016). The poly-aromatic compounds have lower H/C ratios than the mono-aromatic compounds, consistent with less saturation due to the increase in DBE.

The rainwater contains some higher molecular weight compounds, predominantly CHO and CHON compounds, which exceed 600 Da whereas the aerosol sample compounds do not exceed 600 Da, regardless of air mass origin. Most compounds in the marine and

continental rain have compounds ≤ 600 Da whereas the majority of neutral masses in the Saharan rain are ≤ 400 Da, despite containing significantly more formulae assignments overall than the marine rain. The continental rain sample R50 shows horizontal bands of high molecular weight CHON, CHOS and CHONS compounds with little change in O/C ratio. These may be oligomer products formed via oxidative and non-oxidative processes.

The marine rain contains very few mono-aromatic compounds compared with the Saharan and continental rain. The Saharan rain mono-aromatic and poly-aromatic compounds appear to occupy a lower mass range (100–250 Da and 270–410 Da respectively) than the marine and continental aromatic compounds (100–350 Da for mono-aromatics compounds and 345–520 Da for poly-aromatics). This difference could be due to stronger forest fire influence in the marine and continental rain. Since there were no marine-influenced summer samples, it is not possible to make a strong comparison of the marine influence in different seasons.

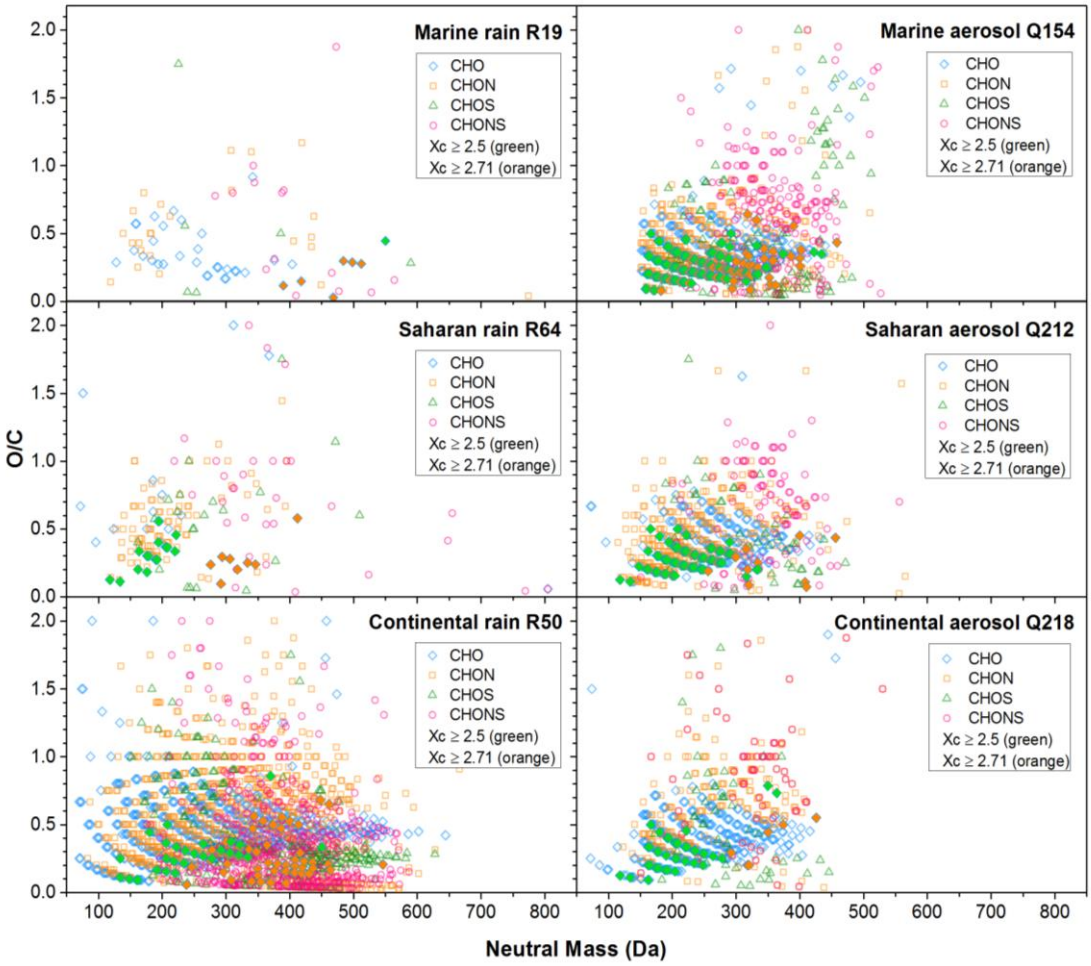

Figure 7.5. Oxygen to carbon (O/C) ratios for a representative pair of samples (one rain, one aerosol) from the same rain event, influenced by the marine, Saharan and continental air mass back trajectories shown in Figure 7.1. CHO, CHON, CHOS and CHONS formulae sub groups presented alongside mono-aromatic CHO compounds (solid green diamonds) and poly-aromatic CHO compounds (solid orange diamonds), identified using Aromaticity Equivalent, X_C.

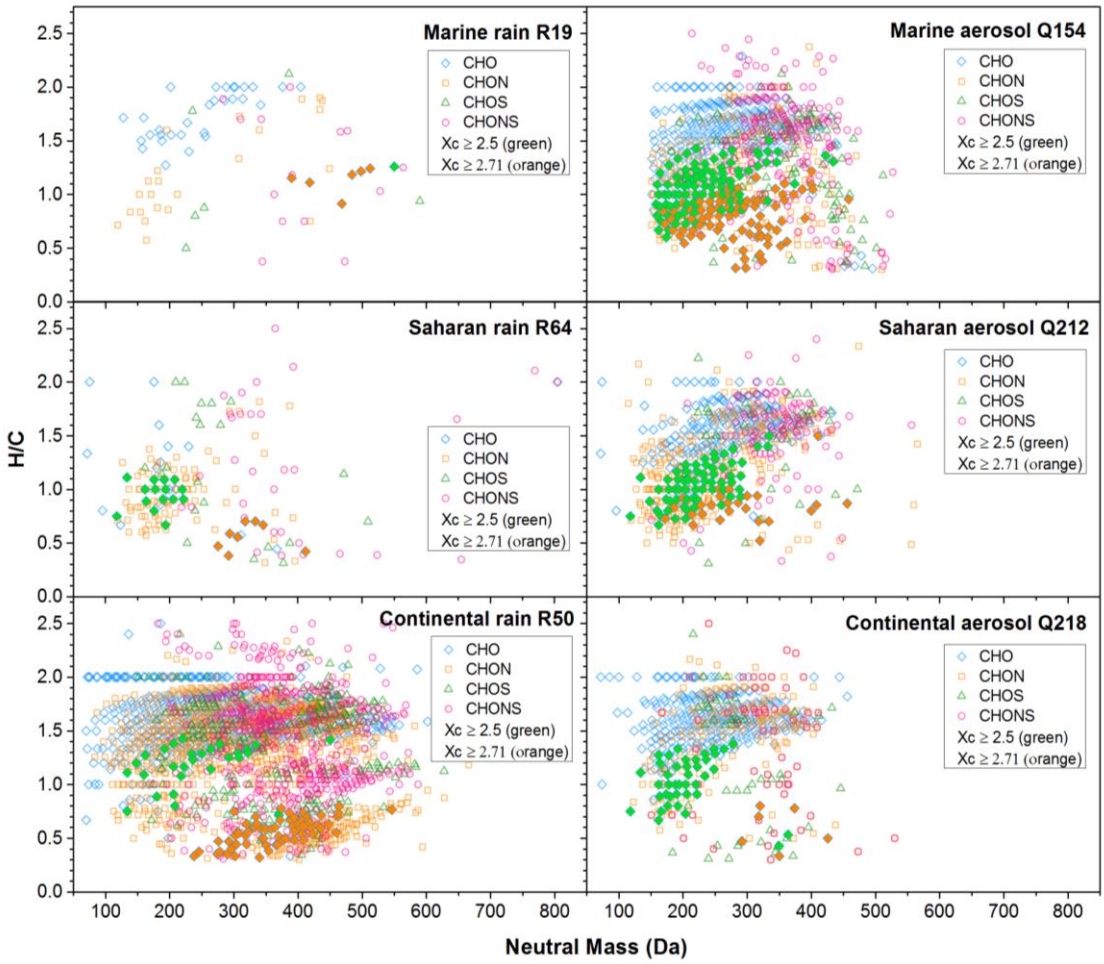

Figure 7.6. Hydrogen to carbon (H/C) ratios for a representative pair of samples (one rain, one aerosol) from the same rain event, influenced by the marine, Saharan and continental air mass back trajectories shown in Figure 7.1. CHO, CHON, CHOS and CHONS formulae sub groups presented alongside mono-aromatic CHO compounds (solid green diamonds) and poly-aromatic CHO compounds (solid orange diamonds), identified using Aromaticity Equivalent, X_C.

Table 7.6 shows the total number of aromatic compounds, mono-aromatic and poly-aromatic compounds, averaged across all of the rainwater and aerosol samples from each air mass origin, expressed as a percentage of the total number of formulae assignments in the samples. The overall percentage of aromatic compounds in the rain and aerosol samples are of a similar magnitude (30–37% for rain and 34–47% for aerosol) but regardless of air mass origin, the aerosol samples contain more aromatic compounds than their rainwater sample counterparts. This was also observed in the seasonal comparison (Figure 6.3 and Figure 6.4). Of the rainwater samples, the continental rain contains the highest and the Saharan rain contains the lowest percentage of aromatic compounds. This coincides with the seasonal trend (Figure 6.3 and Figure

6.4) where 78% of the continental rain samples were winter samples which also exhibited the highest percentage of aromatic compounds, and the Saharan samples comprised 40% summer samples which had the lowest percentage of aromatic compounds. In contrast, for the aerosol samples, the marine aerosol contains the highest and the Saharan aerosol contains the lowest percentage of aromatic compounds. This, again, reflects the seasonal trend because the marine aerosol comprises 73% spring and 18% winter samples, both of which have more aromatic compounds than the summer aerosol which makes up 57% of the Saharan aerosol.

The marine aerosol contained the highest percentage of mono-aromatics; 38% more than the Saharan aerosol ($p = < 0.05$) and 3% more than the continental aerosol ($p = > 0.05$), and Saharan aerosol contains the least. However, in the rain samples, the continental rain has the highest percentage of mono-aromatics; 24% more than the marine rain ($p = > 0.05$) and 40% more than the Saharan rain ($p = > 0.05$). There is very little difference ($\leq$ 10%) between the poly-aromatic percentages for the rainwater samples but the continental aerosol has a very low poly-aromatic content; 75% less than the marine aerosol ($p = < 0.05$) and 56% less than the Saharan aerosol ($p = > 0.05$).

Both the rainwater and aerosol samples have a higher percentage of mono-aromatic compounds than poly-aromatic compounds, although these differences are not statistically significant ($p = > 0.05$). There is a much larger difference in the percentage of mono-aromatic and poly-aromatic compounds in the aerosol than in the rainwater which could be a result of the rainwater removing many of the poly-aromatic compounds from the atmosphere and thus leaving as little as 6% of the aerosol sample composition attributable to poly-aromatic compounds.

Table 7.6. Mono-aromatic and poly-aromatic CHO compounds identified using the aromaticity equivalent, X_C, presented as averages ± 1 standard deviation across all rainwater and aerosol samples, according to air mass origin.

	Total Aromatic ($X_C \geq 2.5$) (%)	**Poly-Aromatic ($X_C \geq 2.7143$) (%)**	**Mono-aromatic (X_C 2.5-2.7143) (%)**
Marine Rain	34 ± 18.8	16 ± 5.2	18 ± 17.9
Saharan Rain	30 ± 21.9	15 ± 9.4	15 ± 14.9
Continental Rain	37 ± 11.4	14 ± 4.0	22 ± 12.5
Marine Aerosol	47 ± 10.8	13 ± 4.1	34 ± 8.0
Saharan Aerosol	34 ± 14.2	11 ± 10.6	23 ± 7.6
Continental Aerosol	39 ± 16.9	6 ± 3.7	33 ± 16.2

O/C ratios can be misleading in assessing the degree of oxidation of organic compounds because they are unaffected by non-oxidative atmospheric processes such as hydration or dehydration (Kourtchev et al. 2014a, Tong et al. 2016). To provide a more accurate idea of the oxidation of organic compounds, the average carbon oxidation state ($\overline{OS_C}$) (Kroll et al. 2011) is used as a function of the number of carbon atoms. $\overline{OS_C}$ is calculated using the following equation:

$$\overline{(OS_C)} = -\sum_i OS_i \frac{n_i}{n_C}, \tag{7.1}$$

where OS_i is the oxidation state of element *i* and n_i/n_C is the molar ratio of element *I* and carbon. Since nitrogen and sulphur species are present in multiple oxygen states, $\overline{OS_C}$ is used for CHO compounds only and Equation 7.1 is simplified to the following:

$$\overline{(OS_C)} \approx 2\frac{O}{C} - \frac{H}{C}. \tag{7.2}$$

$\overline{OS_C}$ increases upon oxidation since it takes into account both the formation of bonds between carbon and oxygen and/or the breaking of bonds between carbon and hydrogen. When plotting $\overline{OS_C}$ as a function of the number of carbon atoms, *C*, all organic species, ultimately, will oxidise to CO_2 which requires both the addition of oxygen-containing functional groups and breaking of C–C single bonds. Three classes of reactions contribute to this process; functionalisation (oxidative adding of polar functional groups to the carbon skeleton which increases $\overline{OS_C}$), fragmentation (oxidative

cleavage of C-C single bonds) and oligomerisation (association of two organic molecules) (Kroll et al. 2011). Most organic aerosol species have $\overline{OS_C}$ values between −2 and +1. Organic species with higher oxidation states are generally associated with small, low volatile or semi-low volatile aerosol (Tong et al. 2016).

Figure 7.7 shows the $\overline{OS_C}$ values, plotted as a function of the number of carbon atoms, from the Nano-ESI-MS data for the same representative rain and aerosol samples; R19 and Q154 for the marine-influenced samples, R64 and Q212 for the Saharan-influenced samples and R50 and Q218 for the continental-influenced samples. The majority of the compounds in the rain and aerosol have $\overline{OS_C}$ values between +1.0 and −1.8 with ≤ 25 carbon atoms. The continental rain contains the largest range of carbon numbers. The C_2–C_5 compounds which are not present in the marine rain and aerosol and only slightly in the Saharan rain and aerosol could be products of biogenically-emitted isoprene and α-pinene oxidation including small carboxylic acids, aldehydes and ketones. The significant presence of these compounds in the continental rain show that a lot of oxidation is happening within the continental air mass and these oxidation products are being removed efficiently from the atmosphere via wet deposition.

The C_4–C_{13} compounds with $\overline{OS_C}$ values between 0 and +1 are likely to be LV-OOA and correspond to "aged" SOA, produced by multistep oxidation reactions. All of the samples in Figure 7.7 appear to contain SV-OOA which have $\overline{OS_C}$ values between 0 and −0.5 and correspond to "fresh" SOA (Kroll et al. 2011). The compounds with ≤ 30 carbon atoms in a horizontal line, exhibiting little change in $\overline{OS_C}$ in the continental rain, suggest oligomerisation from accretion reactions which produce high molecular weight species with low volatility (Kroll and Seinfeld 2008). All of the samples in Figure 7.7, excluding the Saharan rain sample, contain some compounds with $\overline{OS_C}$ values < −1.0. The C_7–C_{22} compounds with $\overline{OS_C}$ values between +0.5 and −1.5; present in the marine rain and aerosol and Saharan aerosol but mainly in the continental rain and aerosol; are likely to be BBOA, corresponding to POA emitted directly into the atmosphere (Kroll et al. 2011). Compounds with $\overline{OS_C}$ ≤ 0 are reduced and include monoterpenes, toluene, isoprene, carboxylic acids, aldehydes and ketones. There are a few compounds with longer carbon chains (C_{18}–C_{30}) with $\overline{OS_C}$ values between −1 and −2 in the continental rain which could be primary HOA. These have been observed in boreal forest samples (Kourtchev et al. 2013). A small number of compounds in the marine aerosol and continental rain and aerosol have $\overline{OS_C}$ > +1.0 These are volatile although highly

oxidised, and are likely to be mostly in the gas phase in the atmosphere because they are photochemically or thermodynamically unstable and decompose rapidly into smaller species (Kroll et al. 2011). Similar OS_C values have been observed in laboratory-produced biogenic SOA and boreal forest aerosol (Kourtchev et al. 2014a).

The oxidation patterns for the mono-aromatic and poly-aromatic compounds, inferred by the O/C values in Figure 7.5 and the $\overline{OS_C}$ values appear to be largely similar. In general, the mono-aromatic compounds cover a wider range of oxidation states than the poly-aromatic compounds and the poly-aromatic oxidation states lie between the minimum and maximum oxidation states of the mono-aromatic compounds. However, Figure 7.7 indicates that many of the poly-aromatic compounds in the continental rain, and a few in the marine aerosol, have higher $\overline{OS_C}$ values (> 0) than the mono-aromatic compounds whereas the majority of the aromatic compounds in the other samples are reduced ($\overline{OS_C}$ < 0). The oxidised aromatic compounds are likely to be BBOA emitted from the forest fires.

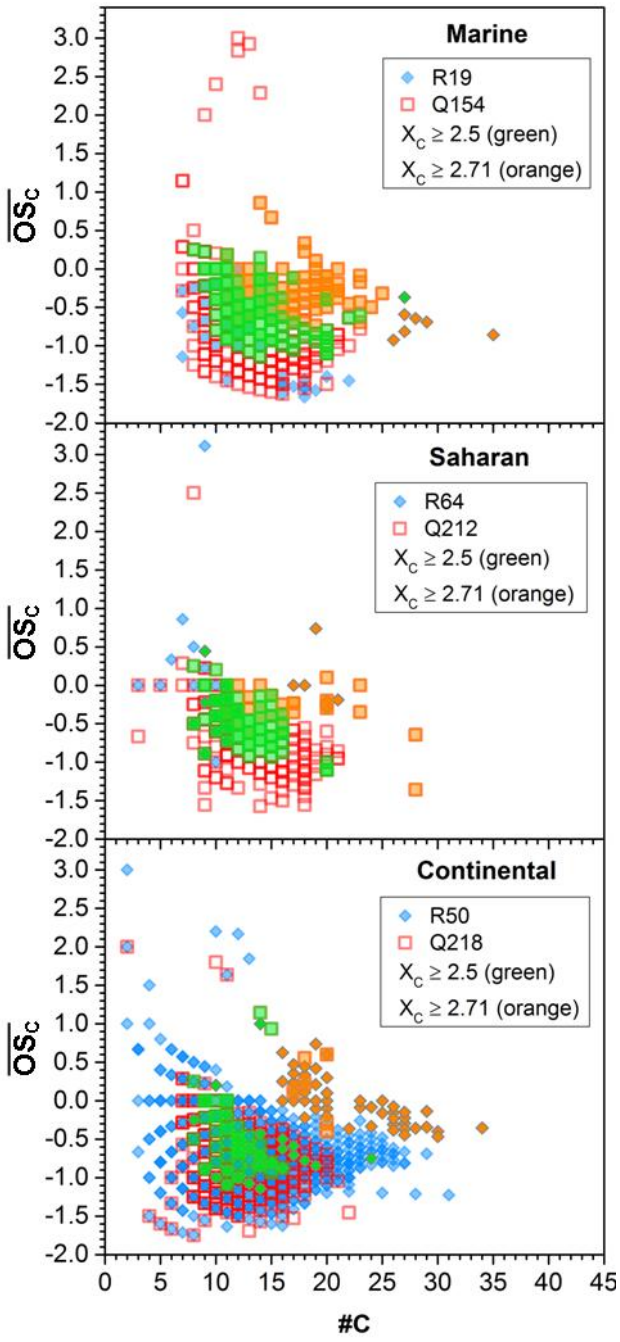

Figure 7.7. $\overline{OS_C}$ values for the CHO compounds in representative rain (blue, solid diamonds) and aerosol (red, open squares) samples. Marine-influenced rain and aerosol sample (top) corresponding to the air mass on 16.04.16, a Saharan rain and aerosol sample (middle) corresponding to air mass on 04.11.16 and a continental rain and aerosol sample (bottom) corresponding to air mass on 25.08.16. Mono-aromatic CHO compounds for rain (green, solid diamonds) and aerosol (green, solid squares) and poly-aromatic CHO compounds for rain (orange, solid diamonds) and aerosol (orange, solid squares) also included.

7.5 Conclusions

120 hour back trajectories were plotted for the AERORAIN rainwater and aerosol samples using HYSPLIT to determine air mass origin. Air mass origin was found to be one of the dominant influences on the rainwater and aerosol sample composition. 90% of the spring samples and 25% of the winter samples were marine-influenced and the distributions of CHO, CHON, CHOS and CHONS as a function of seasonality and air mass origin were very similar.

The CHO compounds in the rainwater and aerosol samples were deemed to be largely of oceanic origin because the spring and summer Saharan-influenced samples had slightly more influence from the Atlantic Ocean and Mediterranean Sea and these samples had more CHO compounds while the winter Saharan-influenced samples had less oceanic influence and more CHON compounds. Within the solely marine-influenced samples, the spring trajectories had a stronger Atlantic Ocean influence and more CHO compounds than the winter marine trajectories which had weaker Atlantic Ocean influence and more CHON compounds.

Marine-influenced samples were the least acidic and had the lowest concentrations of PM_{10}, OC, EC, SO_4^{2-}, NH_4^+ and NO_3^- compared with the continental and Saharan-influenced samples. The winter marine-influenced samples appeared to have an extra source of nitrogen and sulphur producing more CHON/CHOS/CHONS compounds than were present in the spring marine samples. This could be a combination of organic nitrogen from marine biological sources and terrestrial nitrogen and sulphur influencing the samples in the last couple of days before rain deposition. The CHOS compounds in the aerosol were more oxidised and more saturated in the spring than in the winter and this could be due more fatty acids being present. Marine CHON and CHONS compounds were also more saturated (higher H/C ratios) in the spring than in the winter, in both the rain and aerosol samples.

CHON compounds dominated the Sahara desert-influenced samples and the number of CHO compounds in these samples decreased throughout the year. The Saharan aerosol also contained higher concentrations of SO_4^{2-} and NO_3^- than the continental aerosol which is most likely due to the Saharan air masses picking up desert dust and industrial emissions from North Africa, as indicated by the backwards trajectories, which provide an additional source of SO_4^{2-} and NO_3^-. Highly oxidised compounds were observed in

the Saharan rainwater and aerosol. Overall, the winter rain CHO, CHON, CHOS and CHONS compounds had higher O/C ratios and lower H/C ratios than the spring/summer rain, meaning that the winter rainwater contains more oxidised and less saturated compounds. PAHs may have contributed to the lower average H/C ratio for the winter rain samples. However, the spring/summer aerosol CHO, CHON and CHOS compounds have higher O/C ratios than the winter aerosol.

Continental-influenced samples comprised 50% of the summer samples and 59% of the winter samples. They were the most acidic and had the highest PM_{10}, OC, EC and NH_4^+ concentrations due to greater terrestrial influence, including anthropogenic and biogenic emissions from forest fires in Spain and Portugal. The continental rainwater contained, on average, four times as many compounds as the marine rain (91% more CHO, 132% more CHON, 124% more CHOS and 136% more CHONS) and twice as many compounds as the Saharan rainwater (including 78% more CHOS). This could be due to stronger influence from coal combustion from the coal-powered plants in Northern Spain. The number of CHON, CHOS and CHONS compounds decreased throughout the year in the continental samples, particularly between the summer and winter period, reflecting reduced photochemistry and fewer forest fires in the winter compared with the summer.

All continental aerosol formulae sub-groups and CHON compounds in the continental rainwater showed statistically-significant positive correlations between the number of forest fires in Spain in 2016 and the number of compounds. Saharan rainwater CHONS also showed a significant positive correlation and non-statistically-significant positive correlations were observed for all other Saharan formulae sub-groups in the rain and aerosol. Marine samples were generally less affected by forest fires because the air mass passed over fewer forested areas than the Saharan and continental air masses. However, the marine aerosol did show significant positive correlation between number of compounds and number of forest fires but this was not observed for the marine rainwater, perhaps due to the reduced number of forest fires occurring on the days when rain samples were collected.

The aerosol OC was more strongly influenced by the biomass burning from the forest fires than the rainwater DOC. The OC, SO_4^{2-} and NO_3^- concentrations in the marine aerosol were heavily influenced by the forest fires. Forest fires in Spain contributed significantly to the continental aerosol OC concentrations whereas the Saharan aerosol OC was probably more influenced by the industrial and agricultural emissions from

North Africa because there were fewer forest fires on the days when the Saharan samples were collected.

Marine, Saharan and continental aerosol all contained significantly higher percentages of mono-aromatic compounds than poly-aromatic compounds. The percentages of mono-aromatic and poly-aromatic compounds are much more similar in the rainwater although continental rain contains slightly more mono-aromatic compounds than poly-aromatic compounds. The continental rain shows the largest range of $\overline{OS_C}$ values, including highly oxidised, small C_2–C_5 carboxylic acids which could be SOA products from isoprene oxidation and are not present in the continental aerosol, indicating efficient scavenging of these compounds by the rain droplets. The continental rain also has high molecular weight products which may be oligomerisation products from accretion reactions and have low volatility. All of the samples appear to contain SV-OOA or "fresh" SOA and the continental rain contains more LV-OOA or "aged" SOA.

8 INVESTIGATING SCAVENGING OF ORGANIC COMPOUNDS IN AEROSOL BY RAINWATER DURING THE AERORAIN CAMPAIGN

The previous analysis of the Nano-ESI-MS data for the AERORAIN samples in this thesis has highlighted clear differences in the compound distributions in the rainwater and aerosol as well as seasonal impacts and influences from air mass origin. The analysis in this chapter focuses on quantifying the aerosol scavenging occurring in the samples and how air mass origin influences scavenging.

8.1 Introduction

Wet deposition of atmospheric compounds occurs through *washout* or *below-cloud scavenging* which scavenges airborne particulates between the cloud and Earth's surface, and *rainout* or *in-cloud scavenging* where compounds are incorporated into droplets within a cloud via nucleation, condensation and gas dissolution (Seinfeld and Pandis 2006, Peña et al. 2002). Air mass origin has been shown to influence scavenging (Sasakawa and Uematsu 2002, Hu, Balasubramanian and Wu 2003). Measurements of precipitation and aerosol composition and the associated scavenging of compounds is important for understanding which compounds are more efficiently removed from the

atmosphere and which have more longevity and are thus more likely to influence aerosol climate forcing (Gioda et al. 2011).

Previous studies have investigated the scavenging of organic compounds in rainwater over time (Kawamura et al. 1996) and distributions of compounds in aerosol and rainwater (Mace et al. 2003) and in aerosol and cloud water (Boone et al. 2015, van Pinxteren et al. 2016). However, to our knowledge, none have directly compared the molecular composition of rainwater and aerosol collected from the same rain event.

8.2 Aims

The overall aim of this work was to assess the conservation of compounds between rainwater and aerosol sampled during the AERORAIN campaign and see if this is linked to below-cloud scavenging of the aerosol by the falling precipitation.

The specific objectives of this work were to:

- Determine the extent of scavenging of compounds in aerosol samples by rainwater during the rain events in León.
- Investigate the influence of air mass origin on the extent of scavenging of organic compounds.

8.3 Analysis and Discussion

8.3.1 'Cleaning' of atmosphere during long rain event

There is strong evidence of aerosol scavenging occurring in the León samples. A good example of this is the large spring rain event which began on 05.05.16 and ended on 11.05.16. Figure 8.1 shows the number of formulae assignments in the rain samples and aerosol samples collected during the event as well as the rainwater DOC and $PM_{2.5}$ concentrations in the 'RE aerosol'. There is a general decrease in the number of compounds in the rain and aerosol between the first day and seventh day of rain. The rainwater DOC concentration appears to decrease significantly after the first day of rain and as previously mentioned, the O/C ratios for the rainwater in the long rain event

decreased from 0.51 to 0.22 which shows that the scavenging has changed the composition of the aerosol by removing the more oxidised and, thus, more water-soluble compounds from the atmosphere earlier on in the rain event. This indicates that the aerosol scavenged by the rain towards the end of the rain event is less aged and less complex than the aerosol scavenged at the beginning of the rain event.

On the fourth and sixth days of the rain event, there are spikes in the DOC concentration. These peaks are echoed to a lesser extent in the number of rainwater compounds. These correspond to slight decreases in the measured rain intensity (Figure 5.8) and therefore may indicate fewer rain droplets available to remove the organic compounds from the atmosphere. The $PM_{2.5}$ concentration of the 'RE' aerosol collected during the rain event shows a strong decrease over time, indicating clear 'cleaning' of the atmosphere over the course of the rain event.

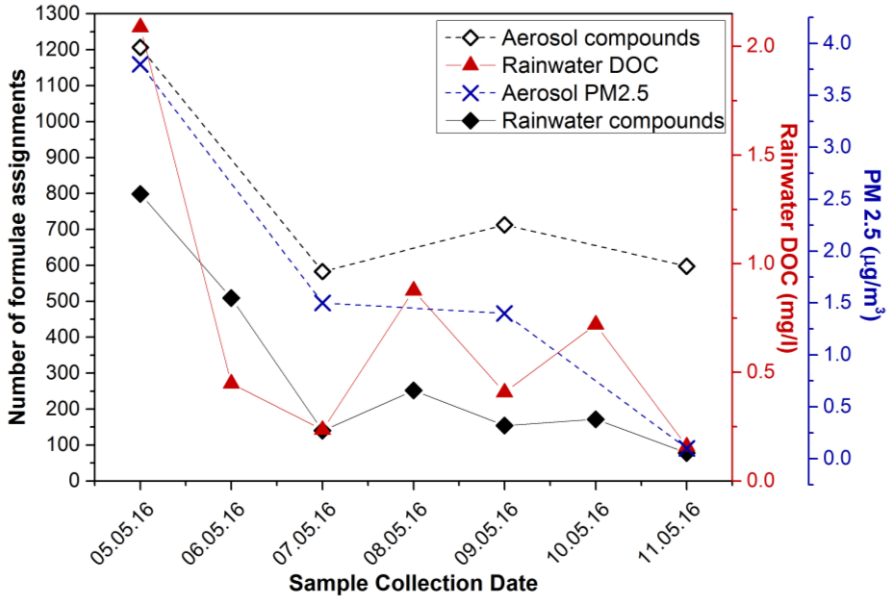

Figure 8.1. Rainwater and RE aerosol number of compounds (filled diamonds for rain, open diamonds for aerosol), rainwater DOC (red triangles) and aerosol PM 2.5 (blue crosses) for the spring rain event from 05.05.16 to 11.05.16.

8.3.2 Change in aerosol composition before and after rain event

The '24 hr' aerosol, collected on the same day a rain event occurred, show evidence of aerosol scavenging when compared with the '24 hr' aerosol sample collected on the day before the rain event. Of the five available sets of aerosol samples, all except one show a decrease in the number of compounds and the concentrations of PM_{10}, OC, EC, SO_4^{2-}, NH_4^+ and NO_3^- on the day when the rain event occurred compared with the previous day, as shown in Table 8.1. This is a strong indicator that the rain events are removing aerosol from the atmosphere.

Table 8.1. Number of compounds, PM_{10} concentrations, carbon concentrations and inorganic ion concentrations for the '24 hr' aerosol samples collected on a day when a rain event occurred (white rows) and on the day before the rain event (grey rows).

Date	Sample ID	Number of compounds	PM_{10} (μg/m^3)	OC (μg/m^3)	EC (μg/m^3)	SO_4^{2-} (μg/m^3)	NH_4^+ (μg/m^3)	NO_3^- (μg/m^3)
05.07.16	Q169	2248	21.26	3.16	0.46	0.0221	0.0873	0.0429
06.07.16	Q170	1370	15.16	2.49	0.55	0.0269	0.0808	0.0470
13.08.16	Q259	1883	20.09	3.41	0.66	0.0338	0.1188	0.0457
14.08.16	Q260	1312	20.57	3.48	1.22	0.0336	0.1144	0.0408
24.08.16	Q272	1462	28.91	3.91	1.13	0.0652	0.2390	0.0722
25.08.16	Q273	1967	27.06	3.18	1.08	0.0420	0.1695	0.0710
18.11.16	Q366	896	9.83	2.37	0.62	0.0203	0.0587	0.0505
19.11.16	Q367	871	7.67	2.00	0.36	0.0294	0.0496	0.0557
13.12.16	Q392	1019	18.35	2.43	0.97	0.1586	0.1624	0.2701
14.12.16	Q393	951	13.66	2.26	0.71	0.0372	0.0312	0.0777

8.3.3 Influence of air mass origin on extent of scavenging

There were 18 pairs of rainwater and aerosol samples collected during rain events; six marine-influenced pairs, six Saharan-influenced pairs and six continental-influenced pairs. These are listed in Table 8.2. To determine the extent of scavenging in each rain event, the number of formulae assignments in the aerosol sample which were also present in the rain sample, was calculated as a percentage of the total number of formulae assignments in the aerosol sample, as shown in Equation 8.1, and the results are shown in Figure 8.2.

$$\frac{\text{Number of aerosol compounds present in rainwater sample}}{\text{Total number of compounds in aerosol sample}} \times 100 \,. \qquad (8.1)$$

Table 8.2. 18 pairs of rainwater and aerosol samples collected during rain events. Total numbers of compounds in the aerosol samples used in the calculation of the percentage of aerosol compounds in the rainwater samples.

	Date of rain event	Rainwater Sample	Total number of rainwater compounds	Aerosol Sample	Total number of aerosol compounds
Marine	14.04.16	R19	81	Q154 RE	1029
	16.04.16	R21	134	Q155 RE	852
	07.05.16	R29	140	Q201 RE	583
	09.05.16	R31	154	Q202 RE	713
	11.05.16	R33	78	Q203 RE	598
	19.11.16	R69	332	Q367 24 hr	871
Saharan	05.05.16	R27	799	Q200 RE	1206
	05.07.16	R47	589	Q170 24 hr	1370
	05.07.16	R47	589	Q206 RE	592
	06.07.16	R48	426	Q172 RE	1593
	04.11.16	R63	326	Q212 RE	703
	04.11.16	R64	177	Q212 RE	703
Continental	14.08.16	R49	1350	Q260 24 hr	1312
	25.08.16	R50	2224	Q273 24 hr	1967
	13.10.16	R57	532	Q211 RE	239
	24.11.16	R71	309	Q214 RE	207
	14.12.16	R73	667	Q232 RE	255
	14.12.16	R73	667	Q393 24 hr	951

The percentage of formulae assignments that were observed in both the aerosol and rainwater sample, for each pair of samples in Table 8.2, are shown in Figure 8.2. Higher percentages indicate more compounds removed from the air by wet deposition and, hence, stronger scavenging. On average, the continental rain events show the most scavenging; 43% of the compounds in the aerosol were removed via wet deposition and were subsequently present in the rainwater. This is 53% ($p = < 0.05$) more than the Saharan samples and 116% ($p = < 0.05$) more than the marine samples. The previous analysis of the O/C ratios (Figure 7.5) and the $\overline{OS_C}$ ratios (Figure 7.7) indicates that there was a greater number of highly oxidised compounds including aged SOA in the continental rain compared with the other samples. OOA are more water-soluble (Aiken et al. 2008) so there were more water-soluble compounds available in the continental aerosol for the rainwater to scavenge than there were in the marine or Saharan aerosol.

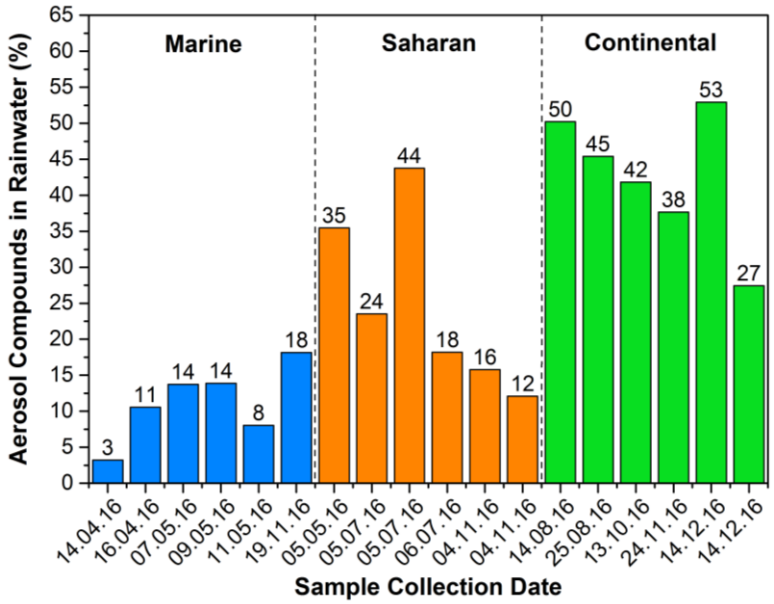

Figure 8.2. Percentage of aerosol compounds also present in the rainwater sample from the same rain event Marine samples (blue), Saharan samples (orange) and continental samples (green).

The distribution of the percentages of CHO and CHON compounds scavenged in the marine samples were very similar, as were the Saharan and continental CHO and CHON compound scavenging distributions. Therefore, they have been presented as a combined figure for each air mass origin in Figure 8.3. The same was done for the CHOS and CHONS compounds. It is evident from Figure 8.3 that the CHO and CHON compounds were scavenged far more effectively than the CHOS and CHONS

compounds; 97% (p = 0.02) more effectively in the marine samples, 106% (p = 0.01) more effectively in the Saharan samples and 74% (p = 0.001) more effectively in the continental samples. CHO compounds were generally more efficiently scavenged in the marine and Saharan samples whereas CHON compounds are the most scavenged for the continental aerosol although it is noted that these differences are not statistically-significant. The absolute number distribution of formulae assignments in the rainwater shown in Figure 7.2 (A) showed that CHO compounds were present in the highest numbers in the marine rain so this could explain why more CHO were scavenged in the marine samples. CHON compounds dominated the continental rain and Figure 7.5 and Figure 7.6 showed that a significant portion of the CHON compounds in the continental rainwater had O/C ratios > 1.0 and H/C ratios < 1.0 which is consistent with highly oxygenated organic compounds. These compounds were more water-soluble so were more easily scavenged by the rainwater in the continental samples.

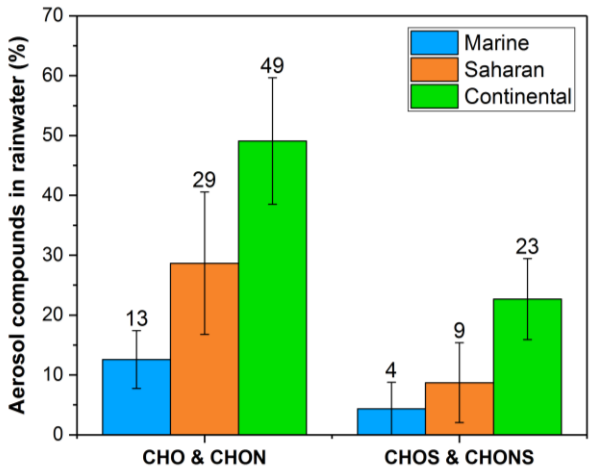

Figure 8.3. Percentage of CHO, CHON, CHOS and CHONS aerosol compounds also present in the rainwater samples from the same rain event. Marine (blue), Saharan (orange) and continental (green) averages shown ± 1 standard deviation.

8.4 Conclusions

The aim of this work was to determine if there was significant scavenging of the compounds from the atmosphere by the rainwater which is reflected in the compositional data analysed here. Both the rainwater and aerosol samples show strong evidence of aerosol scavenging. The seven day rain event in May 2016 showed an overall decrease in the number of compounds, DOC concentration, $PM_{2.5}$ concentration and O/C ratios for the rainwater. This shows that the scavenging significantly altered the composition of the aerosol by removing the more oxidised and, thus, more water-soluble compounds from the atmosphere, making the compounds scavenged at the end of the rain event less complex and less aged than those scavenged at the beginning of the rain event.

The rainwater DOC and number of compounds decrease during longer rain events, as does the 'RE' aerosol number of compounds and the $PM_{2.5}$ concentrations. The '24 hr' aerosol samples collected on the day of a rain event have lower concentrations of OC, EC, PM_{10}, sulphate, ammonium and nitrate concentrations compared with the '24 hr' aerosol from the day before the rain event. This is clear evidence of removal of aerosol particles via wet deposition.

This is the first study to investigate aerosol scavenging using rainwater and aerosol composition from the same rain event and to suggest preferential scavenging of more "aged" aerosol. Continental samples exhibited the most efficient aerosol scavenging and marine samples exhibited the least scavenging. CHO and CHON compounds were scavenged more efficiently than CHOS and CHONS compounds regardless of air mass origin. CHON compounds were scavenged very efficiently in the continental rainwater which may be due to a significant fraction of the CHON being highly oxidised and therefore more water-soluble so were more readily available for scavenging by the rainwater.

9 Identification of Organic Compounds in Rainwater and Aerosol Samples using LC-ESI-MS

Molecular characterisation using direct infusion ESI-MS such as that covered in Chapters 5–8 is very useful for providing an overview of the distribution of organic species in ambient samples, but it is a qualitative approach. LC-MS, however, provides a (semi)-quantitative method of identifying compounds in the ambient rain and aerosol samples and it allows the separation of isomers.

9.1 Introduction

Liquid Chromatography Mass Spectrometry (LC-MS), or HPLC, combines the separation capabilities of liquid chromatography with the mass analysis precision and accuracy of mass spectrometry. Reversed Phase (RP) Partition Chromatography is the most commonly used form of HPLC which uses a non-polar stationary phase and polar mobile phase. In RP-HPLC, a sample is loaded onto a column containing a non-polar stationary phase which is a long-chain alkyl group chemically bonded to porous silica.

Non-polar, hydrophobic analytes interact strongly with the stationary phase and are retained for longer than hydrophilic analytes which spend more time in the polar mobile phase; usually a mixture of water and methanol or acetonitrile. Using a gradient program allows the user to strengthen the elution solvent to elute more strongly retained hydrophobic compounds from the column (Dass 2007).

LC analysis has an advantage over GC analysis in that both the stationary phase and the mobile phase in the LC column are used in the separation and can each be modified to achieve the most efficient separation for the target compounds, whereas only the stationary phase in a GC column achieves the separation (Noziere et al. 2015).

LC-MS has been used for general molecular characterisation of ambient and laboratory-generated aerosol samples to investigate SOA formation, aerosol ageing and identify organosulphates and nitrooxy organosulphates (Glasius et al. 2000, Surratt et al. 2006, Gao et al. 2006, Surratt et al. 2008, Iinuma et al. 2009, Gómez-González et al. 2012). LC-MS is one of the most robust analytical methods for characterising polar organic compounds containing hydroxyl, oxo, carboxylic acid and sulphate functional groups, the latter of which cannot be analysed using GC-based methods.

LC-MS also allows separation of chemical isomers and helps reduce ion suppression (Kourtchev et al. 2013), making it very useful for investigating ageing of SOA in conjunction with ESI-MS because competitive ionisation of analytes in ESI-MS alone does not accurately reflect the concentration of the compounds in the sample.

9.2 Aims

The aim of this work is to build on the general characterisation of the AERORAIN rainwater and aerosol samples completed in the previous chapters of this thesis by using LC-ESI-MS to identify specific compounds in samples.

Specific objectives of this work were to:

- Identify specific organic compounds in the rainwater and aerosol samples including carboxylic acids, organosulphates and organonitrates.
- Compare the distributions of specific compounds in samples from marine, desert dust and continental origins.

9.3 Methodology

Prior to LC-MS analysis, the rain and aerosol samples listed in Table 5.1–Table 5.3 were prepared using the method described in 5.3.1, using the SPE Strata-X method described in Table 4.3 and were evaporated down to 100 µl samples. They were run in batches with each batch running for up to 60 hours.

Three external standards were added to the 100 µl rainwater and aerosol samples to detect any shifting of retention times which may occur during the long sequence runs, to detect degradation of samples and to identify any variability in recovery between samples. SOA oxidation products from biogenic precursors were expected to be present in the samples. The three chosen external standards were deuterated succinic acid; a representative for carboxylic acids, 4-nitrocatechol; a representative for organonitrate compounds and camphorsulphonic acid; a representative for organosulphate compounds. These compounds were chosen because they produced stable retention times in areas of the chromatograms of the test rainwater and aerosol samples, where there were no or very few peaks from samples ions.

The standards were prepared by making separate stock solutions of the compounds in a solvent of 0.1% formic acid in water (LC-MS, Fisher Scientific). The stock solution concentrations were as follows; 0.1 mg/ml of deuterated succinic acid (98%, Sigma-Aldrich), 0.001 mg/ml of camphorsulphonic acid (99%, Sigma-Aldrich) and 0.001 mg/ml of 4-nitrocatechol (97%, Sigma-Aldrich). 50 µl of each of the three standard stock solutions was added to each 100 µl rain and aerosol sub-sample which diluted the stock solution concentration by 80% so that the resulting concentrations of the three standards in the samples were 20 ng/µl of deuterated succinic acid, 0.2 ng/µl camphorsulphonic acid and 0.2 ng/µl of 4-nitrocatechol.

The extracted ion chromatograms (EIC) from one sequence run for the three standard compounds are shown in Figure 9.1. Over the period in which all of the rain and aerosol LC-MS analysis was completed, the retention times were found to vary by $\pm \leq 0.30$ minutes, averaged over 10 individual EICs for the standard compounds. It is noted that using internal standards prior to the filter extraction would have yielded more accurate results regarding degradation as it would have accounted for inconsistencies in the filter extraction and SPE. However, half of the eluted analyte solution from the SPE was to be used for direct infusion ESI-MS. Since these standards are not necessary for direct

infusion ESI-MS spectra, they were only added to the 100 µl LC-MS sub-samples once the samples had been split into the LC-MS and direct infusion ESI-MS sub-samples, to avoid introduction of contaminants.

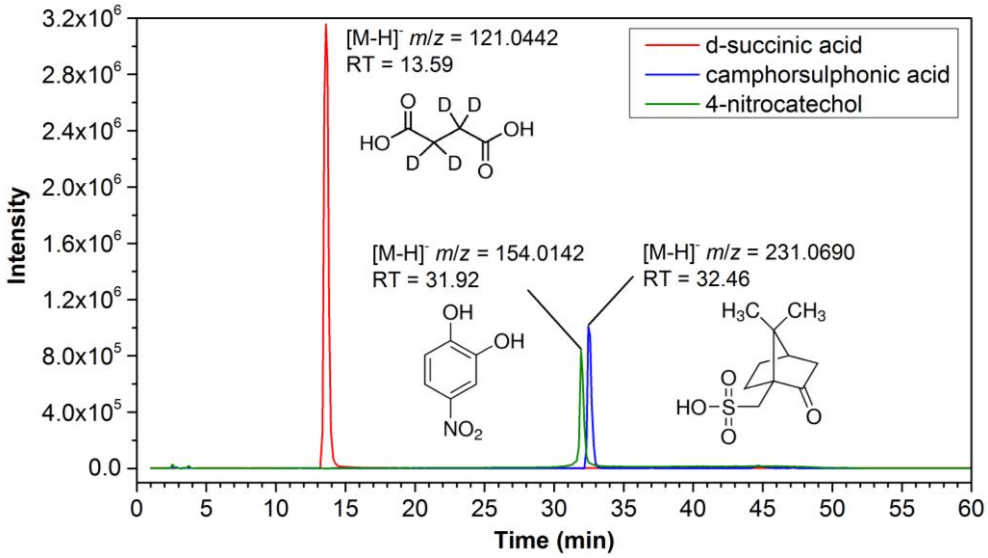

Figure 9.1. (−)LC-ESI-MS Extracted Ion Chromatogram (EIC) showing retention times (RT) for the three standards; deuterated succinic acid ($[M-H]^-$ *m/z* 122.11 (red)), camphorsulphonic acid ($[M-H]^-$ *m/z* 232.30 (blue)) and 4-nitrocatechol ($[M-H]^-$ *m/z* 32.01 (green)).

LC-ESI-MS analysis of the León samples was conducted using an Accela Autosampler and Pump System (Thermo Scientific, San Jose, USA) coupled to the same LTQ Orbitrap Velos MS that was used for the Nano-ESI source direct infusion, with a heated ESI source attached. A T3 Atlantis C18 reversed phase column (3 µm, 3.0 × 150 mm; Waters, Milford USA) was used to separate the organic compounds from the rain and aerosol samples, before detection by the ESI-MS. C18 columns are capable of withstanding high mass loading of highly polar compounds and are widely used for analysing environmental samples (Kourtchev et al. 2013, Mace et al. 2003, Surratt et al. 2006, Gao et al. 2006, Surratt et al. 2008, Iinuma et al. 2009, Cooporation 2007, Scientific 2009a). The LC-MS sequences were run using *Xcalibur* software (Thermo Scientific) and 0.1% formic acid in water, and methanol (both LC-MS grade, Fisher Scientific, Loughborough) were used for the mobile phase.

The method used for the LC analysis is described as follows. Prior to each sequence run, the two LC lines loading the solvent onto the column were washed with their respective solvents (0.1% formic acid in water and methanol) for 10 minutes at a flush

speed of 1000 µl/min, to remove any previous solvent and contaminants from the lines. The column was washed with 0.1% formic acid in water (LC-MS, Fisher Scientific, Loughborough) for 10 minutes at 200 µl/min and the autosampler syringe and needle were washed with methanol.

The gradient program in Table 9.1 was used to elute as many compounds from the LC column as possible, using two solvents; 0.1% formic acid in water, and methanol (both LC-MS grade, Fisher Scientific, Loughborough). Before any of the samples were loaded onto the column, 15 µl of methanol (UHPLC, Fisher Scientific, Venezuela) was loaded onto the column and run three times using the gradient program on Table 9.1, with each run lasting 60 minutes. This eluted any organic compounds which may have been retained on the column and had not been previously removed by the water. 15 µl of the blank samples were then loaded onto the column using the autosampler, followed by 15 µl of each sample. Each blank and sample was run for 60 minutes and data was acquired as two replicates over the scan range *m*/*z* 60-650. To monitor the quality of the chromatograms over the long sequences, a methanol run was included every 8 or 9 sample replicates and compared with the initial methanol chromatograms. Once all of the samples had been analysed, data was acquired as two replicates over *m*/*z* 60–650 for a mixed solution containing 100 µl of each of the three external standard solutions only (deuterated succinic acid, camphorsulphonic acid and 4-nitrocatechol). Once the sequence was complete, the LC-MS column was washed with methanol to remove any compounds remaining on the column and was stored in acetonitrile between sequence runs to prevent column degradation. The Accela pump was also flushed with 2-propanol to maintain good working order.

Table 9.1. LC-MS Gradient Program used to elute rainwater and aerosol analytes from the LC column. The increases and decreases in solvent proportions were linear. Reagents used were either LC-MS or UHPLC-MS grade for all samples.

Time (min)	0.1% formic acid / water (%)	Methanol (%)
0	97	3
3	97	3
25	50	50
43	10	90
48	97	3
60	97	3
-	100	0

9.3.1.1 LC-MS Data Treatment

The LC-MS chromatograms and mass spectra were analysed using the same *Xcalibur* software (Thermo Scientific) as the Nano-ESI-MS spectra. Species in the samples were tentatively identified by comparing the mass spectral data with those for identified compounds reported in the literature. Only *m*/*z* values with at least 10% relative abundance were considered when identifying the compound for each chromatographic peak. Similar to the mass shift validation used for treating the Nano-ESI-MS data, described in 4.5.2, a mass error limit of ± 4.0 ppm was used in the *Xcalibur* software for formulae assignments and any *m*/*z* values which fell outside of the limit were not used for the species identification. The mass error is the difference between the measured and theoretical mass and is expressed in parts per million (Noziere et al. 2015) and was calculated using the following equation:

$$\text{Mass Error} = \left(\frac{m/z_{\text{experimental}} - m/z_{\text{theoretical}}}{m/z_{\text{theoretical}}}\right) \times 10^6 , \qquad (9.1)$$

where $m/z_{experimental}$ is the detected *m*/*z* value in the mass spectra and $m/z_{theoretical}$ is the value calculated from the molecular formula using the *Xcalibur* software.

9.4 Results and Discussion

Table 9.2–Table 9.7 show the retention times (RT), detected $[M-H]^-$ ions, mass error (calculated using Equation 9.1), molecular formula and possible identified compounds in the same representative samples for the marine rain and aerosol (R19/Q154, 14.04.16), Saharan rain and aerosol (R64/Q212, 04.11.16) and continental rain and aerosol (R50/Q218, 25.08.16), which correspond to the air mass back trajectories in Figure 7.1. The following discussion applies to these representative samples only.

It is noted at this stage that the compounds reported from LC-MS analysis in this sub-chapter, are suggestions but have not been confirmed. In order to make an unambiguous identification of organic compounds using LC-MS, in addition to matching literature values, an internal reference standard is required to definitively confirm and match the retention times of the chromatographic peaks in the rain and aerosol samples.

Many of the short chained (C_1–C_2) carboxylic acids identified in previous rainwater studies in Northern Spain (Peña et al. 2002, Durana et al. 1992) including acetic acid, formic acid, oxalic acid and propionic acid were not identified in the León samples. Formic acid (CH_2O_2, $[M-H]^-$ *m*/*z* 44.9982) and acetic acid ($C_2H_4O_2$, $[M-H]^-$ *m*/*z* 59.0139) were outside the *m*/*z* 60–550 scan range used to acquire the rain and aerosol spectra in this study so they were not detected.

A comparison between the 'No SPE' and 'Strata-X' sub-samples R47 and R50 from the second batch of test rainwater samples investigated in Chapter 4 revealed very small peaks with very low intensities ($\times10^3$–10^4) and less than 10% Relative Abundance (RA) in both 'No SPE' samples for *m*/*z* 88.9880 which is the $[M-H]^-$ *m*/*z* value for oxalic acid ($C_2H_2O_4$). This peak was not present in either of the sub-samples which had had SPE applied. This suggests that SPE could have removed oxalic acid from the sample. Losses of highly polar organic compounds with low molecular weights, including short chain (C_1–C_2) carboxylic acids, does sometimes occur during SPE because they are only weakly retained on the reversed phase substrate in the column (Mazzoleni et al. 2012b). However, the fact that the *m*/*z* 88.9880 peak was in the "No SPE" samples also suggests that oxalic acid could have been susceptible to competitive ionisation which was also observed in the complex organic mixtures ionised with the EESI source studied in Chapter 3 of this thesis. Highly polar compounds have been observed to be more susceptible to ion suppression from MS matrix effects (Taylor 2005).

Similarly, there was a very small peak ($\times 10^3$) with less than 10% RA at *m*/*z* 73.0294 in both the R47 and R50 "No SPE" samples which could correspond to propionic acid ($C_3H_6O_2$). These peaks were also present in the mass spectra but the intensities were so low ($\times 10^1$–10^2) that they were indistinguishable from the noise in the spectra and had shifted retention times so were not used for compound identification.

Lactic and citric acid were tentatively identified in the León marine rainwater and aerosol. Other C_3–C_9 monocarboxylic acids and C_3–C_{10} dicarboxylic acids including aromatic diacids (phthalic acid and methylphthalic acid) were identified which were reported in previous rainwater studies from the USA (Kawamura et al. 1996, Avery et al. 2006, Willey et al. 2000). The continental rainwater contains the highest number of carboxylic acids and the marine rainwater contains the lowest. Previous studies comparing marine and continental influences on rainwater have shown that both biogenic and anthropogenic emissions are important sources of organic acids. Organic acid precursors emitted from biogenic emissions are an important source of carboxylic acids. Previous studies have observed higher concentrations of organic acids during the "growing season" (April-September) compared with the non-growing season (Avery et al. 2006, Avery Jr et al. 2001). Anthropogenic emissions; fuel combustion in particular, are also an important source of organic acids (Peña et al. 2002). The continental rainwater has significantly more biogenic and anthropogenic influence than the marine rain which is the likely explanation for more different carboxylic acids being detected relative to the marine rainwater.

In contrast, the marine aerosol contained more carboxylic acids than the Saharan and continental aerosol. As indicated by previous analysis of the direct infusion ESI-MS data, the marine and Saharan aerosol samples overall contained more compounds than their rainwater counterparts and this is evident in the LC-MS analysis of the representative marine and Saharan aerosol samples (Q154 and Q212 respectively). The opposite is true for the continental samples and the significant number of carboxylic acids in the continental rainwater reiterate the idea of preferential scavenging of the carboxylic acids from the continental air mass.

Previous studies of rainwater in Northern Spain (Peña et al. 2002) and in the US (Kawamura et al. 1996, Sakugawa, Kaplan and Shepard 1993) have observed aldehydes produced from photo-oxidation of biogenic and anthropogenic emitted hydrocarbons. Since the air mass trajectories and previous analysis has shown that the León rainwater and aerosol samples have been influenced by biogenic emissions, biomass burning and

industrial emissions from Africa, it is likely that these samples do contain aldehydes. However, no aldehydes were detected with LC-MS but this is likely a result of the lack of a hydroxyl group for deprotonation in (−)ESI-MS and is not a reflection on the aldehyde distribution in the samples.

Most of the compounds listed for each rainwater and aerosol sample are SOA products from the oxidation of biogenic monoterpenes; mainly *α*-pinene, *β*-pinene, Δ_3-carene and *d*-limonene. These products were reported elsewhere in forest aerosol (Kourtchev et al. 2013, Yasmeen et al. 2011) and include terpynilic acid, 3-methyl-1,2,3-butanetricarboxylic acid (MBTCA), deterpenylic acid acetate, terebic acid, 2-hydroxyterpenylic acid, norpionic acid, *cis*-norpionic acid and 1-hydroxy-3-(hydroxymethyl)-2,2-dimethylcyclobutane-carboxylic acid (HHDCA). The LC-MS analysis separated *α*-pinene/*β*-pinene SOA oxidation product *cis*-pinonic acid from Δ_3-carene SOA oxidation product caronic acid; two isomers with the formula $C_{10}H_{16}O_3$ and *m*/*z* 183.1025 ± 0.0000. The *d*-limonene oxidation products limonic acid and ketolimononic acid, formed in the presence of NO_x (Jaoui et al. 2006) were also separated from the *α*-pinene/*β*-pinene/Δ_3-carene SOA oxidation products; homoterpenylic acid, *cis*-pinic acid and *cis*-caric acid. These five compounds had the molecular formula $C_9H_{14}O_4$ and *m*/*z* 185.0817 ± 0.0002. Isomers azelaic acid and 2-hydroxyterpenylic acid with the formulae $C_9H_{16}O_4$ and *m*/*z* 187.0975 ± 0.0002 were also separated. 3,3-dimethyl-2-(3-oxobutyl)cyclobutanecarboxylic acid (DCCA); an oxidation product of the sesquiterpene β-caryophyllene (Li et al. 2011) was also identified.

Compounds associated with biomass burning are identifiable in the samples, particularly in the continental rainwater. Levoglucosan; a pyrolysis product of cellulose and a well-known marker for biomass burning (Simoneit et al. 1999), was identified in the continental rainwater (*m*/*z* 161.0452). Peaks at *m*/*z* 161.0355, 161.0356 and 161.0353 were detected in the marine, Saharan and continental aerosol respectively which could have been levoglucosan but their mass error was > 4.0 ppm so they were not included for formulae identification. A methyl nitro-catechol compound with the molecular formula $C_7H_7NO_4$; another biomass burning marker which often closely correlates with levoglucosan, was also tentatively identified at *m*/*z* 168.0305 and 168.0299 in the Saharan and continental rainwater respectively and at *m*/*z* 168.0301, 168.0302 and 168.0299 for marine, Saharan and continental aerosol respectively. These correspond to the methyl-nitrocatechol isomers 4-methyl-5-nitrocatechol, 3-methyl-5-

nitrocatechol and 3-methyl-6-nitrocatechol. These methyl-nitrocatechols form via the photo-oxidation, in the presence of NO_x, of *m*-cresol; a methylphenol emitted during biomass burning from the degradation of lignin compound (Iinuma et al. 2010, Claeys et al. 2012). Pyruvic acid, malonic acid and succinic acid were observed in the continental rainwater. These are formed as direct oxidation products and also oligomeric SOA products from photooxidation of methylglyoxal via the hydroxyl radical which occurs when the methylglyoxal has been incorporated into a cloud droplet or aqueous aerosol, irreversibly. Modelling studies have previously suggested that irreversible uptake of methylglyoxal by cloud droplets and aqueous aerosol can contribute more to global SOA production than the reversible partitioning mechanism (Fu et al. 2008). Methylglyoxal is formed via the photooxidation of toluene, *m*-xylene and *p*-xylene by the OH radical in the presence of NO_x and also from biomass burning. Its oligomeric species have also been observed in wildfire-influenced cloud water due to it being highly soluble (Cook et al. 2017, Fu et al. 2008). The presence of these compounds in the León rainwater samples suggests aqueous phase reactive uptake of methylglyoxal could be a significant source of SOA over the forested regions of Spain.

A few amino acids were identified in the rainwater and marine aerosol including aspartic acid (*m*/*z* 132.0302), glutamic acid (*m*/*z* 146.0457) and tyrosine (*m*/*z* 180.0663) which have previously been observed in rainwater in Australia (Mace et al. 2003) and in forest aerosol (Samy, Robinson and Hays 2011). Amino acids are an important contributor to organic nitrogen in rain and aerosol, particularly in marine environments where organic nitrogen accounts for approximately 60% of the total nitrogen in rainwater due to an absence of nitrate and ammonium sources (Cornell et al. 2001).

Most of the organosulphates identified were *α*-pinene SOA oxidation products, also reported in boreal forest aerosol (Kourtchev et al. 2013). These included $C_{10}H_{18}O_5S$ isomers 2,6,6-trimethylbicycloheptane-2,3-diol OS and an unknown OS (*m*/*z* 249.07975 ± 0.0002); and $C_{10}H_{16}O_7S$ isomers 2.3-dihydroxy-2-(hydroxymethyl)-7,7-dimethylbicycloheptan-6-one (DHHMDMCP) OS and 3-(2-hydroxy-3-oxobutyl)-2,2-dimethylsuccinaldehyde (HODSA) OS (*m*/*z* 279.0540 ± 0.0002). Pinanoaldehyde OS; another *α*-pinene SOA organosulphates was identified.

The organosulphate molecular formulae listed in Table 9.2–Table 9.7 with no possible compounds attributed, potentially correspond to SOA products from ozonolysis of *d*-limonene. These compounds were observed in the laboratory from the evaporation and re-dissolution of aqueous d-limonene SOA in the presence of ammonium sulphate

(Nguyen et al. 2012). They were also observed in wildfire and urban-influenced cloud water samples collected in the USA which were characterised by high sulphate cloud water concentrations and were not seen in the biogenic samples analysed in that study (Cook et al. 2017). These compounds were tentatively identified in all of the representative rain and aerosol León samples but a higher number of them were observed in the Saharan and continental rain compared with the marine rain. The higher sulphate concentrations observed in the Saharan and continental samples relative to the marine samples provides an explanation for the increased occurrence of these organosulphates in the Saharan and continental samples. The presence of these compounds in the rainwater more so than the aerosol also suggests that these organosulphates are readily scavenged and are relatively stable towards hydrolysis.

Two nitroxy-organosulphates; pinanediol mononitrate isomers, with the formula $C_{10}H_{17}O_7NS$ (*m*/*z* 294.0651 ± 0.0003) were also identified in most of the representative samples, including the marine-influenced aerosol. These molecular weight 295 compounds have been reported to exist as five isomers; three positional isomers, of which two isomers have enantiomeric forms. They are formed via the photooxidation of α-pinene in the presence of NO_x and have been observed in forest aerosol (Gómez-González et al. 2012, Kourtchev et al. 2013, Maenhaut et al. 2017, Gómez-González et al. 2008). A previous study of forest aerosol (Gómez-González et al. 2008) observed a peak in the concentration of the 295 pinanediol mononitrate compounds during the night-time and suggested this may be due to dark ozonolysis, formation via night-time chemistry or enhanced gas-to-particle partitioning during the cooler night-time temperatures.

Organosulphates and nitrooxy-organosulphates have both biogenic and anthropogenic origins since they require sulphuric acid which is formed via oxidation of SO_2 which is produced by fuel combustion and industrial emissions. The fact that the marine samples contain numerous biogenic SOA compounds and also organosulphates and nitroxy organosulphates shows that even the relatively clean marine air is strongly influenced by the passing of the marine air masses over the forested regions and the coal-fuelled power plants of Northern Spain, even though this accounts for a small fraction of the back trajectory.

Some previous studies have expressed concerns over using SPE to remove salt from organic aerosol prior to MS analysis because it may remove organosulphates which will therefore not be detected by the MS (Surratt et al. 2008, Gao et al. 2006). The results of

the LC-ESI-MS analysis in this study show that some sulphate esters from α-pinene oxidation were detected and this indicates that SPE is a suitable method for preparing ambient precipitation samples. The use of SPE for treating these samples also ensured that any excess inorganic sulphate was removed from the samples which means we can be certain that the sulphate esters detected in the LC-MS were present in the samples and did not occur as a result of inorganic clusters in the MS (Surratt et al. 2007).

Table 9.2. Tentatively identified organic compounds in marine-influenced rainwater sample R19, collected on 14.04.16, using LC-(–)ESI-UHRMS. (*HHDCA*= 1-hydroxy-3-(hydroxymethyl)-2,2-dimethylcyclobutane-carboxylic acid. *DCCA*= 3,3-dimethyl-2-(3-oxobutyl)cyclobutanecarboxylic acid).

Retention Time (min)	Detected $[M-H]^-$ *m/z*	Mass Drift (ppm)	Molecular Formula	Possible Compound
CHO Compounds				
5.09	89.0244	0	$C_3H_6O_3$	lactic acid
5.23	87.0088	0	$C_3H_4O_3$	pyruvic acid
24.60	171.0662	0.6	$C_8H_{12}O_4$	terpynilic acid
32.89	185.0817	1.1	$C_9H_{14}O_4$	limonic acid
33.40	165.0192	0.6	$C_8H_6O_4$	phthalic acid
34.60	183.1025	1.1	$C_{10}H_{16}O_3$	cis-pinic acid
35.22	171.1026	0.6	$C_9H_{16}O_3$	HHDCA
35.88	157.0869	0.6	$C_8H_{14}O_3$	terebic acid
36.52	191.0200	1.6	$C_6H_8O_7$	citric acid
38.61	187.0976	1.6	$C_9H_{16}O_4$	azelaic acid
38.50	171.1025	1.2	$C_9H_{16}O_3$	cis-norpinic acid
38.50	187.0973	1.6	$C_9H_{16}O_4$	2-hydroxyterpenylic acid
41.64	201.1129	1.5	$C_{10}H_{18}O_4$	sebacic acid
43.74	185.0818	0.5	$C_9H_{14}O_4$	ketolimononic acid
44.22	197.1182	0.5	$C_{11}H_{18}O_3$	DCCA
43.49	169.0869	0.6	$C_9H_{14}O_3$	norpinonic acid
46.09	143.1076	1.4	$C_8H_{16}O_2$	octanoic acid
CHON, CHOS and CHONS Compounds				
3.73	132.0302	0	$C_4H_7NO_4$	aspartic acid
13.61	469.1028	1.5	$C_{18}H_{30}O_{12}S$	
45.62	223.0281	0.4	$C_7H_{12}O_6S$	
47.49	265.1476	1.1	$C_{12}H_{26}O_4S$	pinanoaldehyde OS

Table 9.3. Tentatively identified organic compounds in Saharan-influenced rainwater sample R64, collected on 04.11.16, using LC-(–)ESI-UHRMS. (*HHDCA*= 1-hydroxy-3-(hydroxymethyl)-2,2-dimethylcyclobutane-carboxylic acid. *DCCA* = 3,3-dimethyl-2-(3-oxobutyl)cyclobutanecarboxylic acid). *DHHMDMCP OS* = 2,3-dihydroxy-2-(hydroxymethyl)-7,7-dimethylbicycloheptan-6-one organosulphate. *HODSA OS* = 3-(2-hydroxy-3-oxobutyl)-2,2-dimethylsuccininaldehyde organosulphate).

Retention Time (min)	Detected $[M-H]^-$ *m/z*	Mass Drift (ppm)	Molecular Formula	Possible Compound
		CHO Compounds		
18.65	131.0351	0.8	$C_5H_6O_4$	methylmaleic acid
23.14	185.0819	0	$C_9H_{14}O_4$	homoterpenylic acid
24.14	145.0506	0	$C_6H_{10}O_4$	2-methylglutaric acid
24.48	171.0664	0.6	$C_8H_{12}O_4$	terpynilic acid
27.32	185.0821	1.1	$C_9H_{14}O_4$	ketolimononic acid
28.46	165.094	0.6	$C_8H_6O_4$	pthalic acid
29.29	215.0925	0.2	$C_{10}H_{16}O_5$	unknown
29.44	159.0664	0.6	$C_7H_{12}O_4$	pimelic acid
33.53	179.0352	1.1	$C_9H_8O_4$	4-methylphthalic acid
33.84	157.0873	1.5	$C_8H_{14}O_3$	terebic acid
34.64	171.1029	1.1	$C_9H_{16}O_3$	HHDCA
37.62	187.0978	1.1	$C_9H_{16}O_4$	azelaic acid
37.76	187.0978	1.2	$C_9H_{16}O_4$	2-hydroxyterpenylic acid
39.80	197.1186	1.5	$C_{11}H_{18}O_3$	DCCA
40.70	201.1135	1.5	$C_{10}H_{18}O_4$	sebacic acid
42.68	169.0873	1.7	$C_9H_{14}O_3$	norpinonic acid

Table 9.3 continued.

CHON, CHOS and CHONS Compounds				
3.96	146.0457	1.4	$C_5H_9NO_4$	glutamic acid
19.65	279.0541	0.9	$C_{10}H_{16}O_7S$	DHHMDMCP OS
20.14	279.0542	0.7	$C_{10}H_{16}O_7S$	HODSA OS
24.14	235.0281	0.6	$C_8H_{12}O_6S$	
30.93	299.0448	1.9	$C_9H_{16}O_9S$	
35.84	168.0305	1.7	$C_7H_7NO_4$	(4-methyl-5- / 3-methyl-5- / 3-methyl-6-) nitrocatechol
36.89	249.0802	0.0	$C_{10}H_{18}O_5S$	2,6,6-trimethylbicycloheptane-2,3-diol OS
48.15	265.1482	1.1	$C_{12}H_{26}O_4S$	pinanoaldehyde OS
40.55	294.0657	1.3	$C_{10}H_{17}O_7NS$	pinanediol mononitrate (295)
44.66	294.0657	1.5	$C_{10}H_{17}O_7NS$	pinanediol mononitrate (295)
44.79	223.0286	2.1	$C_7H_{12}O_6S$	
46.19	497.1373	7.7	$C_{19}H_{30}O_{13}S$	
50.01	483.1550	1.7	$C_{19}H_{32}O_{12}S$	
58.79	513.1276	1.5	$C_{19}H_{30}O_{14}S$	

Table 9.4. Tentatively identified organic compounds in continental-influenced rainwater sample R50, collected on 25.08.16, using LC-(–)ESI-UHRMS. (*MBTCA* = 3-methyl-1,2,3-butanetricarboxylic acid. *HHDCA* = 1-hydroxy-3-(hydroxymethyl)-2,2-dimethylcyclobutane-carboxylic acid. *DCCA* = 3,3-dimethyl-2-(3-oxobutyl)cyclobutanecarboxylic acid).

Retention Time (min)	Detected $[M-H]^-$ *m/z*	Mass Drift (ppm)	Molecular Formula	Possible Compound
		CHO Compounds		
14.05	117.0192	1.1	$C_4H_6O_4$	methylmalonic acid
14.52	103.0036	0.4	$C_3H_4O_4$	malonic acid
15.19	161.0452	2.5	$C_6H_{10}O_5$	levoglucosan
18.39	117.0191	2.0	$C_4H_6O_4$	succinic acid
18.68	131.0347	1.8	$C_5H_8O_4$	methylsuccinic acid
18.68	131.0347	1.8	$C_5H_8O_4$	glutaric acid
19.84	187.0608	2.4	$C_8H_{12}O_5$	unknown terpenoic acid
20.24	159.0659	2.5	$C_7H_{12}O_4$	pimelic acid
22.05	129.0191	1.6	$C_5H_6O_4$	methylmaleic acid
22.18	87.0087	1.1	$C_3H_4O_3$	pyruvic acid
23.08	185.0816	2.0	$C_9H_{14}O_4$	homoterpenylic acid
24.13	145.0503	2.2	$C_6H_{10}O_4$	adipic acid
24.39	171.0658	2.7	$C_8H_{12}O_4$	terpynilic acid
25.91	203.0556	2.5	$C_8H_{12}O_6$	MBTCA
27.20	185.0814	2.6	$C_9H_{14}O_4$	*cis*-pinic acid
27.65	145.0503	2.4	$C_6H_{10}O_4$	2-methylglutaric acid
28.45	165.0190	2.1	$C_8H_6O_4$	phthalic acid
30.91	231.0869	2.3	$C_{10}H_{16}O_6$	deterpenylic acid acetate
30.27	215.0920	2.2	$C_{10}H_{16}O_5$	unknown
33.46	179.0346	2.2	$C_9H_8O_4$	4-methylphthalic acid
34.08	185.0815	2.3	$C_9H_{14}O_4$	ketolimononic acid
36.28	185.0815	2.3	$C_9H_{14}O_4$	limonic acid
37.46	187.0972	2.3	$C_9H_{16}O_4$	azelaic acid
37.58	171.1024	1.8	$C_9H_{16}O_3$	HHDCA
40.54	201.1128	2.2	$C_{10}H_{18}O_4$	sebacic acid
43.05	197.1181	1.3	$C_{11}H_{18}O_3$	DCCA
30.78	169.0867	1.7	$C_9H_{14}O_3$	norpinonic acid

Table 9.4 continued.

CHON, CHOS and CHONS Compounds				
18.39	253.0381	2.5	$C_8H_{14}O_7S$	
18.83	223.0276	2.6	$C_7H_{12}O_6S$	
19.72	279.0538	2.3	$C_{10}H_{16}O_7S$	DHHMDMCP OS
20.38	279.0537	2.4	$C_{10}H_{16}O_7S$	HODSA OS
23.59	249.0431	2.8	$C_9H_{14}O_6S$	
23.72	263.0599	1.6	$C_{10}H_{16}O_6S$	
25.91	267.0538	2.2	$C_9H_{16}O_7S$	
25.27	265.0382	6.0	$C_9H_{14}O_7S$	
28.07	225.0433	2.5	$C_7H_{14}O_6S$	
28.97	297.0643	2.2	$C_{10}H_{18}O_8S$	
30.41	251.0589	2.4	$C_9H_{16}O_6S$	
30.54	168.0299	1.8	$C_7H_7NO_4$	(4-methyl-5- / 3-methyl-5- / 3-methyl-6-) nitrocatechol
31.17	329.0546	0.5	$C_{10}H_{18}O_{10}S$	
31.55	267.0184	1.3	$C_8H_{12}O_8S$	
34.48	281.0693	2.6	$C_{10}H_{18}O_7S$	
42.94	249.0796	2.3	$C_{10}H_{18}O_5S$	2,6,6-trimethylbicycloheptane-2,3-diol OS
43.18	294.0647	2.0	$C_{10}H_{17}O_7NS$	pinanediol mononitrate (295)
44.21	249.0797	2.3	$C_{10}H_{18}O_5S$	unknown OS
45.35	265.1474	2.0	$C_{12}H_{26}O_4S$	pinanoaldehyde OS
47.93	294.0649	1.5	$C_{10}H_{17}O_7NS$	pinanediol mononitrate (295)

Table 9.5. Tentatively identified organic compounds in marine-influenced aerosol sample Q154, collected on 14.04.16, using LC-(–)ESI-UHRMS. (*HHDCA*= 1-hydroxy-3-(hydroxymethyl)-2,2-dimethylcyclobutane-carboxylic acid. *DCCA* =3,3-dimethyl-2-(3-oxobutyl)cyclobutanecarboxylic acid).

Retention Time (min)	Detected $[M-H]^-$ *m/z*	Mass Drift (ppm)	Molecular Formula	Possible Compound
		CHO Compounds		
7.40	89.0244	0	$C_3H_6O_3$	lactic acid
13.15	117.0193	0.5	$C_4H_6O_4$	methylmalonic acid
16.80	129.0193	0	$C_5H_6O_4$	methylmaleic acid
17.85	131.0350	0.2	$C_5H_8O_4$	glutaric acid
23.98	143.0348	1.0	$C_6H_8O_4$	dimethylmaleic acid
27.16	185.0818	0.8	$C_9H_{14}O_4$	*cis*-caric acid
28.51	179.0348	1.1	$C_9H_8O_4$	4-methylphthalic acid
28.51	185.0817	0.9	$C_9H_{14}O_4$	*cis*-pinic acid
32.15	145.0506	0.4	$C_6H_{10}O_4$	adipic acid
34.10	157.0868	1.1	$C_8H_{14}O_3$	terebic acid
34.21	183.1025	1.0	$C_{10}H_{16}O_3$	caronic acid
34.57	165.0192	1.0	$C_8H_6O_4$	phthalic acid
35.20	145.0505	1.0	$C_6H_{10}O_4$	2-methylglutaric
36.05	171.0662	0.7	$C_8H_{12}O_4$	terpynilic acid
37.97	187.0973	1.4	$C_9H_{16}O_4$	azelaic acid
38.08	171.1025	1.2	$C_9H_{16}O_3$	HHDCA
41.19	201.1130	1.2	$C_{10}H_{18}O_4$	sebacic acid
43.20	169.0869	0.9	$C_9H_{14}O_3$	norpinonic acid
43.79	197.1181	1.0	$C_{11}H_{18}O_3$	DCCA
44.11	129.0921	0.3	$C_7H_{14}O_2$	heptanoic acid
45.73	143.1076	0.9	$C_8H_{16}O_2$	octanoic acid
48.23	157.1232	1.2	$C_9H_{18}O_2$	nonanoic acid

Table 9.5 Continued.

CHON, CHOS and CHONS Compounds				
12.92	267.0541	1.3	$C_9H_{16}O_7S$	
24.97	251.0591	1.7	$C_9H_{16}O_6S$	
29.68	267.0177	1.3	$C_8H_{12}O_8S$	
30.69	294.0649	1.3	$C_{10}H_{17}O_7NS$	pinanediol mononitrate (295)
38.54	168.0301	0.9	$C_7H_7NO_4$	(4-methyl-5- / 3-methyl-5- / 3-methyl-6-) nitrocatechol
41.07	295.0489	1.5	$C_{10}H_{16}O_8S$	
43.20	265.1476	1.2	$C_{12}H_{26}O_4S$	pinanoaldehyde OS
43.89	249.0798	1.6	$C_{10}H_{18}O_5S$	2,6,6-trimethylbicycloheptane-2,3-diol OS
45.05	180.0665	0.9	$C_9H_{11}NO_3$	tyrosine
45.16	294.0650	1.0	$C_{10}H_{17}O_7NS$	pinanediol mononitrate (295)
45.28	223.0281	0.4	$C_7H_{12}O_6S$	

Table 9.6. Tentatively identified organic compounds in Saharan-influenced aerosol sample Q212, collected on 04.11.16, using LC-(–)ESI-UHRMS. (*DCCA* = 3,3-dimethyl-2-(3-oxobutyl)cyclobutanecarboxylic acid).

Retention Time (min)	Detected $[M-H]^-$ *m/z*	Mass Drift (ppm)	Molecular Formula	Possible Compound
CHO Compounds				
23.82	143.0349	0.8	$C_6H_8O_4$	dimethylmaleic acid
27.83	165.0193	0.2	$C_8H_6O_4$	phthalic acid
28.65	159.0661	0.9	$C_7H_{12}O_4$	pimelic acid
28.78	121.0295	0.3	$C_7H_6O_2$	benzoic acid
29.73	145.0506	0	$C_6H_{10}O_4$	2-methylglutaric acid
31.90	87.0088	0	$C_3H_4O_3$	pyruvic acid
33.33	157.0869	0.7	$C_8H_{14}O_3$	terebic acid
33.58	183.1026	0.2	$C_{10}H_{16}O_3$	*cis*-pinonic acid
34.12	171.0663	0	$C_8H_{12}O_4$	terpynilic acid
35.42	183.1025	1.0	$C_{10}H_{16}O_3$	caronic acid
37.15	187.0974	1.2	$C_9H_{16}O_4$	2-hydroxyterpenylic acid
37.26	171.1025	0.9	$C_9H_{16}O_3$	*cis*-norpinic acid
40.27	201.1131	0.9	$C_{10}H_{18}O_4$	sebacic acid
40.40	185.0819	0.2	$C_9H_{14}O_4$	ketolimononic acid
41.28	197.1183	0.3	$C_{11}H_{18}O_3$	DCCA
42.20	169.0869	0.5	$C_9H_{14}O_4$	norpionic acid
42.72	185.0818	0.6	$C_9H_{14}O_4$	limonic acid
44.91	143.1076	1.1	$C_8H_{16}O_2$	octanoic acid
47.37	157.1233	0.7	$C_9H_{18}O_2$	nonanoic acid
CHON, CHOS and CHONS Compounds				
29.86	168.0302	0.4	$C_7H_7NO_4$	(4-methyl-5- / 3-methyl-5- / 3-methyl-6-) nitrocatechol
43.82	294.0652	0.4	$C_{10}H_{17}O_7NS$	pinanediol mononitrate (295)
44.55	223.0283	0.5	$C_7H_{12}O_6S$	
49.10	294.0652	0.3	$C_{10}H_{17}O_7NS$	pinanediol mononitrate (295)

Table 9.7. Tentatively identified organic compounds in continental-influenced aerosol sample Q218, collected on 25.08.16, using LC-(–)ESI-UHRMS. (*DCCA* = 3,3-dimethyl-2-(3-oxobutyl)cyclobutanecarboxylic acid).

Retention Time (min)	Detected $[M-H]^-$ *m/z*	Mass Drift (ppm)	Molecular Formula	Possible Compound
CHO Compounds				
22.87	185.0815	3.3	$C_9H_{14}O_4$	*cis*-pinic acid
26.95	185.0815	3.4	$C_9H_{14}O_4$	*cis*-caric acid
32.38	185.0816	3.9	$C_9H_{14}O_4$	ketolimononic acid
33.65	183.1023	3.9	$C_{10}H_{16}O_3$	*cis*-pinonic acid
35.31	121.0293	7.6	$C_7H_6O_2$	benzoic acid
36.05	183.1023	3.8	$C_{10}H_{16}O_3$	caronic acid
37.11	187.0973	4.0	$C_9H_{16}O_4$	2-hydroxyterpenylic acid
39.34	197.1180	1.8	$C_{11}H_{18}O_3$	DCCA
40.21	201.1128	3.4	$C_{10}H_{18}O_4$	sebacic acid
28.24	185.0815	3.6	$C_9H_{14}O_4$	limonic acid
42.21	169.0868	1.5	$C_9H_{14}O_3$	norpinonic acid
42.49	185.0816	3.9	$C_9H_{14}O_4$	homoterpenylic acid
CHON, CHOS and CHONS Compounds				
30.16	168.0299	2.0	$C_7H_7NO_4$	(4-methyl-5- / 3-methyl-5- / 3-methyl-6-) nitrocatechol
32.24	249.0796	2.6	$C_{10}H_{18}O_5S$	2,6,6-trimethylbicycloheptane-2,3-diol OS
34.72	281.0694	2.3	$C_{10}H_{18}O_7S$	
42.21	265.1474	1.9	$C_{12}H_{26}O_4S$	pinanoaldehyde OS
42.26	294.0648	1.6	$C_{10}H_{17}O_7NS$	pinanediol mononitrate (295)
43.58	249.0796	2.4	$C_{10}H_{18}O_5S$	unknown OS
44.26	223.0279	1.3	$C_7H_{12}O_6S$	

9.5 Conclusions

The LC-(-)ESI-UHRMS analysis revealed a range of biogenic SOA oxidation products from the photooxidation of monoterpenes α-pinene, β-pinene, Δ_3-carene and *d*-limonene and sesquiterpene β-caryophyllene, in the representative rainwater and aerosol samples. The Saharan and continental-influenced rain and aerosol samples contained the most mono-carboxylic and dicarboxylic acids, as expected, due to the strong terrestrial

influence. However, the majority of the compounds identified in the marine rain and aerosol were of biogenic origin which shows that the last few hours of the air mass trajectory over the forested region of Northern Spain have had a major influence on the chemical composition of the samples.

Nitrogen-containing compounds including amino acids and the biomass burning markers levuglucosan and methyl nitrocatechol isomers were identified in the rain and aerosol samples. SOA products from the reactive uptake of methylglyoxal into cloud droplets and aqueous aerosol were also observed in the continental rainwater suggesting that a reactive uptake of methylglyoxal could be a significant source of SOA in the forested regions of Spain.

SOA organosulphates from α-pinene oxidation and *d*-limonene ozonolysis and two nitroxy-organosulphate isomers from α-pinene oxidation were tentatively identified in most of the samples. More species were observed in the Saharan and continental samples than in the marine samples due to the anthropogenic sources of SO_2 on the continent from industry and fuel combustion. However, the representative marine-influenced rain and aerosol samples were found to contain some of the same organosulphates that were observed in the Saharan and continental samples which indicates that the SO_2 emissions picked up from the marine trajectory are from the coal-fuelled power plants in north-west Spain.

The SPE method used prior to the MS analysis does not appear to have removed organosulphates which was a concern in other molecular composition studies. However, the SPE method appears to have removed some of the lower molecular weight organic acids that are usually present in rainwater. The LC-MS data could be used in further quantitative analysis to explore the temporal and seasonal variation or investigate the change in concentration of compounds during longer rain events. To do this requires the use of more reference standards and more lengthy analysis which was beyond the scope of this thesis.

10 CONCLUSIONS

10.1 Summary of Research Findings

Detailed conclusions for the results presented in this thesis are provided at the end of each respective results chapter (3–9). This conclusions chapter provides a brief summary of the results of the studies reported in this thesis, with regards to the original aims and objectives specified for each chapter.

10.1.1 Chemical Characterisation of EESI-MS

The aim of this work was to characterise a newly developed EESI source by testing its susceptibility to competitive ionisation and salt suppression effects; issues commonly associated with ESI techniques. This study was motivated by the need for development of soft ionisation techniques suitable for producing online measurements of the composition of organic compounds.

Three sets of characterisation experiments were conducted to test the susceptibility of the EESI source salt suppression effects and competitive ionisation when ionising organic compounds in complex aerosol with mixed organic and inorganic composition. In addition, the ability of EESI-MS to ionise and detect chamber-generated SOA products generated from the ozonolysis and OH radical-initiated oxidation of mixtures

of BVOCs and AVOCs, was tested. The application of this EESI source to complex mixtures of aerosol had not been tested prior to the experiments described in this chapter, making this a novel study.

10.1.1.1 Simple and complex organic and inorganic aerosol mixtures

There was no significant change in MS signal intensity for *cis*-pinonic acid in the simple aerosol mixtures with 0-91% inorganic molar percentage relative to organic, suggesting that EESI-MS is not significantly affected by salt suppression and outperforms ESI-MS on this issue. At inorganic molar percentages ≤ 70%, the six tested WSOCs in the complex organic aerosol mixtures also showed no significant change in organic signal intensity. However, at inorganic fractions > 80% and total aerosol concentrations > 200µg/m^3, the signal for some of the WSOCs increased significantly. SEM-EDX analysis was conducted but was unable to confirm if the increase in WSOC intensities was due to the organics forming an outer coating around a predominantly inorganic core. Since ambient aerosol rarely exceeds 80% inorganic content, it was concluded that EESI-MS is suitable for analysing a wide range of ambient aerosol and is not significantly affected by salt suppression.

Oxalic acid, arabitol and erythritol all showed reduced ionisation efficiencies compared with the other tested organics in the complex mixtures. This could suggest that EESI is just as susceptible to competitive ionisation as other ESI techniques but further experiments with calibration standards are required to confirm this. The experiments also highlighted that compound residues are an issue for EESI-MS and the source should be cleaned thoroughly between experiments in the future.

10.1.1.2 Chamber-generated SOA

The EESI-MS successfully detected oligomer products from complex BVOC and AVOC oxidation, which had previously been identified in previous chamber studies using simple BVOC mixtures. EESI-MS also demonstrated good sensitivity in detecting the change in ozone concentration and subsequent change in MS signal intensity.

10.1.2 Solid Phase Extraction Method Development

The main aim of Chapter 1.1 was to develop an SPE method that could be used to treat both rainwater and ambient aerosol samples from a campaign, to make the results following Nano-ESI-MS and LC-MS analysis comparable. Three different Reversed-Phase SPE sorbents were tested on test aerosol samples and Strata-X sorbent was found to produce the highest recovery of organic compounds in both the rainwater and aerosol following Nano-ESI-MS, including aliphatic and aromatic compounds. SPE application was essential for the rainwater samples in this study so it was important to understand if SPE would result in significant removal of certain compounds. The SPE method optimisation described in this chapter allowed a suitable sample preparation protocol to be developed for treating the ambient rainwater and aerosol samples and future studies of ambient sample composition could benefit from including such details to improve sample treatment methods required for MS analysis and to allow easier comparison of analytical methodologies in literature.

A novel study comparing the impact of three different blank subtraction approaches on the yield of formulae assignments in the UHRMS sample spectra was conducted as part of the subsequent data treatment. Combining and averaging three separate blank spectra replicates into a ‘master blank’ and subtracting that from each of the sample spectra was found to be a conservative yet manageable approach to blank subtraction and yielded a satisfactory number of formulae assignments in the sample spectra following data processing. It can be concluded from this analysis that using a single blank spectrum is insufficient for producing high quality sample spectra because this method relies too heavily on a high quality blank. The alternative method of using three different blank spectra and subtracting each of these from each sample spectrum was found to be a highly conservative approach but was immensely time consuming and is inappropriate for processing large numbers of sample spectra.

10.1.3 UHRMS analysis of rainwater and aerosol samples from the AERORAIN Campaign

The characterisation of the samples collected during the AERORAIN campaign, presented in Chapters 5–9 is the first study, to our knowledge, to use both direct infusion Nano-ESI-MS and LC-ESI-MS to produce a detailed molecular characterisation of rainwater and aerosol collected during the same rain event. The aims of the study were to identify any seasonal distributions of organic and aromatic compounds in the rainwater and aerosol, assess the influence of air mass origin on the sample composition and, assess the extent of below-cloud scavenging occurring during the different rain events and identify specific compounds in the rainwater and aerosol samples.

The results showed that the aerosol samples generally contained more mono-aromatic compounds whereas the rainwater contained more poly-aromatic compounds. Seasonality and air mass origin had strong influences on the sample composition. Using air mass backward trajectories generated by the HYSPLIT model, to aid source attribution, revealed that the summer and Sahara desert-influenced samples contained the most compounds due to increased photochemical activity and extra industrial emissions from Northern Africa respectively. All samples contained SV-OOA or "fresh" SOA and multiple organosulphates were tentatively identified. The continental rainwater samples contained LV-OOA or "aged" SOA including highly oxidized C_2–C_5 carboxylic acids; potential biogenic VOC oxidation products. Efficient aerosol scavenging was most prevalent in the continental samples and least prevalent in the marine samples with CHO and CHON compounds being preferentially scavenged over CHOS and CHONS compounds.

The combined direct infusion Nano-ESI-MS and LC-ESI-MS analysis of the rainwater and aerosol composition in Chapters 5–9 has provided a proof of concept that these techniques provide a good characterisation of the distribution of organic compounds in the rainwater and aerosol. These MS techniques, coupled with visualisation methods to interpret the complex MS data generated, allowed temporal and seasonal trends to be identified for the number and distribution of compounds. Air mass trajectory analysis allowed source regions to be identified and highlighted the impact of long range transport of emissions from the Saharan desert and industrial emissions from Northern Africa on the composition and ageing of the organic compounds in the samples.

10.2 Future Work and Recommendations

10.2.1 Further Characterisation of EESI in analysing aerosol of highly inorganic composition .

The EESI characterisation study revealed that some WSOC MS intensities increased in mixtures with increasing inorganic solute concentrations whereas others remained relatively constant. These unexpected results may have been partially due to the EESI source failing to fully extract the total particle mass at very high aerosol mass concentrations. It is important to fully understand the limitations of new ionisation techniques in order to further their development and increase their suitability for analysing ambient aerosol from a range of different environments.

An important recommendation from this EESI characterisation study is to conduct further investigation into the ionisation of organic compounds in complex samples with very high inorganic content and aerosol mass loadings, using EESI techniques and also other new soft ionisation tehniques.

10.2.2 Application of EESI to aqueous SOA formation and cloud processing.

The work in section 3.4.3 of this thesis has shown that EESI-MS is able to detect the composition of chamber-generated SOA. A potential application of real time EESI-MS is measuring aqueous pathways of SOA formation and cloud processing. Aerosol-cloud interactions are still rather poorly understood (Giorio et al. 2017b) which is partly due to the complexity and high temporal and spatial variability of clouds in the atmosphere. Therefore, laboratory simulations of clouds are very important in improving our understanding of these complex processes (Schütze and Stratmann 2008). Flow tubes have been developed to study cloud evolution such as the Leipzig Aerosol Interaction Simulator (LACIS) device (Stratmann et al. 2004) which is designed to reproduce realistic thermodynamic conditions of atmospheric clouds and allow the user to control them accurately.

Experiments to develop a small-scale ‘Cloud or Haze Flow Tube’ (CFT) which could be used in conjunction with EESI-MS to investigate aqueous cloud processing of SOA on

short timescales, have been conducted and are discussed in Appendix N. These experiments focussed on the droplet distribution in the CFT. However, they could be adapted to investigate timescales of the uptake of aerosol particles into liquid droplets since the two separate inlets on the CFT allow independent introduction of water droplets from an atomiser and aerosol from a chamber or another source and the different outlets along the top of the CFT allows an SMPS Spectrometer or an Optical Particle Counter (OPC) to measure the concentration and size distribution at different positions during the cloud lifetime. The experiments in Appendix N determined the theoretical cloud lifetime in the CFT to be 2.3 minutes which makes the system suitable for monitoring atmospheric cloud droplet lifetimes on the order of 10-15 minutes. Aqueous atmospheric reactions with short lifetimes such as hydrolysis of organic anhydrides, could be examined using EESI-MS coupled to the CFT which would allow the point at which the resulting organic acids are generated to be detected in real time. Figure 10.1 depicts another future set-up which could be used to investigate cloud processing of SOA generated in the CASC, using EESI-MS to analyse the composition of the evolving haze or cloud at different position during the cloud lifetime.

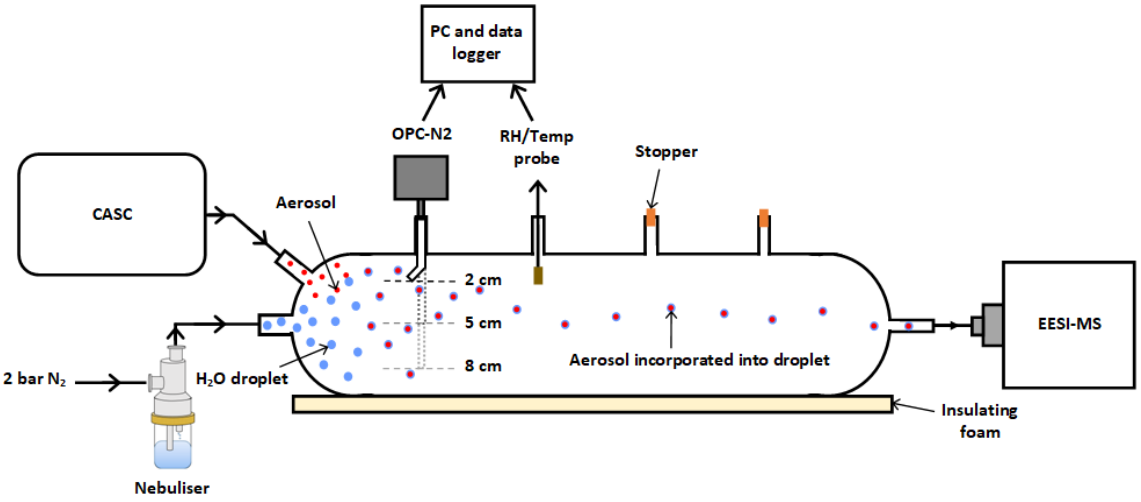

Figure 10.1. Experimental set-up used to generate a cloud. A constant output nebuliser generates a fine spray of water droplets (blue) into the Cloud Flow Tube (CFT) via a central inlet. Aerosol (red) can be introduced from the chamber or nebulised from another source via a second inlet and intercept the water droplets. An OPC monitors the size distribution and droplet concentration at different distances from the point of injection. Aerosol can be extracted from any of the outlets in the CFT and directed into the EESI-MS to measure aqueous phase reactions changing SOA composition.

10.2.3 Inclusion of systematic method development details

Meticulous, detailed sample preparation methodologies and effective quality control in both analytical and data processing methods were described in detail throughout this thesis. Descriptions of such methods are necessary to ensure that the most suitable protocols are applied to ambient samples and to provide consistency and standardisation in analytical methodologies between different research organisations. However, adequate descriptions of traceable, systematic protocols and methodology pathways are lacking in current literature.

The SPE method development for the rainwater and aerosol sample preparation and the comparison of different blank subtraction methods for processing sample mass spectra in Chapter 1.1 of this thesis are prime examples of such details which would be useful in aiding method development in future studies. Including optimisation details may also help prevent repetition of certain procedures such as using a single blank spectrum for blank subtraction of sample spectra when there is a more appropriate alternative method available. Similarly, the decision tree included in Chapter 6 for selecting appropriate metrics to visualise the aromaticity of the compounds in the rainwater and aerosol samples was a useful addition in the method development and similar visual aids could be included in future studies of complex environmental sample composition to provide transparency in protocol development.

10.2.4 Quantifying the concentration of compounds in the AERORAIN samples using LC-ESI-MS.

Several organic compounds including carboxylic acids and organosulphates were tentatively identified in the rainwater and aerosol samples in Chapter 9 using LC-ESI-MS. An important next step for this analysis is to quantify the concentrations of the compounds present in the samples to fully determine the impact of the different marine, desert dust and continental environments on the sample composition.

A current problem for quantifying concentrations of compounds using LC-MS is the lack of calibration standards available for many atmospheric compounds. This presented a limitation for the LC-MS analysis of the rainwater and aerosol samples in this thesis

and is why only ‘tentative’ assignments for compounds could be made based on their *m*/*z* values and comparisons in the literature. Thus, an important recommendation from this thesis is to continue developing calibration standards for atmospherically-relevant compounds.

10.3 Closing Remarks

There have been major advancements in using analytical tools such as UHRMS and LC-MS with soft ionisation techniques, coupled with very useful data visualisation tools, to interpret complex ambient aerosol composition. UHRMS has enormous potential to provide complete molecular characterisation of organic aerosol. However, for ambient aerosol characterisation, meteorology must always be considered. The study of rainwater and aerosol composition from the AERORAIN campaign in this thesis has shown that meteorology and seasonality both have very strong influences on the composition and ageing of aerosol and also aerosol scavenging. Therefore, in future studies of ambient aerosol, techniques to aid source attribution should be employed to help fully understand complex ambient aerosol formation and reactions in the atmosphere.

There are still many gaps in our knowledge of aerosol characterisation and there remains a need for development of new analytical techniques which can efficiently measure organic aerosol composition from a range of environments. However, future research can narrow these gaps considerably through clear reporting of systematic method development in literature, as shown in this thesis, to ensure consistency and transparency throughout the research community.

11 REFERENCES

Advion 2010. Advion TriVersa NanoMate Electrospray Ionizator Robot User Manual. United States of America.

Global Forest Watch Fires (2018).

Abdel-Shafy, H. I. & M. S. Mansour (2016) A review on polycyclic aromatic hydrocarbons: source, environmental impact, effect on human health and remediation. *Egyptian Journal of Petroleum,* 25**,** 107-123.

Advion. 2009. Advion TriVersa ™ User Training Manual.

Advion. 2017. TriVersa NanoMate® – Advion.

Ahmad, M. & H. Subawi (2013) New Van Krevelen diagram and its correlation with the heating value of biomass. *Res. J. Agric. Environ. Manage,* 2**,** 295-301.

Aiken, A. C., P. F. Decarlo, J. H. Kroll, D. R. Worsnop, J. A. Huffman, K. S. Docherty, I. M. Ulbrich, C. Mohr, J. R. Kimmel & D. Sueper (2008) O/C and OM/OC ratios of primary, secondary, and ambient organic aerosols with high-resolution time-of-flight aerosol mass spectrometry. *Environmental Science & Technology,* 42**,** 4478-4485.

Alphasense. 2015. Alphasense User Manual OPC-N2 Optical Particle Counter. Alphasense Ltd.

Altieri, K., M. Hastings, A. Peters & D. Sigman (2012) Molecular characterization of water soluble organic nitrogen in marine rainwater by ultra-high resolution electrospray ionization mass spectrometry. *Atmospheric Chemistry and Physics,* 12**,** 3557-3571.

Altieri, K., S. Seitzinger, A. Carlton, B. Turpin, G. Klein & A. Marshall (2008) Oligomers formed through in-cloud methylglyoxal reactions: Chemical composition, properties, and mechanisms investigated by ultra-high resolution FT-ICR mass spectrometry. *Atmospheric Environment,* 42**,** 1476-1490.

Altieri, K., B. Turpin & S. Seitzinger (2009) Oligomers, organosulfates, and nitrooxy organosulfates in rainwater identified by ultra-high resolution electrospray ionization FT-ICR mass spectrometry. *Atmospheric Chemistry and Physics,* 9**,** 2533-2542.

Andreae, M., R. Talbot, T. Andreae & R. Harriss (1988) Formic and acetic acid over the central Amazon region, Brazil: 1. Dry season. *Journal of Geophysical Research: Atmospheres,* 93**,** 1616-1624.

Andrews, E. & S. M. Larson (1993) Effect of surfactant layers on the size changes of aerosol particles as a function of relative humidity. *Environmental science & technology,* 27**,** 857-865.

Atkinson, R. (2000) Atmospheric chemistry of VOCs and NOx. *Atmospheric environment,* 34**,** 2063-2101.

Atkinson, R. & J. Arey (2003a) Atmospheric degradation of volatile organic compounds. *Chemical reviews,* 103**,** 4605-4638.

Atkinson, R & J. Arey (2003b) Gas-phase tropospheric chemistry of biogenic volatile organic compounds: a review. *Atmospheric Environment,* 37**,** 197-219.

Ault, A. P., T. M. Peters, E. J. Sawvel, G. S. Casuccio, R. D. Willis, G. A. Norris & V. H. Grassian (2012) Single-particle SEM-EDX analysis of iron-containing coarse particulate matter in an urban environment: sources and distribution of iron within Cleveland, Ohio. *Environmental science & technology,* 46**,** 4331-4339.

Avery, G. B., R. J. Kieber, M. Witt & J. D. Willey (2006) Rainwater monocarboxylic and dicarboxylic acid concentrations in southeastern North Carolina, USA, as a function of air-mass back-trajectory. *Atmospheric Environment,* 40**,** 1683-1693.

Avery Jr, G. B., Y. Tang, R. J. Kieber & J. D. Willey (2001) Impact of recent urbanization on formic and acetic acid concentrations in coastal North Carolina rainwater. *Atmospheric Environment,* 35**,** 3353-3359.

Avila, A., I. Queralt, F. Gallart & J. Martin-Vide. 1996. African dust over northeastern Spain: mineralogy and source regions. In *The impact of desert dust across the Mediterranean,* 201-205. Springer.

Balakrishnan, V. K., K. A. Terry & J. Toito (2006) Determination of sulfonamide antibiotics in wastewater: A comparison of solid phase microextraction and solid phase extraction methods. *Journal of Chromatography A,* 1131**,** 1-10.

Bandu, M. L., K. R. Watkins, M. L. Bretthauer, C. A. Moore & H. Desaire (2004) Prediction of MS/MS data. 1. A focus on pharmaceuticals containing carboxylic acids. *Analytical chemistry,* 76**,** 1746-1753.

Banerjee, S. & S. Mazumdar (2012) Electrospray ionization mass spectrometry: a technique to access the information beyond the molecular weight of the analyte. *International journal of analytical chemistry,* 2012.

Bateman, A. P., S. A. Nizkorodov, J. Laskin & A. Laskin (2009) Time-resolved molecular characterization of limonene/ozone aerosol using high-resolution electrospray ionization mass spectrometry. *Physical Chemistry Chemical Physics,* 11**,** 7931-7942.

Bateman, A. P., M. L. Walser, Y. Desyaterik, J. Laskin, A. Laskin & S. A. Nizkorodov (2008) The effect of solvent on the analysis of secondary organic aerosol using

electrospray ionization mass spectrometry. *Environmental science & technology,* 42**,** 7341-7346.

Bauer, H., M. Claeys, R. Vermeylen, E. Schueller, G. Weinke, A. Berger & H. Puxbaum (2008) Arabitol and mannitol as tracers for the quantification of airborne fungal spores. *Atmospheric Environment,* 42**,** 588-593.

Bird, R. B., W. E. Stewart & E. N. Lightfoot (1960) Transport phenomena. 1960. *Madison, USA.*

Blando, J. D. & B. J. Turpin (2000) Secondary organic aerosol formation in cloud and fog droplets: a literature evaluation of plausibility. *Atmospheric Environment,* 34**,** 1623-1632.

Boone, E. J., A. Laskin, J. Laskin, C. Wirth, P. B. Shepson, B. H. Stirm & K. A. Pratt (2015) Aqueous processing of atmospheric organic particles in cloud water collected via aircraft sampling. *Environmental science & technology,* 49**,** 8523-8530.

Brooks, S. D., R. M. Garland, M. E. Wise, A. J. Prenni, M. Cushing, E. Hewitt & M. A. Tolbert (2003) Phase changes in internally mixed maleic acid/ammonium sulfate aerosols. *Journal of Geophysical Research: Atmospheres,* 108.

Canagaratna, M., J. Jayne, J. Jimenez, J. Allan, M. Alfarra, Q. Zhang, T. Onasch, F. Drewnick, H. Coe & A. Middlebrook (2007) Chemical and microphysical characterization of ambient aerosols with the aerodyne aerosol mass spectrometer. *Mass spectrometry reviews,* 26**,** 185-222.

Caseiro, A., I. L. Marr, M. Claeys, A. Kasper-Giebl, H. Puxbaum & C. A. Pio (2007) Determination of saccharides in atmospheric aerosol using anion-exchange high-performance liquid chromatography and pulsed-amperometric detection. *Journal of Chromatography A,* 1171**,** 37-45.

Cech, N. B. & C. G. Enke (2000) Relating electrospray ionization response to nonpolar character of small peptides. *Analytical Chemistry,* 72**,** 2717-2723.

Cech, N. B. & C. G. Enke (2001) Practical implications of some recent studies in electrospray ionization fundamentals. *Mass spectrometry reviews,* 20**,** 362-387.

Chen, H., A. Venter & R. G. Cooks (2006) Extractive electrospray ionization for direct analysis of undiluted urine, milk and other complex mixtures without sample preparation. *Chemical Communications***,** 2042-2044.

Chen, H., A. Wortmann & R. Zenobi (2007a) Neutral desorption sampling coupled to extractive electrospray ionization mass spectrometry for rapid differentiation of biosamples by metabolomic fingerprinting. *Journal of Mass Spectrometry,* 42**,** 1123-1135.

Chen, H., A. Wortmann, W. Zhang & R. Zenobi (2007b) Rapid in vivo fingerprinting of nonvolatile compounds in breath by extractive electrospray ionization quadrupole time-of-flight mass spectrometry. *Angewandte Chemie,* 119**,** 586-589.

Chen, H., S. Yang, M. Li, B. Hu, J. Li & J. Wang (2010) Sensitive detection of native proteins using extractive electrospray ionization mass spectrometry. *Angewandte Chemie,* 122**,** 3117-3120.

Chen, H., S. Yang, A. Wortmann & R. Zenobi (2007c) Neutral desorption sampling of living objects for rapid analysis by extractive electrospray ionization mass spectrometry. *Angewandte Chemie International Edition,* 46**,** 7591-7594.

Chen, H. & R. Zenobi (2008) Neutral desorption sampling of biological surfaces for rapid chemical characterization by extractive electrospray ionization mass spectrometry. *Nature Protocols,* 3**,** 1467.

Chingin, K., G. Gamez, H. Chen, L. Zhu & R. Zenobi (2008) Rapid classification of perfumes by extractive electrospray ionization mass spectrometry (EESI-MS). *Rapid Communications in Mass Spectrometry: An International Journal Devoted to the Rapid Dissemination of Up-to-the-Minute Research in Mass Spectrometry,* 22**,** 2009-2014.

Claeys, M., B. Graham, G. Vas, W. Wang, R. Vermeylen, V. Pashynska, J. Cafmeyer, P. Guyon, M. O. Andreae & P. Artaxo (2004) Formation of secondary organic aerosols through photooxidation of isoprene. *Science,* 303**,** 1173-1176.

Claeys, M., Y. Iinuma, R. Szmigielski, J. D. Surratt, F. Blockhuys, C. Van Alsenoy, O. Böge, B. Sierau, Y. Gómez-González & R. Vermeylen (2009) Terpenylic acid and related compounds from the oxidation of α-pinene: Implications for new particle formation and growth above forests. *Environmental science & technology,* 43**,** 6976-6982.

Claeys, M., R. Vermeylen, F. Yasmeen, Y. Gómez-González, X. Chi, W. Maenhaut, T. Mészáros & I. Salma (2012) Chemical characterisation of humic-like substances from urban, rural and tropical biomass burning environments using liquid chromatography with UV/vis photodiode array detection and electrospray ionisation mass spectrometry. *Environmental Chemistry,* 9**,** 273-284.

Cocker, D. R., R. C. Flagan & J. H. Seinfeld (2001) State-of-the-art chamber facility for studying atmospheric aerosol chemistry. *Environmental science & technology,* 35**,** 2594-2601.

Colberg, C. A., U. K. Krieger & T. Peter (2004) Morphological investigations of single levitated H2SO4/NH3/H2O aerosol particles during deliquescence/efflorescence experiments. *The Journal of Physical Chemistry A,* 108**,** 2700-2709.

Cook, R. D., Y. H. Lin, Z. Peng, E. Boone, R. K. Chu, J. E. Dukett, M. J. Gunsch, W. Zhang, N. Tolic, A. Laskin & K. A. Pratt (2017) Biogenic, urban, and wildfire influences on the molecular composition of dissolved organic compounds in cloud water. *Atmos. Chem. Phys. Discuss.,* 2017**,** 1-25.

Cooporation, W. 2007. Atlantis T3 and Acquity UPLC HSS T3 Columns. USA: Waters Cooporation.

Cornell, S., K. Mace, S. Coeppicus, R. Duce, B. Huebert, T. Jickells & L. Z. Zhuang (2001) Organic nitrogen in Hawaiian rain and aerosol. *Journal of Geophysical Research: Atmospheres,* 106**,** 7973-7983.

D'Andrea, S., S. Häkkinen, D. Westervelt, C. Kuang, E. Levin, V. Kanawade, W. Leaitch, D. Spracklen, I. Riipinen & J. Pierce (2013) Understanding global secondary organic aerosol amount and size-resolved condensational behavior. *Atmospheric Chemistry and Physics,* 13**,** 11519-11534.

Dalton, C. N., M. Jaoui, R. M. Kamens & G. L. Glish (2005) Continuous real-time analysis of products from the reaction of some monoterpenes with ozone using

atmospheric sampling glow discharge ionization coupled to a quadrupole ion trap mass spectrometer. *Analytical chemistry,* 77**,** 3156-3163.

Dass, C. (2007) Basics of Mass Spectrometry. *Fundamentals of Contemporary Mass Spectrometry***,** 1-14.

de Hoffmann, E. & V. Stroobant. 2002. *Mass Spectrometry: Principles and Applications*. Chichester, West Sussex PO19 IUD, England: John Wiley and Sons, Inc.

de la Mora, J. F., L. de Juan, T. Eichler & J. Rosell (1998) Differential mobility analysis of molecular ions and nanometer particles. *TrAC Trends in Analytical Chemistry,* 17**,** 328-339.

DeCarlo, P. F., J. R. Kimmel, A. Trimborn, M. J. Northway, J. T. Jayne, A. C. Aiken, M. Gonin, K. Fuhrer, T. Horvath & K. S. Docherty (2006) Field-deployable, high-resolution, time-of-flight aerosol mass spectrometer. *Analytical chemistry,* 78**,** 8281-8289.

Denisov, E., E. Damoc, O. Lange & A. Makarov (2012) Orbitrap mass spectrometry with resolving powers above 1,000,000. *International Journal of Mass Spectrometry,* 325**,** 80-85.

Di Lorenzo, R. A., R. A. Washenfelder, A. R. Attwood, H. Guo, L. Xu, N. L. Ng, R. J. Weber, K. Baumann, E. Edgerton & C. J. Young (2017) Molecular-size-separated brown carbon absorption for biomass-burning aerosol at multiple field sites. *Environmental science & technology,* 51**,** 3128-3137.

Docherty, K. S. & P. J. Ziemann (2003) Effects of stabilized criegee intermediate and OH radical scavengers on aerosol formation from reactions of β-pinene with O 3. *Aerosol Science & Technology,* 37**,** 877-891.

Doezema, L. A., T. Longin, W. Cody, V. Perraud, M. L. Dawson, M. J. Ezell, J. Greaves, K. R. Johnson & B. J. Finlayson-Pitts (2012) Analysis of secondary organic aerosols in air using extractive electrospray ionization mass spectrometry (EESI-MS). *Rsc Advances,* 2**,** 2930-2938.

Drewnick, F., S. S. Hings, P. DeCarlo, J. T. Jayne, M. Gonin, K. Fuhrer, S. Weimer, J. L. Jimenez, K. L. Demerjian & S. Borrmann (2005) A new time-of-flight aerosol mass spectrometer (TOF-AMS)—Instrument description and first field deployment. *Aerosol Science and Technology,* 39**,** 637-658.

Durana, N., H. Casado, C. Garcia, A. Ezcurra, J. Lacaux & D. Encinas (1992) Organic acids in precipitation in the Basque Country (North of Spain). *Atmospheric research,* 28**,** 93-101.

Dzepina, K., C. Mazzoleni, P. Fialho, S. China, B. Zhang, R. C. Owen, D. Helmig, J. Hueber, S. Kumar, J. A. Perlinger, L. J. Kramer, M. P. Dziobak, M. T. Ampadu, S. Olsen, L. R. Mazzoleni (2015) Molecular characterization of free tropospheric aerosol collected at the Pico Mountain Observatory: a case study with a long-range transported biomass burning plume. *Atmospheric Chemistry and Physics,* 15**,** 5047-5068.

Editor, M. B. (2019) What Is the F-test of Overall Significance in Regression Analysis? https://blog.minitab.com/blog/adventures-in-statistics-2/what-is-the-f-test-of-overall-significance-in-regression-analysis (last accessed 18.10.19).

Ehn, M., J. A. Thornton, E. Kleist, M. Sipilä, H. Junninen, I. Pullinen, M. Springer, F. Rubach, R. Tillmann & B. Lee (2014) A large source of low-volatility secondary organic aerosol. *Nature,* 506**,** 476.

Eikel, D., M. Vavrek, S. Smith, C. Bason, S. Yeh, W. A. Korfmacher & J. D. Henion (2011) Liquid extraction surface analysis mass spectrometry (LESA-MS) as a novel profiling tool for drug distribution and metabolism analysis: the terfenadine example. *Rapid Communications in Mass Spectrometry,* 25**,** 3587-3596.

Endo, S., A. Pfennigsdorff & K.-U. Goss (2012) Salting-out effect in aqueous NaCl solutions: trends with size and polarity of solute molecules. *Environmental science & technology,* 46**,** 1496-1503.

Facchini, M. C., S. Decesari, M. Rinaldi, C. Carbone, E. Finessi, M. Mircea, S. Fuzzi, F. Moretti, E. Tagliavini & D. Ceburnis (2008) Important source of marine secondary organic aerosol from biogenic amines. *Environmental science & technology,* 42**,** 9116-9121.

Faria, P., J. Órfão & M. Pereira (2008) Activated carbon catalytic ozonation of oxamic and oxalic acids. *Applied Catalysis B: Environmental,* 79**,** 237-243.

Fox, M. A. & J. K. Whitesell. 1997. *Core Organic Chemistry*. Jones and Bartlett.

Fu, I., E. Woolf & B. Matuszewski (1998) Effect of the sample matrix on the determination of indinavir in human urine by HPLC with turbo ion spray tandem mass spectrometric detection1. *Journal of pharmaceutical and biomedical analysis,* 18**,** 347-357.

Fu, T. M., D. J. Jacob, F. Wittrock, J. P. Burrows, M. Vrekoussis & D. K. Henze (2008) Global budgets of atmospheric glyoxal and methylglyoxal, and implications for formation of secondary organic aerosols. *Journal of geophysical research: atmospheres,* 113.

Fuller, S. J., Y. Zhao, S. S. Cliff, A. S. Wexler & M. Kalberer (2012) Direct surface analysis of time-resolved aerosol impactor samples with ultrahigh-resolution mass spectrometry. *Analytical chemistry,* 84**,** 9858-9864.

Gallimore, P. J., C. Giorio, B. M. Mahon & M. Kalberer (2017a) Online molecular characterisation of organic aerosols in an atmospheric chamber using extractive electrospray ionisation mass spectrometry. *Atmospheric Chemistry and Physics,* 17**,** 14485-14500.

Gallimore, P. J. & M. Kalberer (2013) Characterizing an extractive electrospray ionization (EESI) source for the online mass spectrometry analysis of organic aerosols. *Environmental science & technology,* 47**,** 7324-7331.

Gallimore, P. J., B. M. Mahon, F. P. Wragg, S. J. Fuller, C. Giorio, I. Kourtchev & M. Kalberer (2017b) Multiphase composition changes and reactive oxygen species formation during limonene oxidation in the new Cambridge Atmospheric Simulation Chamber (CASC). *Atmospheric Chemistry and Physics,* 17**,** 9853-9868.

Gao, S., J. D. Surratt, E. M. Knipping, E. S. Edgerton, M. Shahgholi & J. H. Seinfeld (2006) Characterization of polar organic components in fine aerosols in the southeastern United States: Identity, origin, and evolution. *Journal of Geophysical Research: Atmospheres,* 111.

Gao, S., Z.-P. Zhang & H. Karnes (2005) Sensitivity enhancement in liquid chromatography/atmospheric pressure ionization mass spectrometry using derivatization and mobile phase additives. *Journal of Chromatography B,* 825**,** 98-110.

Gard, E., J. E. Mayer, B. D. Morrical, T. Dienes, D. P. Fergenson & K. A. Prather (1997) Real-time analysis of individual atmospheric aerosol particles: Design and performance of a portable ATOFMS. *Analytical Chemistry,* 69**,** 4083-4091.

Gill, P., T. Graedel & C. Weschler (1983) Organic films on atmospheric aerosol particles, fog droplets, cloud droplets, raindrops, and snowflakes. *Reviews of Geophysics,* 21**,** 903-920.

Gioda, A., G. J. Reyes-Rodríguez, G. Santos-Figueroa, J. L. Collett Jr, S. Decesari, M. d. C. K. Ramos, H. J. Bezerra Netto, F. R. de Aquino Neto & O. L. Mayol-Bracero (2011) Speciation of water-soluble inorganic, organic, and total nitrogen in a background marine environment: Cloud water, rainwater, and aerosol particles. *Journal of Geophysical Research: Atmospheres,* 116.

Giorio, C., S. J. Campbell, M. Bruschi, F. Tampieri, A. Barbon, A. Toffoletti, A. Tapparo, C. Paijens, A. J. Wedlake & P. Grice (2017a) Online Quantification of Criegee Intermediates of α-Pinene Ozonolysis by Stabilization with Spin Traps and Proton-Transfer Reaction Mass Spectrometry Detection. *Journal of the American Chemical Society,* 139**,** 3999-4008.

Giorio, C., A. Monod, L. Brégonzio-Rozier, H. L. DeWitt, M. Cazaunau, B. Temime-Roussel, A. Gratien, V. Michoud, E. Pangui & S. Ravier (2017b) Cloud processing of secondary organic aerosol from isoprene and methacrolein photooxidation. *The Journal of Physical Chemistry A,* 121**,** 7641-7654.

Giorio, C., E. Moyroud, B. J. Glover, P. C. Skelton & M. Kalberer (2015) Direct surface analysis coupled to high-resolution mass spectrometry reveals heterogeneous composition of the cuticle of Hibiscus trionum petals. *Analytical chemistry,* 87**,** 9900-9907.

Glasius, M., M. Duane & B. R. Larsen (1999) Determination of polar terpene oxidation products in aerosols by liquid chromatography–ion trap mass spectrometry. *Journal of Chromatography A,* 833**,** 121-135.

Glasius, M. & A. H. Goldstein. 2016. Recent discoveries and future challenges in atmospheric organic chemistry. ACS Publications.

Glasius, M., M. Lahaniati, A. Calogirou, D. Di Bella, N. R. Jensen, J. Hjorth, D. Kotzias & B. R. Larsen (2000) Carboxylic acids in secondary aerosols from oxidation of cyclic monoterpenes by ozone. *Environmental Science & Technology,* 34**,** 1001-1010.

Gómez-González, Y., W. Wang, R. Vermeylen, X. Chi, J. Neirynck, I. Janssens, W. Maenhaut & M. Claeys (2012) Chemical characterisation of atmospheric aerosols during a 2007 summer field campaign at Brasschaat, Belgium: sources and source processes of biogenic secondary organic aerosol. *Atmospheric Chemistry and Physics,* 12**,** 125-138.

Gómez-González, Y., J. D. Surratt, F. Cuyckens, R. Szmigielski, R. Vermeylen, M. Jaoui, M. Lewandowski, J. H. Offenberg, T. E. Kleindienst & E. O. Edney (2008) Characterization of organosulfates from the photooxidation of isoprene and unsaturated fatty acids in ambient aerosol using liquid chromatography/(−)

electrospray ionization mass spectrometry. *Journal of Mass Spectrometry,* 43**,** 371-382.

Hallquist, M., J. C. Wenger, U. Baltensperger, Y. Rudich, D. Simpson, M. Claeys, J. Dommen, N. Donahue, C. George & A. Goldstein (2009) The formation, properties and impact of secondary organic aerosol: current and emerging issues. *Atmospheric chemistry and physics,* 9**,** 5155-5236.

Hamilton, J., M. Alfarra, N. Robinson, M. Ward, A. Lewis, G. McFiggans, H. Coe & J. Allan (2013) Linking biogenic hydrocarbons to biogenic aerosol in the Borneo rainforest. *Atmospheric Chemistry and Physics,* 13**,** 11295-11305.

Heald, C., J. Kroll, J. Jimenez, K. Docherty, P. DeCarlo, A. Aiken, Q. Chen, S. Martin, D. Farmer & P. Artaxo (2010) A simplified description of the evolution of organic aerosol composition in the atmosphere. *Geophysical Research Letters,* 37.

Hennigan, C. J., M. H. Bergin, J. E. Dibb & R. J. Weber (2008) Enhanced secondary organic aerosol formation due to water uptake by fine particles. *Geophysical Research Letters,* 35.

Hennigan, C. J., M. H. Bergin, A. G. Russell, A. Nenes & R. J. Weber (2009) Gas/particle partitioning of water-soluble organic aerosol in Atlanta. *Atmospheric Chemistry and Physics,* 9**,** 3613-3628.

Henriksen, T., R. K. Juhler, B. Svensmark & N. B. Cech (2005) The relative influences of acidity and polarity on responsiveness of small organic molecules to analysis with negative ion electrospray ionization mass spectrometry (ESI-MS). *Journal of the American Society for Mass Spectrometry,* 16**,** 446-455.

Henze, D., J. Seinfeld, N. Ng, J. Kroll, T.-M. Fu, D. J. Jacob & C. Heald (2008) Global modeling of secondary organic aerosol formation from aromatic hydrocarbons: high-vs. low-yield pathways. *Atmospheric Chemistry and Physics,* 8**,** 2405-2420.

Hodzic, A., J. L. Jimenez, S. Madronich, M. Canagaratna, P. F. DeCarlo, L. Kleinman & J. Fast (2010) Modeling organic aerosols in a megacity: potential contribution of semi-volatile and intermediate volatility primary organic compounds to secondary organic aerosol formation. *Atmospheric Chemistry & Physics,* 10.

Holzinger, R., J. Williams, F. Herrmann, J. Lelieveld, N. Donahue & T. Röckmann (2010) Aerosol analysis using a Thermal-Desorption Proton-Transfer-Reaction Mass Spectrometer (TD-PTR-MS): a new approach to study processing of organic aerosols. *Atmospheric chemistry and physics,* 10**,** 2257-2267.

Hop, C. E., Y. Chen & L. J. Yu (2005) Uniformity of ionization response of structurally diverse analytes using a chip-based nanoelectrospray ionization source. *Rapid Communications in Mass Spectrometry: An International Journal Devoted to the Rapid Dissemination of Up-to-the-Minute Research in Mass Spectrometry,* 19**,** 3139-3142.

Hu, G., R. Balasubramanian & C. Wu (2003) Chemical characterization of rainwater at Singapore. *Chemosphere,* 51**,** 747-755.

Huck, C. & G. Bonn (2000) Recent developments in polymer-based sorbents for solid-phase extraction. *Journal of Chromatography A,* 885**,** 51-72.

Huffman, B. A., M. L. Poltash & C. A. Hughey (2012) Effect of polar protic and polar aprotic solvents on negative-ion electrospray ionization and chromatographic separation of small acidic molecules. *Analytical chemistry,* 84**,** 9942-9950.

Hyde, A. M., S. L. Zultanski, J. H. Waldman, Y.-L. Zhong, M. Shevlin & F. Peng (2017) General principles and strategies for salting-out informed by the Hofmeister series. *Organic Process Research & Development,* 21**,** 1355-1370.

Hyder, M. & J. Å. Jönsson (2012) Hollow-fiber liquid phase microextraction for lignin pyrolysis acids in aerosol samples and gas chromatography–mass spectrometry analysis. *Journal of Chromatography A,* 1249**,** 48-53.

Ifa, D. R., C. Wu, Z. Ouyang & R. G. Cooks (2010) Desorption electrospray ionization and other ambient ionization methods: current progress and preview. *Analyst,* 135**,** 669-681.

Iinuma, Y., O. Böge, T. Gnauk & H. Herrmann (2004) Aerosol-chamber study of the α-pinene/O3 reaction: influence of particle acidity on aerosol yields and products. *Atmospheric Environment,* 38**,** 761-773.

Iinuma, Y., O. Böge, R. Gräfe & H. Herrmann (2010) Methyl-nitrocatechols: atmospheric tracer compounds for biomass burning secondary organic aerosols. *Environmental science & technology,* 44**,** 8453-8459.

Iinuma, Y., O. Böge, A. Kahnt & H. Herrmann (2009) Laboratory chamber studies on the formation of organosulfates from reactive uptake of monoterpene oxides. *Physical Chemistry Chemical Physics,* 11**,** 7985-7997.

Incorporated, T. 2011. Scanning Mobility Particle Sizer Spectrometer (SMPS) Model 3936. In *Particle Instruments,* ed. T. Incorporated. USA.

Izquierdo, R., A. Avila & M. Alarcón (2012) Trajectory statistical analysis of atmospheric transport patterns and trends in precipitation chemistry of a rural site in NE Spain in 1984–2009. *Atmospheric environment,* 61**,** 400-408.

Jackson, A. U., N. Talaty, R. G. Cooks & G. J. Van Berkel (2007) Salt tolerance of desorption electrospray ionization (DESI). *Journal of the American Society for Mass Spectrometry,* 18**,** 2218-2225.

Jackson, A. U., S. R. Werner, N. Talaty, Y. Song, K. Campbell, R. G. Cooks & J. A. Morgan (2008) Targeted metabolomic analysis of Escherichia coli by desorption electrospray ionization and extractive electrospray ionization mass spectrometry. *Analytical biochemistry,* 375**,** 272-281.

Jaitz, L., B. Mueller, G. Koellensperger, D. Huber, E. Oburger, M. Puschenreiter & S. Hann (2011) LC–MS analysis of low molecular weight organic acids derived from root exudation. *Analytical and bioanalytical chemistry,* 400**,** 2587-2596.

Jaoui, M., E. Corse, T. E. Kleindienst, J. H. Offenberg, M. Lewandowski & E. O. Edney (2006) Analysis of Secondary Organic Aerosol Compounds from the Photooxidation of d-Limonene in the Presence of NO X and their Detection in Ambient PM2. 5. *Environmental science & technology,* 40**,** 3819-3828.

Jardine, K. J., R. K. Monson, L. Abrell, S. R. Saleska, A. Arneth, A. Jardine, F. Y. Ishida, A. M. Y. Serrano, P. Artaxo & T. Karl (2012) Within-plant isoprene oxidation confirmed by direct emissions of oxidation products methyl vinyl ketone and methacrolein. *Global Change Biology,* 18**,** 973-984.

Jayne, J. T., D. C. Leard, X. Zhang, P. Davidovits, K. A. Smith, C. E. Kolb & D. R. Worsnop (2000) Development of an aerosol mass spectrometer for size and composition analysis of submicron particles. *Aerosol Science & Technology,* 33**,** 49-70.

Jenkin, M. (2004) Modelling the formation and composition of secondary organic aerosol from α-and β-pinene ozonolysis using MCM v3. *Atmospheric Chemistry and Physics,* 4**,** 1741-1757.

Jimenez, J. L., M. R. Canagaratna, N. M. Donahue, A. S. H. Prevot, Q. Zhang, J. H. Kroll, P. F. DeCarlo, J. D. Allan, H. Coe, N. L. Ng, A. C. Aiken, K. S. Docherty, I. M. Ulbrich, A. P. Grieshop, A. L. Robinson, J. Duplissy, J. D. Smith, K. R. Wilson, V. A. Lanz, C. Hueglin, Y. L. Sun, J. Tian, A. Laaksonen, T. Raatikainen, J. Rautiainen, P. Vaattovaara, M. Ehn, M. Kulmala, J. M. Tomlinson, D. R. Collins, M. J. Cubison, E., J. Dunlea, J. A. Huffman, T. B. Onasch, M. R. Alfarra, P. I. Williams, K. Bower, Y. Kondo, J. Schneider, F. Drewnick, S. Borrmann, S. Weimer, K. Demerjian, D. Salcedo, L. Cottrell, R. Griffin, A. Takami, T. Miyoshi, S. Hatakeyama, A. Shimono, J. Y. Sun, Y. M. Zhang, K. Dzepina, J. R. Kimmel, D. Sueper, J. T. Jayne, S. C. Herndon, A. M. Trimborn, L. R. Williams, E. C. Wood, A. M. Middlebrook, C. E. Kolb, U. Baltensperger & D. R. Worsnop (2009) Evolution of Organic Aerosols in the Atmosphere.

Johnston, M. V. & D. Kerecman (2019) Molecular Characterization of Atmospheric Organic Aerosol by Mass Spectrometry. *Annual Review of Analytical Chemistry,* 12.

Kalberer, M., D. Paulsen, M. Sax, M. Steinbacher, J. Dommen, A. Prevot, R. Fisseha, E. Weingartner, V. Frankevich & R. Zenobi (2004) Identification of polymers as major components of atmospheric organic aerosols. *Science,* 303**,** 1659-1662.

Kalberer, M., J. Yu, D. Cocker, R. Flagan & J. H. Seinfeld (2000) Aerosol formation in the cyclohexene-ozone system. *Environmental science & technology,* 34**,** 4894-4901.

Kampf, C. J., B. Bonn & T. Hoffmann (2011) Development and validation of a selective HPLC-ESI-MS/MS method for the quantification of glyoxal and methylglyoxal in atmospheric aerosols (PM2. 5). *Analytical and bioanalytical chemistry,* 401**,** 3115-3124.

Kanakidou, M., J. Seinfeld, S. Pandis, I. Barnes, F. Dentener, M. Facchini, R. V. Dingenen, B. Ervens, A. Nenes & C. Nielsen (2005) Organic aerosol and global climate modelling: a review. *Atmospheric Chemistry and Physics,* 5**,** 1053-1123.

Karagulian, F., A. S. Lea, C. W. Dilbeck & B. J. Finlayson-Pitts (2008) A new mechanism for ozonolysis of unsaturated organics on solids: phosphocholines on NaCl as a model for sea salt particles. *Physical chemistry chemical physics,* 10**,** 528-541.

Kaufman, Y. J., D. Tanré & O. Boucher (2002) A satellite view of aerosols in the climate system. *Nature,* 419**,** 215-223.

Kawamura, K., S. Steinberg & I. R. Kaplan (1996) Concentrations of monocar□ ylic and dicar□ ylic acids and aldehydes in southern California wet precipitations: Comparison of urban and nonurban samples and compositional changes during scavenging. *Atmospheric Environment,* 30**,** 1035-1052.

Kessler, S. H., J. D. Smith, D. L. Che, D. R. Worsnop, K. R. Wilson & J. H. Kroll (2010) Chemical sinks of organic aerosol: Kinetics and products of the heterogeneous oxidation of erythritol and levoglucosan. *Environmental science & technology,* 44**,** 7005-7010.

Kim, S., R. W. Kramer & P. G. Hatcher (2003) Graphical method for analysis of ultrahigh-resolution broadband mass spectra of natural organic matter, the van Krevelen diagram. *Analytical Chemistry,* 75**,** 5336-5344.

Kind, T. & O. Fiehn (2007) Seven Golden Rules for heuristic filtering of molecular formulas obtained by accurate mass spectrometry. *BMC Bioinformatics,* 8**,** 105.

King, R., R. Bonfiglio, C. Fernandez-Metzler, C. Miller-Stein & T. Olah (2000) Mechanistic investigation of ionization suppression in electrospray ionization. *Journal of the American Society for Mass Spectrometry,* 11**,** 942-950.

Kleindienst, T., D. Smith, W. Li, E. Edney, D. Driscoll, R. Speer & W. Weathers (1999) Secondary organic aerosol formation from the oxidation of aromatic hydrocarbons in the presence of dry submicron ammonium sulfate aerosol. *Atmospheric Environment,* 33**,** 3669-3681.

Koch, B. P., & T. Dittmar (2006) From mass to structure: an aromaticity index for high-resolution mass data of natural organic matter. *Rapid Communications in Mass Spectrometry,* 20**,** 926-932.

Komjarova, I. & R. Blust (2006) Comparison of liquid–liquid extraction, solid-phase extraction and co-precipitation preconcentration methods for the determination of cadmium, copper, nickel, lead and zinc in seawater. *Analytica Chimica Acta,* 576**,** 221-228.

Kostiainen, R. & T. J. Kauppila (2009) Effect of eluent on the ionization process in liquid chromatography–mass spectrometry. *Journal of Chromatography A,* 1216**,** 685-699.

Kourtchev, I., J.-F. Doussin, C. Giorio, B. Mahon, E. M. Wilson, N. Maurin, E. Pangui, D. S. Venables, J. C. Wenger & M. Kalberer (2015) Molecular composition of fresh and aged secondary organic aerosol from a mixture of biogenic volatile compounds: a high-resolution mass spectrometry study. *Atmospheric Chemistry and Physics,* 15**,** 5683-5695.

Kourtchev, I., S. Fuller, J. Aalto, T. M. Ruuskanen, M. W. McLeod, W. Maenhaut, R. Jones, M. Kulmala & M. Kalberer (2013) Molecular composition of boreal forest aerosol from Hyytiala, Finland, using ultrahigh resolution mass spectrometry. *Environmental science & technology,* 47**,** 4069-4079.

Kourtchev, I., S. Fuller, C. Giorio, R. M. Healy, E. Wilson, I. O'Connor, J. C. Wenger, M. McLeod, J. Aalto & T. M. Ruuskanen (2014a) Molecular composition of biogenic secondary organic aerosols using ultrahigh-resolution mass spectrometry: comparing laboratory and field studies. *Atmospheric Chemistry and Physics,* 14**,** 2155-2167.

Kourtchev, I., C. Giorio, A. Manninen, E. Wilson, B. Mahon, J. Aalto, M. Kajos, D. Venables, T. Ruuskanen & J. Levula (2016a) Enhanced Volatile Organic Compounds emissions and organic aerosol mass increase the oligomer content of atmospheric aerosols. *Scientific reports,* 6**,** 35038.

Kourtchev, I., R. H. Godoi, S. Connors, J. G. Levine, A. T. Archibald, A. F. Godoi, S. L. Paralovo, C. G. Barbosa, R. A. Souza & A. O. Manzi (2016b) Molecular composition of organic aerosols in central Amazonia: an ultra-high-resolution mass spectrometry study. *Atmospheric Chemistry and Physics,* 16**,** 11899-11913.

Kourtchev, I., I. O'Connor, C. Giorio, S. Fuller, K. Kristensen, W. Maenhaut, J. Wenger, J. Sodeau, M. Glasius & M. Kalberer (2014b) Effects of anthropogenic emissions on the molecular composition of urban organic aerosols: An ultrahigh resolution mass spectrometry study. *Atmospheric Environment,* 89**,** 525-532.

Kourtchev, I., T. Ruuskanen, W. Maenhaut, M. Kulmala & M. Claeys (2005) Observation of 2-methyltetrols and related photo-oxidation products of isoprene in boreal forest aerosols from Hyytiälä, Finland. *Atmospheric Chemistry and Physics,* 5**,** 2761-2770.

Kristensen, K., T. Cui, H. Zhang, A. Gold, M. Glasius & J. Surratt (2014) Dimers in α-pinene secondary organic aerosol: effect of hydroxyl radical, ozone, relative humidity and aerosol acidity. *Atmospheric Chemistry and Physics,* 14**,** 4201-4218.

Kristensen, K., K. L. Enggrob, S. King, D. Worton, S. Platt, R. Mortensen, T. Rosenoern, J. Surratt, M. Bilde & A. Goldstein (2013) Formation and occurrence of dimer esters of pinene oxidation products in atmospheric aerosols. *Atmospheric Chemistry and Physics,* 13**,** 3763-3776.

Kroll, J. H., N. M. Donahue, J. L. Jimenez, S. H. Kessler, M. R. Canagaratna, K. R. Wilson, K. E. Altieri, L. R. Mazzoleni, A. S. Wozniak & H. Bluhm (2011) Carbon oxidation state as a metric for describing the chemistry of atmospheric organic aerosol. *Nature Chemistry,* 3**,** 133-139.

Kroll, J. H., N. L. Ng, S. M. Murphy, R. C. Flagan & J. H. Seinfeld (2006) Secondary organic aerosol formation from isoprene photooxidation. *Environmental science & technology,* 40**,** 1869-1877.

Kroll, J. H. & J. H. Seinfeld (2008) Chemistry of secondary organic aerosol: Formation and evolution of low-volatility organics in the atmosphere. *Atmospheric Environment,* 42**,** 3593-3624.

Kruve, A., K. Kaupmees, J. Liigand & I. Leito (2014) Negative electrospray ionization via deprotonation: predicting the ionization efficiency. *Analytical chemistry,* 86**,** 4822-4830.

Kumbhani, S., T. Longin, L. Wingen, C. Kidd, V. Perraud & B. Finlayson-Pitts (2018) New Mechanism of Extractive Electrospray Ionization Mass Spectrometry for Heterogeneous Solid Particles. *Analytical chemistry,* 90**,** 2055-2062.

Lambe, A., T. Onasch, P. Massoli, D. Croasdale, J. Wright, A. Ahern, L. Williams, D. Worsnop, W. Brune & P. Davidovits (2011) Laboratory studies of the chemical composition and cloud condensation nuclei (CCN) activity of secondary organic aerosol (SOA) and oxidized primary organic aerosol (OPOA). *Atmospheric Chemistry and Physics,* 11**,** 8913-8928.

Laskin, A. & J. P. Cowin (2001) Automated single-particle SEM/EDX analysis of submicrometer particles down to 0.1 μm. *Analytical Chemistry,* 73**,** 1023-1029.

Lauder, R. 2008. Practical Skills. Pearson.

Law, W. S., R. Wang, B. Hu, C. Berchtold, L. Meier, H. Chen & R. Zenobi (2010) On the mechanism of extractive electrospray ionization. *Analytical chemistry,* 82**,** 4494-4500.

Lee, A., A. H. Goldstein, M. D. Keywood, S. Gao, V. Varutbangkul, R. Bahreini, N. L. Ng, R. C. Flagan & J. H. Seinfeld (2006a) Gas-phase products and secondary

aerosol yields from the ozonolysis of ten different terpenes. *Journal of Geophysical Research: Atmospheres,* 111.

Lee, A., A. H. Goldstein, J. H. Kroll, N. L. Ng, V. Varutbangkul, R. C. Flagan & J. H. Seinfeld (2006b) Gas-phase products and secondary aerosol yields from the photooxidation of 16 different terpenes. *Journal of Geophysical Research: Atmospheres,* 111.

Lee, S. H., J. Uin, A. B. Guenther, J. A. de Gouw, F. Yu, A. B. Nadykto, J. Herb, N. L. Ng, A. Koss & W. H. Brune (2016) Isoprene suppression of new particle formation: Potential mechanisms and implications. *Journal of Geophysical Research: Atmospheres,* 121**,** 14,621-14,635.

Leslie, S. A. & J. C. Mitchell (2007) Removing gold coating from SEM samples. *palaeontology,* 50**,** 1459-1461.

Li, Y., Q. Chen, M. Guzman, C. K. Chan & S. Martin (2011) Second-generation products contribute substantially to the particle-phase organic material produced by β-caryophyllene ozonolysis. *Atmospheric Chemistry and Physics,* 11**,** 121-132.

Lim, Y., Y. Tan, M. Perri, S. Seitzinger & B. Turpin (2010) Aqueous chemistry and its role in secondary organic aerosol (SOA) formation. *Atmospheric Chemistry and Physics,* 10**,** 10521-10539.

Lin, P., A. G. Rincon, M. Kalberer & J. Z. Yu (2012) Elemental composition of HULIS in the Pearl River Delta Region, China: Results inferred from positive and negative electrospray high resolution mass spectrometric data. *Environmental science & technology,* 46**,** 7454-7462.

Liu, X., J. Zhu, P. Van Espen, F. Adams, R. Xiao, S. Dong & Y. Li (2005) Single particle characterization of spring and summer aerosols in Beijing: Formation of composite sulfate of calcium and potassium. *Atmospheric Environment,* 39**,** 6909-6918.

Louchouarn, P., S. Opsahl & R. Benner (2000) Isolation and quantification of dissolved lignin from natural waters using solid-phase extraction and GC/MS. *Analytical Chemistry,* 72**,** 2780-2787.

Mace, K. A., R. A. Duce & N. W. Tindale (2003) Organic nitrogen in rain and aerosol at Cape Grim, Tasmania, Australia. *Journal of Geophysical Research: Atmospheres,* 108.

Maenhaut, W., X. Chi, W. Wang, J. Cafmeyer, F. Yasmeen, R. Vermeylen, K. Szmigielska, I. A. Janssens & M. Claeys (2017) Contribution from Selected Organic Species to PM2. 5 Aerosol during a Summer Field Campaign at K-Puszta, Hungary. *Atmosphere,* 8**,** 221.

Maenhaut, W., F. Francois & J. Cafmeyer (1992) The "Gent" stacked filter unit (SFU) sampler for the collection of atmospheric aerosols in two size fractions: description and instructions for installation and use. *IAEA CRP E,* 4.

Majors, R. E. (2010) Solid-Phase Extraction. *Handbook of Sample Preparation***,** 53-79.

Mallet, C. R., Z. Lu & J. R. Mazzeo (2004) A study of ion suppression effects in electrospray ionization from mobile phase additives and solid-phase extracts. *Rapid Communications in Mass Spectrometry,* 18**,** 49-58.

Matuszewski, B., M. Constanzer & C. Chavez-Eng (2003) Strategies for the assessment of matrix effect in quantitative bioanalytical methods based on HPLC− MS/MS. *Analytical chemistry,* 75**,** 3019-3030.

Mazzoleni, L. R., B. M. Ehrmann, X. Shen, A. G. Marshall & J. L. Collett Jr (2010a) Water-soluble atmospheric organic matter in fog: exact masses and chemical formula identification by ultrahigh-resolution Fourier transform ion cyclotron resonance mass spectrometry. *Environmental science & technology,* 44**,** 3690-3697.

Mazzoleni, L. R., B. M. Ehrmann, X. Shen, A. G. Marshall & J. Jeffrey L. Collett (2010b) Water-Soluble Atmospheric Organic Matter in Fog: Exact Masses and Chemical Formula Identification by Ultrahigh-Resolution Fourier Transform Ion Cyclotron Resonance Mass Spectrometry. *Environmental Science and Technology,* 44**,** 3690-3697.

Mazzoleni, L. R., P. Saranjampour, M. M. Dalbec, V. Samburova, A. G. Hallar, B. Zielinska, D. H. Lowenthal & S. Kohl (2012) Identification of water-soluble organic carbon in non-urban aerosols using ultrahigh-resolution FT-ICR mass spectrometry: organic anions. *Environmental Chemistry,* 9**,** 285-297.

McFiggans, G., T. F. Mentel, J. Wildt, I. Pullinen, S. Kang, E. Kleist, S. Schmitt, M. Springer, R. Tillmann & C. Wu (2019) Secondary organic aerosol reduced by mixture of atmospheric vapours. *Nature,* 565**,** 587.

McNeill, V. F., G. M. Wolfe & J. A. Thornton (2007) The oxidation of oleate in submicron aqueous salt aerosols: Evidence of a surface process. *The Journal of Physical Chemistry A,* 111**,** 1073-1083.

Mirante, F., C. Alves, C. Pio, O. Pindado, R. Perez, M. A. Revuelta & B. Artiñano (2013) Organic composition of size segregated atmospheric particulate matter, during summer and winter sampling campaigns at representative sites in Madrid, Spain. *Atmospheric Research,* 132**,** 345-361.

Miyazaki, Y., K. Kawamura & M. Sawano (2010) Size distributions of organic nitrogen and carbon in remote marine aerosols: Evidence of marine biological origin based on their isotopic ratios. *Geophysical Research Letters,* 37.

Mochida, M., Y. Kitamori, K. Kawamura, Y. Nojiri & K. Suzuki (2002) Fatty acids in the marine atmosphere: Factors governing their concentrations and evaluation of organic films on sea-salt particles. *Journal of Geophysical Research: Atmospheres,* 107.

Mohr, C., J. A. Huffman, M. J. Cubison, A. C. Aiken, K. S. Docherty, J. R. Kimmel, I. M. Ulbrich, M. Hannigan & J. L. Jimenez (2009) Characterization of primary organic aerosol emissions from meat cooking, trash burning, and motor vehicles with high-resolution aerosol mass spectrometry and comparison with ambient and chamber observations. *Environmental Science & Technology,* 43**,** 2443-2449.

Molteni, U., F. Bianchi, F. Klein, I. E. Haddad, C. Frege, M. J. Rossi, J. Dommen & U. Baltensperger (2018) Formation of highly oxygenated organic molecules from aromatic compounds. *Atmospheric Chemistry and Physics,* 18**,** 1909-1921.

Mouli, P. C., S. V. Mohan & S. J. Reddy (2005) Rainwater chemistry at a regional representative urban site: influence of terrestrial sources on ionic composition. *Atmospheric environment,* 39**,** 999-1008.

Myhre, G., D. Shindell, F.-M. Bréon, W. Collins, J. Fuglestvedt, J. Huang, D. Koch, J.-F. Lamarque, D. Lee & B. Mendoza (2013) Anthropogenic and natural radiative forcing. *Climate change,* 423**,** 658-740.

Müller, L., M.-C. Reinnig, J. Warnke & T. Hoffmann (2008) Unambiguous identification of esters as oligomers in secondary organic aerosol formed from cyclohexene and cyclohexene/α-pinene ozonolysis. *Atmospheric Chemistry and Physics,* 8**,** 1423-1433.

Ng, N., M. Canagaratna, J. Jimenez, P. Chhabra, J. Seinfeld & D. Worsnop (2011) Changes in organic aerosol composition with aging inferred from aerosol mass spectra. *Atmospheric Chemistry and Physics,* 11**,** 6465-6474.

Ng, N., M. Canagaratna, Q. Zhang, J. Jimenez, J. Tian, I. Ulbrich, J. Kroll, K. Docherty, P. Chhabra & R. Bahreini (2010) Organic aerosol components observed in Northern Hemispheric datasets from Aerosol Mass Spectrometry. *Atmospheric Chemistry and Physics,* 10**,** 4625-4641.

Ng, N. L., J. H. Kroll, M. D. Keywood, R. Bahreini, V. Varutbangkul, R. C. Flagan, J. H. Seinfeld, A. Lee & A. H. Goldstein (2006) Contribution of first-versus second-generation products to secondary organic aerosols formed in the oxidation of biogenic hydrocarbons. *Environmental science & technology,* 40**,** 2283-2297.

Nguyen, T. B., P. B. Lee, K. M. Updyke, D. L. Bones, J. Laskin, A. Laskin & S. A. Nizkorodov (2012) Formation of nitrogen-and sulfur-containing light-absorbing compounds accelerated by evaporation of water from secondary organic aerosols. *Journal of Geophysical Research: Atmospheres,* 117.

Noziere, B., M. Kalberer, M. Claeys, J. Allan, B. D'Anna, S. Decesari, E. Finessi, M. Glasius, I. Grgic & J. F. Hamilton (2015) The molecular identification of organic compounds in the atmosphere: state of the art and challenges. *Chemical reviews,* 115**,** 3919-3983.

O'dowd, C. D., M. C. Facchini, F. Cavalli, D. Ceburnis, M. Mircea, S. Decesari, S. Fuzzi, Y. J. Yoon & J.-P. Putaud (2004) Biogenically driven organic contribution to marine aerosol. *Nature,* 431**,** 676-680.

Odum, J. R., T. Hoffmann, F. Bowman, D. Collins, R. C. Flagan & J. H. Seinfeld (1996) Gas/particle partitioning and secondary organic aerosol yields. *Environmental Science & Technology,* 30**,** 2580-2585.

OriginLab. 2019. Help Online - Origin Help - Interpreting Regression Results. In *Origin Help*.

Oss, M., A. Kruve, K. Herodes & I. Leito (2010) Electrospray ionization efficiency scale of organic compounds. *Analytical Chemistry,* 82**,** 2865-2872.

Paerl, H. W. (1985) Enhancement of marine primary production by nitrogen-enriched acid rain. *Nature,* 315**,** 747.

Pankow, J. F. (1994) An absorption model of gas/particle partitioning of organic compounds in the atmosphere. *Atmospheric Environment,* 28**,** 185-188.

Parshintsev, J., M. Kivilompolo, J. Ruiz-Jimenez, K. Hartonen, M. Kulmala & M.-L. Riekkola (2010) Particle-into-liquid sampler on-line coupled with solid-phase extraction-liquid chromatography–mass spectrometry for the determination of organic acids in atmospheric aerosols. *Journal of Chromatography a,* 1217**,** 5427-5433.

Peña, R. M., S. García, C. Herrero, M. Losada, A. Vázquez & T. Lucas (2002) Organic acids and aldehydes in rainwater in a northwest region of Spain. *Atmospheric Environment,* 36**,** 5277-5288.

Phenomenex. 2011. TN-013: A Simple Approach to Fast and Practical Solid Phase Extraction (SPE) Method Development | Phenomenex UHPLC, HPLC, SPE and GC.

Phenomenex. 2015. Solid Phase Extraction (SPE) Method Development Guide.

Piccolo, A., P. Conte, R. Spaccini & M. Chiarella (2003) Effects of some dicarboxylic acids on the association of dissolved humic substances. *Biology and Fertility of Soils,* 37**,** 255-259.

Pluskal, T., S. Castillo, A. Villar-Briones & M. Orešič (2010) MZmine 2: Modular framework for processing, visualizing, and analyzing mass spectrometry-based molecular profile data. *BMC Bioinformatics,* 11**,** 395.

Pope, F., P. Gallimore, S. Fuller, R. Cox & M. Kalberer (2010) Ozonolysis of maleic acid aerosols: Effect upon aerosol hygroscopicity, phase and mass. *Environmental science & technology,* 44**,** 6656-6660.

Pramanik, B. N., A. K. Ganguly & M. L. Gross. 2002. *Applied electrospray mass spectrometry: practical spectroscopy series*. CRC Press.

Pratt, K. A., M. N. Fiddler, P. B. Shepson, A. G. Carlton & J. D. Surratt (2013) Organosulfates in cloud water above the Ozarks' isoprene source region. *Atmospheric environment,* 77**,** 231-238.

Pratt, K. A. & K. A. Prather (2012) Mass spectrometry of atmospheric aerosols—Recent developments and applications. Part II: On-line mass spectrometry techniques. *Mass Spectrometry Reviews,* 31**,** 17-48.

Putman, A. L., J. H. Offenberg, R. Fisseha, S. Kundu, T. A. Rahn & L. R. Mazzoleni (2012) Ultrahigh-resolution FT-ICR mass spectrometry characterization of α-pinene ozonolysis SOA. *Atmospheric environment,* 46**,** 164-172.

Pósfai, M., H. Xu, J. R. Anderson & P. R. Buseck (1998) Wet and dry sizes of atmospheric aerosol particles: An AFM-TEM Study. *Geophysical Research Letters,* 25**,** 1907-1910.

Pöschl, U. (2005) Atmospheric aerosols: composition, transformation, climate and health effects. *Angewandte Chemie International Edition,* 44**,** 7520-7540.

Raffaelli, A. & A. Saba (2003) Atmospheric pressure photoionization mass spectrometry. *Mass Spectrometry Reviews,* 22**,** 318-331.

Ramanathan, V., P. Crutzen, J. Kiehl & D. Rosenfeld (2001) Aerosols, climate, and the hydrological cycle. *science,* 294**,** 2119-2124.

Ranninger, C., L. E. Schmidt, M. Rurik, A. Limonciel, P. Jennings, O. Kohlbacher & C. G. Huber (2016) Improving global feature detectabilities through scan range splitting for untargeted metabolomics by high-performance liquid chromatography-Orbitrap mass spectrometry. *Analytica chimica acta,* 930**,** 13-22.

Rayleigh, L. (1882) XX. On the equilibrium of liquid conducting masses charged with electricity. *The London, Edinburgh, and Dublin Philosophical Magazine and Journal of Science,* 14**,** 184-186.

Reinhardt, A., C. Emmenegger, B. Gerrits, C. Panse, J. Dommen, U. Baltensperger, R. Zenobi & M. Kalberer (2007) Ultrahigh mass resolution and accurate mass measurements as a tool to characterize oligomers in secondary organic aerosols. *Analytical Chemistry,* 79**,** 4074-4082.

Rellán-Álvarez, R., S. López-Gomollón, J. Abadía & A. Álvarez-Fernández (2011) Development of a new high-performance liquid chromatography–electrospray ionization time-of-flight mass spectrometry method for the determination of low molecular mass organic acids in plant tissue extracts. *Journal of agricultural and food chemistry,* 59**,** 6864-6870.

Reynolds, O. (1883) XXIX. An experimental investigation of the circumstances which determine whether the motion of water shall be direct or sinuous, and of the law of resistance in parallel channels. *Philosophical Transactions of the Royal Society of London***,** 935-982.

Robinson, A. L., N. M. Donahue, M. K. Shrivastava, E. A. Weitkamp, A. M. Sage, A. P. Grieshop, T. E. Lane, J. R. Pierce & S. N. Pandis (2007) Rethinking organic aerosols: Semivolatile emissions and photochemical aging. *Science,* 315**,** 1259-1262.

Rodríguez González, S., A. Alastuey, S. Alonso-Pérez, X. Querol, E. Cuevas Agulló, J. Abreu Afonso, M. Viana, N. Pérez, M. Pandolfi & J. D. d. l. Rosa (2011) Transport of desert dust mixed with North African industrial pollutants in the subtropical Saharan Air Layer.

Rudich, Y., N. M. Donahue & T. F. Mentel (2007) Aging of organic aerosol: Bridging the gap between laboratory and field studies. *Annu. Rev. Phys. Chem.,* 58**,** 321-352.

Röhrl, A. & G. Lammel (2002) Determination of malic acid and other C4 dicarboxylic acids in atmospheric aerosol samples. *Chemosphere,* 46**,** 1195-1199.

Safai, P., P. Rao, G. Momin, K. Ali, D. Chate & P. Praveen (2004) Chemical composition of precipitation during 1984–2002 at Pune, India. *Atmospheric Environment,* 38**,** 1705-1714.

Sakugawa, H., I. R. Kaplan & L. S. Shepard (1993) Measurements of H2O2, aldehydes and organic acids in Los Angeles rainwater: their sources and deposition rates. *Atmospheric Environment. Part B. Urban Atmosphere,* 27**,** 203-219.

Salve, P., A. Maurya, S. Wate & S. Devotta (2008) Chemical composition of major ions in rainwater. *Bulletin of environmental contamination and toxicology,* 80**,** 242-246.

Samy, S. & M. D. Hays (2013) Quantitative LC–MS for water-soluble heterocyclic amines in fine aerosols (PM2. 5) at Duke Forest, USA. *Atmospheric environment,* 72**,** 77-80.

Samy, S., J. Robinson & M. D. Hays (2011) An advanced LC-MS (Q-TOF) technique for the detection of amino acids in atmospheric aerosols. *Analytical and bioanalytical chemistry,* 401**,** 3103-3113.

Sangster, T., M. Spence, P. Sinclair, R. Payne & C. Smith (2004) Unexpected observation of ion suppression in a liquid chromatography/atmospheric pressure chemical ionization mass spectrometric bioanalytical method. *Rapid communications in mass spectrometry,* 18**,** 1361-1364.

Sasakawa, M. & M. Uematsu (2002) Chemical composition of aerosol, sea fog, and rainwater in the marine boundary layer of the northwestern North Pacific and its marginal seas. *Journal of Geophysical Research: Atmospheres,* 107.

Schmidt, A., M. Karas & T. Dülcks (2003) Effect of different solution flow rates on analyte ion signals in nano-ESI MS, or: when does ESI turn into nano-ESI? *Journal of the American Society for Mass Spectrometry,* 14**,** 492-500.

Schmitt-Kopplin, P., A. Gelencsér, E. Dabek-Zlotorzynska, G. Kiss, N. Hertkorn, M. Harir, Y. Hong & I. Gebefügi (2010) Analysis of the Unresolved Organic Fraction in Atmospheric Aerosols with Ultrahigh-Resolution Mass Spectrometry and Nuclear Magnetic Resonance Spectroscopy: Organosulfates As Photochemical Smog Constituents†. 82**,** 8017-8026.

Schütze, M. & F. Stratmann (2008) Numerical simulation of cloud droplet formation in a tank. *Computers & Geosciences,* 34**,** 1034-1043.

Scientific, T. 2009a. Thermo Scientific Chromatography: Columns and Consumables. ed. T. Scientific.

Scientific, T. F. 2009b. LTQ Orbitrap Velos^{TM} Hardware Manual. In *LTQ Orbitrap Velos* ^{TM}, ed. T. F. S. Inc.

Scigelova, M. & A. Makarov (2006) Orbitrap mass analyzer–overview and applications in proteomics. *Proteomics,* 6**,** 16-21.

Seinfeld, J. H. & S. N. Pandis. 2006. *Atmospheric Chemistry and Physics: From Air Pollution to Climate Change*. Hoboken, New Jersey, USA: John Wiley & Sons, Inc.

Shrivastava, M., C. D. Cappa, J. Fan, A. H. Goldstein, A. B. Guenther, J. L. Jimenez, C. Kuang, A. Laskin, S. T. Martin & N. L. Ng (2017) Recent advances in understanding secondary organic aerosol: Implications for global climate forcing. *Reviews of Geophysics,* 55**,** 509-559.

Simoneit, B. R., J. J. Schauer, C. Nolte, D. R. Oros, V. O. Elias, M. Fraser, W. Rogge & G. R. Cass (1999) Levoglucosan, a tracer for cellulose in biomass burning and atmospheric particles. *Atmospheric Environment,* 33**,** 173-182.

Singh, S., P. Khare, G. Satsangi, A. Lakhani, K. M. Kumari & S. Srivastava (2001) Rainwater composition at a regional representative site of a semi-arid region of India. *Water, air, and soil pollution,* 127**,** 93-108.

Sleighter, R. L. & P. G. Hatcher (2007) The application of electrospray ionization coupled to ultrahigh resolution mass spectrometry for the molecular characterization of natural organic matter. *Journal of Mass Spectrometry,* 42**,** 559-574.

Sorooshian, A., N. L. Ng, A. W. Chan, G. Feingold, R. C. Flagan & J. H. Seinfeld (2007) Particulate organic acids and overall water-soluble aerosol composition measurements from the 2006 Gulf of Mexico Atmospheric Composition and Climate Study (GoMACCS). *Journal of Geophysical Research: Atmospheres,* 112.

Sorooshian, A., V. Varutbangkul, F. J. Brechtel, B. Ervens, G. Feingold, R. Bahreini, S. M. Murphy, J. S. Holloway, E. L. Atlas & G. Buzorius (2006) Oxalic acid in clear and cloudy atmospheres: Analysis of data from International Consortium for Atmospheric Research on Transport and Transformation 2004. *Journal of Geophysical Research: Atmospheres,* 111.

Stein, A., R. R. Draxler, G. D. Rolph, B. J. Stunder, M. Cohen & F. Ngan (2015) NOAA's HYSPLIT atmospheric transport and dispersion modeling system. *Bulletin of the American Meteorological Society,* 96**,** 2059-2077.

Stratmann, F., A. Kiselev, S. Wurzler, M. Wendisch, J. Heintzenberg, R. Charlson, K. Diehl, H. Wex & S. Schmidt (2004) Laboratory studies and numerical simulations of cloud droplet formation under realistic supersaturation conditions. *Journal of Atmospheric and Oceanic Technology,* 21**,** 876-887.

Sullivan, R. C. & K. A. Prather (2005) Recent advances in our understanding of atmospheric chemistry and climate made possible by on-line aerosol analysis instrumentation. *Analytical Chemistry,* 77**,** 3861-3886.

Sunghwan Kim, a. Robert W. Kramer & P. G. Hatcher* (2003) Graphical Method for Analysis of Ultrahigh-Resolution Broadband Mass Spectra of Natural Organic Matter, the Van Krevelen Diagram.

Supelco. 1998. Guide to Solid Phase Extraction. Sigma Aldrich Co.

Surratt, J. D., Y. Gómez-González, A. W. Chan, R. Vermeylen, M. Shahgholi, T. E. Kleindienst, E. O. Edney, J. H. Offenberg, M. Lewandowski & M. Jaoui (2008) Organosulfate formation in biogenic secondary organic aerosol. *The Journal of Physical Chemistry A,* 112**,** 8345-8378.

Surratt, J. D., J. H. Kroll, T. E. Kleindienst, E. O. Edney, M. Claeys, A. Sorooshian, N. L. Ng, J. H. Offenberg, M. Lewandowski & M. Jaoui (2007) Evidence for organosulfates in secondary organic aerosol. *Environmental Science & Technology,* 41**,** 517-527.

Surratt, J. D., S. M. Murphy, J. H. Kroll, N. L. Ng, L. Hildebrandt, A. Sorooshian, R. Szmigielski, R. Vermeylen, W. Maenhaut & M. Claeys (2006) Chemical composition of secondary organic aerosol formed from the photooxidation of isoprene. *The Journal of Physical Chemistry A,* 110**,** 9665-9690.

Szeto, P. 2014. Mass Spectrometry Analysis of Organic Compounds in Atmospheric Aerosols (2014). In *Chemistry Department*. University of Cambridge.

Taflin, D. C., T. L. Ward & E. J. Davis (1989) Electrified droplet fission and the Rayleigh limit. *Langmuir,* 5**,** 376-384.

Takats, Z., J. M. Wiseman, B. Gologan & R. G. Cooks (2004) Mass spectrometry sampling under ambient conditions with desorption electrospray ionization. *Science,* 306**,** 471-473.

Taylor, P. J. J. C. b. (2005) Matrix effects: the Achilles heel of quantitative high-performance liquid chromatography–electrospray–tandem mass spectrometry. 38**,** 328-334.

Tervahattu, H., K. Hartonen, V. M. Kerminen, K. Kupiainen, P. Aarnio, T. Koskentalo, A. F. Tuck & V. Vaida (2002) New evidence of an organic layer on marine aerosols. *Journal of Geophysical Research: Atmospheres,* 107.

Thorsten Reemtsma, †, Anja These, Prasanna Venkatachari, Xiaoyan Xia, Phillip K. Hopke, a. Andreas Springer & M. Linscheid§ (2006) Identification of Fulvic Acids and Sulfated and Nitrated Analogues in Atmospheric Aerosol by Electrospray Ionization Fourier Transform Ion Cyclotron Resonance Mass Spectrometry. 78**,** 8299-8304.

Tolman, R. C. (1949) The effect of droplet size on surface tension. *The journal of chemical physics,* 17**,** 333-337.

Tolocka, M. P., M. Jang, J. M. Ginter, F. J. Cox, R. M. Kamens & M. V. Johnston (2004) Formation of oligomers in secondary organic aerosol. *Environmental Science & Technology,* 38**,** 1428-1434.

Tong, H., I. Kourtchev, P. Pant, I. J. Keyte, I. P. O'Connor, J. C. Wenger, F. D. Pope, R. M. Harrison & M. Kalberer (2016) Molecular composition of organic aerosols at urban background and road tunnel sites using ultra-high resolution mass spectrometry. *Faraday discussions,* 189**,** 51-68.

Topping, D., G. McFiggans, G. Kiss, Z. Varga, M. Facchini, S. Decesari & M. Mircea (2007) Surface tensions of multi-component mixed inorganic/organic aqueous systems of atmospheric significance: measurements, model predictions and importance for cloud activation predictions. *Atmospheric Chemistry and Physics,* 7**,** 2371-2398.

Tost, H., P. Jöckel, A. Kerkweg, A. Pozzer, R. Sander & J. Lelieveld (2007) Global cloud and precipitation chemistry and wet deposition: tropospheric model simulations with ECHAM5/MESSy1. *Atmospheric Chemistry and Physics,* 7**,** 2733-2757.

Tröstl, J., W. K. Chuang, H. Gordon, M. Heinritzi, C. Yan, U. Molteni, L. Ahlm, C. Frege, F. Bianchi & R. Wagner (2016) The role of low-volatility organic compounds in initial particle growth in the atmosphere. *Nature,* 533**,** 527.

TSI. 2005. Model 3076 Constant Output Atomsier. In *Instruction Manual,* ed. T. I. T. Incorporated.

TSI. 2011. Scanning Mobility Particle Sizer Model 3936. In *Particle Instruments,* ed. T. Incorporated. USA: TSI Incorporated.

TSI. 2012. Series 3080 Electrostatic Classifiers - Operation and Service Manual. In *Particle Instruments - Aerosol Neutralizers,* ed. T. Incorporated. Shoreview, Minnesota, USA: TSI Incorporated.

Ulbrich, I., M. Canagaratna, Q. Zhang, D. Worsnop & J. Jimenez (2009) Interpretation of organic components from Positive Matrix Factorization of aerosol mass spectrometric data. *Atmospheric Chemistry and Physics,* 9**,** 2891-2918.

Van De Steene, J. C., K. A. Mortier & W. E. Lambert (2006) Tackling matrix effects during development of a liquid chromatographic–electrospray ionisation tandem mass spectrometric analysis of nine basic pharmaceuticals in aqueous environmental samples. *Journal of Chromatography A,* 1123**,** 71-81.

Van Krevelen, D. (1950) Graphical-statistical method for the study of structure and reaction processes of coal. *Fuel,* 29**,** 269-284.

van Pinxteren, D., K. W. Fomba, S. Mertes, K. Müller, G. Spindler, J. Schneider, T. Lee, J. L. Collett & H. Herrmann (2016) Cloud water composition during HCCT-2010: Scavenging efficiencies, solute concentrations, and droplet size dependence of inorganic ions and dissolved organic carbon. *Atmospheric Chemistry and Physics,* 16**,** 3185-3205.

Vidal, L., J. Parshintsev, K. Hartonen, A. Canals & M.-L. Riekkola (2012) Ionic liquid-functionalized silica for selective solid-phase extraction of organic acids, amines and aldehydes. *Journal of chromatography A,* 1226**,** 2-10.

Volkamer, R., P. Ziemann & M. Molina (2009) Secondary organic aerosol formation from acetylene (C 2 H 2): seed effect on SOA yields due to organic photochemistry in the aerosol aqueous phase. *Atmospheric Chemistry and Physics,* 9**,** 1907-1928.

Wang, C., Y. D. Lei, S. Endo & F. Wania (2014) Measuring and modeling the salting-out effect in ammonium sulfate solutions. *Environmental science & technology,* 48**,** 13238-13245.

Wang, G., C. Chen, J. Li, B. Zhou, M. Xie, S. Hu, K. Kawamura & Y. Chen (2011) Molecular composition and size distribution of sugars, sugar-alcohols and carboxylic acids in airborne particles during a severe urban haze event caused by wheat straw burning. *Atmospheric Environment,* 45**,** 2473-2479.

Wang, R., A. J. Gröhn, L. Zhu, R. Dietiker, K. Wegner, D. Günther & R. Zenobi (2012) On the mechanism of extractive electrospray ionization (EESI) in the dual-spray configuration. *Analytical and bioanalytical chemistry,* 402**,** 2633-2643.

Wang, W., I. Kourtchev, B. Graham, J. Cafmeyer, W. Maenhaut & M. Claeys (2005) Characterization of oxygenated derivatives of isoprene related to 2-methyltetrols in Amazonian aerosols using trimethylsilylation and gas chromatography/ion trap mass spectrometry. *Rapid Communications in Mass Spectrometry: An International Journal Devoted to the Rapid Dissemination of Up-to-the-Minute Research in Mass Spectrometry,* 19**,** 1343-1351.

Warscheid, B. & T. Hoffmann (2002) Direct analysis of highly oxidised organic aerosol constituents by on-line ion trap mass spectrometry in the negative-ion mode. *Rapid communications in mass spectrometry,* 16**,** 496-504.

Willey, J. D., R. J. Kieber, M. S. Eyman & G. B. Avery (2000) Rainwater dissolved organic carbon: concentrations and global flux. *Global Biogeochemical Cycles,* 14**,** 139-148.

Williams, B. J., A. H. Goldstein, D. B. Millet, R. Holzinger, N. M. Kreisberg, S. V. Hering, A. B. White, D. R. Worsnop, J. D. Allan & J. L. Jimenez (2007) Chemical speciation of organic aerosol during the International Consortium for Atmospheric Research on Transport and Transformation 2004: Results from in situ measurements. *Journal of Geophysical Research: Atmospheres,* 112.

Wilm, M. S. & M. Mann (1994) Electrospray and Taylor-Cone theory, Dole's beam of macromolecules at last? *International Journal of Mass Spectrometry and Ion Processes,* 136**,** 167-180.

Winterhalter, R., M. Kippenberger, J. Williams, E. Fries, K. Sieg & G. K. Moortgat (2009) Concentrations of higher dicarboxylic acids C 5–C 13 in fresh snow samples collected at the High Alpine Research Station Jungfraujoch during CLACE 5 and 6. *Atmospheric Chemistry and Physics,* 9**,** 2097-2112.

Wisthaler, A., N. Jensen, R. Winterhalter, W. Lindinger & J. Hjorth (2001) Measurements of acetone and other gas phase product yields from the OH-initiated oxidation of terpenes by proton-transfer-reaction mass spectrometry (PTR-MS). *Atmospheric Environment,* 35**,** 6181-6191.

Wozniak, A. S., J. E. Bauer, R. L. Sleighter, R. M. Dickhut, P. G. Hatcher (2008) Molecular characterization of aerosol-derived water soluble organic carbon using ultrahigh resolution electrospray ionization Fourier transform ion cyclotron resonance mass spectrometry. *Atmospheric Chemistry and Physics,* 8**,** 5099-5111.

Xiang, X., C. Y. Ko & H. Guh (1996) Ion-exchange chromatography/electrospray mass spectrometry for the identification of organic and inorganic species in topiramate tablets. *Analytical chemistry,* 68**,** 3726-3731.

Yasmeen, F., R. Szmigielski, R. Vermeylen, Y. Gómez-González, J. D. Surratt, A. W. Chan, J. H. Seinfeld, W. Maenhaut & M. Claeys (2011) Mass spectrometric characterization of isomeric terpenoic acids from the oxidation of α-pinene, β-pinene, d-limonene, and Δ3-carene in fine forest aerosol. *Journal of Mass Spectrometry,* 46**,** 425-442.

Yasmeen, F., R. Vermeylen, R. Szmigielski, Y. Iinuma, O. Böge, H. Herrmann, W. Maenhaut & M. Claeys (2010) Terpenylic acid and related compounds: precursors for dimers in secondary organic aerosol from the ozonolysis of α-and β-pinene. *Atmospheric Chemistry and Physics,* 10**,** 9383-9392.

Yassine, M. M., M. Harir, E. Dabek-Zlotorzynska & P. Schmitt-Kopplin (2014) Structural characterization of organic aerosol using Fourier transform ion cyclotron resonance mass spectrometry: aromaticity equivalent approach. *Rapid Communications in Mass Spectrometry,* 28**,** 2445-2454.

Zhang, Q., J. L. Jimenez, M. Canagaratna, J. Allan, H. Coe, I. Ulbrich, M. Alfarra, A. Takami, A. Middlebrook & Y. Sun (2007) Ubiquity and dominance of oxygenated species in organic aerosols in anthropogenically-influenced Northern Hemisphere midlatitudes. *Geophysical Research Letters,* 34.

Zhang, X. & P. McMurry (1987) Theoretical analysis of evaporative losses from impactor and filter deposits. *Atmospheric Environment (1967),* 21**,** 1779-1789.

Zhang, X. & P. H. McMurry (1991) Theoretical analysis of evaporative losses of adsorbed or absorbed species during atmospheric aerosol sampling. *Environmental science & technology,* 25**,** 456-459.

Zhang, X., R. C. McVay, D. D. Huang, N. F. Dalleska, B. Aumont, R. C. Flagan & J. H. Seinfeld (2015) Formation and evolution of molecular products in α-pinene secondary organic aerosol. *Proceedings of the National Academy of Sciences,* 112**,** 14168-14173.

Zhang, Y., L. Zheng, X. Liu, T. Jickells, J. N. Cape, K. Goulding, A. Fangmeier & F. Zhang (2008) Evidence for organic N deposition and its anthropogenic sources in China. *Atmospheric Environment,* 42**,** 1035-1041.

Zhao, Y., A. Hallar & L. Mazzoleni (2013) Atmospheric organic matter in clouds: exact masses and molecular formula identification using ultrahigh-resolution FT-ICR mass spectrometry. *Atmospheric Chemistry and Physics,* 13**,** 12343-12362.

Zhu, L., G. Gamez, H. Chen, K. Chingin & R. Zenobi (2009) Rapid detection of melamine in untreated milk and wheat gluten by ultrasound-assisted extractive electrospray ionization mass spectrometry (EESI-MS). *Chemical Communications***,** 559-561.

Zielinski, A. T., M. Kalberer, R. L. Jones, A. Prasad & A. A. Seshia. 2016. Particulate mass sensing with piezoelectric bulk acoustic mode resonators. In *Frequency Control Symposium (IFCS), 2016 IEEE International*, 1-6. IEEE.

Zielinski, A. T., I. Kourtchev, C. Bortolini, S. J. Fuller, C. Giorio, O. A. Popoola, S. Bogialli, A. Tapparo, R. L. Jones & M. Kalberer (2018) A new processing scheme for ultra-high resolution direct infusion mass spectrometry data. *Atmospheric Environment,* 178**,** 129-139.

Ziemann, P. J. & R. Atkinson (2012) Kinetics, products, and mechanisms of secondary organic aerosol formation. *Chemical Society Reviews,* 41**,** 6582-6605.

Àvila i Castells, A. & F. Roda (1991) Red rains as major contributors of nutrients and alkalinity to terrestrial ecosystems at Montseny (NE Spain). *Orsis: organismes i sistemes,* 6**,** 215-229.

12 APPENDICES

Appendix A. Statistical Tests used during Data Analysis.

A.1 Linear Regression Analysis

Linear Regression Analysis was used in Chapters 0 and 7 of this thesis to identify significant relationships between the dependent and independent variables. It is often used when underlying theory or empirical graphical analysis indicates that a linear relationship exists between an independent and dependent variable.

The Coefficient of Determination, R^2, is equivalent to the square of the Pearson Correlation Coefficient (r) and used to provide a measure of the goodness of fit of the dependent variable to the regression line. The R^2 value varies between 0 and +1, a value closer to 1 has a better fit, and thus a stronger linear relationship. It indicates how much of the variance of the dependent variable can be accounted for by the regression equation (Lauder 2008). An adjusted version of the Coefficient of Determination, known as *Adjusted R Square* is provided in this analysis as it accounts for the number of terms in the model so provides a more conservative value and allows for easier comparison with other models with different numbers of independent and dependent variables (OriginLab 2019).

Using an *F-test* in regression analysis allows the user to compare the fit of different of different linear models. The F-test has a benefit over the *t-test* in that the F-test can assess multiple coefficients simultaneously whereas a t-test can only assess one regression coefficient at a time.

The *F-test of Overall Significance* is a specific form of the F-test, used in linear regression. It compares the user-specified linear fit with the intercept-only model and provides a formal hypothesis test of the strength of the relationship between the dependent variable and the linear fit. The null hypothesis for the F-test of overall significance is that the fit of the intercept-only model and the user-specified model are equal. The alternative hypothesis for the F-test is that the fit of the intercept-only model and the user-specified model are significantly different. The F-test of overall significance is the F-test value quoted in this thesis.

The *p-value* for the F-test indicates whether the linear fit is statistically-significant or not. A significance level of significance of 0.05 was used. A p-value of less than 0.05 indicates that the null hypothesis can be rejected and the user-specified model and the intercept-only model are statistically-significantly different (Editor 2019).

A.2 T-tests.

T-tests were used in Chapters 5 and 6 of this thesis to determine if there were significant differences between the means of two different data populations such as the number of aromatic compounds in the rainwater and aerosol samples and during different seasons. Student t-tests are the most common statistical tests used when comparing two normally distributed, independent data sets.

The null hypothesis was that the two samples were from the same population and there was no significant difference between the means. The alternative hypothesis was that the two samples were significantly different and the difference was not due to chance. For each comparison, a t-value was generated for the two samples in question using a t-test, for two samples assuming equal variance, in Microsoft Excel. If the t-value equaled or exceeded the *critical t-value* at a probability level of 5% then the null hypothesis was rejected. A p-value with a significance level of 0.05 was also used with the t-tests. A p-value of greater than or equal to 0.05 indicated that there was at least a 5% chance of the difference in the two sample means being due to chance and the null hypothesis was accepted. A p-value of less than 0.05 was used to reject the null hypothesis and accept the alternative hypothesis that the two groups are significantly different and the difference is not due to chance (Lauder 2008).

Appendix B. Total aerosol concentrations and size distributions for the different mixed organic and inorganic solutions in the WSOC/AS characterisation experiments.

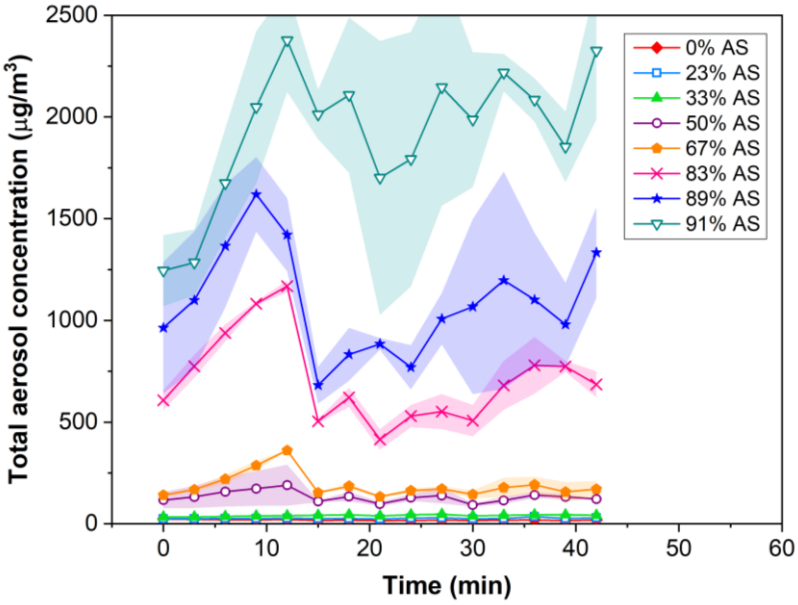

Figure B.1. Time series of the total aerosol concentration for each WSOC/AS solution. Data points shown are averaged over two experiments with error bars denoting ± 1 standard deviation.

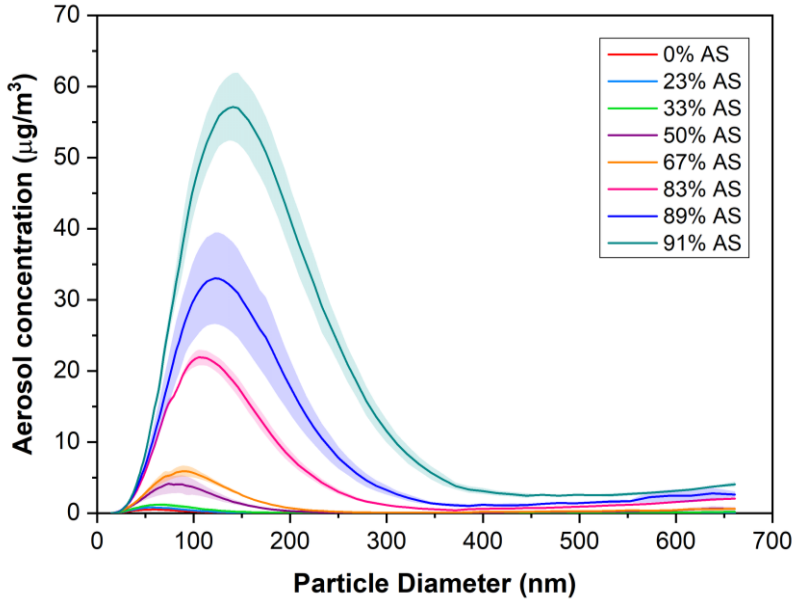

Figure B.2. Size distribution of the aerosol produced for the WSOC/AS solutions. Particle diameters between 14.6 and 661.2 nm were separated into 106 size bins by the DMA and the aerosol mass concentrations recorded for each bin via the CPC. The thick lines represent the average concentration in that size bin for the duration of the experiment and ± 1 standard deviation is represented as shading.

Appendix C. Mass values used in Equation 3.3 for calculating the WSOC mass fractions, w_{WSOC}, for the WSOC/AS characterisation experiments.

Table C.1. Individual WSOC molar masses and masses in the WSOC/AS solutions.

WSOC/AS	Molar Mass, M_{WSOC}, (g/mol)	Mass of WSOC in each solution, m_{WSOC}, (g)	Total WSOC mass ($m_{TotalWSOC}$) (g)
Oxalic acid	90.03	0.90	7.51
Salicylic acid	138.12	1.38	
Maleic acid	116.07	1.16	
Glutaric acid	132.12	1.32	
Arabitol	152.14	1.52	
Erythritol	122.12	1.22	
AS	132.14	-	-

Table C.2. Molar percentage of ammonium sulphate (AS) and mass of AS in each solution.

AS molar percentage (%)	Mass of AS in each solution, m_{AS} (g)
0	0
23	2.38
33	3.96
50	7.93
67	15.86
83	39.64
89	63.43
91	79.28

Appendix D. WSOC aerosol concentration for the WSOC/AS characterisation experiments.

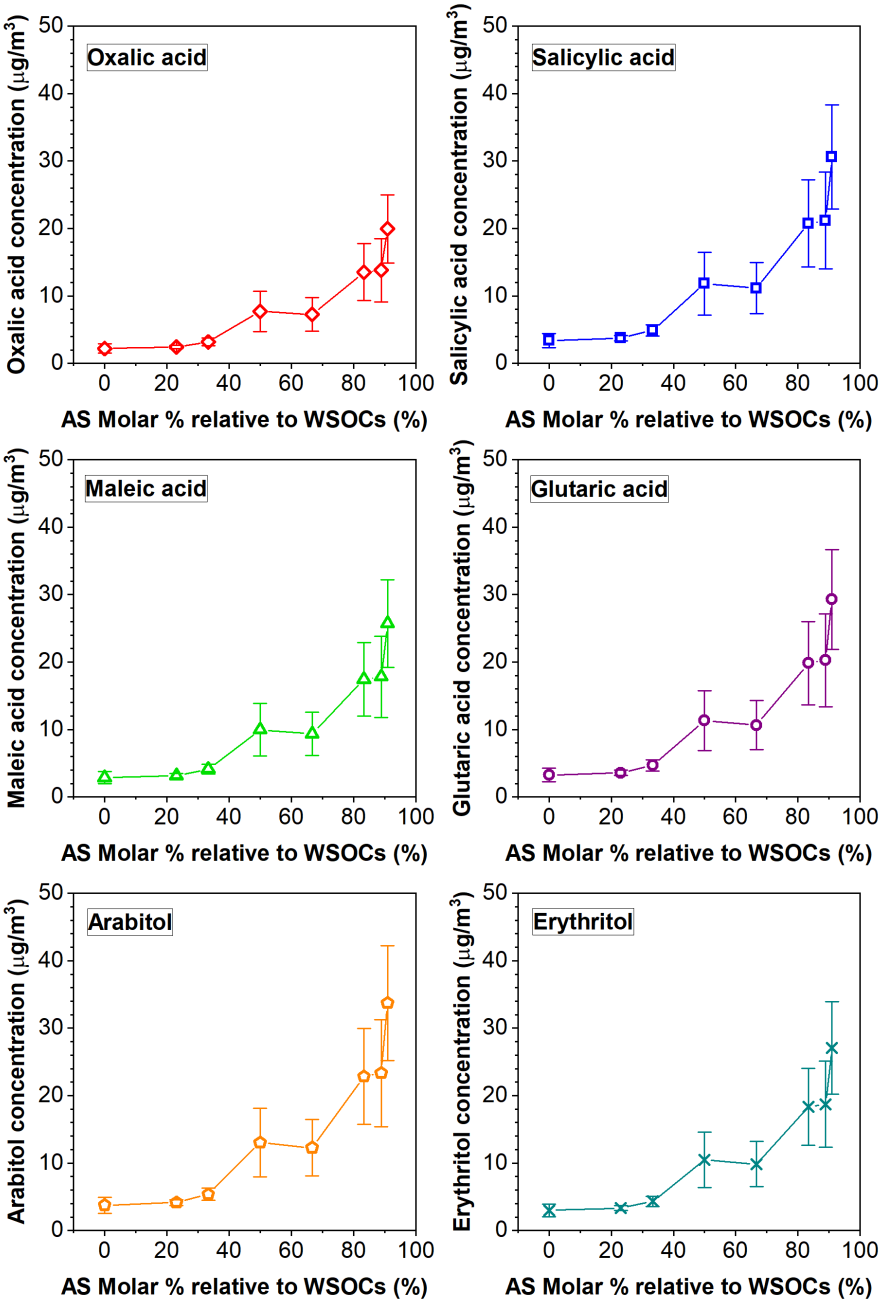

Figure D. Weighted aerosol mass concentrations for each WSOC calculated using the mass fraction of each WSOC and the total aerosol concentration measured using the SMPS. Presented data points are an average of two experiments for each WSOC/AS solution and error bars denote ± 1 standard deviation.

Appendix E. Correlation between *cis*-pinonic acid (CPA)-weighted aerosol mass concentration, and EESI-MS detected intensity for CPA.

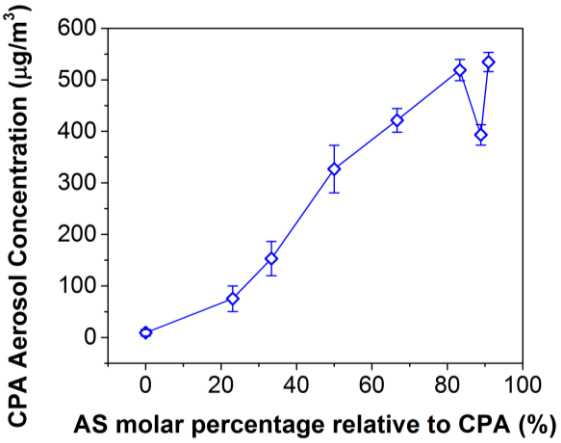

Figure E.1. Weighted aerosol mass concentration for *cis*-pinonic acid (CPA), calculated using the mass fraction of CPA and the total aerosol concentration measured using the SMPS and expressed as a function of increasing molar percentage of ammonium sulphate (%). Each data point is averaged over 42 measurements in a single experiment for each CPA/AS solution and error bars denote ± 1 standard deviation.

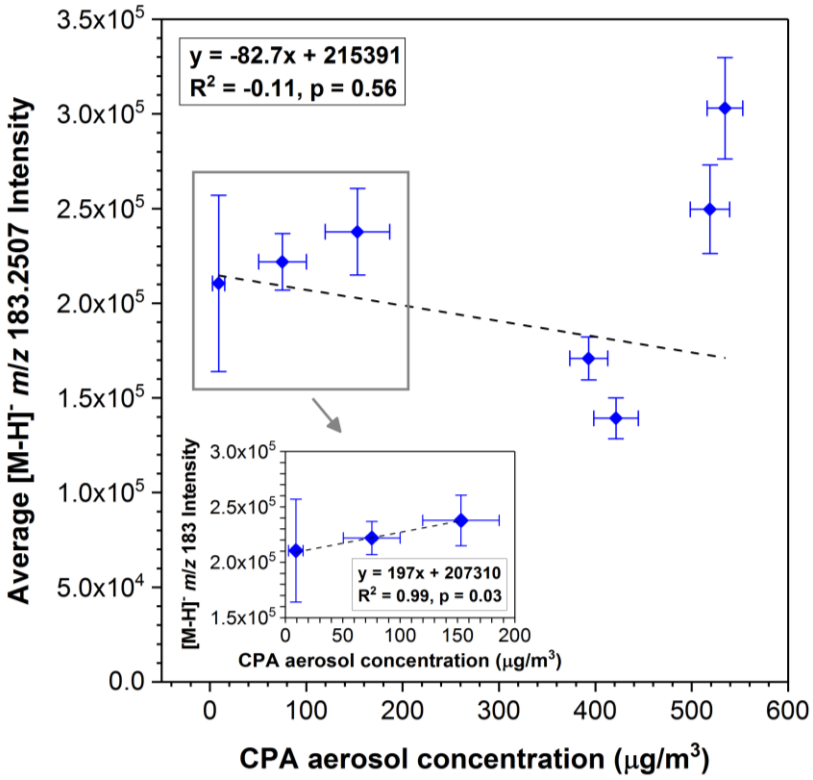

Figure E.2. (−)EESI-MS deprotonated CPA ion ($[M-H]^-$ *m/z* 183.2507) as a function of the weighted CPA aerosol concentration, calculated using the molar mass of CPA and the total aerosol concentration measured by the SMPS. Inset highlights linear relationship at lower CPA aerosol concentrations (~9–155 μg/m^3).

Appendix F. Reference compounds used to calculate the mass shift of each spectrum in the first data processing code for the AERORAIN Campaign and pre-campaign rainwater and aerosol samples.

Table F. The measured mass errors of 20 reference compounds, expected to occur in the solvents and ambient organic samples, were obtained from previous experiments based on source and polarity used. These values were used to evaluate the mass shift for each mass spectrum in the test and main AERORAIN campaign rainwater and aerosol samples, during the data processing described in 4.5.2.

Neutral Molecular Formula
$C_8H_{13}O_2$
$C_9H_{17}O_2$
$C_{10}H_{19}O_2$
$C_{12}H_{23}O_2$
$C_{14}H_{27}O_2$
$C_{15}H_{29}O_2$
$C_{16}H_{31}O_2$
$C_{18}H_{33}O_2$
$C_{18}H_{35}O_2$
$C_{16}H_{25}O_3S$
$C_{17}H_{27}O_3S$
$C_{18}H_{29}O_3S$
$C_{19}H_{31}O_3S$
$C_{20}H_{33}O_6S$
$C_2H_3O_3$
$C_{32}H_{43}O_2$
$C_9H_{13}O_4$
$C_{10}H_{15}O_3$
$C_{10}H_{15}O_4$
$C_{18}H_{29}O_7$

Appendix G. Comparison of total number of formulae assignments in test rainwater and aerosol samples following application of three different types of Solid Phase Extraction (SPE) sorbent, and no SPE application.

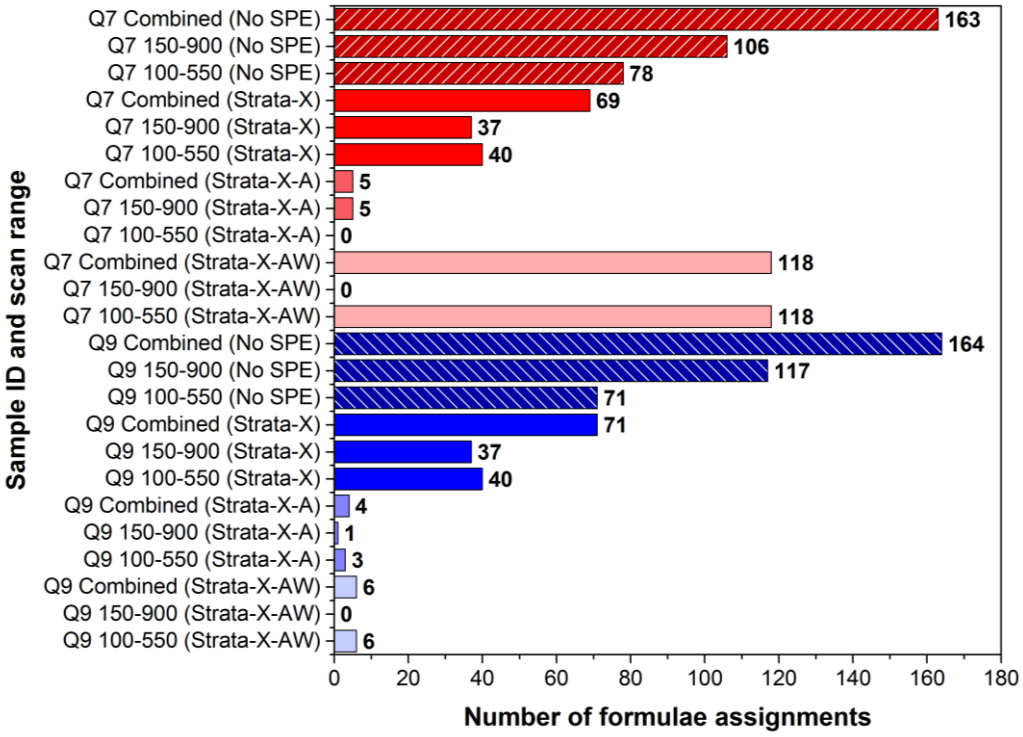

Figure G. Number of formulae assignments in the Q7 and Q9 test aerosol samples. The values for the individual scan ranges; *m*/*z* 100–550 and *m*/*z* 150–900, are shown as well as for the combined spectra. Each sample was split into four sub-samples; three sub-samples had SPE applied with three different SPE sorbent types and the fourth sub-sample had no SPE applied for comparison.

Appendix H. Direct infusion (−)nano-ESI-MS mass spectra for formulae sub groups detected for the AERORAIN 2016 rainwater and aerosol samples.

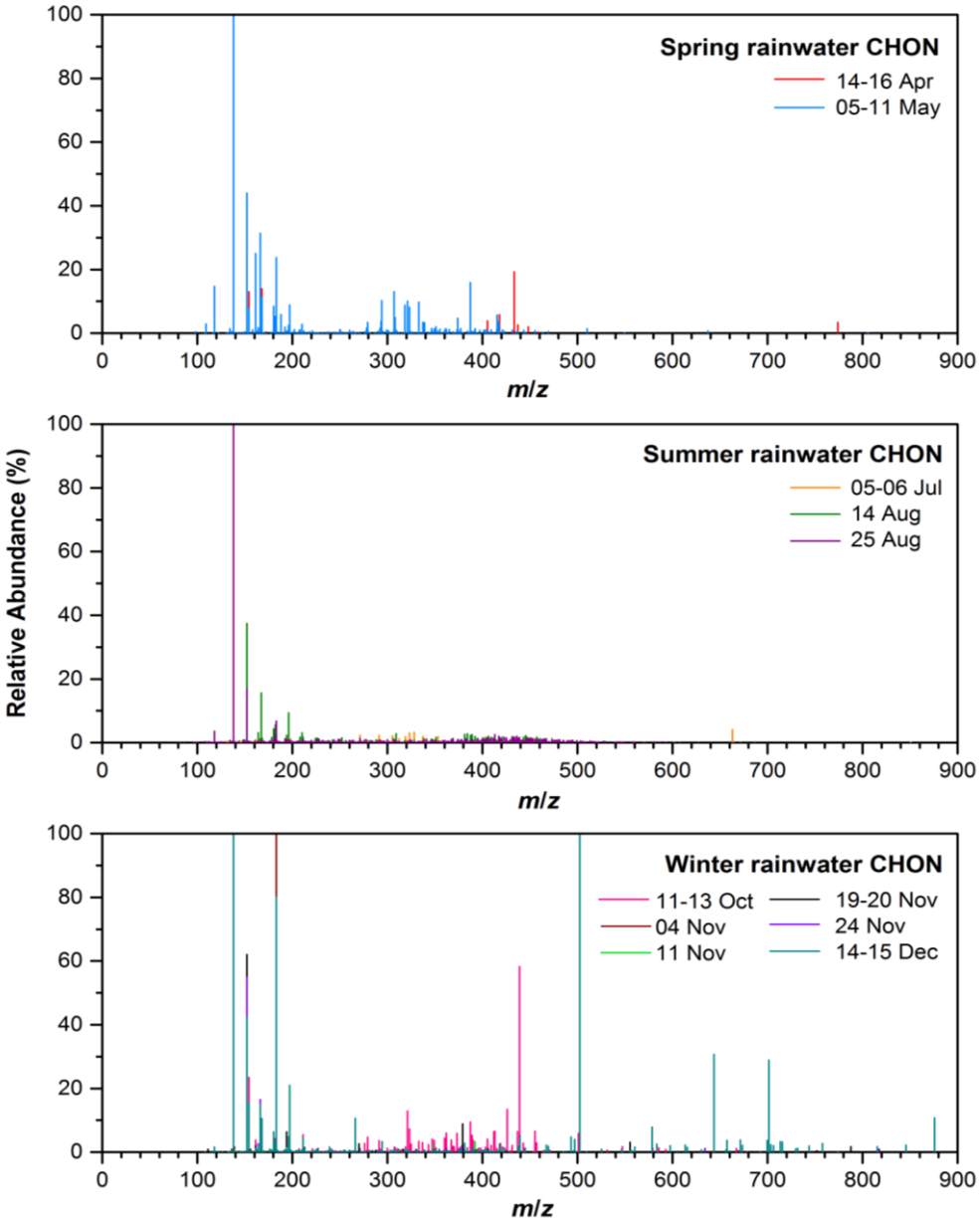

Figure H.1. Reconstructed (−)ESI mass spectra showing common ions for the CHON compounds only in the rainwater samples across spring, summer and winter 2016. Samples are colour coded according to the rain events they were collected during.

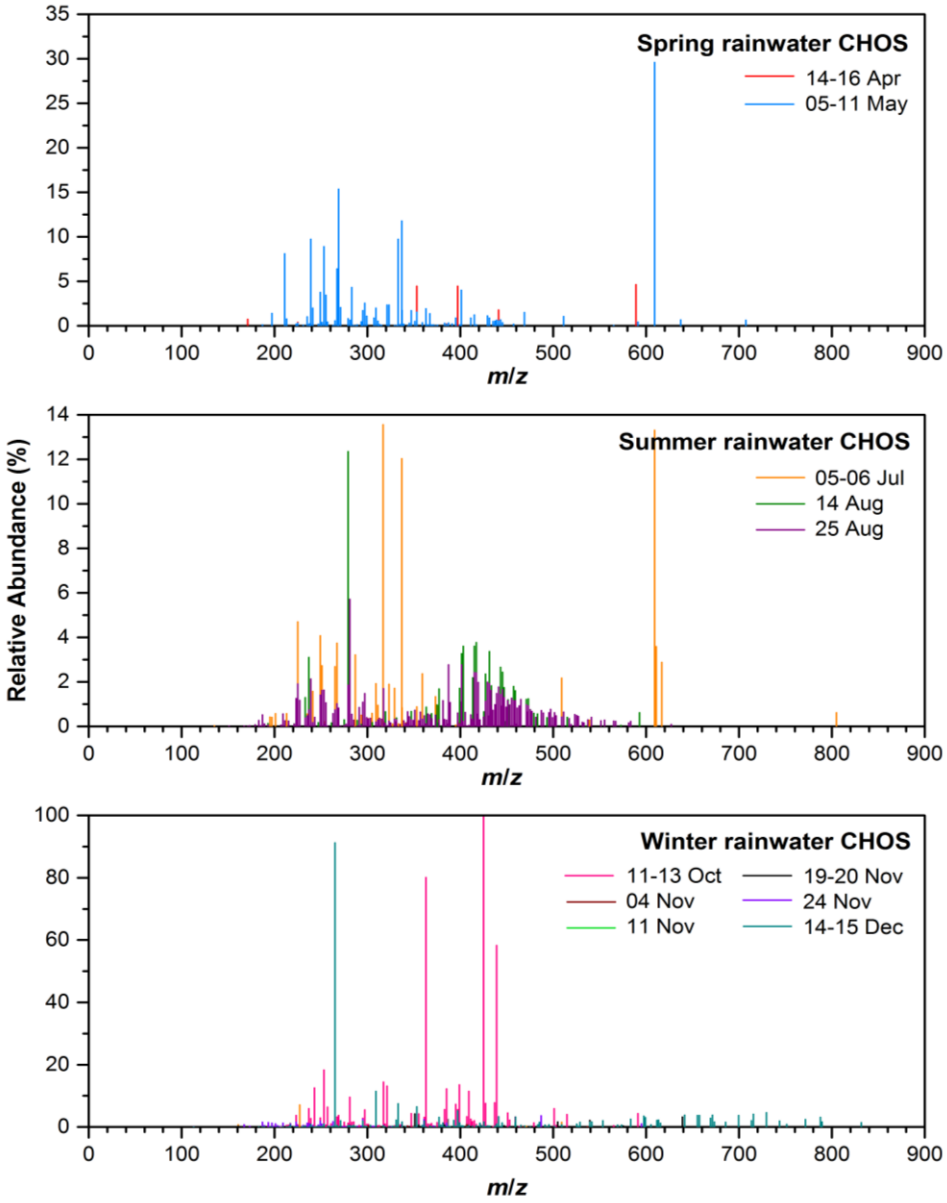

Figure H.2. Reconstructed (−)ESI mass spectra showing common ions for the CHOS compounds only in the rainwater samples across spring, summer and winter 2016. Samples are colour coded according to the rain events they were collected during.

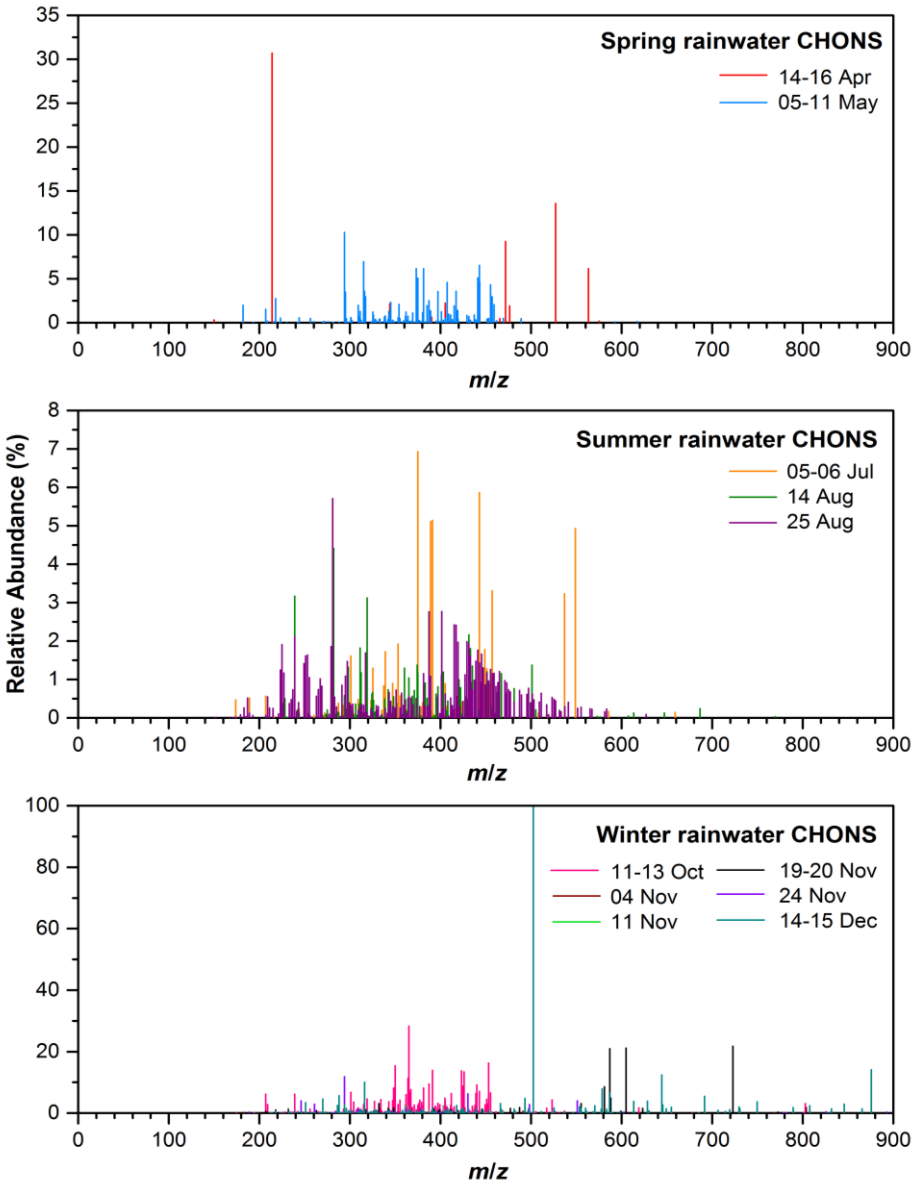

Figure H.3. Reconstructed (−)ESI mass spectra showing common ions for the CHONS compounds only in the rainwater samples across spring, summer and winter 2016. Samples are colour coded according to the rain events they were collected during.

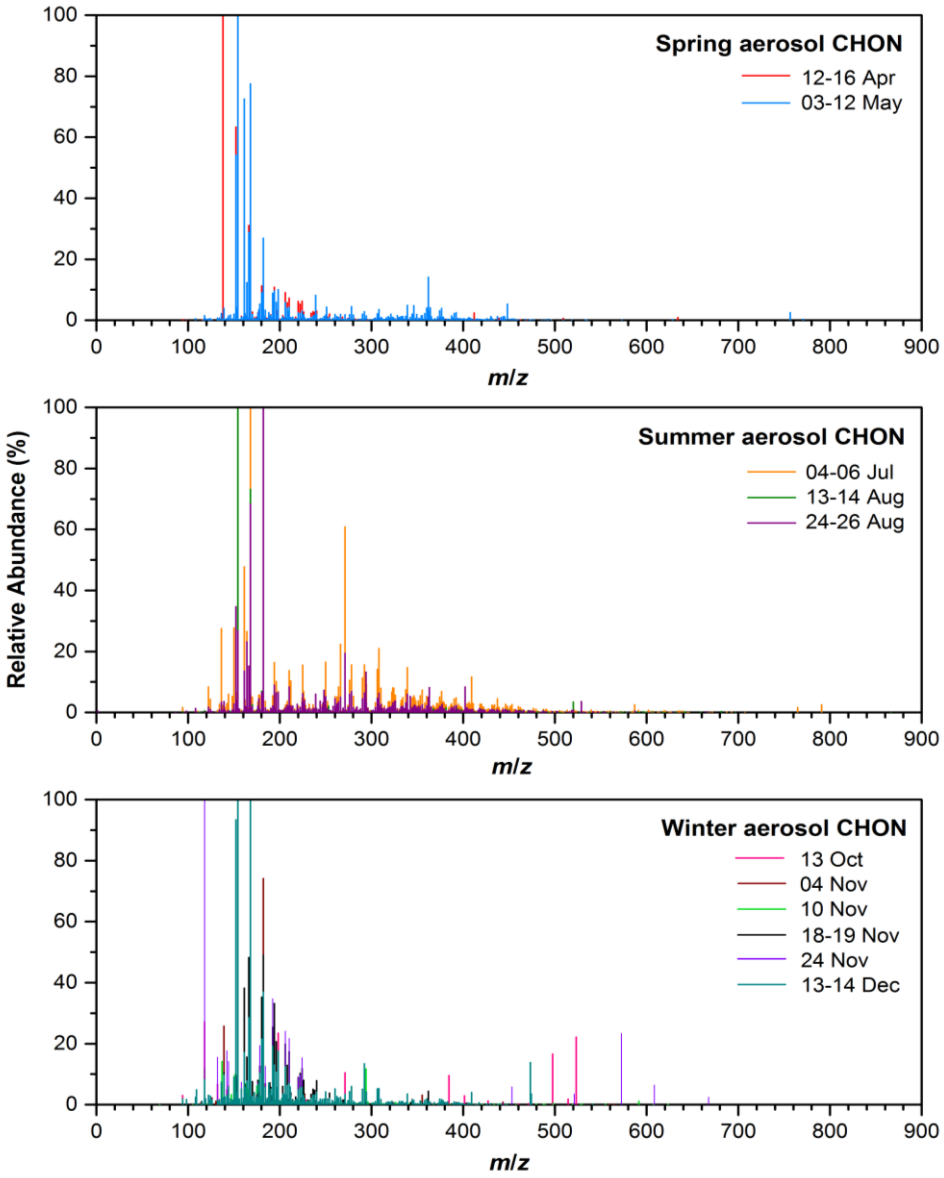

Figure H.4. Reconstructed (−)ESI mass spectra showing common ions for the CHON compounds only in the aerosol samples across spring, summer and winter 2016. Samples are colour coded according to the rain events they were collected during.

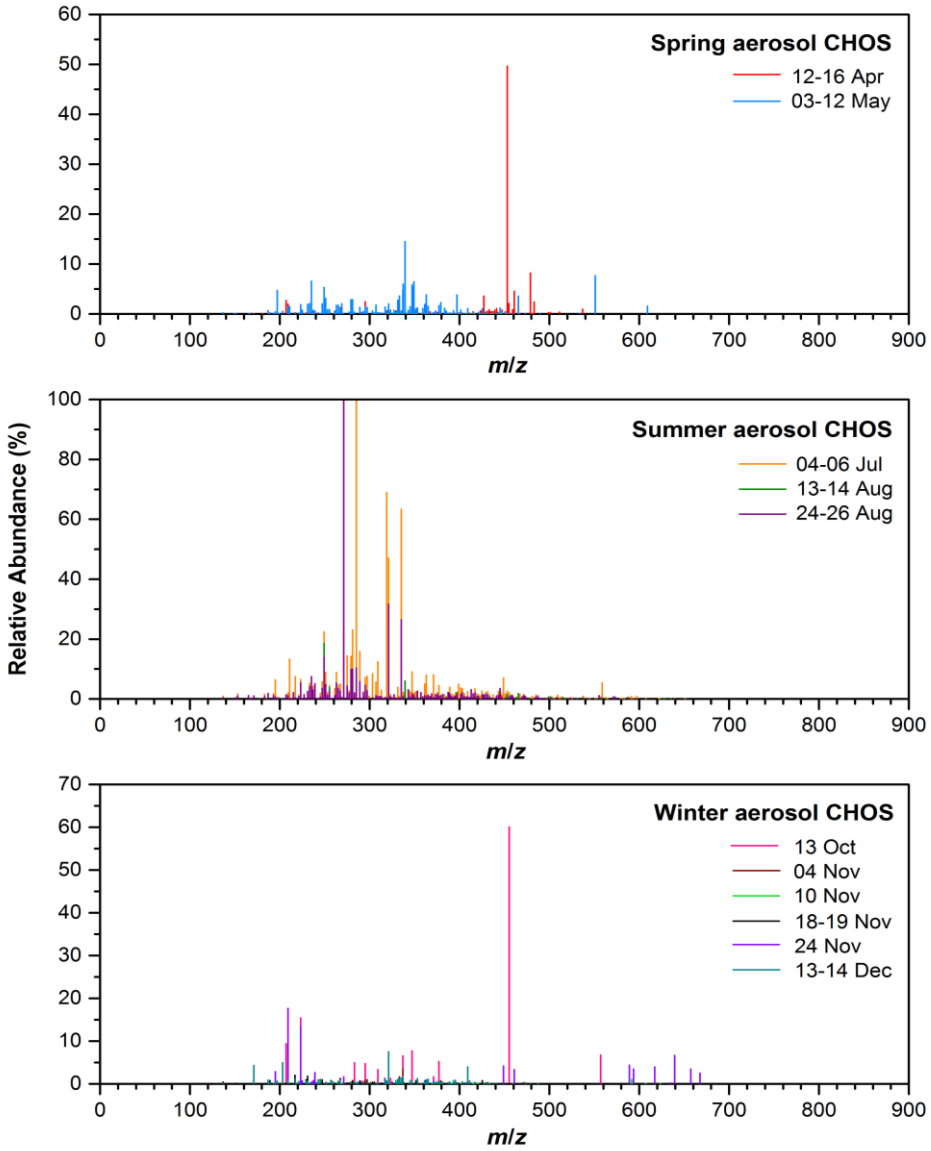

Figure H.5. Reconstructed (−)ESI mass spectra showing common ions for the CHOS compounds only in the aerosol samples across spring, summer and winter 2016. Samples are colour coded according to the rain events they were collected during.

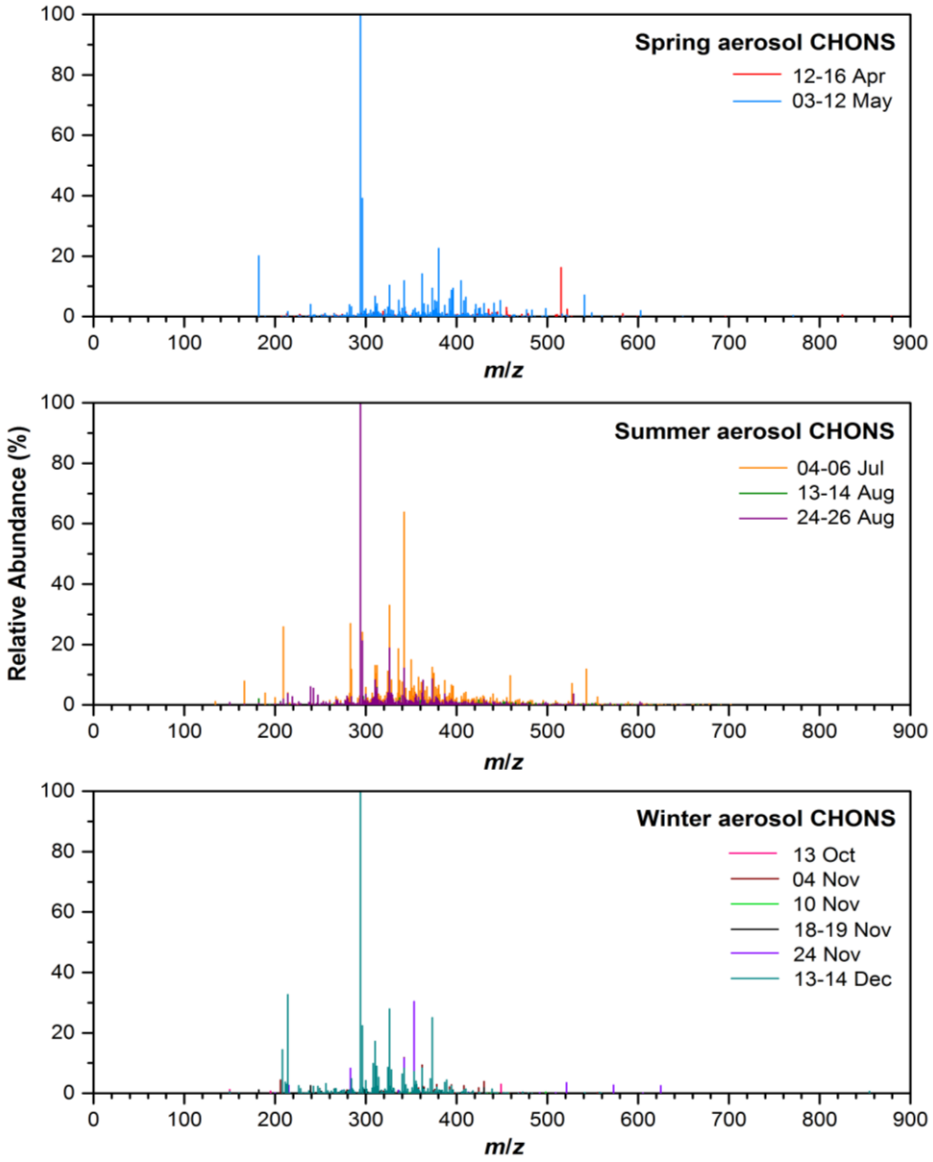

Figure H.6. Reconstructed (−)ESI mass spectra showing common ions for the CHONS compounds only in the aerosol samples across spring, summer and winter 2016. Samples are colour coded according to the rain events they were collected during.

Appendix I. SO_4^{2-}, NH_4^+, NO_3^- and NO_2^- concentrations measured for the 24 hr aerosol samples.

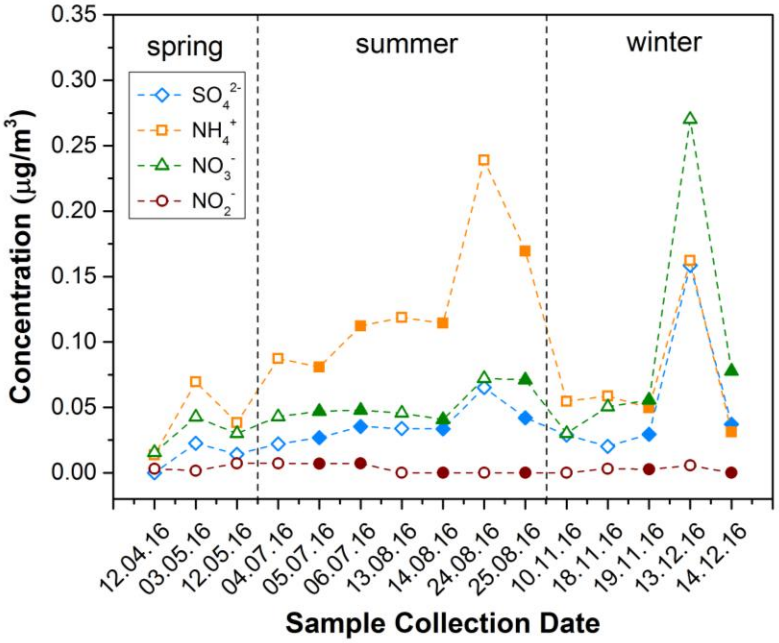

Figure I. Sulphate, ammonium, nitrate and nitrite concentrations for the 24 hr aerosol collected in León, regardless of whether a rain event occurred or not.

Appendix J. Van Krevelen plots for rainwater and aerosol samples collected in León, across different seasons.

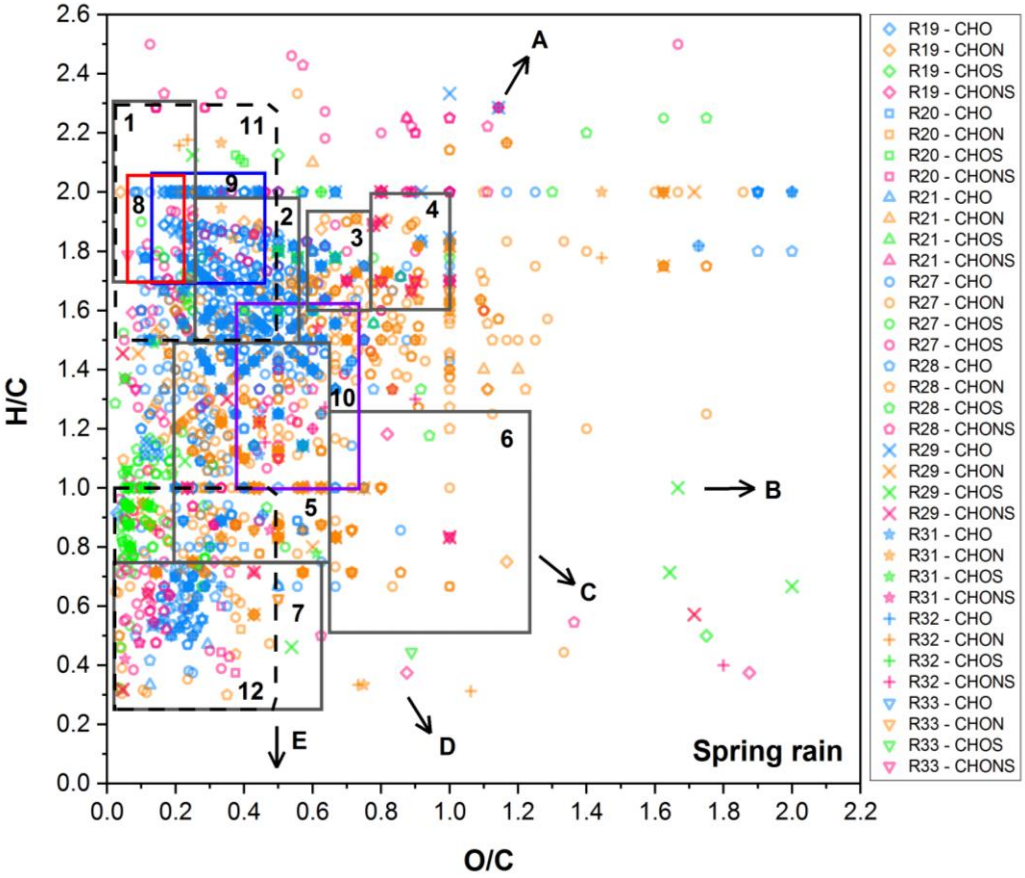

Figure J.1. Van Krevelen plots showing oxygen to carbon (O/C) and hydrogen to carbon (H/C) elemental ratios for CHO (blue), CHON (orange), CHOS (green) and CHONS (pink) compounds in every spring rain sample from León. Boxes represent potential sources of molecular classes. Grey boxes: (1) Lipids, (2) Proteins, (3) Aminosugars, (4) Cellulose, (5) Lignin, (6) Tannins, (7) Poly-Aromatic Hydrocarbons. Red box (8) and blue box (9) are monocarboxylic and dicarboxylic acids respectively. Purple box (10) is SOA and dashed boxes (11) and (12) are aliphatic and aromatic compounds respectively. Arrows indicate potential chemical reactions; (A) hydration, gradient = 2, (B) addition of OH group, gradient = 0, (C) simultaneous addition of C=O and OH group, gradient = −1, (D) replacement of CH_2 group with C=O group, gradient = −2, (E) dehydrogenation, gradient = −4.

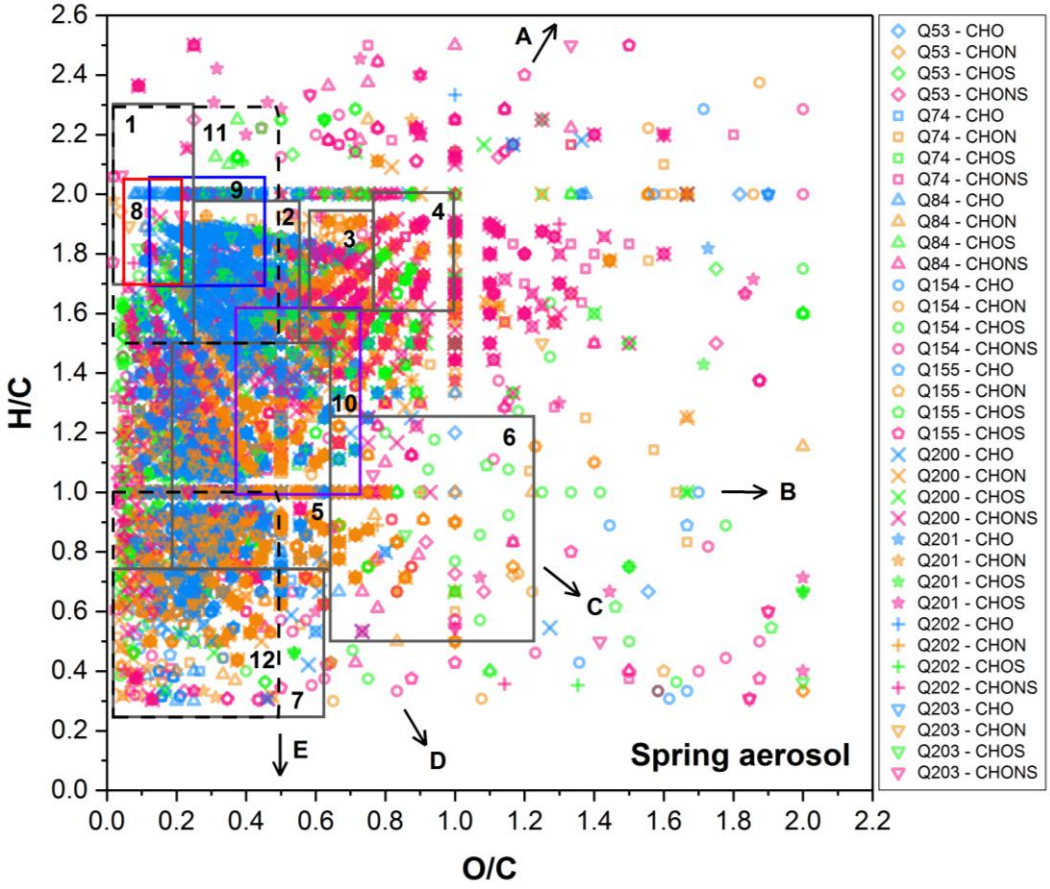

Figure J.2. Van Krevelen plots showing oxygen to carbon (O/C) and hydrogen to carbon (H/C) elemental ratios for CHO (blue), CHON (orange), CHOS (green) and CHONS (pink) compounds in every spring aerosol sample from León. Boxes represent potential sources of molecular classes. Grey boxes: (1) Lipids, (2) Proteins, (3) Aminosugars, (4) Cellulose, (5) Lignin, (6) Tannins, (7) Poly-Aromatic Hydrocarbons. Red box (8) and blue box (9) are monocarboxylic and dicarboxylic acids respectively. Purple box (10) is SOA and dashed boxes (11) and (12) are aliphatic and aromatic compounds respectively. Arrows indicate potential chemical reactions; (A) hydration, gradient = 2, (B) addition of OH group, gradient = 0, (C) simultaneous addition of C=O and OH group, gradient = −1, (D) replacement of CH_2 group with C=O group, gradient = −2, (E) dehydrogenation, gradient = −4.

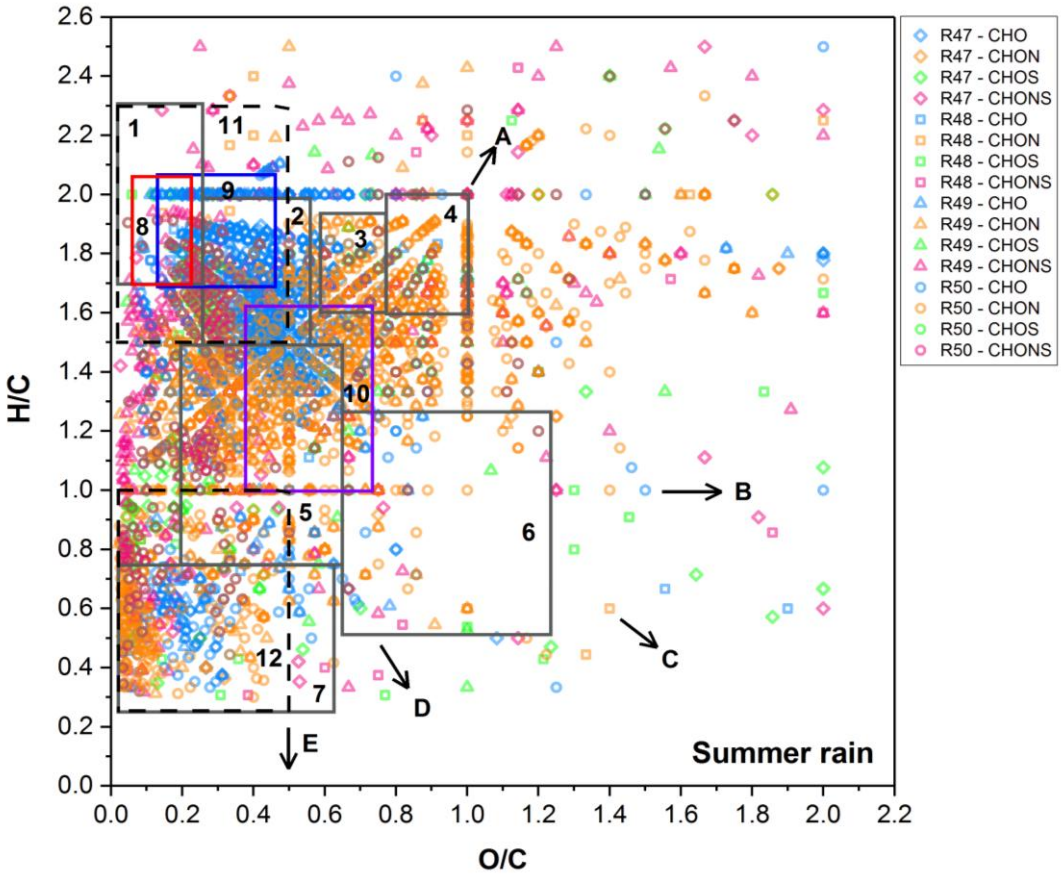

Figure J.3. Van Krevelen plots showing oxygen to carbon (O/C) and hydrogen to carbon (H/C) elemental ratios for CHO (blue), CHON (orange), CHOS (green) and CHONS (pink) compounds in every summer rain sample from León. Boxes represent potential sources of molecular classes. Grey boxes: (1) Lipids, (2) Proteins, (3) Aminosugars, (4) Cellulose, (5) Lignin, (6) Tannins, (7) Poly-Aromatic Hydrocarbons. Red box (8) and blue box (9) are monocarboxylic and dicarboxylic acids respectively. Purple box (10) is SOA and dashed boxes (11) and (12) are aliphatic and aromatic compounds respectively. Arrows indicate potential chemical reactions; (A) hydration, gradient = 2, (B) addition of OH group, gradient = 0, (C) simultaneous addition of C=O and OH group, gradient = −1, (D) replacement of CH_2 group with C=O group, gradient = −2, (E) dehydrogenation, gradient = −4.

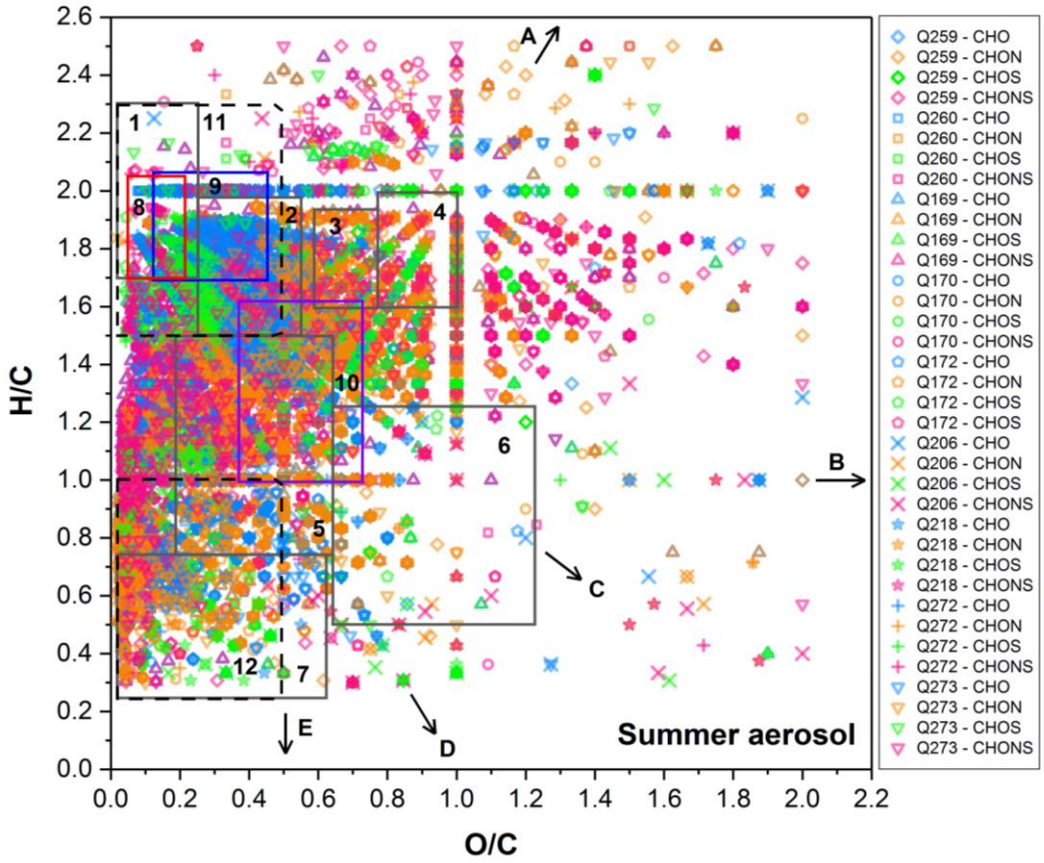

Figure J.4. Van Krevelen plots showing oxygen to carbon (O/C) and hydrogen to carbon (H/C) elemental ratios for CHO (blue), CHON (orange), CHOS (green) and CHONS (pink) compounds in every summer aerosol sample from León. Boxes represent potential sources of molecular classes. Grey boxes: (1) Lipids, (2) Proteins, (3) Aminosugars, (4) Cellulose, (5) Lignin, (6) Tannins, (7) Poly-Aromatic Hydrocarbons. Red box (8) and blue box (9) are monocarboxylic and dicarboxylic acids respectively. Purple box (10) is SOA and dashed boxes (11) and (12) are aliphatic and aromatic compounds respectively. Arrows indicate potential chemical reactions; (A) hydration, gradient = 2, (B) addition of OH group, gradient = 0, (C) simultaneous addition of C=O and OH group, gradient = −1, (D) replacement of CH_2 group with C=O group, gradient = −2, (E) dehydrogenation, gradient = −4.

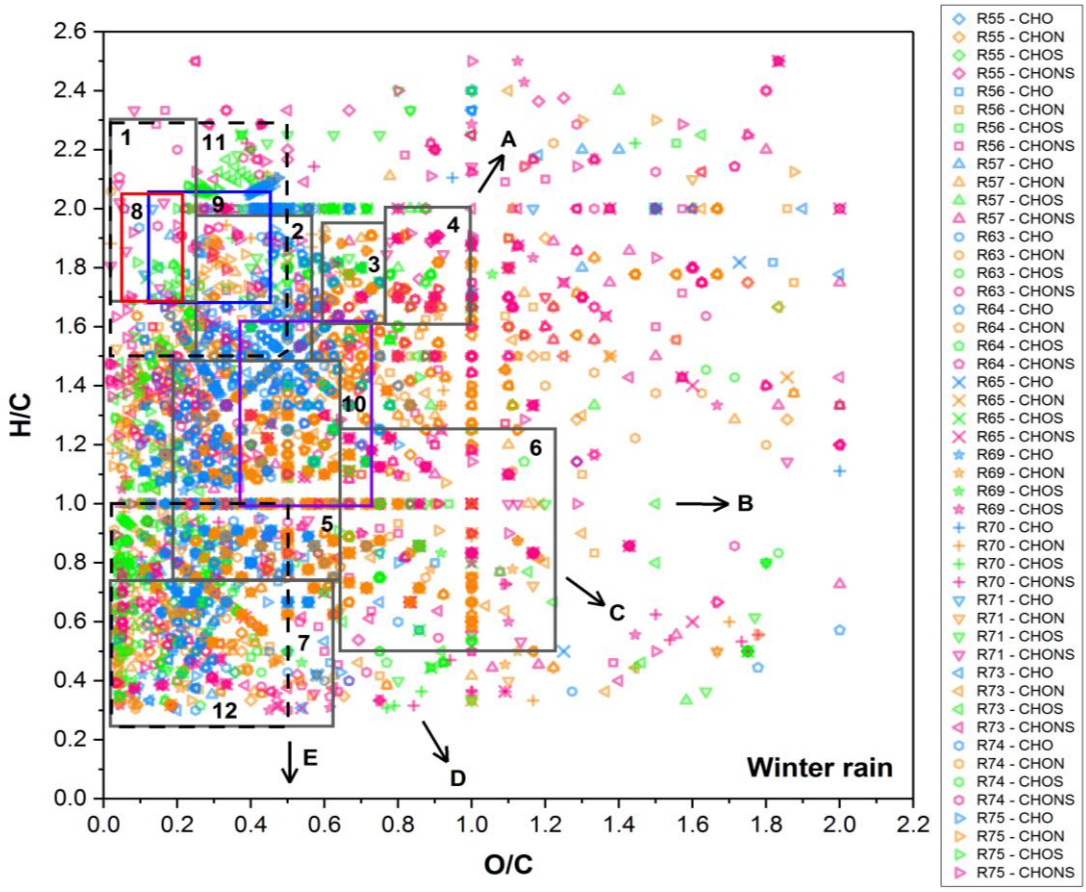

Figure J.5. Van Krevelen plots showing oxygen to carbon (O/C) and hydrogen to carbon (H/C) elemental ratios for CHO (blue), CHON (orange), CHOS (green) and CHONS (pink) compounds in every winter rain sample from León. Boxes represent potential sources of molecular classes. Grey boxes: (1) Lipids, (2) Proteins, (3) Aminosugars, (4) Cellulose, (5) Lignin, (6) Tannins, (7) Poly-Aromatic Hydrocarbons. Red box (8) and blue box (9) are monocarboxylic and dicarboxylic acids respectively. Purple box (10) is SOA and dashed boxes (11) and (12) are aliphatic and aromatic compounds respectively. Arrows indicate potential chemical reactions; (A) hydration, gradient = 2, (B) addition of OH group, gradient = 0, (C) simultaneous addition of C=O and OH group, gradient = −1, (D) replacement of CH_2 group with C=O group, gradient = −2, (E) dehydrogenation, gradient = −4.

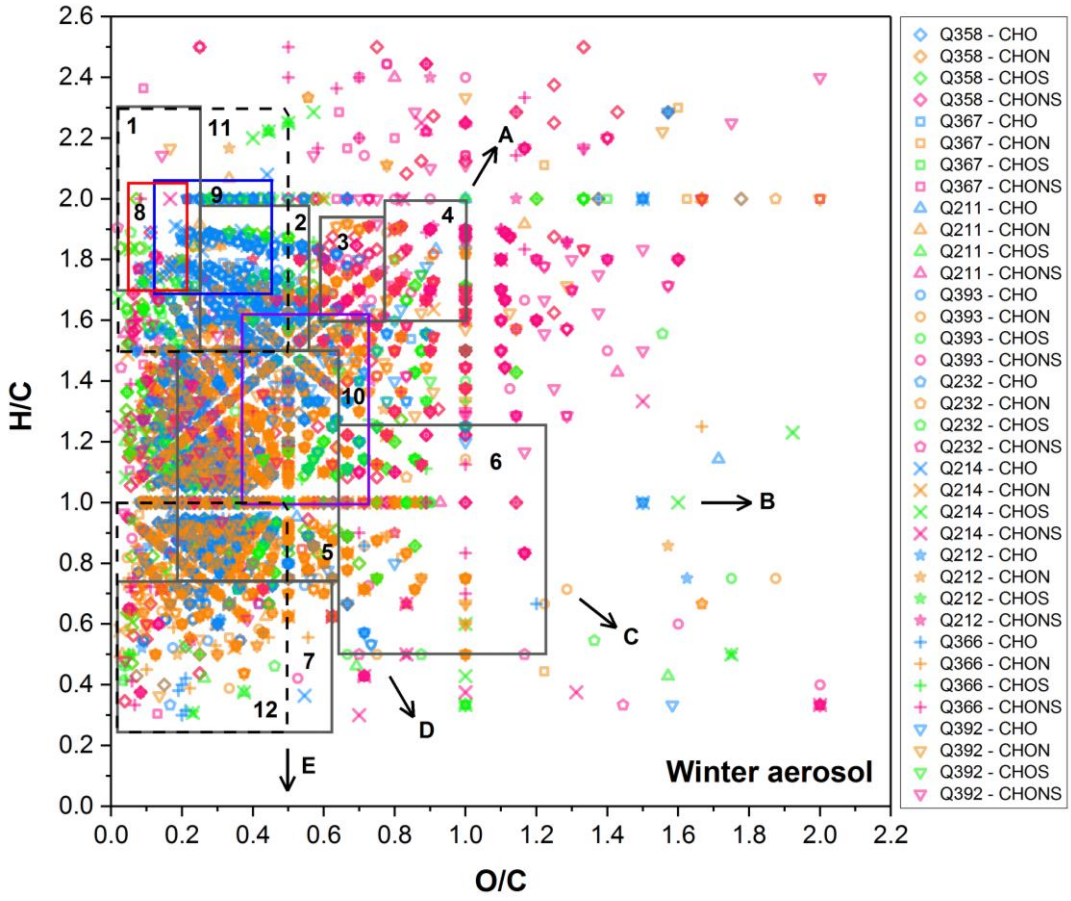

Figure J.6. Van Krevelen plots showing oxygen to carbon (O/C) and hydrogen to carbon (H/C) elemental ratios for CHO (blue), CHON (orange), CHOS (green) and CHONS (pink) compounds in every winter aerosol sample from León. Boxes represent potential sources of molecular classes. Grey boxes: (1) Lipids, (2) Proteins, (3) Aminosugars, (4) Cellulose, (5) Lignin, (6) Tannins, (7) Poly-Aromatic Hydrocarbons. Red box (8) and blue box (9) are monocarboxylic and dicarboxylic acids respectively. Purple box (10) is SOA and dashed boxes (11) and (12) are aliphatic and aromatic compounds respectively. Arrows indicate potential chemical reactions; (A) hydration, gradient = 2, (B) addition of OH group, gradient = 0, (C) simultaneous addition of C=O and OH group, gradient = −1, (D) replacement of CH_2 group with C=O group, gradient = −2, (E) dehydrogenation, gradient = −4.

Appendix K. HYSPLIT Air mass backward trajectories used to classify air mass origins influencing León samples.

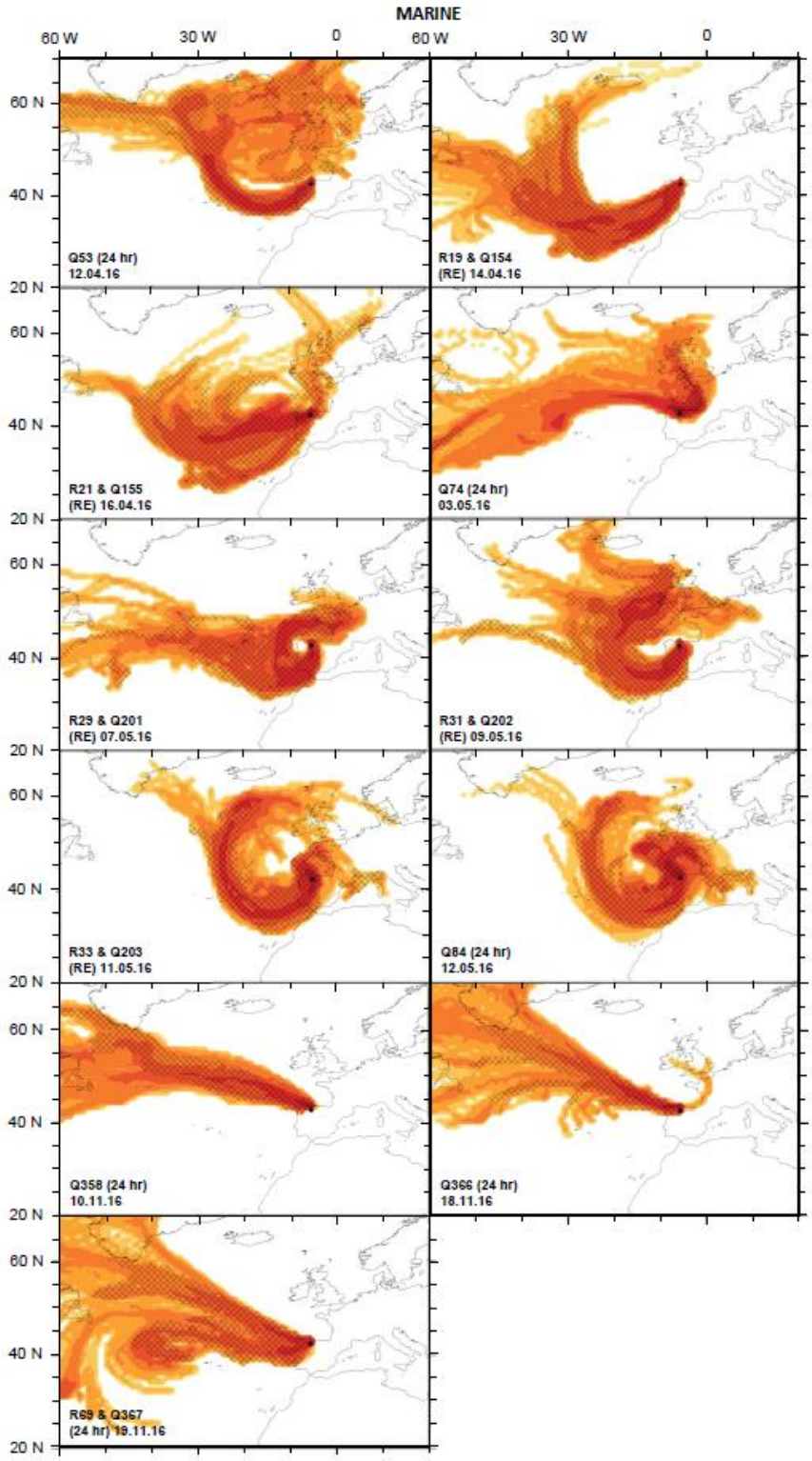

Figure K.1. Marine-influenced HYSPLIT air mass backward trajectories run for 5 days from the sampling start time (10:00 UTC for 24 hour samples or as close as possible to the sampling start time of the samples collected during the rain event) at altitudes of 500 m, 1500 m and 3000 m (Dr C Rae, Cambridge).

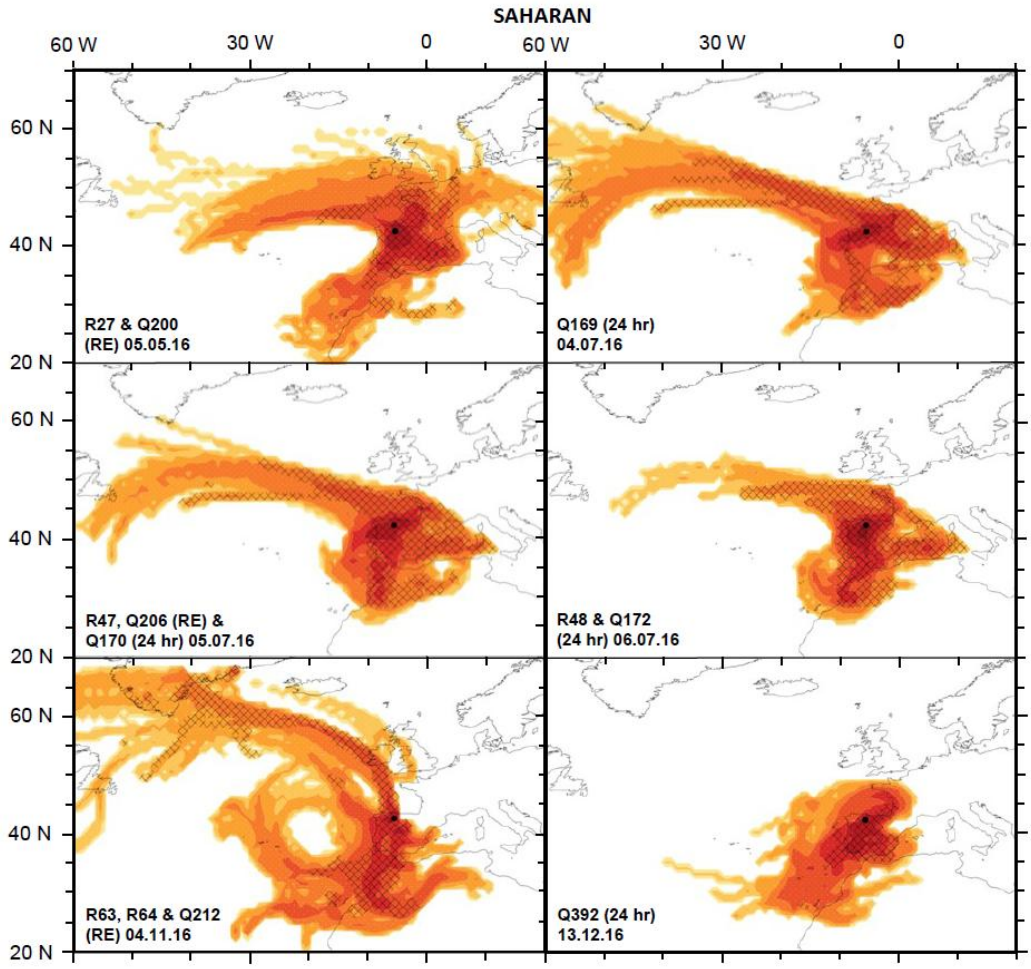

Figure K.2. Saharan-influenced HYSPLIT air mass back trajectories run for 5 days from the sampling start time (10:00 UTC for 24 hour samples or as close as possible to the sampling start time of the samples collected during the rain event) at altitudes of 500 m, 1500 m and 3000 m (Dr C Rae, Cambridge).

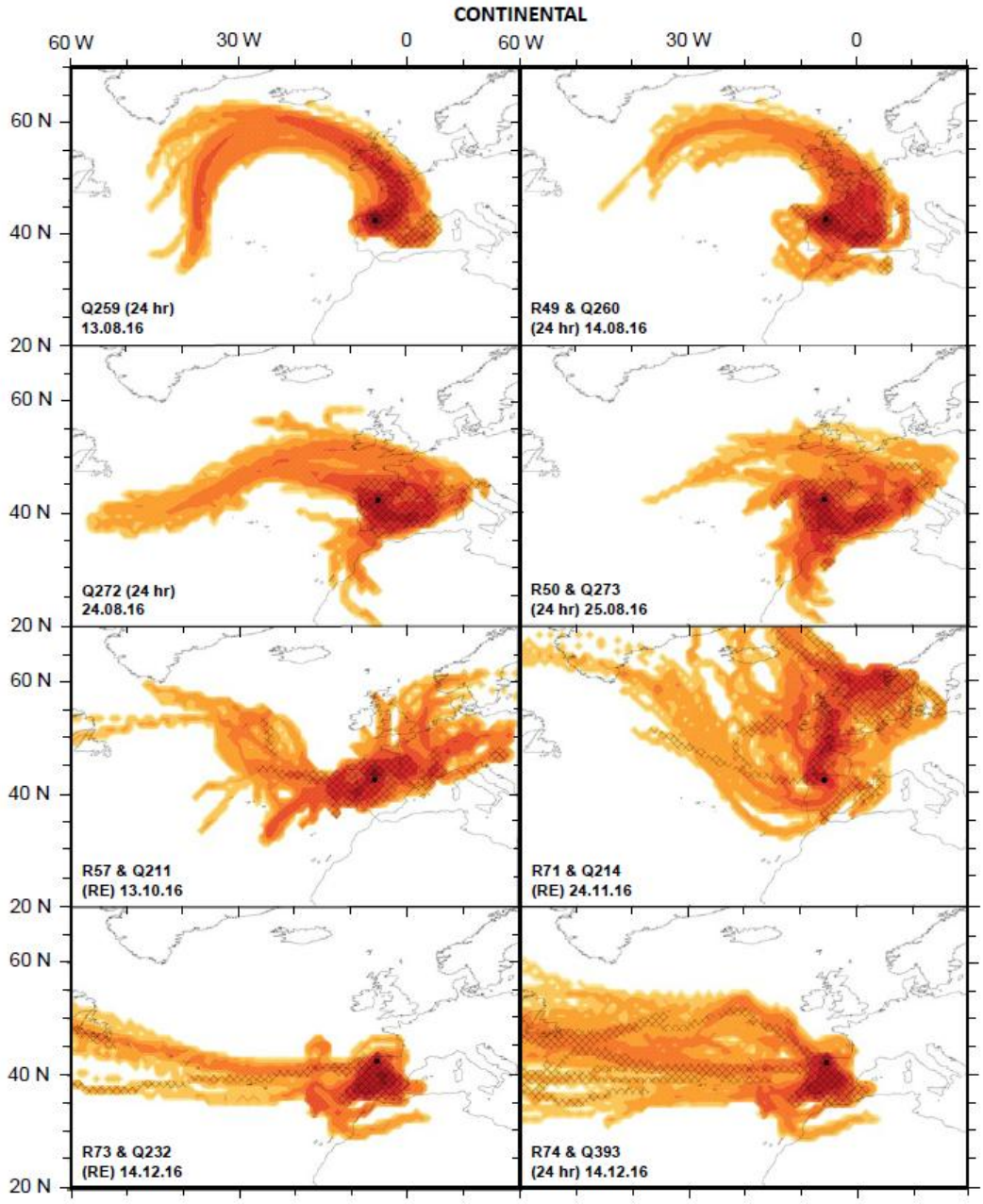

Figure K.3. Continental-influenced HYSPLIT air mass back trajectories run for 5 days from the sampling start time (10:00 UTC for 24 hour samples or as close as possible to the sampling start time of the samples collected during the rain event) at altitudes of 500 m, 1500 m and 3000 m (Dr C Rae, Cambridge).

Appendix L. Linear correlation between inorganic ion concentrations and CHON compounds in the AERORAIN '24 hr' aerosol samples.

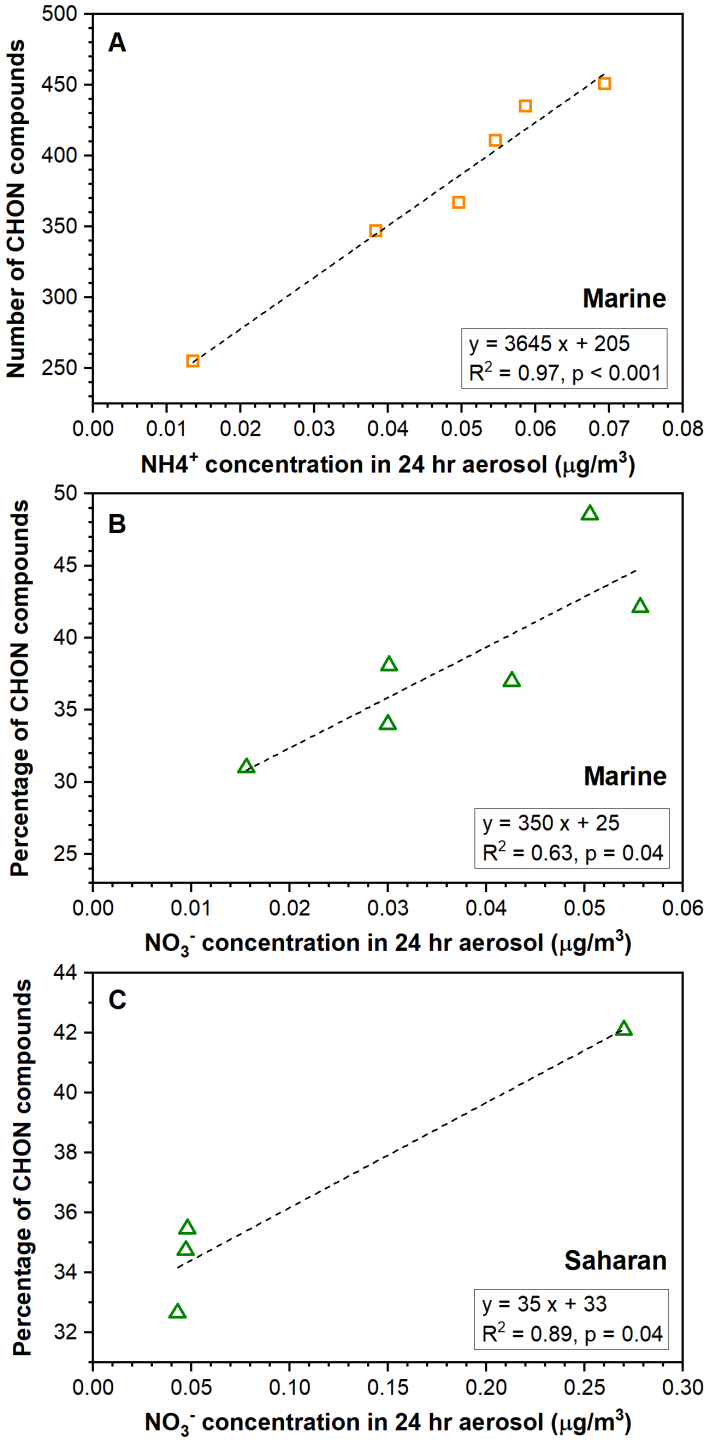

Figure L. Number and percentage of CHON compounds as a function of the corresponding NH_4^+ and NO_3^- concentrations in the marine 24 hr aerosol (A and B respectively); and (C) the percentage of CHON compounds and the NO_3^- concentration in the Saharan 24 hr aerosol. F-test linear regression analysis included, using a significance level of 0.05.

Appendix M. Example of Global Forest Watch Fires Fire Alert map used to provide the number of forest fires in Spain during AERORAIN sample collection.

Figure M. Screen shot of the Fire Alert map from the *Global Forest Watch Fire (2018)* 'Fire Report for Spain', showing the number and distribution of forest fires reported in Spain from 14.08.16 to 15.08.16; when the R49 summer rainwater sample was collected. *VIIRS Fires* (red) denote fires detected using the Visible Infrared Imaging Radiometer Suite onboard the Suomi NPP Satellite and *MODIS Fires* (orange) denote fires detected using the Moderate Resolution Imaging Spectroradiometer sensor onboard NASA's Terra and Aqua satellites.

Appendix N. Droplet Profile Experiments for the development of a Cloud or Haze Flow Tube (CFT) for investigating Aqueous SOA Formation and Cloud Processing.

A small-scale Cloud Flow Tube (CFT) has been developed to generate a haze or cloud to allow investigation of aqueous cloud processing of SOA and in particular, processes occurring on short timescales. The system has been designed to be coupled to EESI-MS and an SMPS or OPC for real time aerosol composition and droplet size distribution and concentration measurements.

N.1 Methodology

The CFT is shown in Figure N.1. A 7.8 L glass tube (length = 0.86 m, diameter = 0.11 m, reaction volume = 7.45 L), was fitted with two separate inlets to allow independent introduction of water droplets from a nebuliser and aerosol from a chamber or another source which are then incorporated into the water droplets. Five outlets position along the top and at the end of the CFT allow the system to be coupled to EESI-MS to measure changes in aerosol composition in real time and to an SMPS Spectrometer or OPC to monitor changes in cloud droplet size distribution and concentration during the cloud lifetime.

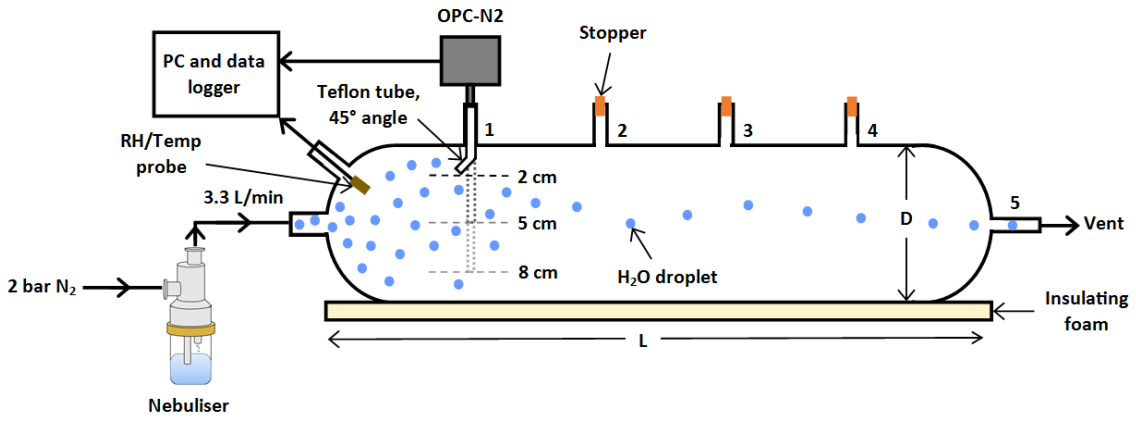

Figure N.1. Experimental set-up used for droplet radial profile experiments. A constant output nebuliser generates a fine spray of water droplets (blue) into the Cloud Flow Tube (CFT) via a central inlet. An OPC monitors the size distribution and droplet concentration from five outlets and at 2 cm, 5 cm and 8 cm from the point of injection.

Droplet radial profile experiments were conducted using the set-up in Figure N.1 to determine if there were any differences in the cloud droplet number concentration and size distribution in different areas of the CFT once the cloud was generated, for example due to evaporation, which could affect the rate of reaction when aerosol was generated. The following procedure was used. An OPC (OPC-N2, Alphasense Ltd.) was used to record the background droplet count per second and size distribution for 20 minutes. A nebuliser (same as the one described in 3.3.1.1), filled with water (HPLC grade, Fisher Scientific), then sprayed water droplets into the CFT via the central inlet, at a flow rate of 3.3 L/min under 2 bar of nitrogen, for 30 minutes. The nebuliser was then switched off and the OPC continued to measure the droplet count/s and size distribution for a further 20 minutes.

This procedure was carried out twice for outlets 1–5 and at three different depths; 2 cm, 5 cm and 8 cm, using a piece of Teflon tubing at a 45° angle to sample the haze from each depth. RH and temperature measurements were made using a humidity sensor (Sensirion, model SHT1x). During these experiments, the flow tube was placed on insulating foam and polystyrene, away from the cold bench surface, to prevent a temperature difference between the top and bottom of the CFT which could affect the water droplet distribution. The CFT was also dried with N_2 for 20 minutes in between each experiment to evaporate any water which had collected on the bottom of the CFT.

The OPC-N2 used for these experiments classifies up to ~10,000 particles per second, assigning each particle to one of 16 size bins, ranging from 0.38 to 17.5 µm in diameter, shown in Table N. (Alphasense 2015). An elliptical mirror and photodetector is used to measure the light scattered by individual droplets as the sample air stream passes through a laser beam at 1.2 L/min. This scattering is calibrated based on Mie scattering theory and is used to determine the particle size and particle number concentration. PM_1, $PM_{2.5}$ and PM_{10} mass loading are then calculated from the particle concentration and size spectra data, assuming a particle density of 1.65 g/ml and a refractive index of 1.5+i0.

Table N. Particle size bins used by the Alphasense OPC-N2 to generate the aerosol size distribution.

Bin number	Particle diameter size range (µm)
0	0.38 – 0.54
1	0.54 – 0.78
2	0.78 – 1.05
3	1.05 – 1.34
4	1.34 – 1.59
5	1.59 – 2.07
6	2.07 – 3.00
7	3.00 – 4.00
8	4.00 – 5.00
9	5.00 – 6.50
10	6.50 – 8.00
11	8.00 – 10.00
12	10.00 – 12.00
13	12.00 – 14.00
14	14.00 – 16.00
15	16.00 – 17.50

N.2 Results and Discussion

N.2.1 Cloud Droplet Radial Profile

Figure N.2 shows a representative example of the RH, temperature and droplet count/s time series data, collected at a depth of 8 cm, from the 4th outlet on the CFT. The RH increases rapidly when water droplet injection is initiated (blue shading), coinciding with the initial spike in water droplets (black line), and remains constant at ~100% for the duration of the water droplet injection period and for the 20 minutes after the nebuliser was switched off. This is a positive indicator for a stable cloud. The variation in temperature in Figure N.2 (red line) is inversely proportional to the droplet concentration due to the high pressure of the nebuliser producing a cold spray which lowers the temperature of the CFT. This temperature change would need to be

accounted for in future experiments with temperature-dependent or temperature-sensitive reactions.

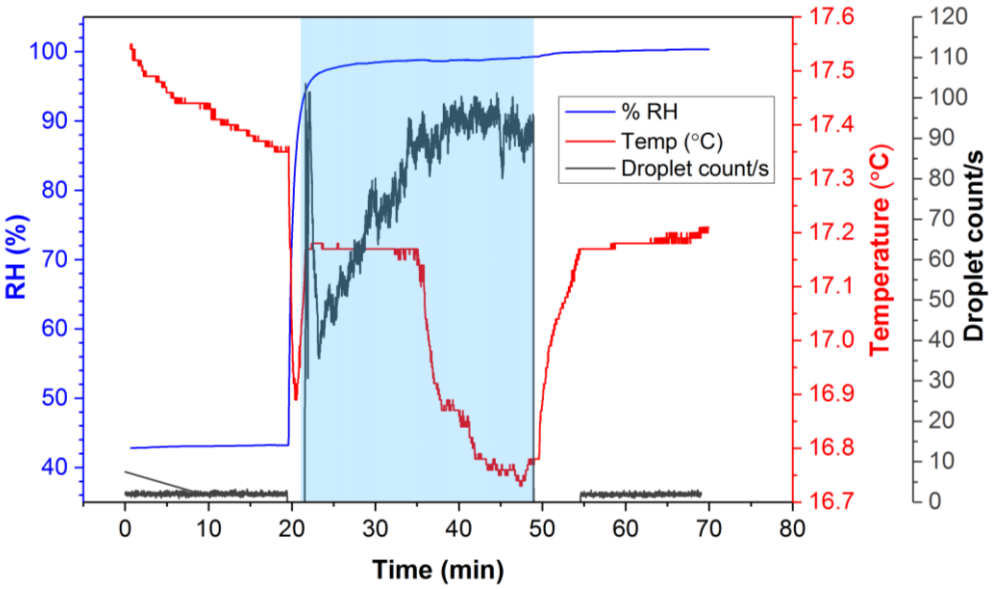

Figure N.2. Time series of RH, temperature and droplet count/s measured by the humidity sensor and OPC 8 cm from the 4th outlet. Blue shading indicates 30 minute period with nebuliser on, injecting water droplets into CFT.

Figure N.3 shows a comparison of the average droplet count for each of the three tested depths from each outlet. The values shown are averaged over two experiments for each outlet and depth. The overall droplet count variation is within a factor of 10, with the majority of the measurements lying within ~30 and 70 droplets/s. This indicates that the droplet concentration remains relatively constant throughout the CFT.

A time series of the droplet counts/s for the last 10 minutes of the 30 minute droplet injection period is shown in Figure N.4 and it shows that the droplet concentration remains relatively constant for the whole 10 minutes. The droplet count/s data for the fourth outlet at 2 cm was inconsistent due to a fault with the OPC and was omitted from Figure N.4. The droplet concentrations for the first outlet in Figure N.4 (orange, red and dark red lines) show more variation during the 10 minutes than the other outlets. This could be due to eddies occurring when the water droplets initially enter the CFT, moving from a smaller diameter into a larger one.

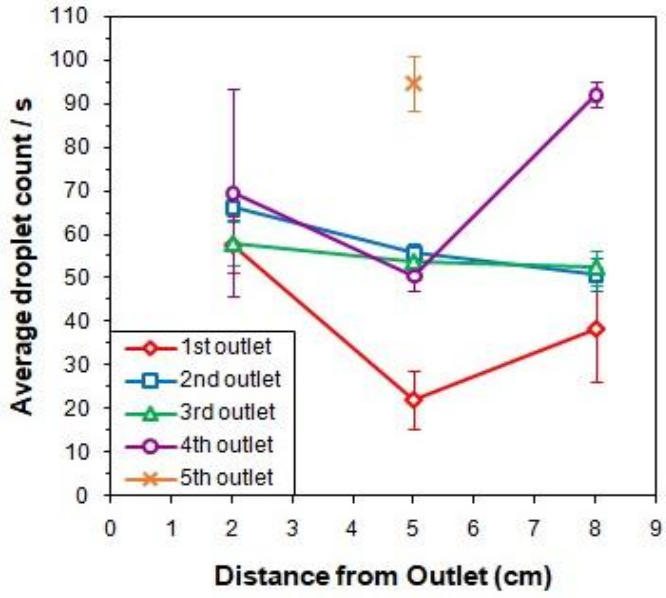

Figure N.3. Average droplet concentration at 2 cm, 5 cm and 8 cm from each outlet. Values averaged over last 10 minutes of water droplet injection period and error bars denote ± 1 standard deviation.

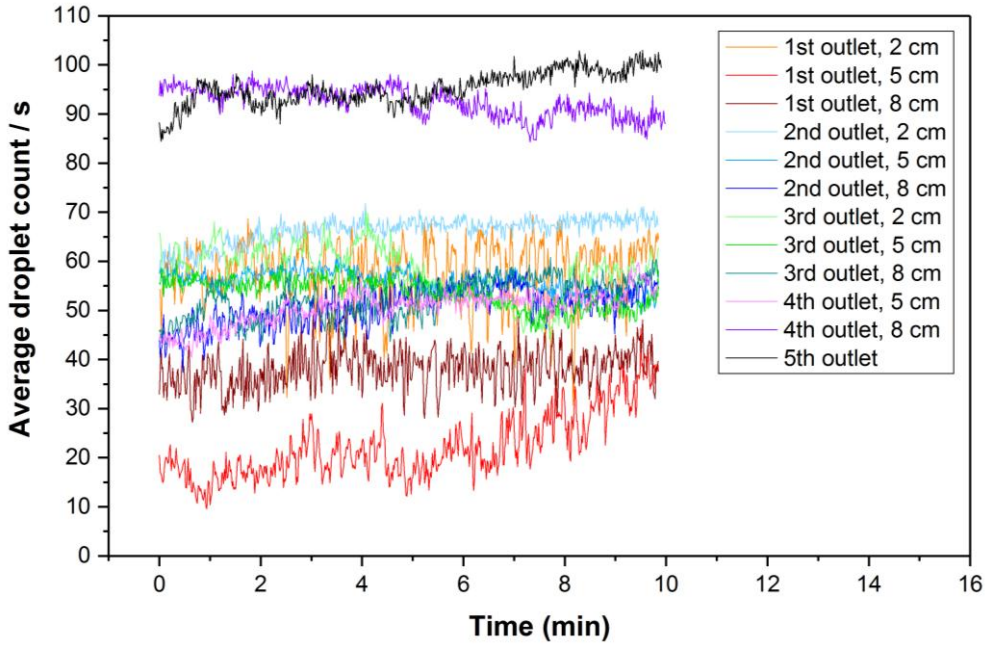

Figure N.4. Time series of droplet counts/sec over the last 10 minutes of the water injection period, measured by the OPC-N2 at 2 cm, 5 cm and 8 cm from the four top CFT outlets and the end (fifth) outlet. Data is averaged over two experiments for each outlet and depth.

Figure N.5 shows the average droplet count/s for each of the 16 particle size bins (defined in Table N.) used by the OPC-N2. The droplet diameters in this study ranged from 2.07 µm to 12.00 µm with the modal size range being 5.0-6.5 µm. The largest droplets in the CFT were measured at 5 cm from the first outlet. This may be due to the close proximity of the first outlet 5 cm sampling point to the central inlet where the droplet spray enters the CFT, which may have resulted in more of the larger droplets being detected before settling to the bottom of the tube. The average droplet number concentration also increases with distance from the point of injection. The first outlet had 624 droplets/s on average whereas the fifth outlet had 1519 droplets/s. This difference is likely a result of turbulences in the CFT which need further detailed flow characterisation experiments and modelling for a complete understanding of the measured evolution of droplet size distribution.

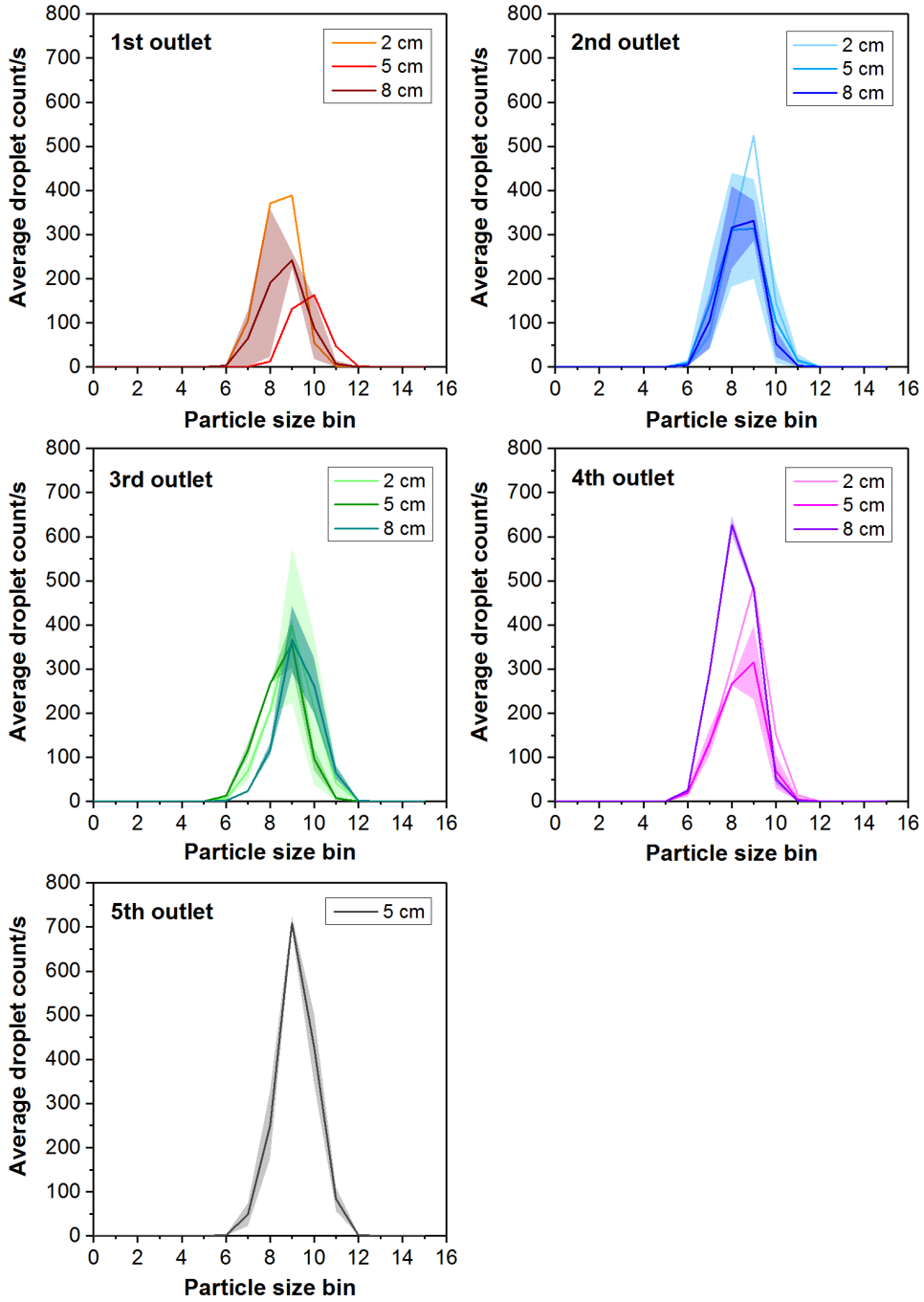

Figure N.5. Average droplet count/s in each of the OPC-N2 16 particle size bins for the last 10 minutes of the water injection period, measured at 2 cm, 5 cm and 8 cm from the five outlets. Data is averaged over two experiments for each outlet and depth and shading denotes ± 1 standard deviation.

N.2.2 Calculation of Reynolds Number and cloud lifetime

The Reynolds number, Re_D, (Reynolds 1883) was calculated to determine if the flow in the CFT was laminar (Re < 2100) or turbulent (Re > 2100) (Bird, Stewart and Lightfoot 1960). Ideally, the flow should be laminar to allow the aerosol to be incorporated into the water droplets and not be lost on the inner walls of the CFT. The Reynolds number, Re_D, for the CFT was calculated using Equation N.1:

$$\mathrm{Re_D} = \frac{\rho v \mathrm{D}}{\mu}, \tag{N.1}$$

where v is the velocity of the stream of water droplets, ρ is the density of the fluid (air, 1.19 kg m^{-3}), D is the diameter of the CFT (0.11 m) and μ is the dynamic viscosity of air (18.2×10^{-6}) Pa.

The velocity of the water droplets, v, was calculated using Equation N.2:

$$v = \frac{\mathrm{Q}}{\mathrm{A}}, \tag{N.2}$$

where Q is the total flow rate (5.5×10^{-5} m^3/s) and A is the cross-sectional area of the CFT (8.83×10^{-3} m^2). This produced a velocity of 6.23×10^{-3} m/s for Equation N.1.

The overall calculated Reynolds number is 43 which is much lower than 2100 and confirms that the flow in the CFT is laminar.

The entrance length, Le, is the distance from the point of injection, after which the flow in the tube becomes fully developed and uniform (Bird et al. 1960) and is a function of Re_D. The calculation for Le in laminar flow is

$$\mathrm{Le} = 0.06\ \mathrm{D}\ \mathrm{Re_D}\ . \tag{N.3}$$

The calculated entrance length for the CFT is 0.28 m. The distance between the central inlet and the first outlet is 0.22 m, indicating that there may still be some small turbulence in this area and the flow is not completely laminar. This is the likely explanation for the observed increase in variation in droplet count/s over time in Figure N.4 for the first outlet compared with the other outlets and it should be accounted for when using the CFT for future experiments.

Since the CFT is a small bench-top system, knowledge of the lifetime of the haze or cloud in the CFT is important for selecting appropriate aqueous reactions to study in

future experiments. The theoretical residence time, or lifetime, of the water droplets in the CFT was calculated as shown in Equation N.4, using the length of the CFT, *L*, (0.86 m) and the flow velocity, *v*, previously calculated (Equation N.2).

$$\text{cloud lifetime} = \frac{\text{L}}{v} \tag{N.4}$$

The theoretical cloud lifetime under the tested flow rate of 3.3 L/min using Equation N.4 is 2.30 minutes. The LACIS device operates on a timescale of 1 minute due to its laminar flow profile (Schütze and Stratmann 2008) so this result for the CFT in this work is acceptable.

Wall losses are a major issue in large atmospheric simulation chambers (Cocker, Flagan and Seinfeld 2001). The problem is emphasised in smaller chambers like aerosol flow tubes where the surface area-to-volume ratio is much larger. The total surface area of the CFT is approximately 0.3 m^2 and the total surface area of the water droplets in the CFT, based on an average water droplet count/s from the droplet radial profile experiments, is 1.09×10^{-13} m^2. Therefore, wall losses are likely to be a critically important factor for future experiments using this CFT and the extent should be determined experimentally to produce a wall loss correction factor.

N.3 Conclusions

Droplet radial profile experiments were performed to identify any significant variation in droplet distribution in the tube. A homogenous haze was successfully generated and maintained in the CFT and the droplet count and size distribution were relatively uniform throughout the tube. The CFT flow was found to be laminar and the cloud lifetime was calculated to be 2.3 minutes which is suitable for monitoring atmospheric cloud droplet lifetimes of typically ~10-15 minutes. This initial characterisation of the CFT recommends it as a useful tool for future experiments investigating aqueous SOA formation and cloud processing. The multiple inlets and outlets make the system versatile for online measurements of particle composition from laboratory or chamber-generated SOA using EESI-MS.